# Adequate model complexity and data resolution for effective constraint of simulation models by 4D seismic data

Ildar Sagitov

Submitted for the degree of Doctor of Philosophy

Heriot-Watt University

Institute of Petroleum Engineering

October 2014

# Abstract

4D seismic data bears valuable spatial information about production-related changes in the reservoir. It is a challenging task though to make simulation models honour it. Strict spatial tie of seismic data requires adequate model complexity in order to assimilate details of seismic signature. On the other hand, not all the details in the seismic signal are critical or even relevant to the flow characteristics of the simulation model so that fitting them may compromise the predictive capability of models. So, how complex should be a model to take advantage of information from seismic data and what details should be matched? This work aims to show how choices of parameterisation affect the efficiency of assimilating spatial information from the seismic data. Also, the level of details at which the seismic signal carries useful information for the simulation model is demonstrated in light of the limited detectability of events on the seismic map and modelling errors.

The problem of the optimal model complexity is investigated in the context of choosing model parameterisation which allows effective assimilation of spatial information in the seismic map. In this study, a model parameterisation scheme based on deterministic objects derived from seismic interpretation creates bias for model predictions which results in poor fit of historic data. The key to rectifying the bias was found to be increasing the flexibility of parameterisation by either increasing the number of parameters or using a scheme that does not impose prior information incompatible with data such as pilot points in this case.

Using the history matching experiments with a combined dataset of production and seismic data, a level of match of the seismic maps is identified which results in an optimal constraint of the simulation models. Better constrained models were identified by quality of their forecasts and closeness of the pressure and saturation state to the truth case. The results indicate that a significant amount of details in the seismic maps is not contributing to the constructive constraint by the seismic data which is caused by two factors. First is that smaller details are a specific response of the system-source of observed data, and as such are not relevant to flow characteristics of the model, and second is that the resolution of the seismic map itself is limited by the seismic bandwidth and noise. The results suggest that the notion of a good match for 4D seismic maps commonly equated to the visually close match is not universally applicable.

*This thesis is dedicated to my wife, my son and my parents*

# Acknowledgements

I would like to thank my family for their support during the work on this thesis.

I would like to thank my supervisor Dr Karl Stephen for many interesting discussions, working a lot with my texts and presentations and all the support given to me throughout the PhD course. My work greatly benefited from his contribution and expertise.

I would like to thank Dr Michael King and Dr Rink van Dijke for their time and effort in evaluating my thesis.

I would like to thank all the staff of IPE HW and my friends who were very helpful during the PhD course. Special thank goes to Juergen Munz for providing so necessary support at the right time. Also, I would like to thank Kevin Parker (KKI Associates Ltd) and Tore F Munck (Resoptima) for showing and teaching inspiring examples of work. I would like to thank prof. Yaser Abu-Mostafa (California Institute of Technology) and David Johnston (ExxonMobil) for their excellent courses that significantly affected my work.

# Declaration statement

# Table of contents

# List of tables

## List of figures

## Glossary

Units of measurement are given in SI

| | |
|---|---|
| *PSO* | particle swarm optimization |
| *NA* | neighbourhood algorithm |
| ACO | ant colony optimization |
| *DE* | differential evolution |
| *SA* | simulated annealing |
| *VFSA* | very fast *SA* |
| *McMC* | Markov chain Monte-Carlo |
| EnKF | ensemble Kalman filter |
| PCA | principle component analysis |
| KPCA | kernel PCA |
| KL | Karhunen-Loeve |
| DCT | discrete cosine transform |
| GDM | gradual deformation method |
| *GoM* | Gulf of Mexico |
| UKCS | United Kingdom Continental Shelf |
| OWC | oil-water contact |
| GOC | gas-oil contact |
| WCT | water cut |
| GOR | gas-oil ratio |
| WAG | water alternating gas |
| *PLT* | production log tool |
| *CI* | coloured inversion |
| DFT | discrete Fourier transform |
| IDFT | inverse DFT |
| MPI | Message Passing Interface |
| TVD | true vertical depth |
| TDVSS | TVD subsea |
| PVT | pressure volume temperature |

| | |
|---|---|
| $\widehat{\mathcal{M}}$ | space with the number of dimensions equal to the number of all possible model parameters |
| $\mathcal{M}$ | subspace of $\widehat{\mathcal{M}}$ with the number of dimensions equal to the number of actual model parameters |
| $A$ | basis vector in $\widehat{\mathcal{M}}$ |
| $\delta m$ | variation of model parameters in $\widehat{\mathcal{M}}$ |
| $\delta p$ | variation of model parameters in $\mathcal{M}$ |
| $m$ | vector of model parameters |
| $m_{prior}$ | vector $m$ with prior values |
| $C_M$ | model covariance matrix |
| $C_D$ | data error covariance matrix |
| $C_s$ , $C_p$ | $C_D$ for seismic and production data respectively |
| $d_{obs}$ | vector of observed data |
| $g(m)$ | vector of predicted data |
| $p(m)$, $s(m)$ | g(m) for seismic and production data respectively |
| $J(m)$ | objective function of $m$ |
| $P(m\|d_{obs})$ | probability of $m$ given $d_{obs}$ |
| $a$ | normalisation constant |
| $\langle m_i \rangle$ | mean value of $i^{th}$ component of $m$ |
| $P(m)$ | posterior probability distribution on $\widehat{\mathcal{M}}$ |
| $M(m_i)$ | marginal posterior probability distribution of $i^{th}$ component of $m$ |
| $y$ | state vector |
| $y_j^a$ | $y$ for $j^{th}$ model realisation in the analysis step of EnKF |
| $y_j^f$ | $y$ for $j^{th}$ model realisation in the forecast step of EnKF |
| $C_{yd}$ | matrix of covariance between data and model and state variables |
| $C_{dd}$ | data covariance matrix |
| $d_j^f$ | predicted data of $j^{th}$ model realisation in EnKF |
| $RMS$ | root mean square |
| $NRMS$ | normalised $RMS$ |
| $SoN$ | sum of negatives |
| $a_t$ and $b_t$ | seismic traces of surveys $a$ and $b$ |
| $Vp$ | compressional velocity (P-wave velocity), m/s |
| $Vs$ | shear velocity (S-wave velocity), m/s |
| $\Delta V_p$ , $\Delta V_s$ | time-lapse change of $V_p$ and $V_s$ respectively, m/s |

| | |
|---|---|
| $K$ | bulk modulus, Pa |
| $\mu$ | shear modulus, Pa |
| $\rho$ | density, kg/m$^3$ |
| $I$ | acoustic impedance, Pa·s/m |
| $I_p$, $I_s$ | P-wave and S-wave $I$ respectively, Pa·s/m |
| $\Delta I$ | time-lapse change of acoustic impedance, Pa·s/m |
| $\Delta I_p$ , $\Delta I_s$ | time-lapse change of $I_p$, $I_s$ respectively, Pa·s/m |
| $Ar$, $Ai$ | displacement amplitudes of reflected and incident waves respectively, m |
| $r_{12}$ | reflection coefficient for an interface between media 1 and 2, fraction |
| $K_{sat}$ | effective bulk modulus of saturated rock, Pa |
| $K_{dry}$ | effective bulk modulus of dry rock, Pa |
| $K_f$ | bulk modulus of fluid, Pa |
| $K_0$ | bulk modulus of mineral material making up rock, Pa |
| $\mu_{sat}$ | effective shear modulus of saturated rock, Pa |
| $\mu_{dry}$ | effective shear modulus of dry rock, Pa |
| $m_{dry}$ | either $K$ or $\mu$ of dry rock |
| $P_{eff}$ | effective pressure, Pa |
| $E_{v,r}$, $P_{v,r}$ | stress-sensitivity constants |
| $M_{eff}$ | effective modulus, Pa |
| $M_{sand}$ , $M_{shale}$ | modulus of sand and shale respectively |
| $\varphi$ | porosity, fraction |
| NTG | net to gross, fraction |
| $k$ | permeability, $m^2$ |
| $k_{rw}$ | water relative permeability |
| $k_{ro}$ | oil relative permeability |
| $K_w, K_o, K_g$ | bulk modulus of water, oil and gas respectively, Pa |
| $S_w, S_o, S_g$ | saturation of water, oil and gas respectively, fraction |
| $\Delta S_w$, $\Delta S_o$, $\Delta S_g$ | time-lapse change of $S_w, S_o, S_g$ respectively |
| $\rho_f$ | effective density of fluid mixture, kg/m$^3$ |
| $\rho_w, \rho_o, \rho_g$ | density of water, oil and gas respectively, kg/m$^3$ |
| $x(t)$ | seismic trace in convolutional model |
| $w(t)$ | seismic wavelet |
| $r(t)$ | time function of seismic reflectivities |
| $n(t)$ | time function of added noise in the convolutional model |

| | |
|---|---|
| $r(f)$ | frequency function of amplitude spectrum of reflectivities |
| $I(f)$ | frequency function of amplitude spectrum of impedance |
| $\beta$ | parameter used in description of $r(f)$ |
| $\alpha$ | parameter used in description of $I(f)$ |
| $f$ | frequency |
| $\omega$ | angular frequency |
| $F_w$ | fractional water flow |
| $xf$ | position of water front in Buckley-Leverett calculation, m |
| $Q$ | liquid rate in Buckley-Leverett calculation, $m^3/s$ |
| $t$ | time in Buckley-Leverett calculation, s |
| $A$ | cross-section area in Buckley-Leverett calculation, $m^2$ |
| $tp$ | time of pressure wave travel, s |
| $c_t$ | total compressibility, 1/Pa |
| $r$ | radius in calculation of $tp$, m |
| $\mu$ | viscosity in calculation of $tp$, Pa·s |
| $x_p$ | position of particle in *PSO* |
| $v_p$ | velocity of particle in *PSO* |
| $c_1$, $c_2$ | parameters of *PSO* |
| $x_{pbest}$ | local best position of particle in *PSO* |
| $x_{gbest}$ | global best position of particle in *PSO* |
| $\varphi_1, \varphi_2$ | random functions used in *PSO* |
| $w[i]$ | inertia time variant constant applied to $i^{th}$ particle in *PSO* |
| $Np$ | number of particles in *PSO* |
| $Nn$ | number of neighbours in *PSO* |
| $N_d$ | number of dimensions |
| $f_G$ | Griewank function |
| $TWT$ | two way time, s |
| $\Delta z$ | distance between two vertical points in the grid, m |
| $h(t)$ | time function of filter |
| $H(f)$ | frequency function of amplitude spectrum of filter |
| $X(f)$ | frequency function of amplitude spectrum of seismic trace |
| $\overline{X(f)}$ | average $X(f)$ of all traces |
| $X_{CI}(f)$ | $X(f)$ of seismic trace with applied CI |
| $H_D(\omega)$ | angular frequency function of the desired frequency response |

| | |
|---|---|
| $h_D(t)$ | time function of the ideal infinite impulse response |
| $W(\omega)$ | angular frequency function of frequency response of window function |
| $\Delta \mathrm{Pr}, \Delta \mathrm{Sat}$ | time lapse change of pressure and saturation respectively, Pa,fraction |

## List of publications

Part of this work is presented in the following publications:

Sagitov, I. and Stephen, K. D. 2012. Assisted seismic history matching in different domains: what seismic data should we compare? SPE15403. Presented at the EAGE Annual Conference & Exhibition incorporating SPE EUROPEC held in Copenhagen, Denmark, 4-7 June 2012.

Sagitov, I. and Stephen, K. D. 2013. Optimizing the Integration of 4D Seismic Data in History Matching: Which Data Should We Compare?. SPE164852. Presented at the 75th EAGE Conference and Exhibition incorporating EUROPEC 2013. London, 10-13 June 2013

Stephen, K. D. and Sagitov, I. 2013. When closing the loop with reservoir simulations, size matters. Prepared for presentation at the SPE/EAGE joint workshop, Lisbon, 17-20 November 2013

# Chapter 1. Introduction

## 1.1 Background and context to this work: 4D seismic method and its application in history matching

4D seismic method is based on repeated seismic surveys conducted at different times during field development which aim to detect changes in a reservoir occurring due to hydrocarbon displacement (*Yilmaz, 2001*). Processes such as water floods, gas or steam injection, gas exsolution and significant variation of reservoir pressure cause changes in acoustic properties of rocks that may be detectable in seismic data provided conditions are favourable. Such conditions include sufficient repeatability of seismic surveys and significant magnitude of those dynamic effects. 4D seismic method has a pure geophysical nature of course, but the very purpose of shooting 4D seismic surveys is to help engineers with reservoir management decisions. *Johnston, 2013* described the role of 4D seismic method in a company's business as follows: "Your company is offered a tool that can tell you whether a field is performing according to plan and that can help you locate undrained hydrocarbons, optimize infill well and workover opportunities, manage injection and offtake, and help ensure maximum recovery. The cost is less than that of drilling a single well. Would you purchase that tool? Chances are you will."

The advantages of using 4D seismic surveys have not always been so clear. The method have gone through a few stages of development in the last 30 years before becoming (in many cases) an attractive investment opportunity for companies and a tool engineers can benefit from. Most often, the application of 4D seismic method is associated with repeated 3D surveys (rather than 2D). The 3D seismic acquisition itself has almost a half-century long history. The first experimental 3D seismic survey was shot in 1967 by Exxon Production Research. The experimental surveys continued until 1973 when the first commercial land 3D survey was shot in Lea County NM USA by Geophysical services, inc. Same company shot the first marine 3D survey in 1975 in the High Island area, Gulf of Mexico. By the end of 1980s, the use of the 3D seismic method has grown substantially and accounted for more than a half of seismic surveys in the industry (*Robertson, 1989*). First publications discussing the potential of the 4D seismic for monitoring thermal recovery were based on laboratory tests and field pilot projects and appeared in 1980s (*Nur, 1982; Pullin et al, 1987; Greaves and Fulp, 1987*). Subsequent applications of the method in the early 1990s relied on legacy data and surveys not specifically designed for 4D analysis – 4D seismic was an emerging technology at that time. By the late 1990s, successful applications of the method had proven its economic viability so companies started shooting dedicated 4D seismic surveys at that time (*Lumley, 1994; Jack, 1997; Koster et al, 2000*). As a result, repeatability of 4D seismic data improved dramatically. The technical advancement of the acquisition process has gone as far as installing permanent seabed cables for seismic monitoring, although there are questions on cost-effectiveness of current implementation of that technology (*Watts, 2011*).

The state of the art of 4D seismic method is represented by its effective applications in reservoir management. Seismic attributes derived from the data can be interpreted in terms of areas of bypassed oil, hydrodynamic compartmentalisation, extent of water or gas floods, movement of oil-water contact and other production-related effects (*Yilmaz, 2001; Johnston, 2013*). This information can be fed into the decision making process on the conceptual, qualitative level. For example, to decide on location for infill drilling, or to adjust a simulation model guided by visual inspection of seismic attributes. However, information from seismic data can be taken beyond the qualitative interpretations if the seismic signal is used quantitatively to infer information about pressure and saturation changes in reservoir or even about properties of rocks that allowed those changes. This is a problem of finding models constrained by a given response (observed data) which is known as an inverse problem. Essential for solving it is having the ability to match the observed seismic data by model, that is we need to employ methods of seismic modelling and knowledge about the rock physics.

Quantitative inversion of seismic data opens up great opportunities for exploring the variety of realisations of a model based on data fit instead of working with a single model. Although the inversion process can be organised as estimation of virtually any property with the condition of fitting the data, a few paradigms exist that adopt the general idea of parameter estimation within the geomodel-to-seismic framework. The first proceeds similar to the traditional (of a single survey) seismic inversion by estimating elastic properties of rocks, impedance and seismic velocity. While with a single survey the inversion results in absolute values of the elastic properties, the results of 4D inversion are their time-lapse changes (*Sarkar et al, 2003*). Another option is to invert for pressure and saturation changes (*Landrø, 2001*). Finally, the third approach is taking one step further in complexity of forward modelling by including the flow simulation too. The target for inversion in this case is properties of the simulation model that affect fluid flow such as permeability. In this case the whole process includes perturbing simulation model properties (e.g. permeability), running flow simulation, predicting seismic response based on pressure and saturation calculated by the simulation model, and comparing predicted seismic with the observed counterpart. The comparison of predicted and observed data itself can be carried out in different domains such as seismic attributes, impedance domain, or the observed seismic data can be inverted for pressures and saturations for comparison with simulation results (*Gosselin et al, 2003*).

The last approach mentioned above within the context of inverting 4D seismic data in fact represents a bridge between the disciplines of geophysics and reservoir engineering. Indeed, we use a complex knowledge of flow characteristics, elastic properties of rocks, and seismic modelling methods in order to obtain a response of our simulation model in the seismic domain. When a history matching algorithm is employed to iteratively update the simulation models guided by a match of data (seismic and production), the approach constitutes a history matching loop. From the perspective of history matching of simulation models, the approach where modelling goes as far as predicting the seismic response essentially adds this new constraint, 4D seismic data, to traditional history matching. What does it mean for results of history matching? First of all, with more informative data, history matching yields better constrained models in general. But when this new data is 4D seismic, the extra information contributes even more substantially because it is spatial and covers areas between wells, whereas the traditional well production logs are limited to observation of integral properties at well locations. The potential of 4D seismic as a new effective constraint for history matching of simulation models was recognised by the community and triggered active research in this area. *Gosselin et al, 2003, Stephen et al, 2006, Roggero et al, 2007* formalised matching the seismic data along with production data as an automatic history matching loop. Authors point out that adding the new constraint by 4D seismic data resulted in better constrained, more reliable models and reduced uncertainty of predictions.

Although the prospect of improving simulation models by adding 4D seismic data is attractive, difficulties await a practitioner who has decided to go down that road. Integrating seismic data and flow simulations is a non-trivial task because models in seismic and flow simulation domains use different physical laws, assumptions and scales of space- and time-discretization. The differences between the domains together with uncertainties in petro-elastic properties of rocks and techniques of petro-elastic and seismic modelling make the predicted seismic signal only approximately compatible with the observed data. On the other hand, the observed seismic data itself is a quite distorted response of the true Earth because it is contaminated with errors from acquisition and processing. In other words, errors are contained both in model-predicted and observed data. Although these errors have different causes, their adverse effect on results of history matching is similar: if a model tries to fit an erroneous component of data at the expense of a part it can model, overfitting occurs and the model loses its predictive capability (*Abu-Mostafa et al, 2012*). This machine learning principle appears to be particularly applicable when matching 4D seismic data by simulation results. Indeed, the extra layer of uncertainties when overcoming the gap between the domains only weakens the link between the details of seismic signature and flow characteristics of reservoir. As a result, details appear in seismic data that are specific to the process that generated the seismic response rather than being relevant to a more general characterisation of the flow regime. Most likely, these details will be local and less correlated across the entire volume of investigation than the true response of the pressure-saturation state of the reservoir which is of interest to us. If this is the case then we can take similar approach to the one generally used to prevent fitting noise. That is weight data in the objective function so that the level of match of local variations is reduced in favour of more general information from the entire dataset. Normally, data are weighted by their error estimates which can be obtained from the analysis of observed data itself (*Gouveia and Scales, 1998; Aanonsen et al, 2003*), or we can try to estimate the likely distribution of the model error directly where possible (*Stephen, 2007*). Although the question of errors in seismic data has been studied in the literature, there is no indication of the level of details at which seismic data (such as 4D seismic map) constrains reservoir simulations effectively. Moreover, the term ‘good’ match of a seismic map has universally become equivalent to the closest match possible. There is no question that the close match can be achieved one way or another. The real question is will it improve the model?

Another aspect of integrating 4D seismic data in simulation models is adequate model complexity for assimilating useful information from the new constraint. Complexity of a model is defined here as a number of parameters that control the model response. How complex should our models be for effectively learning from the observed data in order to give meaningful predictions? In scientific problem solving, the heuristic preference is a tendency to simpler, more parsimonious models consistent with observations – a principle known as Occam's razor (*The Stanford Encyclopedia of Philosophy*), or a more cautious formulation by Albert Einstein warning against promoting the simplicity above useful heuristic: "Everything should be kept as simple as possible, but no simpler". This principle sometimes is contrasted with Bayesian inference (*Gouveia and Scales, 1997*) where multiple hypotheses of arbitrary complexity are tested instead of a single parsimonious solution. So where are we with history matching simulation models using 4D seismic data? As far as the complexity of models is concerned, we can see that the reservoir models clearly are not getting simpler. Nowadays, they are built on finer grids which are capable of accommodating complex geological concepts including interpretations of seismic data or other structural ideas of modeller being imposed on the model prior to history matching. In order to avoid bias from all this prior complexity, we need to use many parameters in history matching. *Oliver and Chen, 2011* in their comprehensive review of history matching problems in the literature summarize findings in support of using many parameters. In particular, the authors point out that using a small number of parameters leads to solutions that are too specific to the information in the part of the model not varied as parameters, that is in the prior structure. As a result, predictions are biased and perception of uncertainty of predictions is inadequate (*Hunt et al, 2007; Chen et al, 2010; Kravaris et al, 1985; Fienen et al, 2009*). Engineers still choose to work with few parameters sometimes because it is computationally easier. Parker (*Parker, 1977*) describing this tendency in a more general context concludes that sometimes too few parameters are used for convenience of problem solving rather than for any convincing geological reason. Underparameterisation of the problem does not fit to the abovementioned principle of parsimony either. Choosing just a few parameters for history matching does not make the model simpler, but it only makes it less flexible. With more parameters on the other hand, we can still seek the simplest and smoothest (in a mathematical sense, that is without extreme values) solution commensurate with data. This may require an extra ingredient though which is a regularisation. Indeed, using more parameters will make the model more susceptible to learning from data, and the regularisation will avoid overfitting and make the solution smoother. Although the pitfalls associated with insufficient parameterisation of history matching problems are generally understood, the question is not studied in the context of matching 4D seismic data which requires different considerations about model complexity because of its spatial constraint. Moreover, with the advent of seismic methods, more detailed interpretations of seismic material are being introduced into the simulation models in a form of geobodies (*Martin and Macdonald, 2010*). These form a structural framework which may produce bias as described above if not parameterised properly.

In the last two paragraphs, questions were raised regarding two aspects of seismic history matching: parameterisation of the reservoir model and matching the data. Figure 1.1 illustrates how these aspects fit into the history matching scheme. The scheme shown in this figure describes a history matching formulated as a parameter estimation problem. Constituents of such formulation are discussed in more details in Chapter 2 while here only a brief overview will be given. History matching is a process where some of the model parameters are adjusted so that the model response better fits the data. Additionally, it can be required that the resulting parameter values do not deviate much from a pre-defined prior values. The aim of history matching is calibration of model's response against the historic data intended to improve the predictive capability of the model. The process starts with a geological model built using multiple sources of data and knowledge (see section 2.2 for more details). In the next step, a decision is made on what parameters should be calibrated in the history matching. This is an important and difficult part of the process. The number of parameters and their type and scale define the model resolution which should be adequate to the constraint of the available calibration data. As noted before, choosing too few parameters or insensitive parameters will be an obstacle for assimilating the information from the dynamic historic data. The key to maximizing the value of information from different sources is the balance between the model resolution and the prior knowledge embedded into the model such as geological concepts (see 'parameterisation' sections of chapters 2 and 3 for more discussion on the parameters). This aspect of history matching will be discussed in this work in the context of integrating 4D seismic data within the reservoir simulation models.

The following steps of the history matching workflow shown in Figure 1.1 usually are encountered in a stochastic multiple model optimization approach (see Chapter 3 for discussion on the optimization methods). In such an approach, multiple models (forward models) are run for each iteration. An iteration starts with setting values to the parameters: initial (often random) values if it is the first iteration or optimized (based on minimizing the objective function) values for subsequent iterations. A forward model here includes a reservoir simulation and seismic modelling followed by a comparison of predicted and observed data numerically defined by the objective function (which may also include a comparison with a prior model, hence the block in Figure 1.1 is called data/prior match). For a seismic history matching scenario, the observed data includes both production data such as well rates and pressures and also seismic data in a form of seismic attributes. In reflection seismology, a seismic attribute is defined as a quantity extracted or derived from seismic data that can be analysed in order to enhance information that might be more subtle in a traditional seismic image, leading to a better geological or geophysical interpretation of the data (*Yilmaz, 2001*). Therefore, the objective function consists of 'production' and 'seismic' terms. The balance between matching production and seismic terms is an important question which is addressed in this work. After the objective function is evaluated for each of the models, the resulting values are fed into the optimization algorithm which, if the match criteria is not met (or a maximum of the number of iterations is not reached), calculates updated values of parameters for multiple models of the next iteration thus closing the loop, or ends the process otherwise.

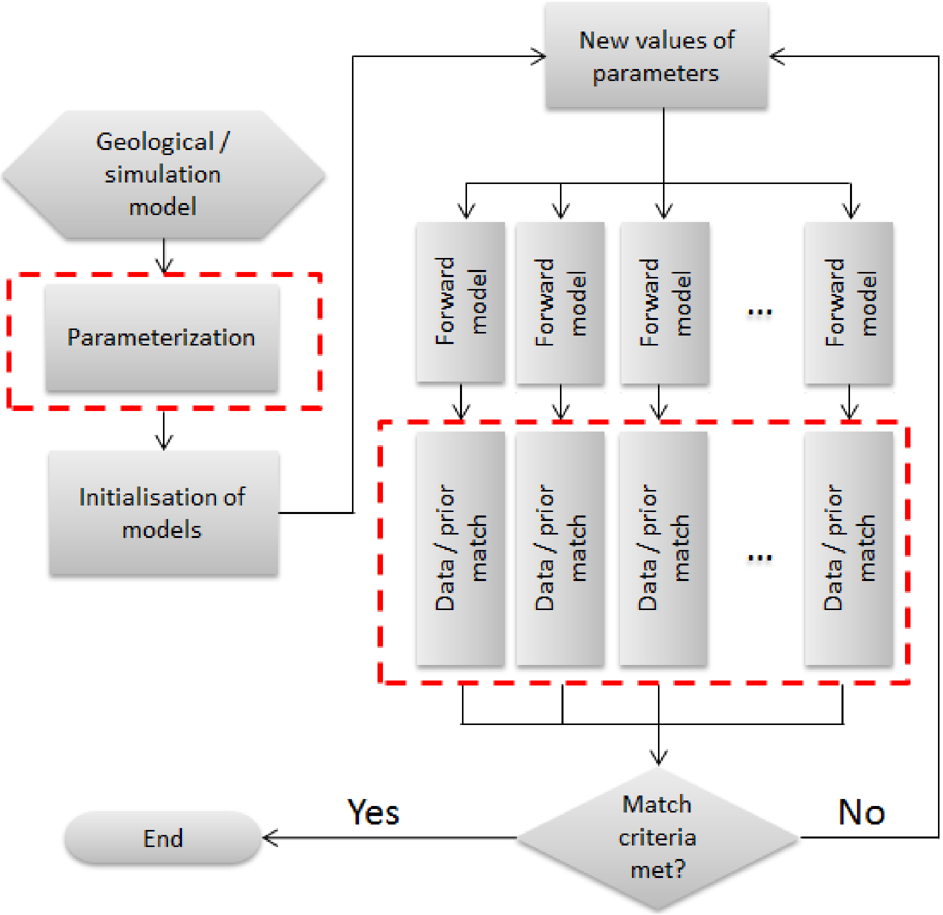

**Figure 1.1. Scheme of history matching for an iterative parameter estimation formulation using multiple-model approach such as a stochastic automatic history matching. Dashed red rectangles indicate the parts of the workflow on which the present work focusses.**

## 1.2 Objectives and scope of this work

As mentioned before the problem of integrating 4D seismic data within the process of history matching of simulation models is non-trivial and many-sided. It is only by collective knowledge based on many case studies from around the world can we assure progress in this field. This work aims to make its contribution in the field by analysing the questions raised in the previous paragraphs and answering them within the scope of a few realistic scenarios constructed as part of this work with the available resources including field data and models of the Schiehallion field. This work aims to achieve the following main goals:

1. Study the seismic response of models covering various distributions of properties. Investigate to what extent the limited resolution of seismic data and associated effects such as tuning and also noise affect the detectability of production-related effects in reservoir. What is the impact on history matching?
2. Study the impact of model complexity and flexibility of parameterisation on the results of history matching. What is the impact of deterministic inclusions in models such as geobodies from seismic interpretation?
3. How to achieve a more flexible parameterisation? Is history matching in high-dimensional parameter spaces a feasible and practical solution for conditioning reservoir simulation models?
4. Investigate differences in constraints by production and seismic data, and the impact of those differences on combining the two data types within a single dataset. How to judge the quality of constraint by data and why one model is better than another?
5. Identify the level of details at which the seismic map constructively constraints flow properties of simulation model. What constitutes a good match?

Achieving those goals has required solving a number of technical problems mainly associated with organising the process of seismic history matching within an automatic loop. This loop integrates a number of processes that bridge the gap between geophysics and simulations domains: petro-elastic and seismic modelling, calculation of seismic attributes, signal processing and seismic inversion.

## 1.3 Outline of the thesis

The remainder of the thesis is organised as follows:

Chapter 2. Theory. This chapter provides definitions and the theoretical context to the methods applied in this work.

Chapter 3. Literature review. The aim of this chapter is describing the progress made so far in addressing the problems of combining seismic and production data within the history matching process.

Chapter 4. Methodology. Conducting the history matching experiments required development of software tools which adopt standard methods and algorithms. The work-specific implementations of those are described here.

Chapter 5. Seismic response study. This chapter focuses on the seismic modelling side of the process by studying the relationship between reservoir properties and the seismic response (4D seismic map in this case). It explains the choice of seismic attributes for history matching. Particular emphasize is put on detectability of production related effects as a basis for seismic history matching.

Chapter 6. Problems of incorporating seismic interpretations in simulation models. This chapter studies how including deterministic seismic interpretations such as geobodies in simulation models affects their flexibility and impacts results of history matching. The question of model complexity is addressed in the context of choosing a parameterisation that allows better assimilation of details from the seismic data and reduces bias from the imposed prior structure.

Chapter 7. Integrating data in seismic history matching: scale of constituents. In this chapter, scenarios of history matching using a combined dataset of production and seismic data are tested to identify the level of details in the seismic map that effectively constrain flow properties of the model. The constraints by production and seismic data are compared in terms of the result of history matching.

Chapter 8. Conclusions and recommendations. Most important results of the work are summarized and also recommendations are made for using the results and improving them.

# Chapter 2. Overview of theory

## 2.1 Introduction

The work of this thesis integrates methods from two disciplines, reservoir simulation and geophysics such as history matching, petro-elastic and seismic modelling and inversion. It is important therefore to establish a theoretical background for the work which is a focus of this chapter. Main definitions and place of the methods in a broader context of the subjects are discussed. The chapter starts with an introduction to the history matching including parameterisation and optimization methods. In the following part, 4D seismic method is introduced by its applications. The central topic in this part is the rock physics foundations. These describe the relationships between production-related pressure and saturation effects occurring in reservoir and petro-elastic properties of rocks that are detectable in 4D seismic data. In the final sections of the chapter, methods of seismic modelling and inversion are discussed. Seismic modelling is used as a part of the forward modelling routine in this work. It facilitates the integration of 4D seismic data within the history matching workflow. Seismic modelling also is a part of the seismic inversion procedure. The latter is used in this work for deriving data-specific distributions of properties in models.

## 2.2 Building of reservoir models

Reservoir models represent aggregated knowledge about reservoirs in a mathematical form. This knowledge comes from field measurements and their interpretations tied together with understanding of geology of the reservoir. A geological model of reservoir consists of the following components:

- Structural framework (reservoir geometry and faults)
- Stratigraphic layering
- Facies model
- Petrophysical model

The geological model serves as a basis for the simulation model which additionally includes properties necessary for fluid flow simulation: properties of fluids, aquifers, relative permeabilities and capillary pressures of rocks, initial pressure and saturation conditions, boundary conditions and well locations and regimes.

The dynamic response of a model such as predicted well rates and pressures is defined by those model constituents for which reason model errors are the factor that reduces the reliability of model predictions. Model error is reduced if some of the model parameters are tuned by calibrating the model response against historic data – well rates, pressures, and 4D seismic data, in a process called history matching. Not all the model parameters can be tuned in history matching as discussed in the parameterisation section below. Some part of the model will have to remain intact (fixed) during history matching because the historic dynamic data may not provide enough information for constraining more parameters and also the history matching with too many parameters may not be feasible. Most often the history matching parameters include those directly affecting the flow: permeabilities, barrier transmissibilities, relative permeabilities and others. The fixed part on the other hand usually is comprised of the structural framework: reservoir geometry, fault locations, facies definitions – those parameters for which the input from the static geological model is less uncertain. This is where the geology is important: any solution for the history matching problem will be found only within the bounds set by the geological model realisation.

These bounds help obtaining geologically plausible models in history matching and also make the search in parameter space more efficient by reducing its size. Geological description such as the type of depositional environment and the definition of facies forms the basis for building a model. For example, seismically derived geobodies in Schiehallion field were integrated in the model of the channelized turbidite reservoir which provided valuable pressure constraint even before the history matching (*Miranda, 2007, Martin and Macdonald, 2010*). In another example, the model of sand lobes interbedded with shales in stacked turbidites of the Magnus reservoir allowed obtaining an effective permeability model and helped planning the tertiary recovery optimization (*King et al, 1998, Moulds et al, 2005, Erbas et al, 2014*).

Together with valuable information, the geological realisation brings an element of subjectivity too because a geological description is to a great extent uncertain. In this situation, considering multiple probable geological realisations helps understating the uncertainty and also provides means for screening of the possible outcomes (while sticking with a particular realisation and hence not thoroughly exploring the parameter space is sometimes called anchoring, see *Aggarwal et al, 2012*). In some cases regeneration of geological realisations can also be included in the history matching itself, although this can significantly slow down the process (*Maucec et al, 2011*).

Building a model requires integration of data from different sources. These data have different uncertainty as well as different characteristic scales which makes their integration challenging. For example, structural framework is built by mapping horizons in 3D seismic data with the structural data updated at well locations. This requires tying vertically coarse seismic data to the detailed well logs for which reason the synthetic seismogram is used (*Yilmaz, 2001*). Relative permeability can be measured directly on core samples in laboratory but upscaling the results to the reservoir scale requires many assumptions about the representativeness of the conditions of the experiment and overall, the results are non-unique and require further calibration (see for example, *Yang et al, 1994*). There are multiple-scale sources for the absolute permeability too: core measurements, mini-permeameter, well test, and even estimates from 4D seismic data (*Durlofsky, 2002*). The most relevant to the present work is reconciling the results of reservoir simulator and observed 4D seismic data. Because these data are discretized at different scale upscaling and downscaling can be required for integrating 4D seismic data within the reservoir model (see Chapter 3 for more details).

## 2.3 History matching

In the history matching process, parameters of the model affecting its predictions are adjusted until the mismatch between the model predictions and observed well rates, pressures, seismic attributes is minimized to a certain degree. Adjustments to the parameters are made iteratively, and at each iteration, new values of parameters, new parameters or a new direction of parameters change, are devised from the current state of the model, and whether this state changes as desired. This iterative process may include a great deal of repetitive computations and therefore is automated where it is possible. Automated history matching algorithms generally require interaction with human for heuristic guidance and the process therefore is called assisted history matching. If automation of the history matching steps is not applied, the process is called manual history matching. Manual history matching relies on good engineering judgement and experience for updating simulation models, but can be limited in the number of runs and width of exploration of parameters. Although manual history matching can follow a structural, well organised approach (*Williams et al, 1998*), it may still result in geologically implausible distributions of properties due to local changes to match individual wells or connections. For these reasons, assisted history matching methods represent an improvement over the traditional manual approach.

In order to formalise the history matching problem and apply mathematical methods to it, such as automation of history matching, the problem is usually formulated as an inverse problem of parameter estimation. The parameters to be estimated in this case are those affecting the dynamic predictions of the model: porosity, permeability, geometric factors of the reservoir, and any other parameters that are thought to improve match of historic data.

The formulation of an inverse problem of parameter estimation includes:

1) Mathematical model (forward model)
2) Parameterisation
3) Objective function
4) Algorithm for minimizing the objective function

With the above formulation, the history matching process represents a series of iterations to minimize the objective function which is a sum of specifically weighted residuals of the difference between predicted and observed data. The predictions are calculated at each iteration using a mathematical model also called a forward model. The optimization algorithm is responsible for updating the parameters with a view to minimize the objective function.

### *2.3.1 Mathematical model*

Prediction of well rates and pressures as well as oil recovery fractions in reservoir simulation is carried out using analytical techniques and numerical methods. The former include material balance equations, fractional flow methods (1D Buckley-Leverett equation), and decline curve analysis. The analytical methods appeared in reservoir engineering before the computation-expensive numerical methods became available. At present, the analytical techniques are still useful for preliminary assessment of well potentials or when data is limited, for example in new developments. However, the discrete models of reservoir now contain detailed spatial information about rock and fluid properties and multiple wells with changing regimes. The complexity of such models implies that it is not possible to obtain an analytical solution for the non-stationary pressure and saturation within them and it should be found numerically. The mathematical model simulating fluid flow in porous media is based on the following fundamental laws (*Donnez, 2007*):

1) Mass conservation law
2) Darcy's law
3) Equation of state
4) Relative permeability and capillary pressure relationships
5) Wells and/or surface facility models for boundary conditions

The respective partial differential equations are solved by simulators using a finite-difference approximation on the simulation grid. The finite-difference simulators are the most common tool for reservoir simulation, and such a simulator is used in this work.

To speed up the simulations, one may opt for an alternative simulator, a streamline simulator instead of a conventional finite-difference simulator (*Datta-Gupta and King, 2007*). It solves the transport equations along streamlines drawn from the velocity field. The streamline simulation method provides faster simulations especially when using finer grids and convective-dominated systems: slightly compressible systems, principally governed by pressure gradients rather than absolute pressure, such as water or gas displacing oil.

### *2.3.2 Parameterization of the model*

Building a model involves integrating many types of imprecise information about rock and fluid properties, every piece of which can potentially be adjusted in order to improve flow predictions of a model. The number of parameters in a history matching problem therefore can be very large exceeding the number of independent data by many orders of magnitude. Such history matching problem will be extremely ill-posed so that even though solutions can be found matching the data, they will be so non-unique that their usefulness for making predictions will be questionable. One way of tackling the non-uniqueness problem is applying a regularisation which would narrow down the range of solution to those meeting imposed criteria such as the smoothness (*Tikhonov and Arsenin, 1977*). Pure generic regularisation does not bear any geological knowledge though, and also, not all optimization algorithms are capable of working in high dimensional spaces. Therefore, we need the parameterisation too. The parameterisation reduces the number of parameters to be modified for updating the model. Choosing parameters for history matching is very important as it defines not only the performance of the history matching algorithm but also the form of the final solution, that is the model and its predictive capability. Generally, parameters are chosen based on their impact on the misfit reduction, and also with a view to improving prediction of a particular data type. For example, relative permeabilities for correcting phase flows, absolute permeability and strength of aquifer for reservoir pressures, areal distribution of permeability and flow barriers for desired more complex flow patterns. In the context of simulation models, the parameters can be those controlling the model as a whole (or big parts of it) such as aquifer strength, oil-water contact depth, petro-elastic constants, PVT properties and so on, and those representing properties on the grid such as porosity and permeability in cells. It is the latter category that normally requires reparameterisation due to the massive amount of potential parameters in it.

One of the most basic parameterisations is called zonation (*Jacquard and Jain, 1965*). It divides a model into regions of constant properties which are then used as parameters in history matching. The scheme leads to very fast initial reduction of misfit, but results in a too coarse model. Problems of the method are addressed in the multi-scale adaptive approach where the parameterisation is refined at different stages of history matching based on reduction of misfit (*Yoon et al, 2001; Grimstad et al, 2003*). In other schemes, solutions are found in the form of smoother property fields in the first place. This is achieved by using an interpolation between the locations of parameter updates. Very popular example is the pilot points scheme which uses krigging to spread the influence of the points at which the property is updated to the adjacent cells in a model (*Marsily et al, 1984*). Other methods may use spline functions for interpolation (*Lee et al, 1986*). Efficient parameterisation of the history matching problem can be achieved by calculating eigenvectors of decomposition of either the prior model covariance matrix such as Karhunen-Loeve (KL) expansion (also known as the principle component analysis (PCA), *Gavalas et al, 1976*) or that of the data-sensitivity matrix, that is by finding the number of parameters determined by data (*Rodrigues, 2006*).

A parameterisation scheme can be viewed as a method of applying an update to all possible parameters in a model through modification of only a few of them. One way of representing the relationship between a high-dimensional vector of the model update $\delta m$ (in space $\widehat{\mathcal{M}}$) and a vector of the parameter update in a lower-dimensional space (subspace $\mathcal{M} \in \widehat{\mathcal{M}}$) $\delta p$ is the linear combination of basis vectors specific to that parameterisation scheme scaled by the components of $\delta p$ (*Oliver and Chen, 2011*):

$$\delta m = A\delta p \tag{2.1}$$

where columns of matrix $A$ are basis vectors in $\widehat{\mathcal{M}}$. These encapsulate the spatial (in $\widehat{\mathcal{M}}$) characteristics of a parameterisation such as smoothness of interpolation or radius of influence of parameter updates. The spatial characteristics of the parameterisation schemes discussed above are illustrated in Figure 2.1 which compares the corresponding basis vectors for an example of parameterising a problem of property estimation on 100 grid blocks using 2 parameters (after *Oliver and Chen, 2011*). Blocky character of the zonation scheme contrasts with smooth fields of other methods. The 2 pilot points in Figure 2.1, b are distributed evenly across the model. The two eigenvectors of KL-expansion method in Figure 2.1,c are determined by the prior covariance matrix only, while the two vectors in Figure 2.1, d result from the data-sensitivity of parameters, hence distributed unevenly in space.

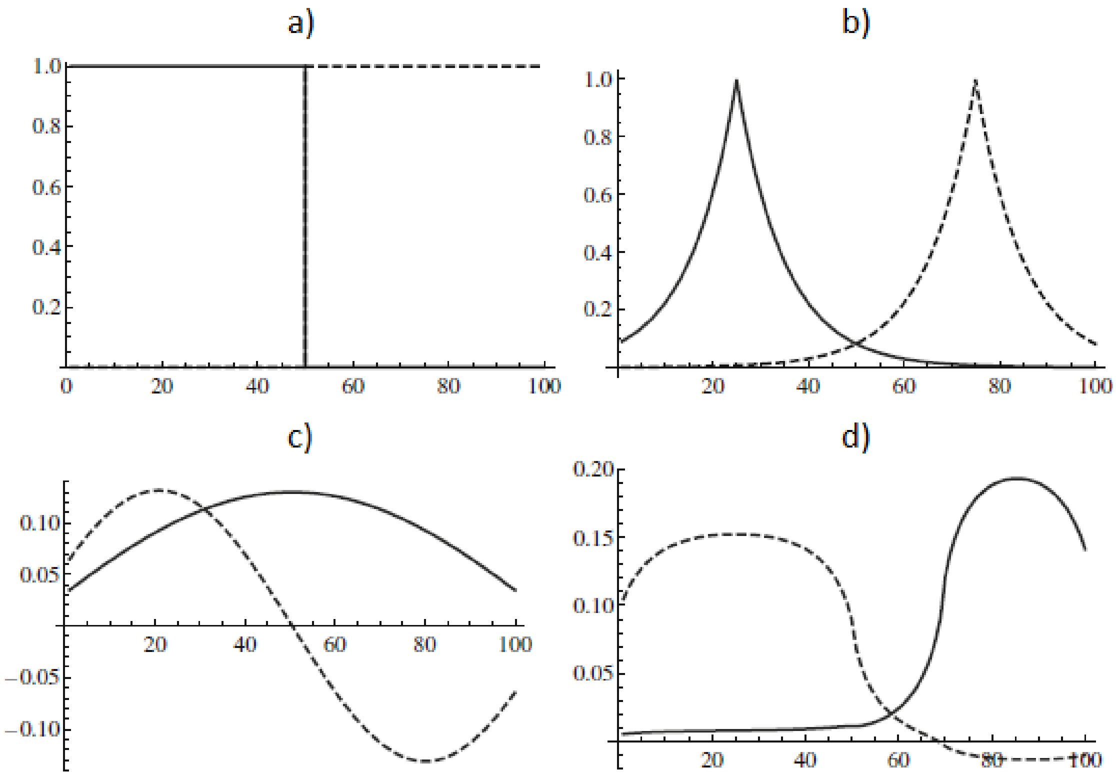

**Figure 2.1. Basis vectors for parameterisation methods: a) zonation, b) pilot points, c) KL expansion, d) singular vectors of (regularized) data-sensitivity matrix. After *Oliver and Chen, 2011***

Modelling complex and geologically realistic properties and distributions of facies requires parameterizing the models with discrete quantities such as appearance of geobodies, placement of channel boundaries, switching facies. History matching can handle this kind of variation of properties too for which it is more convenient to convert them into the continuous form. This can be achieved by reparameterising the problem using multiple-point statistics. Plurigaussian models are used in the Gradual deformation method which works with a series of Gaussian model realisations to find the one that minimizes the objective function (*Hu et al, 2001*). The method preserves the spatial variability of the defined stochastic model. Sometimes, additional constraints are set to the property trends in stochastic realisations such as to control the average spatial proportion of facies (*Roggero et al, 2007*). In a related probability perturbation approach, the probability is updated in the sequential simulations of properties until a realisation is found minimizing the objective function (*Caers and Hoffman, 2006*).

### *2.3.3 Objective function*

History matching algorithms use the objective function to calculate goodness of a given model $m$ which guides them in searching the parameter space $\mathcal{M}$ consisting of models $m$. First of all, the objective function measures the misfit of model prediction, $g(m)$, and the observed data $d_{obs}$, by a weighted sum of residuals. The weighting takes into account units of different data types and also correlations of residuals which are based on the noise statistics. These statistics are encapsulated by the data error covariance matrix $C_D$ *(Tarantola, 1987)*. The mismatch between predicted and observed quantities can also be corrected if predicted data contains errors for which the covariance information is available, for example in upscaling studies (*Stephen, 2007*).

Underdetermined nature of the parameter estimation problem such as history matching requires regularisation to ensure smoothness of its solutions. Regularisation can be implemented explicitly in the objective function by adding a term which penalizes deviations of solutions from certain prior solution ($m_{prior}$). That deviation is measured by the model covariance matrix, $C_M$, which indicates parameter correlations too. The most popular expression for the objective function that has the described characteristics is as follows:

$$\begin{aligned} J(m) = {} & (g(m) - d_{obs})^T C_D^{-1} (g(m) - d_{obs}) \\ & + \left(m - m_{prior}\right)^T C_M^{-1} \left(m - m_{prior}\right) \end{aligned} \tag{2.2}$$

The rationale behind using the squares of the residuals is that the values of the objective function, provided the errors are Gaussian, can be used in the Bayes' formula to calculate the probability of models, *m*:

$$P(m|d_{obs}) = a\,exp\left(-\frac{1}{2}(g(m) - d_{obs})^T C_D^{-1}(g(m) - d_{obs}) - \frac{1}{2}\left(m - m_{prior}\right)^T C_M^{-1}\left(m - m_{prior}\right)\right) = a\exp\left(-\frac{1}{2}J(m)\right), \tag{2.3}$$

where $P(m|d_{obs})$ is the posterior probability of the model *m* given the data $d_{obs}$, $a$ is a normalisation constant.

The above expression is derived from the multiplication of Gaussian probabilities of errors of all individual data points. If the ensemble of models is assigned probabilities as shown above then the posterior probability distribution, *P(m)*, is defined on $\mathcal{M}$ (provided the distribution of *m* is known, or $\mathcal{M}$ can be resampled with a required distribution). Subsequently, known *P(m)* can be used to calculate Bayesian integrals, such as the mean value of the models

$$\langle m_i \rangle = \int_{\mathcal{M}} m_i P(m) dm, \tag{2.4}$$

and the marginal posterior probability distribution

$$M(m_i) = \int \dots \int P(m) \prod_{\substack{k=1 \\ k\neq i}}^{d} dm_k \tag{2.5}$$

### *2.3.4 Algorithm for history matching*

Historically, the manual history matching was the main approach for conditioning reservoir simulation models to field data. It is still widely used as automation may not be possible due to technical or organisational limitations. In the manual history matching, properties that are known to have largest impact on the flow are adjusted. Although it is recognized that the resulting changes to the model should be realistic from the geological point of view, the results of history matching sometimes include localised, unrealistic changes to the model properties. This happens because matching data, especially at the well level is a difficult, time-consuming process, and engineers have to resort to these easier solutions. A systematic approach to the history matching will include (*Donnez, 2007*):

1) Matching data at the field level: aquifer strength (size and permeability), reservoir pressures (using pressures from build ups and RFTs)
2) Matching phase rates (WCT, GOR).
3) Matching bottom hole flowing pressures by adjusting productivity indexes of wells.

When the automation of the history matching process is feasible, different options exist for an algorithm of minimization of the objective function. If the objective function is believed to be relatively smooth then gradient-based methods (*Nocedal and Wright, 2006*) may offer fast convergence with very few iterations and, more importantly, few estimations of the objective function. Gauss-Newton method operates with both gradient and an approximation to Hessian (2nd order derivative) matrixes for estimation of the parameter updates. The method can converge to the solution very rapidly but may become impractical for large number of data and parameters due to the size of the matrices. An improvement to the Hessian calculation is offered by the Levenberg-Marquardt algorithm, but the cost of a single iteration remains high. More practical gradient-based algorithms use the conjugate-gradient method where the Hessian is not used, and the subsequent search directions are estimated as linear combinations of the previous directions.

Gradient methods can handle history matching problems with many parameters and offer fast convergence rates but may fail to overcome the non-linearities of the objective function in a sense that a solution may be found in a local minimum of it. Also, accurate computation of data-sensitivities is computationally expensive. Stochastic algorithms on the other hand do not use sensitivities while relying on the random sampling of the response surface. For that reason the stochastic algorithms are capable of avoiding local minima. The major weakness of these algorithms though is the need for many models to explore the parameter space efficiently. This limits the dimensionality of the parameter space, that is it reduces the number of parameters that can be used in history matching compared to the gradient-based methods.

Stochastic algorithms are often based on analogy with natural processes of evolution of populations. Genetic algorithms use mutations and recombinations of models which are performed randomly but are conditioned on the current value of the misfit (*Winter et al, 1995*). Simulated annealing algorithm simulates a controlled cooling of the system where the probability of accepting worse solutions (jumps) decreases with temperature (*Reeves, 1995*). The Particle swarm optimization (PSO) algorithm is inspired by social behaviour of bird flocking or fish schooling (*Kennedy and Eberhart, 1995*). Each particle in the population moves randomly but is attracted towards the best solution found by itself and towards the best solution found by the population as a whole or as a group. PSO method is used in this work so the algorithm is described in more details in the Methodology chapter.

Different approach to history matching is represented by the ensemble Kalman filter (EnKF) method which results in multiple history matched models (rather than a single deterministic model). The resulting ensemble of models gives an estimate of uncertainty (although this estimate generally appears to be too low, according to *Oliver and Chen, 2011*). The method was only recently brought to the petroleum science (*Lorentzen et al, 2001*). EnKF is based on a sequential data assimilating scheme and is capable of estimating large numbers of model variables (*Aanonsen et al, 2009; Zhang and Oliver, 2011*). Not only the model variables such as porosity and permeability, but also the state variables such as pressures and phase saturations are estimated in this method. Both model and state variables are combined within a single state vector. The method consists of two main steps, forecasting and analysis (data assimilation step). At the forecasting step reservoir simulator and a seismic forward model (if any) are used to propagate the state vectors forward in time. At the analysis step, each realisation of the state vector $y$ is updated according to the data assimilation equation:

$$y_j^a = y_j^f + C_{yd}(C_{dd} + C_D)^{-1}\left(d_{obs,j} - d_j^f\right) \tag{2.6}$$

where $j$ is the index of model realisation, $a$ and $f$ refer to the analysis and forecast steps, $C_D$ is the data error covariance matrix, $d^f$ and $d_{obs}$ are predicted and observed data, $C_{yd}$ is the matrix of covariance between data and model and state variables, and $C_{dd}$ is data covariance matrix.

The size of the ensemble of models and variation of properties within the ensemble define the quality of covariance estimates and ultimately the final parameter estimates. Provided the parameters are backed by sufficient variation of properties within the ensemble, the method is not sensitive to the number of parameters being estimated which is the reason for its computational efficiency for estimating large numbers of parameters. The drawbacks of the method are caused by the abovementioned limitation due to the ensemble size and also by the Gaussian and linear assumptions of the analysis step. These include unphysical estimates of state variables and limited ability to assimilate large volumes of independent data such as 4D seismic data.

## 2.4 4D seismic method

4D seismic data, along with production data, forms the basis for constraining simulation models in this work. Prediction of 4D seismic data is therefore a part of the forward modelling step of the history matching process. This section builds up the theoretical background for linking the production-related effects in reservoir with the elastic properties of rocks. Fundamental laws of rock physics and empirical relationships are given here explaining their assumptions and a broader context, whereas the methodology chapter details the exact workflow for predicting seismic properties.

4D seismic method is based on repeated (most often 3D) seismic surveys. 3D seismic acquisition is a geophysical technique that has undergone a significant growth in the last 45 years and has largely replaced 2D seismic acquisition in the seismic industry (*Eaton et al, 1997, Biondi, 2006*). 3D seismic data has superior resolution compared to 2D seismic data because of the reduced spacing of the seismic grid (25 or less metres for 3D compared to a kilometre for 2D) and improved positioning of reflections by the application of 3D sampling and migration algorithms. As high resolution data, 3D seismic data represents a critical component for reservoir description as it bears information about the inter-well space not available from wells. Typical applications of the 3D seismic method include (*Jourdan and Ekern, 1996*):

- Structural analysis and identification of top of reservoir: mapping of horizons and faults.
- Stratigraphic and sedimentological analysis: sequence stratigraphic analysis, the analysis of reservoir architecture, bounding surfaces and reservoir heterogeneities. At this level, the high-resolution seismic data is integrated with the geological concepts.

- Estimation of petrophysical parameters and rock properties. Estimation of porosity and net to gross 3D properties by calibrating seismic attributes at well locations, or deriving trends of properties rather than their values.
- Fluid detection. Analysis of seismic attributes for direct hydrocarbon indicators (bright spots, flat spots) or detection of hydrocarbon bearing reservoirs from the amplitude versus offset (AVO) analysis.

As follows from the list of applications, 3D seismic method provides necessary input for the static geological model. 4D seismic data on the other hand is a reservoir management tool which provides information about the dynamic characteristic of the reservoir and as such can be used to constrain the response of the simulation model. 4D seismic method has evolved from an academic research topic into a practical tool for reservoir management during the last 20 years due to the advances in acquisition and processing techniques and the advent of new technologies such as repeated marine streamers. First publications on the applicability of the 4D method were related to the thermal recovery monitoring (*Nur, 1982*). Early 4D studies used legacy seismic data to detect production related changes, mainly associated with water flooding, before the companies started shooting specifically designed 4D surveys (*Koster et al, 2000*). Today, the 4D seismic effects are well understood, mostly for monitoring of thermal recovery, $CO_2$ enhanced recovery, water flooding, pressuring up and compacting reservoirs.

Applications of the 4D seismic method are summarized below:

1) Monitoring the spatial extent of the steam front following in-situ combustion or steam injection used for thermal recovery
2) Monitoring the spatial extent of the injected water front used for secondary recovery
3) Imaging bypassed oil
4) Determining flow properties of sealing or leaking faults, identifying compartmentalisation
5) Detecting changes in oil-water contact
6) Monitoring $CO_2$ enhanced recovery or $CO_2$ sequestration in order to minimize $CO_2$ loss and recycling
7) Monitoring compaction or over-pressuring of reservoirs

The state of the art of 4D seismic method is quantitative use of 4D seismic attributes as discussed in Chapter 1. These require more information available from 4D seismic data which means better data quality ensured by higher repeatability and lower noise. Several strategies exist today that improve on these parameters (*Johnston, 2013*). First of all, dedicated 4D seismic surveys provide far better repeatability than those using legacy data. The dedicated surveys can be acquired using either towed streamers or using permanent installations such as ocean bottom cables (OBC) or ocean bottom sensors/nodes (OBS/N). For the towed-streamer surveys the following strategies improve the repeatability:

- Using the same line orientation and direction
- Matching the source positions
- Overlapping streamers
- Matching streamer feathering
- Using non-standard dual vessel geometries
- Shooting infill lines on the basis of repeatability criteria
- Designing baseline survey to be easy to repeat
- Tightening survey specifications
- Considering alternative acquisition methods under facilities

Although the permanent monitoring systems (OBC and OBS) benefit from better repeatability parameters, their market penetration remains low. The main reason is that the economic benefit of the technology is difficult to prove in the life of field scale. Figure 2.2 illustrates the cost difference between the towed-streamer and permanent systems for a scenario where the surveys are shot twice a year. The difference increases however if one survey a year is assumed.

The majority of 4D seismic surveys have been acquired offshore. The land application of 4D seismic method is limited by the land seismic data quality issues and also by the economic factor: 4D survey offshore is easier to justify due to the high cost of facilities.

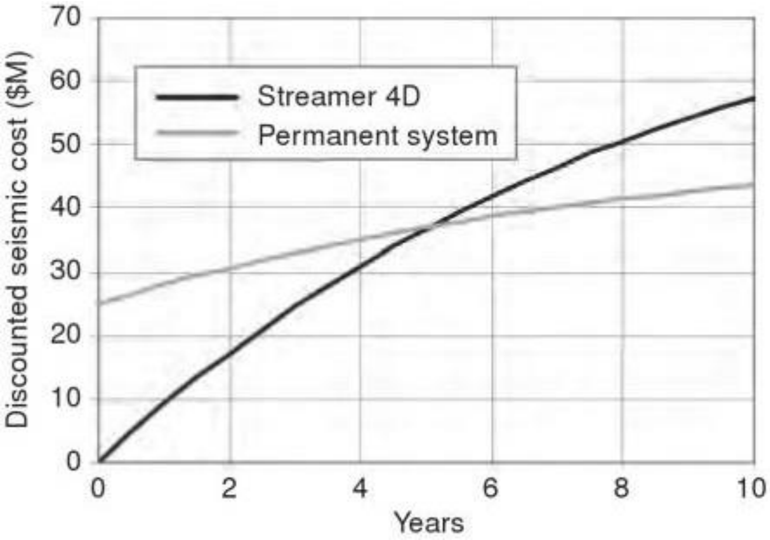

**Figure 2.2. Comparison of costs of 4D acquisition types: towed-streamer and permanent installation. After *Johnston, 2013***

The time lapse (4D) seismic method works with seismic images of same subsurface target taken at different times to reveal production-related effects in them. Production of hydrocarbons, injection of water, steam or gases change pressure and saturation of the reservoir, cause reservoir compaction or pressuring up, may also change the temperature field resulting in changes of the elastic properties of the subsurface rocks (Figure 2.3). These changes can be detected on the differences of seismic surveys taken at different stages of production. Ideally, the first survey is pre-production and is called a baseline survey, and the subsequent surveys are called monitor surveys.

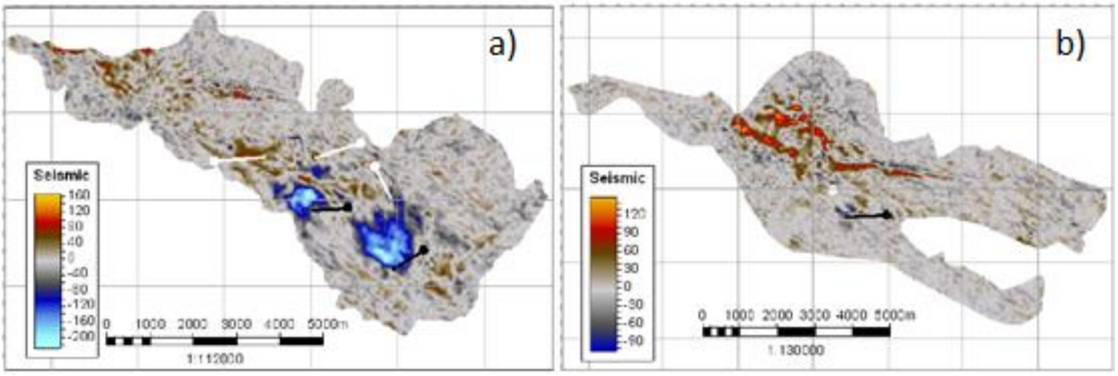

**Figure 2.3. 4D signal associated with water injection (negative anomalies): a) Block 6 of Marlim Sul field, b) 4D signal associated with gas anomalies (positive values), Block 4 of Marlim Sul field. After *Thedy et al, 2007*.**

Taking the difference of the two seismic volumes aims to amplify the production-related effects while attenuating signal due to lithology variations. This can only be achieved if the two surveys are as identical as possible everywhere except for the production affected areas. The similarity among the baseline and monitor surveys is called repeatability. Repeatability is a critical factor for a 4D study which determines how much information can ultimately be extracted from the 4D seismic data. Similarity of the geometries of surveys is a prerequisite of good repeatability (Figure 2.4), but repeatability also depends on many other factors. Usually the repeatability is measured by the normalized RMS difference of the surveys (NRMS):

$$NRMS = \frac{200\ \times RMS(a_t - b_t)}{RMS(a_t) + RMS(b_t)} \tag{2.7}$$

where $a_t$ and $b_t$ are seismic traces of the two surveys, *RMS* is root mean square taken within a time window. The repeatability of 4D seismic surveys has improved in the recent decade because of technological advances and improved design of surveys. If in early 2000s the typical NRMS values for the North Sea region were greater than 30%, the later surveys see values as low as 10-20%. The operators of Schiehallion field report repeatability noise to be as low as 7% (*Staples et al, 2006*).

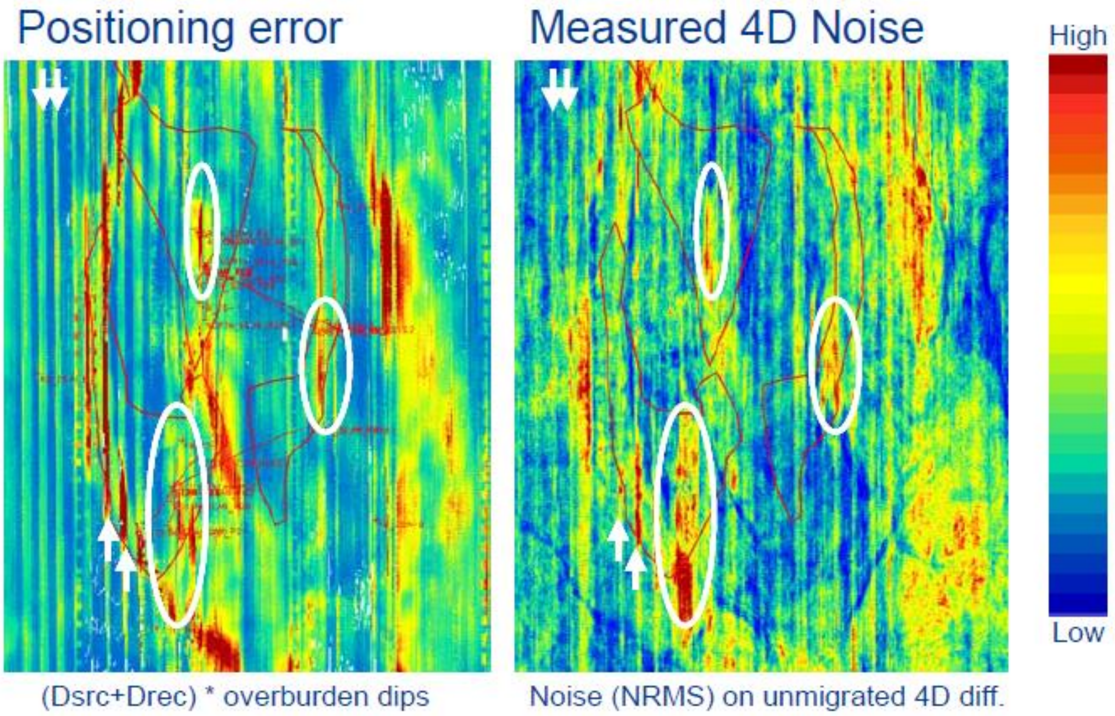

**Figure 2.4. Demonstration of the link between acquisition repeatability (steamer data) and 4D noise. After *Staples, 2006*.**

Another factor controlling the success of the 4D study is detectability of the production related effects. It is a function of the magnitude of pressure and saturation changes, sensitivity of seismic signal to those changes, and timing of surveys. Sensitivity of seismic signal to certain changes of pressure and saturation and also on the rock types is determined by the rock physics as described in the next section. Studying the expected magnitude of 4D signal in a given field for the planned development strategies constitutes 4D seismic feasibility study which helps establishing the economics of the 4D project.

### *2.4.1 Rock physics foundation of the 4D seismic method*

This section gives an overview of rock physics equations required for modelling 4D seismic effects while the values of the petro-elastic properties used in this work are given in sections 4.5 and 5.3.

Pressure and saturation changes due to production of hydrocarbons induce changes to the elastic properties of rocks that we are trying to detect using the 4D seismic method. The 4D signal is caused by changes in the reflectivity of rocks and changes in the seismic wave arrival times, that is time-shifts, which we will express in terms of velocities of seismic waves. The compressional and shear seismic wave velocities in homogeneous, isotropic, elastic media are given by

$$V_p = \sqrt{\frac{K + \frac{4}{3}\mu}{\rho}}, \quad V_s = \sqrt{\frac{\mu}{\rho}} \tag{2.8}$$

where $V_p$ is the P-wave velocity, $V_s$ is the S-wave velocity, $\rho$ is the density, $K$ is the bulk modulus, $\mu$ is the shear modulus. The bulk modulus K is defined as the ratio of the hydrostatic stress to the volumetric strain and measures the incompressibility of the media (liquid, gas or solid). The shear modulus, $\mu$, is defined as the ratio of shear stress to shear strain.

Reflection of seismic waves occurs at boundaries formed by impedance contrasts. The impedance, *I*, of an elastic medium is the ratio of the stress to the particle velocity. At a plane interface between two thick, homogeneous, isotropic, elastic layers, the normal incidence reflectivity for waves traveling from medium 1 to medium 2 is the ratio of the displacement amplitude, *Ar*, of the reflected wave to that of the incident wave, *Ai*, and is given by (*Mavko et al, 2009*)

$$r_{12} = \frac{Ar}{Ai} = \frac{I_2 - I_1}{I_2 + I_1} = \frac{\rho_2 V_2 - \rho_1 V_1}{\rho_2 V_2 + \rho_1 V_1}, \tag{2.9}$$

where subscripts 1 and 2 signify media 1 and 2 respectively.

*Saturation substitution*

4D seismic effect associated with saturation change, or fluid substitution, is caused by differences in the rock bulk moduli saturated by different fluids, whereas shear modulus is insensitive to fluids. This effect is encountered in such cases as water or gas injection, gas coming out of solution, or condensate dropping. However, the problem of fluid substitution originates not in 4D seismic, but arises as a more general problem of estimating seismic velocities of saturated rock using measurements on rocks saturated with different fluids in the rock physics analysis of cores, logs and seismic data. A common solution to the saturation substitution problem is given by the low-frequency Gassmann-Biot (*Gassmann, 1951; Biot, 1956*) theory. The Gassmann's equation predicts the bulk modulus of saturated rock through the values of bulk moduli of dry rock and the fluid:

$$\frac{K_{sat}}{K_0 - K_{sat}} = \frac{K_{dry}}{K_0 - K_{dry}} + \frac{K_f}{\varphi(K_0 - K_f)}, \qquad \mu_{sat} = \mu_{dry} \tag{2.10}$$

where $K_{dry}$ is the effective bulk modulus of dry rock, $K_{\mathrm{sat}}$ is the effective bulk modulus of the rock with pore fluid, $K_0$ is the bulk modulus of mineral material making up rock, $K_f$ is the effective bulk modulus of pore fluid, $\varphi$ is the porosity, $\mu_{dry}$ is the effective shear modulus of dry rock, and $\mu_{sat}$ is the effective shear modulus of rock with pore fluid.

Gassmann's equation is valid under the following assumptions (*Mavko et al, 2009*):

1) Frequencies of waves passing through the media are assumed low so that pore pressures are equilibrated throughout the pore space, i.e., there is sufficient time for the pore fluid to flow and eliminate wave-induced pore-pressure gradients. Seismic frequencies (10-100 Hz) generally are acceptable, while ultrasonic laboratory conditions will generally not be described well with Gassmann equation. Sonic-logging frequencies may or may not be within the range of validity, depending on the rock type and the fluid viscosity,
2) The rock is isotropic,
3) All minerals making up the rock have the same bulk and shear moduli (homogeneous mineral modulus),

4) Fluid-bearing rock is completely saturated with a fluid of constant bulk modulus.

Since the above equation assumes a single fluid saturating the rock, we will have to calculate an effective modulus for a mixture in general case. For the homogeneous mixing of fluids in the pore space, the bulk modulus of the mixture can be described by Reuss average (Wood's average, *Wood, 1955*) of bulk moduli of constituents:

$$\frac{1}{K_f} = \frac{S_w}{K_w} + \frac{S_o}{K_o} + \frac{S_g}{K_g}, \tag{2.11}$$

where $K_f$ is bulk modulus of mixture of fluids, $S_w$, $S_o$, and $S_g$ are saturations of water, oil and gas respectively, $K_w$, $K_o$, and $K_g$ are bulk moduli of water, oil and gas respectively.

*MacBeth and Stephen, 2008* note that better representation of this equation is possible where statistics of fine scale properties are known, but for the coarse model used here the above equation is accurate.

The density of the fluids mixture is calculated as a saturation-weighted average of individual densities:

$$\rho_f = S_w \rho_w + S_o \rho_o + S_g \rho_g \tag{2.12}$$

Figure 2.5 demonstrates application of Gassman's equation for prediction of the velocity of rock saturated with different fluids. Notably, for gas-water system, only a small amount of gas in the mixture results in dramatic decrease of velocity of rock. For normal oil-water systems, velocity increases with water saturation, and for heavy oils, velocity is almost insensitive to the water saturation change.

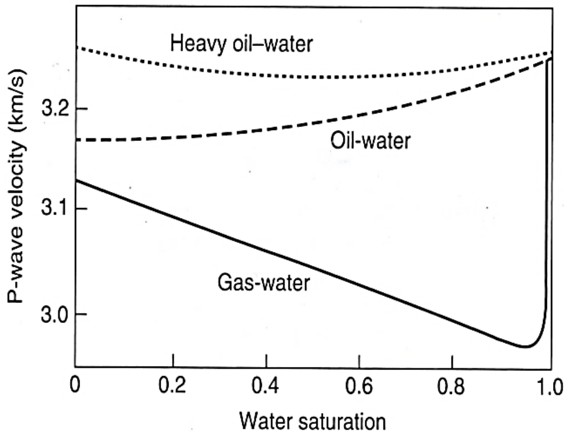

**Figure 2.5. Functions of P-velocity of saturated rock on water saturation for different mixtures of saturation fluids. *After Johnston, 2013.***

*Acoustic properties of fluids*

Seismic velocity and density of fluids are functions of pressure and temperature which are most commonly described by empirical relationships based on laboratory measurements. According to *Johnston, 2013*, the most popular empirical functions were derived by *Batzle and Wang, 1992*, *Han and Batzle, 2000*, and *Han et al, 2008*. Figure 2.6 and Figure 2.7 show the functions of velocity and density of oil and gas on pressure.

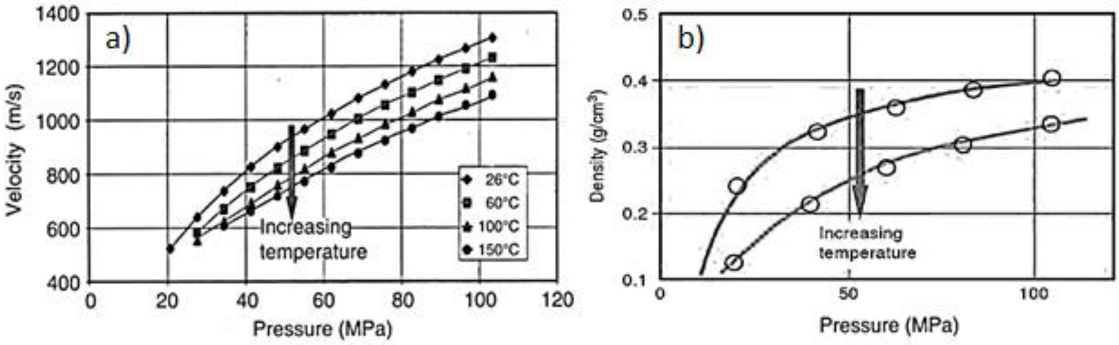

**Figure 2.6. Functions of gas acoustic velocity (a) and density (b) on pressure for different temperatures. After *Han and Batzle, 2000* as shown in *Johnston, 2013*.**

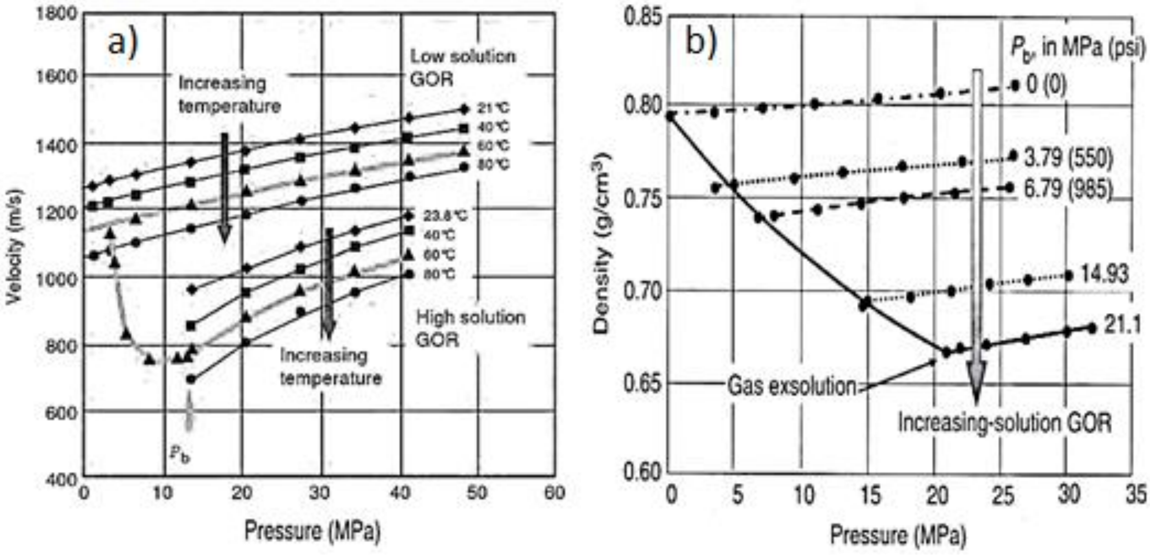

**Figure 2.7. Functions of oil acoustic velocity (a) and density (b) on pressure and temperature for different solution GORs. After *Han and Batzle, 2000* as shown in *Johnston, 2013*.**

While the character of gas functions is straightforward, the functions of oil are conditioned on the presence of dissolved gas as shown by the dissolved GOR factor on the plots. After the pressure is decreased below the bubble point, the velocity of oil rapidly increases as gas leaves the solution. Figure 2.8 shows the dependence of brine velocity and density on pressure, temperature and salinity. Pressure and salinity increase the brine’ velocity and density, but the temperature acts differently – velocity increases with temperature and density decreases.

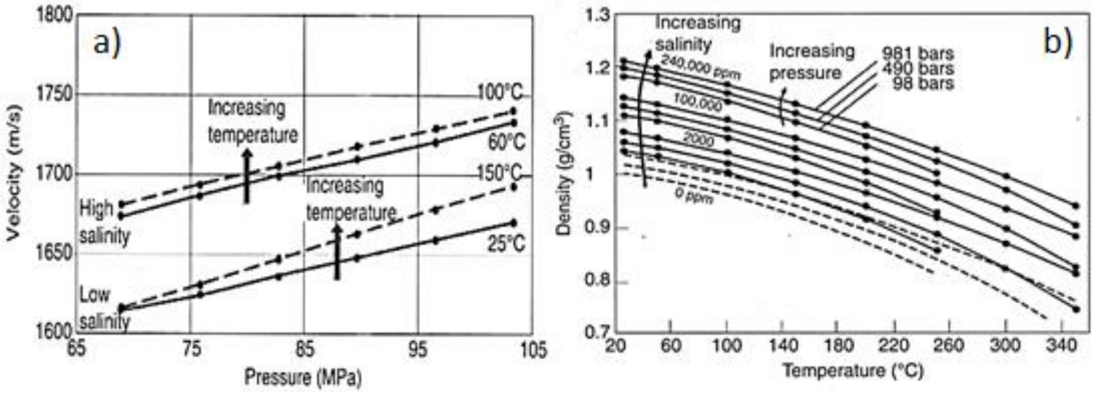

**Figure 2.8. Functions of brine velocity (a) and density (b) on pressure and temperature respectively for different salinity. After *Han and Batzle, 2000* as shown in *Johnston, 2013*.**

### *Effect of lithology and porosity*

The stiffer, more consolidated the rocks are, the less sensitive they are to the fluid saturation changes. Generally carbonates have stiffer rock frameworks and are less sensitive to saturation change than clastics, elastic properties of which are better understood *Johnston, 2013*.

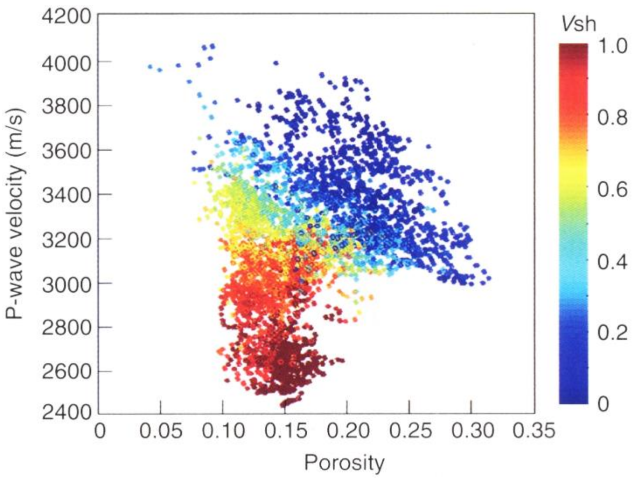

**Figure 2.9. Cross-plot of P-velocity and porosity well-log estimates of a North Sea reservoir. Colour scale is the volume of shale parameter. After *Johnston, 2013*.**

Figure 2.9 demonstrates dependence of P-velocity on porosity for different values of the volume of shale. For clean sands (blue points), velocity decreases with increasing porosity, while for high Vshale values (red points), porosity variation is limited. For this particular case, the clay content (indirectly indicated by Vshale) makes the velocity decrease.

*Pressure dependence of reservoir rocks*

Seismic velocities increase with increasing differential pressure. The differential pressure is defined as a difference between overburden (confining) pressure and pore pressure. Figure 2.10 shows results of different laboratory measurements of P-velocity of rock under varying differential pressure (*Johnston, 2013*) which demonstrate similar exponential character. It suggests different sensitivity of velocity depending on the direction of pressure change: it is more sensitive to an increase of pore pressure (differential pressure decrease) than to a pore pressure depletion. Also, overpressured reservoir will demonstrate high pressure sensitivity. A variant of an exponential rock bulk modulus function on pressure is used in this work.

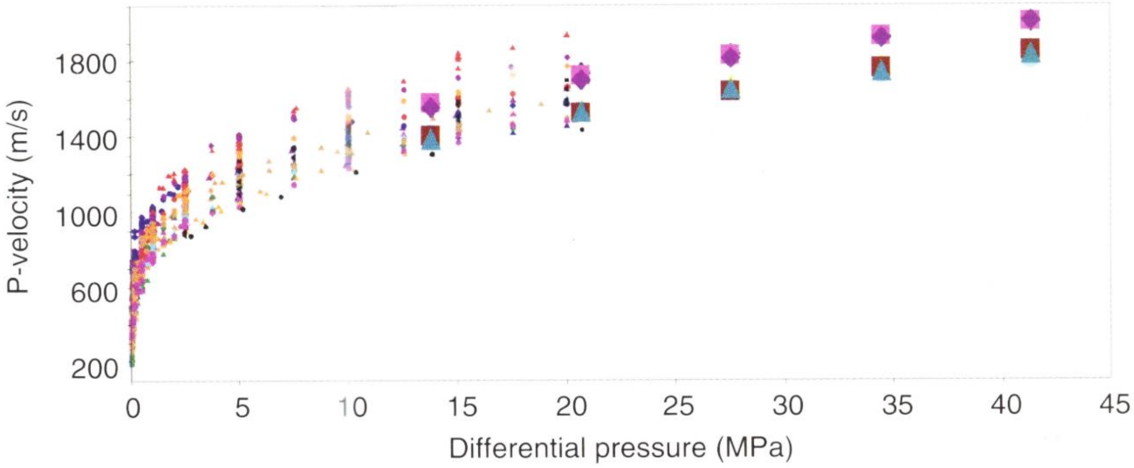

**Figure 2.10. Function of P-velocity of dry, unconsolidated sands on differential pressure from different experiments. After *Johnston, 2013*.**

## 2.5 Seismic modelling

Continuing the discussion of 4D seismic data for constraining simulation models, this section gives a brief overview of practical methods of seismic modelling. These methods were developed with the purpose of modelling single surveys rather than 4D differences of course, but today's view at predicting 4D signal is based on differencing modelled data of individual surveys as it happens with the observed data: surveys are acquired independently (different logic applies in seismic inversion though where individual surveys can be treated as parts of a response of the same system – the reservoir, and processed simultaneously therefore).

The objective of seismic modelling is to predict a seismogram that can be compared to the recorded seismic data in order to infer properties of the subsurface rocks. In the context of 4D seismic, the assumed changes in pressure and saturation will perturb our initial modelled seismogram which can be validated by comparing the synthetics to the observed data. Different methods of seismic modelling can be classified as direct methods, integral-equation methods and ray-tracing methods. For a detailed review of seismic modelling methods see *Carcione et al, 2002; Margrave and Manning, 2004; and Krebes, 2004*.

In the direct methods, the wave field is simulated directly by solving the wave equations on a grid covering the full geological model. For this reason, these methods are also called full wave equation methods. The solution for the wave field can be very accurate at the expense of computation time which can be a very significant factor. Examples of direct methods, in order of increasing accuracy, are finite-difference, pseudospectral, and finite-element methods. The drawback of the finite-difference method is that the solution is distorted by the numerical dispersion on the grid. In the pseudospectral method the problem is partly alleviated by using optimum number of samples per wavelength due to working in the wavenumber domain. In the finite-element method, the wave equation is solved exactly (rather than using finite-difference derivative approximations) in a number of finite regions.

The integral-equation methods originate from integral representation of wave field and are based on Huygens principle which states that the wave field can be represented as a superposition of wave fields from volume point sources or boundary point sources. These two representations are addressed by volume integral equations and boundary integral equations methods. These methods are more restrictive than the direct methods but perform well on models with small inclusions, cracks or fractures in them.

The ray-tracing, or asymptotic, methods do not model the full wave field and therefore greatly benefit from the resulting modelling speed up. Such methods are based on representation of a seismogram as a superposition of reflection events having different arrival times and different amplitudes which is achieved by using an approximate solution to the wave equation. The method is capable of modelling any style of geological sections and produces accurate results for arrival times. The drawbacks of the ray tracing method are that it is not accurate near critical offsets and near caustic zones (where rays converge or focus), does not resolve thin beds well because the method is a high frequency approximation assuming that the medium properties change slowly within dominant wavelength. This leads to difficulties in modelling diffractions and subsequent migration of the traces.

It is also possible to model the target reservoir or other area of interest more accurately while leaving the rest of the model, e.g. the overburden, for the faster methods. This is called hybrid modelling which can combine finite-difference method with faster algorithms such as ray tracing (*Lecomte, 1996; Hokstad et al, 1998; Gjøystdal et al, 2002*).

When calculation of the seismogram requires many iterations not only to cover the volume of the geological model but also to generate many realisations of such seismic cubes, the speed of seismic modelling may become the main factor. For example, in seismic inversion, many realisations of seismic traces are generated during the fitting to the observed data. A particular case of a more general inverse problem is seismic history matching of simulation models which involves frequent rebuilding of the seismic predictions. In these situation, a popular method for seismic modelling is the simplest 1D convolution method. This has been used for calculating synthetic seismograms since the 1950s mainly to tie synthetic seismogram in the well to the observed seismic using the density and sonic logs.

The method is based on a convolutional model which is derived from the Green's theorem stating that the seismogram is a convolution of a source waveform with the impulse response of Earth. The convolutional model is given by (*Yilmaz, 2001*):

$$x(t) = w(t) \otimes r(t) + n(t), \tag{2.13}$$

where $x(t)$ is the recorded seismogram, $w(t)$ is the basic seismic wavelet, $r(t)$ is the Earth's impulse response, $n(t)$ is the random ambient noise, $\otimes$ denotes convolution operator. The random noise in the equation originates from instrumental errors of the recorders, poor geophone coupling, environmental noises. A convolutional model of a seismogram with noise is illustrated in Figure 2.11.

1D convolution method assumes that that the earth is horizontally layered locally, and does not include multiples, converted waves, and attenuation effects, although, it offers excellent level of details in z direction (*Margrave and Manning, 2004*). This is why direct comparisons between 1D convolution and more precise methods such as finite-difference method indicate that the former lacks lateral coherency and horizontal resolution but provides good amplitude information (Figure 2.12, Figure 2.13). At the same time, modelling of the waterfloods shows that the internal multiples in the flooded zones partially subtract out making them less significant for the monitoring projects than for reservoir characterisation (*Shahin et el, 2011*). 1D convolution modelling has been widely used for conditioning simulation models (see for example *Landa and Kumar, 2011*), predicting time-lapse seismic effects from $CO_2$ sequestration (*Arts et al, 2007; Li et al, 2013*), monitoring steam chamber growth (*Lerat et al, 2010*), and so far, is the most popular seismic forward modelling method in closed-loop reservoir model updating workflows.

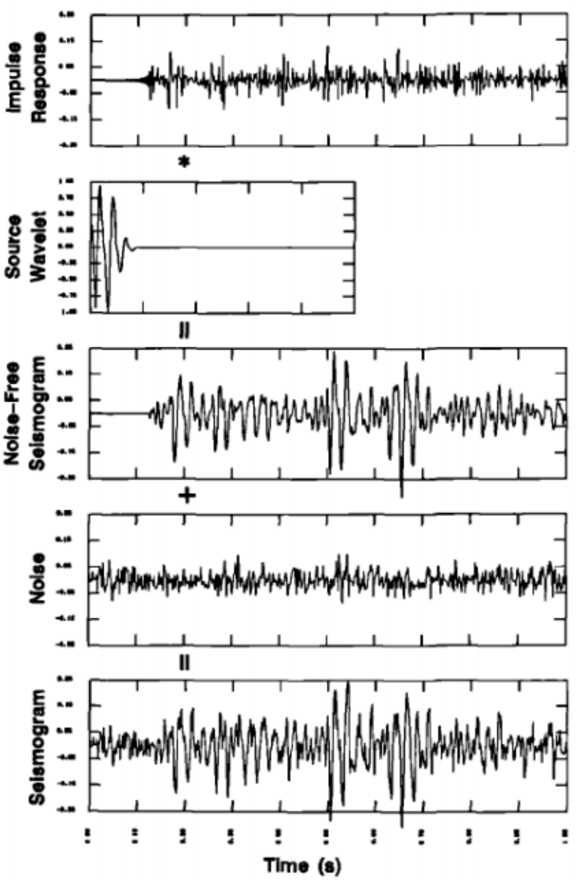

**Figure 2.11. Convolutional model of a seismogram. Asterisks denotes convolution operator. After *Yilmaz, 2001*.**

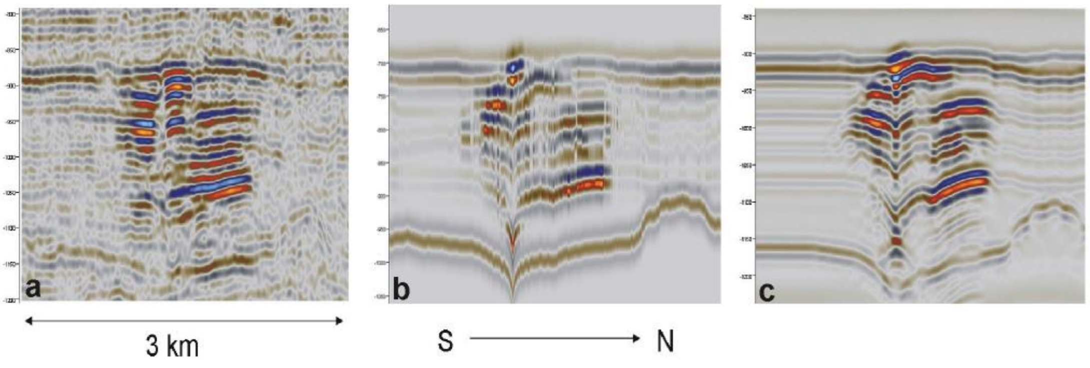

**Figure 2.12. Comparison between observed seismic (a), synthetic by 1D convolution method (b), 2D elastic modelling and processing (c) for the Sleipner $CO_2$ injection project. 4D seismic monitoring aims to image $CO_2$ plume at it migrates in the reservoir. Observed data shows a prominent multi-tier signature, comprising a number of bright sub-horizontal reflections, growing with time, interpreted as arising from up to nine discrete layers of high saturation $CO_2$, each up to a few metres thick. Modelled 4D images show good agreement with the observed data on the main target features. After *Arts et al, 2007*.**

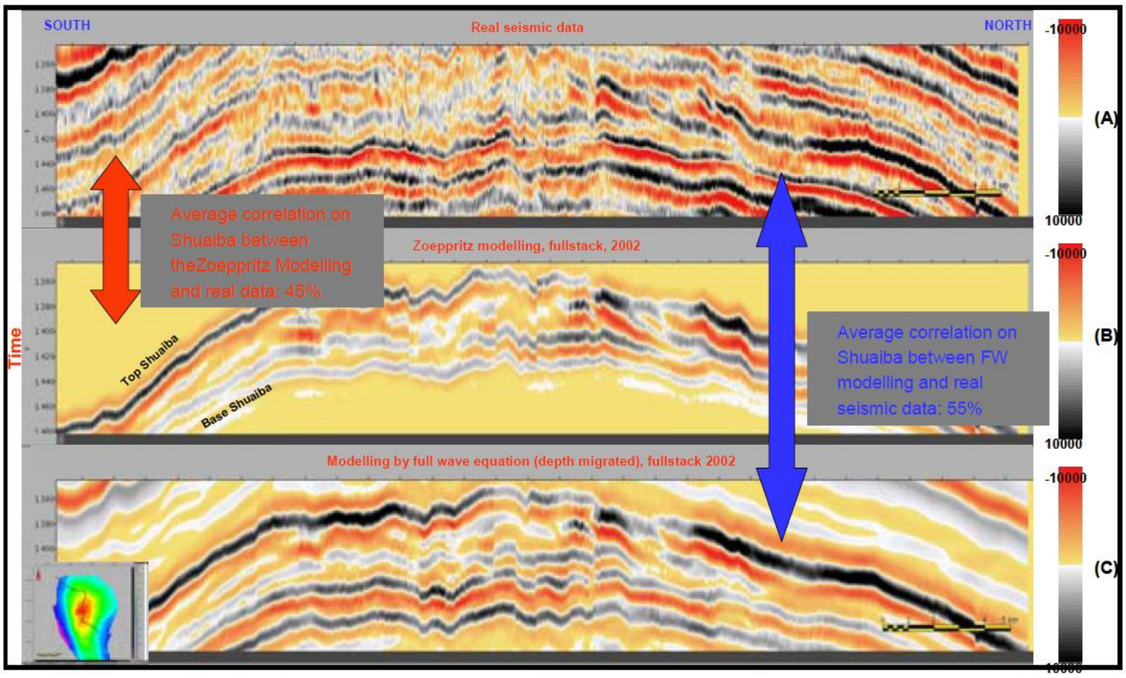

**Figure 2.13. Comparison between real seismic data (A), synthetic by 1D convolution method (B) and by full wave equation (C) for Shuaiba reservoir, Bu Hasa carbonate field. 4D feasibility study of this carbonate reservoir shows applicability of the method for monitoring injection in this reservoir. Results of 1D convolution and full wave equation modelling mostly agree except for some details related to the peripheral water injection areas. After *Marvillet et al, 2007.***

## 2.6 Seismic inversion

This section provides an explanation for the inversion concept and gives a brief overview of different types of the method. Inversion is used in this work for obtaining properties of synthetic models based on data only, thus minimizing input of deterministic information. In particular, history matched models have their NTG properties obtained by inversion rather than copied from the reference (a model providing ‘observed’ seismic response) model. Also, the seismic attribute used for comparing predicted and observed data is a product of the coloured inversion also described in this section.

The objective of seismic inversion in general is estimation of rock properties in the Earth’s model from seismic data in conjunction with other data types, mainly sonic and density well logs. In the traditional problem setting the estimated properties can be relative impedance, acoustic impedance, or compressional and shear velocities and density of rocks, but in general any model property can be varied while fitting the seismic data. Traditionally, the concept of seismic inversion includes different types of the process in terms of the algorithm and data used. For a classification and review of inversion methods see *Cooke and Cant, 2010* and *Curia, 2009*. Inversion can be pre-stack or post-stack depending on the input seismic data. Inversion algorithms that yield a single solution are called deterministic, while the ones searching through many realisations of the input model are called stochastic. Stochastic inversion algorithms that also compute probabilities of the models are called probabilistic. Geostatistical stochastic inversion methods impose variograms on the input models to ensure the desired spatial patterns and statistics in the solutions. Most of the inversion algorithms use seismic forward modelling (usually the convolutional model) in order to compare the model's seismic response with the observed seismic data and determine the goodness of the model. Such inversion algorithms therefore are called model-based, as opposed to the algorithms that calculate the output directly from the seismic trace, such as integration of seismic traces (recursive method) or coloured inversion. If an inversion algorithm finds the solution in the form of absolute properties then the inversion is called broad-band, whereas in the band-limited inversion the solution is relative properties (for example, relative impedance). Different inversion approaches are briefly described below.

### 2.6.1 Trace integration, or recursive, method

The simplest method of inverting seismic data for an estimate of acoustic impedance is based on a recursive calculation as shown below *(Lindseth, 1979)*:

$$r_i = \frac{I_{i+1} - I_i}{I_{i+1} + I_i} \ => I_{i+1} = I_i \frac{1 + r_i}{1 - r_i} \ => \ I_n = I_1 \prod_{i=1}^{n-1} \frac{1 + r_i}{1 - r_i} \ , \tag{2.14}$$

where $r_i$ is the reflection coefficient at the $i$-th interface with P-Impdance $I_i$.

This method assumes that the reflection coefficient can be expressed with the formula for the wave normal incidence as above, and that the seismic trace is given by a convolutional model (given in the seismic modelling section above), so the reflection coefficients can be obtained from the seismic trace by deconvolution. This calculation yields only a band-limited version of impedance because only band-limited version of the reflectivities $r$ is available in the seismic trace. The low frequency component should be extracted from well logs and added to the inversion results. An example of the recursive inversion is shown in Figure 2.14 where it is compared with an inversion

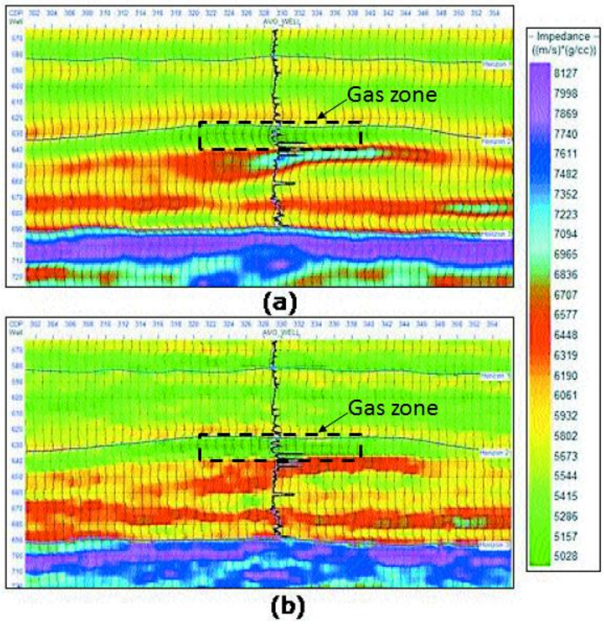

**Figure 2.14. Comparison of inversion results by the recursive method (a) and by the model-based method (b), a seismic section from Alberta. After *Russel and Hampson, 2006***

results by the model-based algorithm. A notable difference is that the model-based inversion results are blockier, with finer details. At the same time, the low impedance gas sand zone is resolved in both sections (marked by black rectangles in Figure 2.14).

### *2.6.2 Coloured inversion*

Another band-limited method is called 'coloured' inversion by (*Lancaster and Whitcombe, 2000*). It is based on mapping of the seismic average spectrum to that of the acoustic impedance logs and performing a -90° constant phase shift. This is achieved by convolving all the traces in the input seismic cube with a specifically designed (antisymmetric) filter. Because the method is based on a simple convolution, it is robust, straightforward to implement, and computationally fast.

*Walden and Hosken (1985)* (as stated in *Lancaster and Whitcombe, 2000*) found that the amplitude spectrum, $r(f)$, of reflectivity coefficients can be described as a function of the frequency $f$ as $r(f)=f^{\beta}$, with a parameter β. The authors found that the parameter β is very stable over a given field or even many fields. *Lancaster and Whitcombe. 2000* observed that the amplitude spectrum of the acoustic impedance shows similar behaviour which can be described as an equivalent function: $I(f)=f^{\alpha}$, where $\alpha$ now is negative. The parameter $\alpha$ gives a slope of the function in semi-log coordinates (Figure 2.15) which is found by analysing well logs of a given field (the resulting $\alpha$ very often will be around -0.85). The next step is designing a filter which, on applying to the input seismic, will map the average spectrum of seismic to the one with a slope $\alpha$ in semi-log coordinates. Moreover, the filter has to perform a -90° constant phase shift which is achieved by making the filter antisymmetric. Results of coloured inversion demonstrate a reasonable match to the results of a more elaborate sparse-spike inversion as shown in

Figure 2.16. The method can be used as an approximate method for obtaining fast-track estimates of relative impedance (*Curia, 2009*).

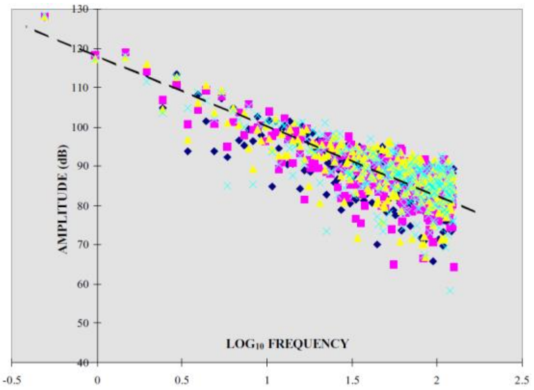

**Figure 2.15. Acoustic impedance amplitude spectra from four logs for a North Sea field. Frequency axis is logarithmic in order to fit the points with a line. After *Lancaster and Whitcombe. 2000***

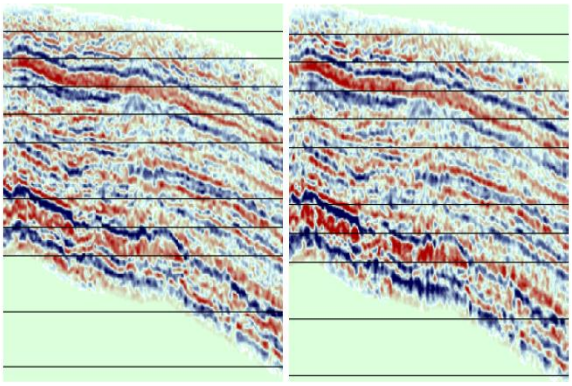

**Figure 2.16. Comparison of results of sparse-spike inversion (left) and coloured inversion (right) on a North Sea field. After *Lancaster and Whitcombe. 2000***

### *2.6.3 Deterministic inversion*

One of the most popular deterministic methods is the sparse spike inversion. In this method, a solution for the inverse problem is found as an Earth's model displaying minimum of structural variation. Such a model would pick up only the major features in the acoustic impedance structure. This concept was formulated by *Oldenburgh et al, 1983* as a linear-programming problem which minimizes the objective function

$$J = \sum_{i=0}^{N-1} |r_i|, \tag{2.15}$$

subject to inequality constraints on analytical expression of real and imaginary parts of the spectrum of reflectivities $r_i$ with added noise, and constraints on the impedance values. The concept of the inversion for the smoothest possible model consistent with the data corresponds to the Occam's inversion which relies only on the information available from the data itself (*Gouveia and Scales, 1997*). This contrasts with other model-based inversion methods where the solution is found in one of the defined forms such as blocky impedance. The latter imposes information that is not supported by the (seismic) data being inverted but reflects our prior knowledge.

The sparse-spike method will not reproduce finer details in a model as follows from its formulation, but it will produce unbiased estimate of the band-limited (relative) impedance. Unbiased means that no subjective model is used, and the band-limited aspect is in that it lacks the low frequency component which should be added separately from the well logs. The high frequency component is present in the inverted data though, it comes from the form in which the solution is found – a series of spikes or equivalently, blocky impedance.

The blocky impedance is the usual model for the model-based inversion methods which is based on our assumption of the Earth's layered structure. To clarify, this is not an assumption that the geology is "blocky" but rather an assumption that discontinuities are part of it with the blocky structure (piecewise constant function) being the simplest model. An example of an alternative form of impedance distribution is shown in Figure 2.17. Specific form of the impedance solution (blocky, controlled by local trends, smooth, etc.) is the information that we supply to the inversion algorithm to complement the solution in the high frequency part of the spectrum which is not covered by the seismic data. It means that the two impedance models in Figure 2.17 may have the same seismic response as they are only different in the high frequencies. But even if the blocky structure assumption is correct (which is true in most cases), the absence of high frequencies in the seismic data leads to infinite number of different solutions for impedance/thickness of thin layers as shown in Figure 2.18 – two different impedance models have similar seismic response with the same RMS amplitude value.

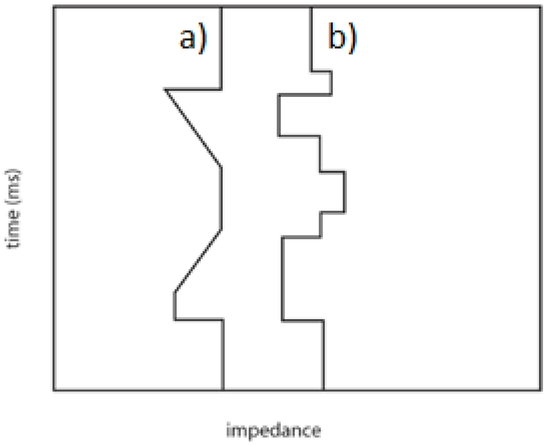

**Figure 2.17. Two representations of the impedance model: a) non-blocky, b) blocky. After Cooke and Cant, 2010.**

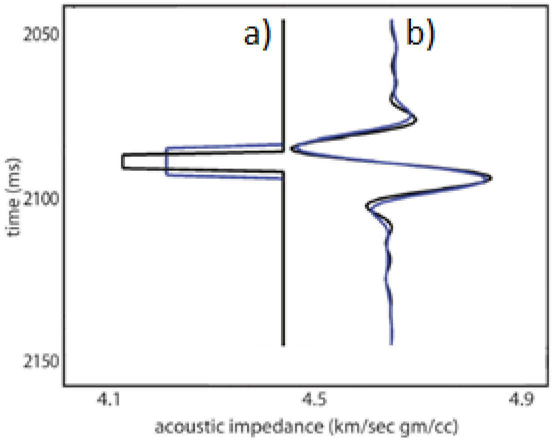

**Figure 2.18. Two different impedance models in (a) produce similar seismic response (b). After *Cooke and Cant, 2010*.**

Another popular method of deterministic inversion is the generalised linear inversion (*Cooke and Schneider, 1983*). It is used to invert both pre- and post-stack data. With an input impedance model as a first guess, the algorithm performs a number of refinements to finally match the data. The impedance model for the inversion is divided into a number of layers, where the impedance and thickness values of each layer are the parameters of the inverse problem. The updates to the parameters at each iteration are calculated from the truncated Taylor series expansion of the forward model.

### *2.6.4 Stochastic inversion*

The stochastic inversion algorithms search through many realisations of the input models and keep those that (through the forward modelling) match the observed data. The input distributions of $V_p$, $V_s$ and ρ (although the last two can be set as functions of $V_p$) are built by analysing well data where average $V_p$ trend and its standard deviation are defined. A technique like the Markov Chain Monte Carlo (MCMC) sampling can be employed to ensure adequate sampling of the input distributions of the models. The realisations are assigned probabilities using the Bayes' theorem (*Pendrel, 2006*).

Figure 2.19 compares the results of the deterministic and probabilistic inversions. The arrows indicate gas reservoirs. For the upper reservoir, the results of the inversions are very similar while the lower reservoir is resolved differently by the two inversions. This difference in the results can be attributed to the different treatment of the low frequency input (*Cooke and Cant, 2010*): the deterministic inversion uses a trend of impedance from the wells, while the probabilistic inversion is fed by distributions of input properties without explicitly specifying the low frequency trend. Another source of the differences is the number of layers – the stochastic inversion uses finer parameterisation.

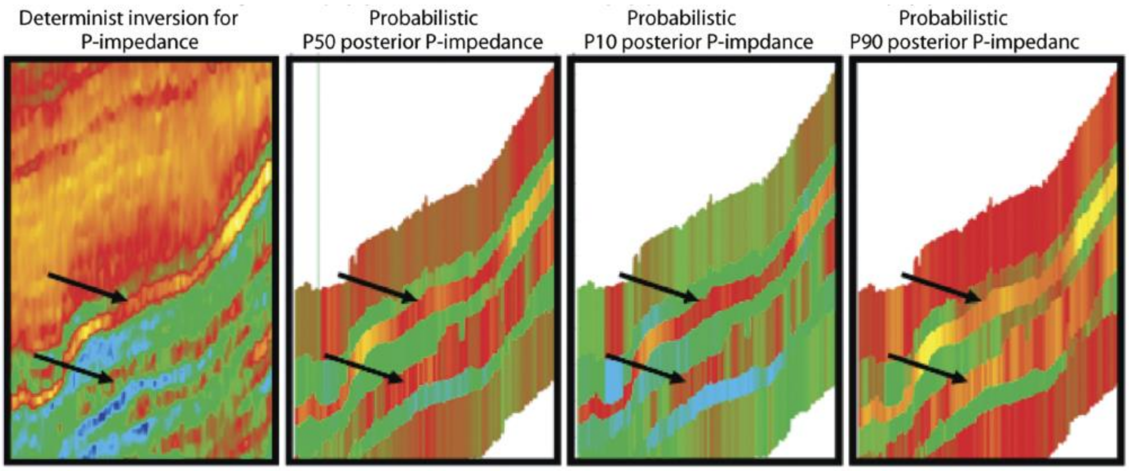

**Figure 2.19. Comparison of P-impedance estimates using the deterministic inversion and P50, P10, P90 solutions of the probabilistic method. After *Cooke and Cant, 2010*.**

# Chapter 3. Using 4D seismic data to constrain reservoir models: a literature review

## 3.1 Introduction

The main goal of this chapter is to review the applications of 4D seismic data to constraining simulation models in history matching. Specifically, how choices of optimization algorithm, parameterisation, and data types affect the process itself and the quality of resulting models. This review does not aim to embrace the variety of methods and case studies but rather aims to give a higher level image of the notable views on the process of integrating 4D seismic data in the literature. The definition of the 4D seismic method itself, physics that cause 4D effects, and constituents of the history matching mechanism are described in the theory chapter.

## 3.2 4D seismic method as a reservoir management tool

4D seismic method has been an efficient reservoir management tool because of its extra spatial resolution compared to the well measurements. The better understanding of flow patterns in the inter-well space has given the operators confidence in business decisions: drilling new wells (Norne field, *El Ouair et al, 2005*), optimising infill wells placement (Heidrun field, *Kolsto et al, 2008*), repositioning planned wells (Marlim field, *Oliveira 2008*), revising the water injection strategy, converting producer into injector, drilling new appraisal wells (Draugen field, *Mikkelsen et al, 2008*).

Generally, the additional spatial information provided by 4D seismic data helps better constraining the reservoir models which then produce more reliable predictions of well rates and recoveries reducing uncertainties in field's economic forecasts. The constraining of reservoir models is implemented at different levels: constraining geological models, constraining predictions of simulation models, qualitatively and quantitatively. *Andersen et al, 2006* present an example of constraining the geological model realisations to the combined 3D and 4D seismic and well data. The model represents fluvial reservoirs of the Oseberg field (North Sea). $I_p$ and $V_p/V_s$ (inverted) properties from 3D seismic data were used to define regions of different confidence of sand (Figure 3.1, a). 4D variation of the same (inverted) properties was used to distinguish pressure and saturation effects (Figure 3.1, b). From that, highest probability of sand was assigned to the gas flooding areas. Combining interpretations of 3D and 4D attributes led to a sand probability cube – basis for geostatistical realisations of the geological model (Figure 3.1, c).

Another level of integration of 4D seismic is constraining predictions of simulation models, also referred to as seismic history matching. This is of primary interest in our study. 4D seismic data in history matching can be used qualitatively and quantitatively. Qualitative use of 4D seismic data is demonstrated by *Seldal et al, 2009* in a history matching study of Snorre field. The Snorre reservoir consists of highly heterogeneous and faulted stratified fluvial deposits, and is depleted using the water alternating gas scheme. These factors result in complex drainage patterns. Volumetric geobodies are extracted from 4D seismic data which represent two types of seismic signal: hardening mainly due to the water saturation increase (dimming effect), and softening mainly due to the gas saturation increase (brightening effect).

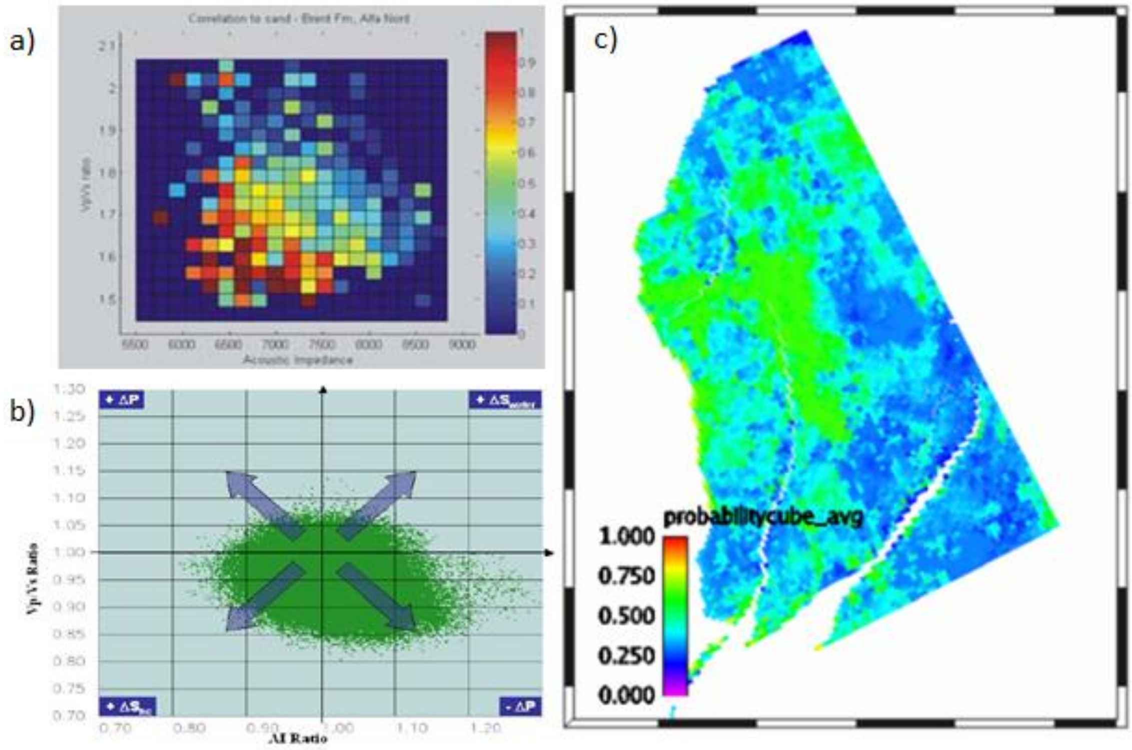

**Figure 3.1. Identification of sands based on combined interpretation of 3D and 4D seismic data: a) probability of sand based on $I_p$ and $V_p/V_s$ attributes of 3D seismic, b) classification of production effects based on (inverted) 4D seismic attributes where gas flood areas are more sandy, and c) the sand probability cube combining the previous two interpretations. After *Andersen et al, 2006*.**

Figure 3.2 illustrates how 4D seismic attributes were used in the history matching workflow in one of the regions of the model. In this example, information is gained from the extent of water encroachment zone shown as a blue geobody in Figure 3.2, a. Its interpretation led to placing the fault A and adjusting transmissibilities of the faults around the two producers which resulted in a good match of water cut in well P-8 (Figure 3.2, b).

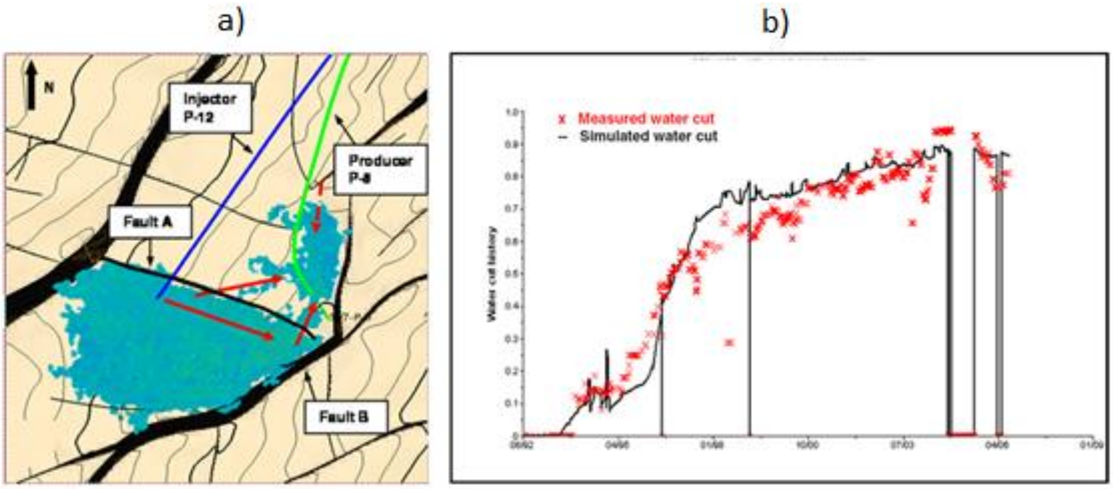

**Figure 3.2. Constraining the simulation model of Snorre field by 4D seismic attributes: a) 4D volumetric attribute (blue geobody) showing water encroachment, b) well P-8 water cut match. After *Seldal et al, 2009*.**

The above example shows a typical qualitative use of 4D seismic attributes. In such cases, indications by the 4D seismic attributes add to the conceptual understanding of flow patterns, and the simulation model is adjusted accordingly. In the rest of the chapter, we will discuss the quantitative use of 4D seismic data within history matching workflows. Using 4D seismic data quantitatively means reading not only the presence and the extent of seismic attributes but also the strength of the signal. It allows calibrating reservoir models to the observed seismic data via seismic modelling which puts results of reservoir simulation to the common domain with seismic data. Also, when comparison of predicted and observed data is formalised in an objective function, we can employ various optimization algorithms in order to automate the process of history matching.

### 3.3 Seismic history matching workflow

Qualitative use of 4D seismic data usually is associated with manual history matching. Although it is possible to use quantitative readings of 4D attributes match quality to perform manual adjustments to the simulation model, the quantitative use of seismic data most often is a part of an iterative process of updating the simulation model, automated to different extents. An example of such history matching loop is illustrated in Figure 3.3. The definitions of different parts of the workflow are given in the theory chapter, while in this review, we will study examples of applications in the published case studies.

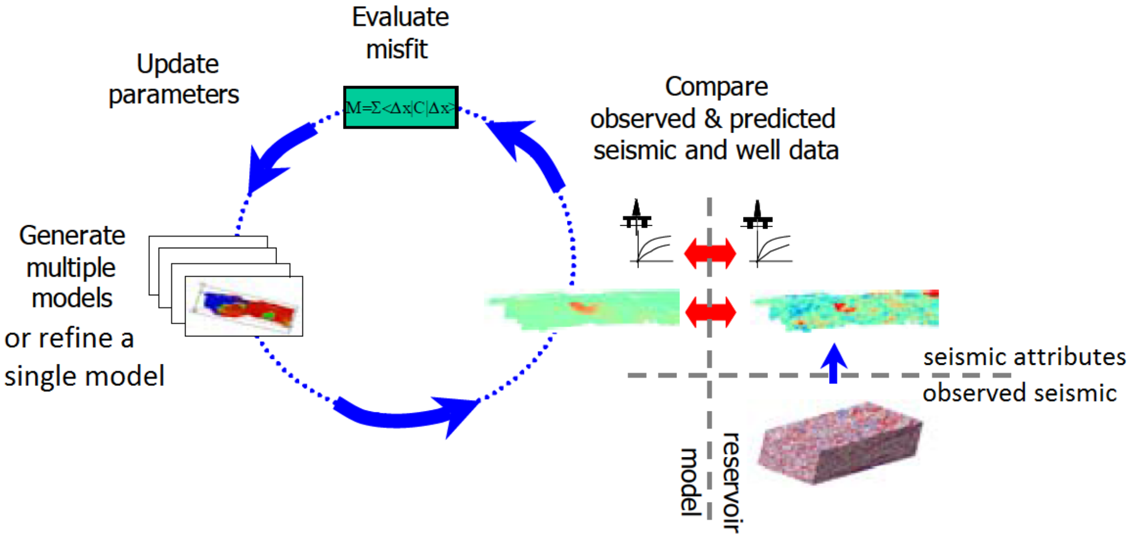

**Figure 3.3. History matching workflow. After *Stephen et al, 2006***

### 3.3.1 *Optimization algorithm*

The decision on updating the model parameters can be based purely on human judgement of goodness of a model which is the manual history matching as discussed before. An alternative approach is the automatic (assisted) history matching in which an optimization algorithm is employed to search for parameter values minimizing the objective function. The algorithms can be divided into two categories: deterministic and stochastic.

*Deterministic algorithms*

Deterministic, mostly gradient, algorithms have been used since the first publications on seismic history matching (*Landa and Horne, 1997; Waggoner et al, 2002; Gosselin et al, 2003; El Ouair et al, 2005; Dadashpour et al, 2007; Dong and Oliver, 2008; Brito et al, 2010; Tillier et al, 2011*). The choice of these algorithms is dictated by faster convergence rates compared to the stochastic algorithms when minimizing the objective function in the history matching problems. *Waggoner et al, 2002* applied the (deterministic) greedy algorithm in history matching of the Grand Isle field model with the retrograde gas reservoir. 1728 parameters were estimated which were values of porosity and permeability in each column of grid cells.

Gradient methods are suitable for minimizing non-linear objective functions occurring in history matching problems and differ in the rates of convergence and memory requirements. Gauss-Newton method is characterised by very fast convergence requiring only few iterations. At the same time, memory requirements of the method make it impractical for problems with large amounts of data and many parameters which is usually the case. *Landa and Horne, 1997* used Gauss-Newton algorithm for their synthetic history matching problem where 4D seismic data was included in the form of water saturation maps. The choice of the algorithm is explained by the need to obtain data sensitivities explicitly. Synthetic studies by *Dadashpour et al, 2007* and *Dickstein et al, 2010* also used the Gauss-Newton algorithm for history matching with 4D seismic data. In both cases, simple models were used. The Levenberg-Marquardt algorithm improves on the previous method by better approximation of the Hessian which leads to faster convergence. In the work by *Gosselin et al, 2003*, the objective function including inverted 4D seismic attributes was minimized using the Levenberg-Marquardt algorithm. The demonstration cases included Oseberg Amelia fields, where the parameters were pore volume and transmissibility multipliers (63 and 55 parameters in the two cases respectively). Quasi-Newton methods such as the conjugate-gradient method do not calculate or store the second order derivate matrix (the Hessian) but only use the gradient. This leads to slower convergence rates but opens up possibilities for using the method for large history matching problems. *Zhang and Reynolds, 2002* compared several optimization algorithms on history matching problems and concluded that the quasi-Newton methods were the most suitable of all gradient methods for history matching problems with big volumes of data and detailed parameterisations. Due to the better memory handling, the quasi-Newton algorithm allowed *Dong and Oliver, 2005* to incorporate 4D seismic data in the objective function which as the authors point out would not be possible with Gauss-Newton.

Although the gradient algorithms can be considered as methods of finding local minima by definition, *Zhang et al, 2003* and *Oliver and Chen, 2011* argue that this may not be a problem for their applicability in real world history matching problems. Finite steps calculated by an algorithm such as the Levenberg-Marquardt algorithm often pass local minima especially those located in narrow valleys as shown in Figure 3.4 so that the algorithm converges to an acceptable minimum near the global minimum. In other words, the algorithm in practice demonstrates the characteristic of a 'broader' search as opposed to the "deep" search as specified by the definition of the gradient algorithms.

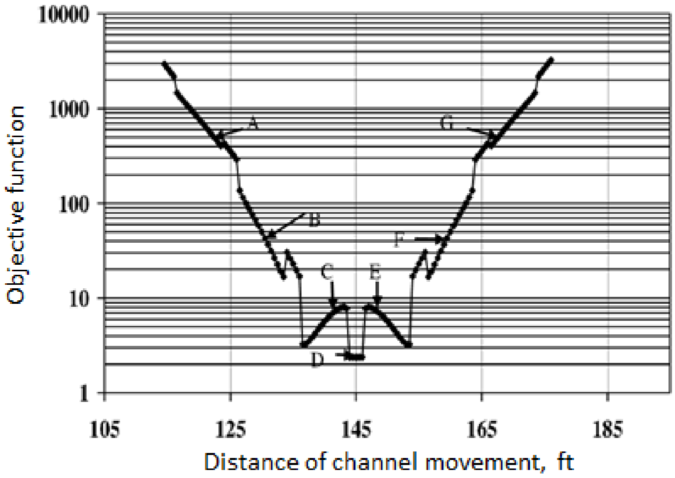

**Figure 3.4. Objective function for a problem of history matching with moving channel. After *Zhang et al, 2003***

*Oliver and Chen, 2011* demonstrate an experiment where an objective function with a highly complex shape is minimized with the Levenberg-Marquardt algorithm and the initial guess of parameters is generated randomly for each realisation of the history matched model. The outcome of the experiment is that 50% of solutions were found around the global minimum, while for the other 50%, it is clear that they have to be discarded (Figure 3.5). The author explains such a good performance by the rapid convergence and the fact that local minima are connected in higher dimensional space.

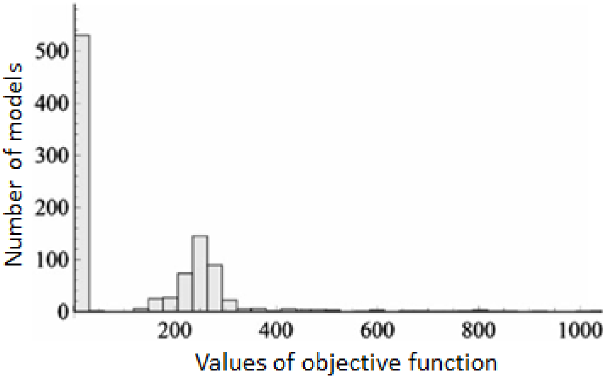

**Figure 3.5. Frequency distribution of values of the objective function for history matched models with different initial guess of parameters. Values around zero correspond to the global minimum, cluster of large values are incorrect local minima. After *Oliver and Chen, 2011***

### *Calculation of sensitivities*

Methods discussed so far require calculating data sensitivities which can be a significant addition to the complexity of the entire history matching problem because of its computational expense. The sensitivities represent partial derivatives of simulated data with respect to model variables. Several methods exist for calculating sensitivities. In the most basic finite-difference method, one function evaluation (forward model) is required per model parameter to explicitly calculate the partial derivatives. This can only be practical for problems with very few parameters. Calculation of sensitivities is faster in the sensitivity equation (or gradient simulator) method (*Anterion et al, 1989 –* first in petroleum engineering*; Bissell, 1994; Rodrigues, 2006; Oliver et al, 2008*). In this method, a preliminary solution is obtained for the state variables of the model by solving a non-linear equation once. With this solution, the system of equations for sensitivity coefficients becomes linear. It has to be solved as many times as there are variables, but the cost of solution to another variable is small.

Far more efficient for calculating the sensitivities is the adjoint (or optimal control) method in which the sensitivities are derived directly from the finite-difference equations of the forward model (*Chen et al, 1974, Chavent et al, 1975*). In this method, the number of linear system solutions is independent of the number of model variables. For this reason the method is suitable for history matching problems with large numbers of parameters. *Wu et al, 1999* applied the adjoint method to conditioning the geostatistical realisations of permeabilities and porosities to well water-cut and pressure data for a two-phase flow problem using the Gauss-Newton algorithm. *Eydinov et al, 2008* applied the method for history matching using their in-house compositional reservoir simulator and showed applicability of the method for the cases with anisotropic permeability fields, multipoint flux approximation, and arbitrary fluid compositions.

Another approach to calculating sensitivities uses the streamline simulator which allows obtaining the sensitivities analytically with only one forward simulation instead of multiple adjoint solutions. *Vasco et al, 2003* applied the streamline simulation in history matching of 4D amplitudes in a synthetic model and also in a model of Bay Marchand field (GoM). An analytical form of sensitivities was derived connecting amplitude changes with variation of porosity and permeability using an expression for travel time of water front along a streamline, an approach borrowed from the high frequency approximation in seismic wave theory. The resolution of the method was limited though to the area along the streamline trajectory and also to the features covered by the water front. It is a critical requirement of the streamline sensitivity formulation that the geometry of streamlines do not vary significantly over 4D seismic survey intervals. This imposes a considerable limitation on the applicability of the method as the flow regime normally changes between the surveys due to the varying well operations as well as changing pressure-saturation state. In a more recent work by *Rey et al, 2012*, this limitation is circumvented by using a recursive formulation of 4D seismic attribute sensitivity to the values of geological property (permeability field). The application of the method includes the synthetic Brugge example as well as Norne field model where more plausible distributions of water saturation were achieved. The saturation-only formulation of sensitivities in the work by *Rey et al, 2012* was extended to include the pressure effect in another work by *Watanabe et al, 2013*. The pressure effect is calculated by distributing the viscous pressure drop along each streamline using the pressure field and the flowing bottom-hole pressure of the well in which the streamline terminates.

*Stochastic algorithms*

Stochastic algorithms operate with random variables in their search process. The randomness added to the model parameters helps overcome noise in the observed data. It also helps to minimize the effect of modelling error (*Hoos and Stützle, 2004*). By their design, stochastic algorithms are capable of avoiding local minima and finding the global minimum. Direct comparisons of stochastic and deterministic algorithms are scarce in the literature. *Liberti and Kucherenko, 2005* compared the deterministic and stochastic approaches using an extensive suite of general-purpose tests and concluded that in general, the stochastic algorithm was more efficient in finding the global minimum but in some cases the deterministic algorithm was faster which was related to the structure of the problem. Similar conclusion was drawn in an analysis by *Wetter and Wright, 2004*. In an optimization problem in the field of building design, they compared gradient and stochastic (PSO and others) algorithms and found that the stochastic algorithms better suited the problems with non-smooth objective functions. The drawback of the stochastic algorithms though is slower convergence rates compared to the gradient algorithms. Stochastic algorithms generate multiple random model realisations to evaluate the shape of the objective function and identify its minimum. Such sampling becomes less efficient with increasing dimensionality of the problem so more simulations are needed. Therefore, the number of model parameters estimated by stochastic algorithms usually is smaller than in the gradient-based optimization. Slow convergence rate of the stochastic algorithms was among the reasons why gradient methods prevailed historically in automatic history matching studies in petroleum engineering. However, growing popularity of geostatistical models since 1990s (*Oliver and Chen, 2011*) and using new data types such as 4D seismic data led to the problems with more complex objective functions for which the stochastic algorithms can be more suitable. Also, the stochastic algorithms better adapt the “black box” notion for the forward model which can include very ill-posed functions while the deterministic algorithms usually assume at least some analytical properties of the objective function (*Liberti and Kucherenko, 2005*). On the other hand, the efficiency of the gradient methods is limited when the adjoint method for calculating gradients can not be applied. This is the case when the adjoint calculation is not included in the commercial reservoir simulators on which the industry depend, or when the adjoint system can not be easily derived from the forward model equations.

These factors most likely affected the growing interest for the stochastic methods within history matching studies in petroleum engineering in the last 20 years. Genetic and evolutionary algorithms were among the first examples to be used in this capacity (*Romero and Carter, 2001*). These algorithms were noted to have slower convergence rates (*Schulze-Riegert et al, 2002*). *Kjelstadli et al, 2005* applied the genetic algorithm in history matching study of a rather unusual for its compaction effects Valhall field. 60 parameters such as porosity and permeability were estimated by matching production and 4D seismic data. *Roggero et al, 2007,* although using the gradient-based methods for matching the production data, point out that applying a method based on response surface would be difficult because of large number of data points in 4D seismic data. The authors also mention the risk of being trapped in a local minimum with a gradient-based algorithm. As a result, they used a variant of the global adaptive learning algorithm for fitting the seismic part of the data. *Stephen et al, 2006* estimated permeability values at pilot-point locations and faults transmissibilities in the Schiehallion field (North Sea) case. They used the Neighbourhood algorithm (NA) which also produces output conveniently suitable for calculation of Bayesian integrals and uncertainty estimation. NA is a stochastic algorithm which approximates the objective function on the entire parameter space by interpolating its values at random locations. The interpolator is based on the Voronoi cells in which the values are constant. The algorithm searches for the minimum by iteratively resampling best Voronoi cells (*Sambridge, 1999*). *Edris et al, 2008* and *Kazemi et al, 2010* applied the neighbourhood algorithm for updating realisations of simulation models of North Sea reservoirs conditioned to production and 4D seismic data simultaneously. While these studies demonstrate good results with NA algorithm using a few parameters, other algorithms perform better when the number of parameters is higher (typically, more than 20). *Hajizadeh et al, 2010* compare the performance of three algorithms that have been applied recently to the history matching problems: ant colony optimization (ACO), differential evolution (DE) and the neighbourhood algorithm. The ACO is a probabilistic technique for solving optimization problems based on finding good paths through graphs (*Dorigo, 1992*). DE is an optimization algorithm in which the population of models is updated by creating new models by combining pairs of existing randomly chosen models (*Storn and Price, 1997*). In the comparative study of *Hajizadeh et al, 2010* the three algorithms are applied in history matching of the PUNQ-S3 reservoir model using the production data from six wells. 45 porosity values were estimated in five layers of the model. The results of the comparison showed better performance of ACO and DE algorithms over the NA in terms of convergence rate and values of misfits (Figure 3.6).

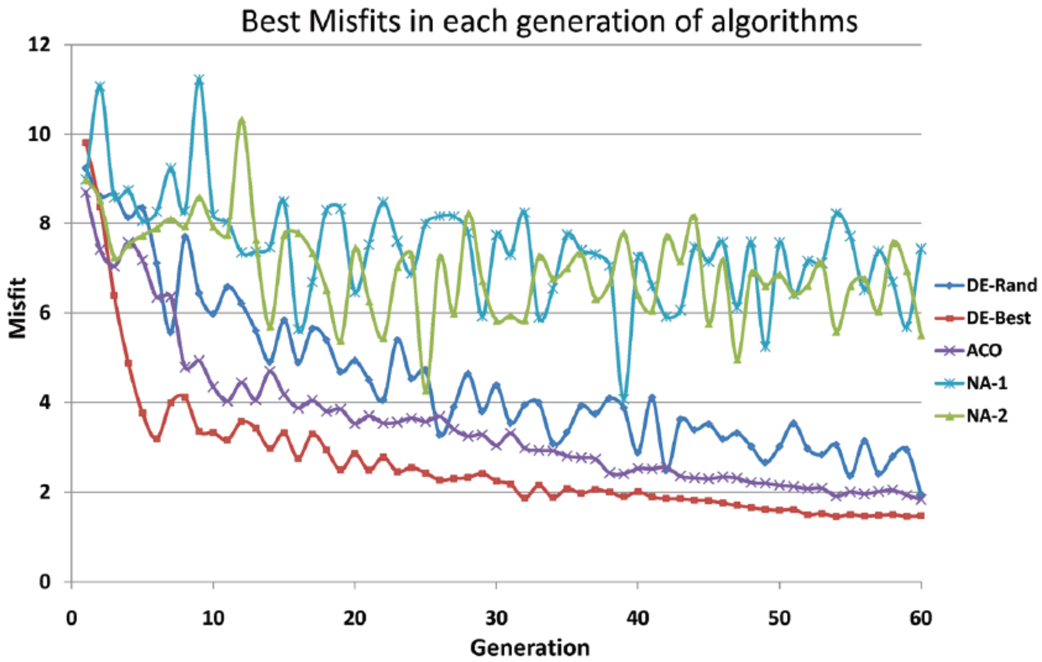

**Figure 3.6. Comparison of misfit functions of stochastic algorithms. DE-Rand is the differential evolution algorithm where base vectors are selected randomly, DE-Best is DE where best solutions are chosen as base vectors, ACO is the ant colony algorithm, NA-1 is the neighbourhood algorithms with extreme-exploration settings, NA-2 is NA with less explorative settings. After *Hajizadeh et al, 2010*.**

*Jin et al, 2011* compare three stochastic algorithms, very fast simulated annealing (VFSA), particle swarm optimization (PSO) and neighbourhood algorithm (NA), in a joint history matching approach using production and 4D seismic data. The study uses a synthetic layered model with uncertain fault throw and permeability of layers (Imperial College Fault Model, *Tavassoli et al, 2004*) and a model of a West African offshore field reservoir. VFSA is based on the simulated annealing (SA) algorithm (SA and PSO are defined in the Theory chapter, section Algorithm for history matching). The results of the objective function minimization in these experiments are shown in Figure 3.7. Compared to the previous comparison study, these do not show as big a difference which probably is because the number of parameters here is small: 9 parameters for the synthetic case and 18 for the real field case. The authors note however, that PSO achieved best results in the misfit reduction in the synthetic case where the objective function is very complex. On the other hand, the West African reservoir case is less complex so VFSA achieves lower misfit there. VFSA, as an algorithm based on a single model rather than a population, also benefits from less computational resources required per iteration than PSO or NA.

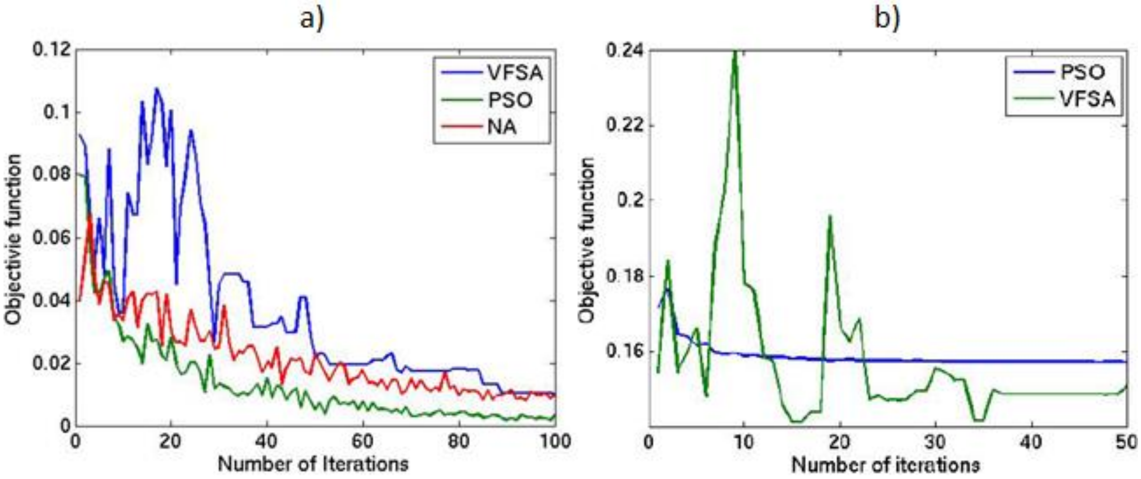

**Figure 3.7. Comparison of misfit functions of stochastic algorithms applied to the cases: a) imperial college fault model, b) West Africa offshore field. After *Jin et al, 2011.***

When considering a history matching problem within the context of Bayesian inversion, Markov chain Monte-Carlo (McMC) methods can be an efficient tool for generating samples from the posterior probability density distribution (pdf) of model parameters. In practice though, their applicability becomes limited when a cost of a single forward model is high as many samples are needed for adequately characterising the posterior pdf. This is particularly the case in probabilistic inversions of dynamic data in reservoir engineering, well production and 4D seismic data, for which running many simulations can be impractical. *Landa and Kumar, 2011* present a method of probabilistic joint inversion of production and 4D seismic data in which the cost of a forward model is reduced significantly by using proxy models for reservoir simulation and seismic modelling. Faster simulations allowed the authors to adapt the Monte-Carlo sampling for obtaining multiple history matched models.

Another probabilistic approach presented by *Castro et al, 2006* allows constructing realistic realisations of the geological model constrained to any geological input, 3D seismic data and also the dynamic data, such as well production logs and 4D seismic. Different sources of information are integrated through conditional probabilities of occurrence of certain facies given observations in the forms of training images, seismic and production data mismatches. Updating of the model is performed using the probability perturbation method which generates realisations minimizing data mismatch.

Different approach for conditioning models to the available dynamic data represents the Ensemble Kalman filter (EnKF) method. As defined in the theory chapter (section Algorithm for history matching), EnKF differs from the traditional methods by sequential assimilation of data and estimation of model and state (pressure and saturation) variables. Also, it is potentially capable of estimating large numbers of parameters if the ensemble of models provides sufficient variation. However, the ensemble size, its variability and Gaussian and linear assumptions in the analysis step of the method limit its ability to assimilate large volumes of independent data making integration of 4D seismic data problematic. In order to alleviate these problems, *Skjervheim et al, 2007* applied subspace inversion and *Zhang and Oliver, 2011* used covariance localisation functions. Another problem of the method is associated with different parameterisation schemes. Discrete properties such as facies and geobodies can not be readily incorporated due to the Gaussian assumption in the analysis step. Modification to the parameterisation is required therefore which accommodates truncated pluri-Gaussian or mixture Gaussian models (*Aanonsen et al, 2009*).

### ***3.3.2 Parameterization***

Most important approaches to parameterizing the history matching problems were defined in the Theory chapter (section Parameterization of the model). The purpose of this section is the discussion of their applications reported in the literature.

Formalized parameterisation schemes normally are designed for updating grid property fields where the number of history matching parameters usually needs to be reduced. However, simulation models in real history matching problems always have parameters such as fault multipliers, aquifer strength and others that should be estimated individually. Choice of such parameters is based on their data sensitivity which can be either estimated or just known from engineering experience. In a history matching study of the Valhall field, *Kjelstadli et al, 2005* chose more than 60 history matching parameters based on experience from previous studies with this field, which included porosity and permeability multipliers, compaction trends, aquifer strength, skin factors. Similarly, the parameters for the history matching of the Norne model were chosen manually in the work by *El Ouair et al, 2005*. Those were fault properties and carbonate barriers. However, assimilation of spatial details such as those imaged by 4D seismic data requires updating 3D properties of the model for which using a parameterisation will most likely be needed.

The zonation method defines regions of constant property change so the resulting model update is a piecewise constant function. Although discontinuities at the boundaries of the zones create bias in the estimated property field, the method allows for rapid initial misfit reduction in history matching. Defining zone is the critical part of the method. *Bissell et al, 1994* calculated data sensitivity of transmissibilities in grid cells then analysed the interpolated values. Regions of high sensitivity formed the basis for the parameterisation. *Gosselin et al, 2003* applied similar technique to find sensitive parameters out of gridcell-based pore-volume and transmissibility multipliers. This made the parameter choice dependent on the data type. For the 4D impedance data, the technique identified 34 transmissibility multipliers as pore volume multipliers were not so sensitive. However, when trying to parameterize the same problem for the Poisson's ratio data, the gradzone analysis showed too many zones with no apparent correlation to group cells in them. This was found to be due to noise in the data.

When the zones are defined prior to the history matching, the final misfit value limited from below by the error of spatial coarsening by the zonation. This of course prevents the model from assimilating spatial details in the data. *Grimstad et al, 2004* address this problem by allowing the parameterisation to be refined during the history matching and wherever more details are warranted by the data. They called this approach Adaptive Multiscale Estimation (AME). Figure 3.8 shows a field scale synthetic example from this study where a series of history matching trials is performed with the aim to restore a permeability field of a reference model. The sequence shows gradual refinement of the zones leading to the concentration of the zones around major reference heterogeneities.

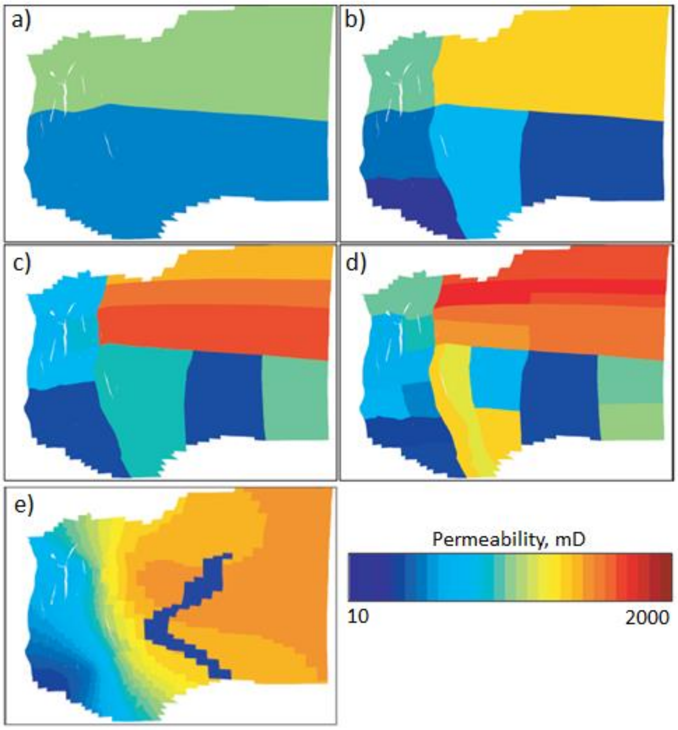

**Figure 3.8. Permeability distribution in history the matched model during different stages of refinement: a)-d) permeability fields parameterized with 2 to 28 value, e) reference permeability. After *Grimstad et al, 2004.***

Smoother property fields result from parameterisation by the pilot points. Similar to the previous method, defining the locations of pilot points is critical for the final solution. Usual practice for locating the pilot points is following the areas of highest sensitivity of data. In the first publication on the pilot points, *Marsily et al, 1984* determined the locations based on the data sensitivity. *Wen et al, 2006* applied the pilot method within a geostatistical inversion of production and 4D seismic data. Locations of the pilot points were determined using the genetic algorithm which did not require calculating sensitivities. *Stephen et al, 2006* used the pilot points along with other parameters for history matching of production and 4D seismic data in the Schiehallion model. The points were located according the observed 4D anomalies for highest anticipated sensitivity of the permeability updates via the pilot points (Figure 3.9). The number of points was further adjusted after trial history matching runs indicating that only the points around well I3 (in addition to some of the fault multipliers and petro-elastic constants) were sensitive to the data.

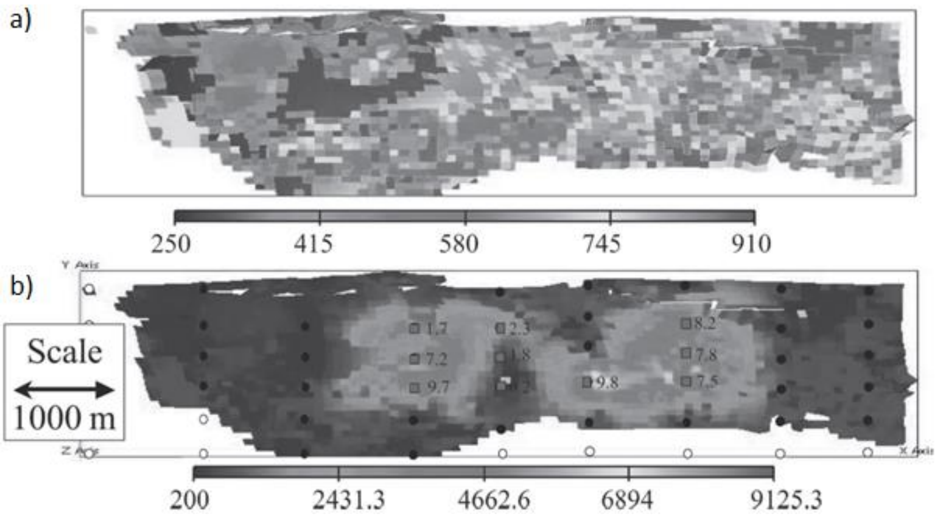

**Figure 3.9. Permeability distributions: a) before history matching, b) after history matching with pilot points. Squares indicate pilot points used in history matching, circles – inactive pilot points with multipliers fixed to 1. After *Stephen et al, 2006***

*Kazemi and Stephen, 2010* investigated the question of optimal locations for the pilot points in an example of history matching with the model of Nelson field (North Sea). Two approached were identified where the placement of pilot points would reflect the importance of model update in respective localities. The first is to allow the points control the major flow paths identified by the streamline analysis and the second is to try to address the mismatch in well directly by placing the points around the wells with highest mismatches. Location of pilot points according the two approaches in shown in Figure 3.10. Results of history matching showed the first approach achieves twice as good an improvement of the data match.

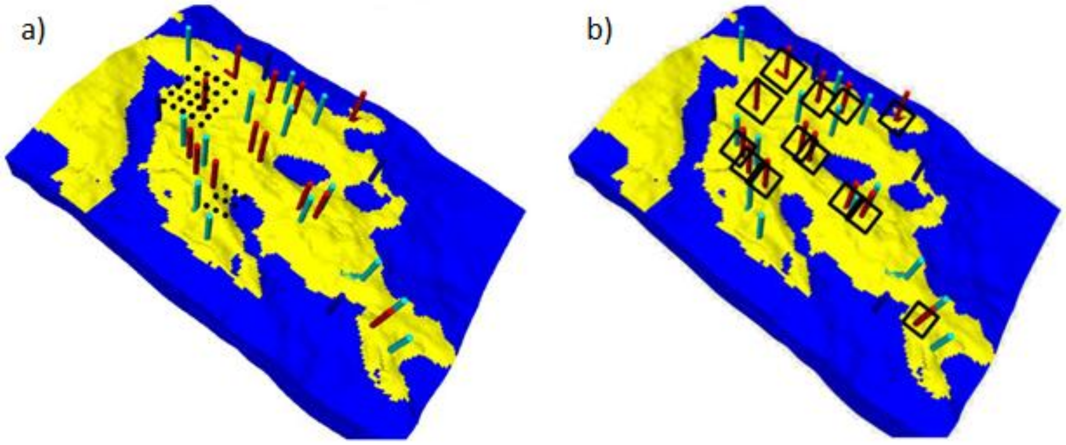

**Figure 3.10. Location of pilot points in the model of Nelson field (saturation is shown, blue-water, yellow-oil): a) pilot points located according to flow paths from streamline analysis, b) pilot points located around wells with high data mismatch (locations are shown by squares). After *Kazemi and Stephen, 2010***

*Jin et al, 2007* used VFSA for inverting 4D seismic data for the porosity field with different numbers of pilot points. The results show that the amount of details in the estimated property is proportional to the number of pilot points (Figure 3.11). The fact that the resolution keeps increasing with the number of points (20 to 50) signify that 4D seismic signal provides the required spatial information.

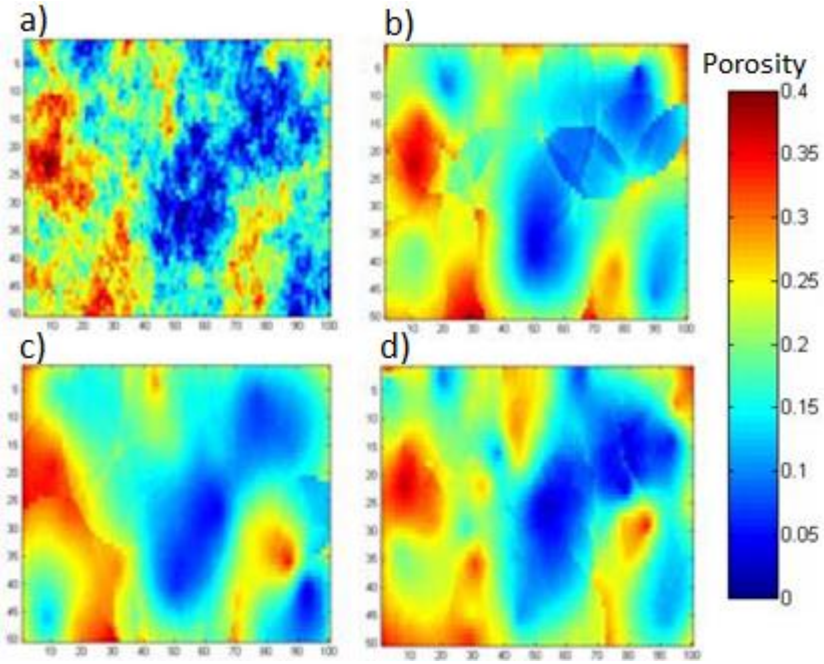

**Figure 3.11. Porosity fields estimated with different numbers of pilot points: a) reference porosity, b) porosity estimated with 20 pilot points, c) with 30 points, d) with 50 points. After *Jin et al, 2007***

In the methods discussed so far, the efficiency of parameterisation is achieved by accounting for data sensitivities of the chosen parameters for which either special analysis of the sensitivity matrix were applied or the performance of history matching was assessed empirically. However, when the history matching is geared towards data fit only, the model starts to lose the geological realism in the distribution of properties, especially if the model updates are strongly localised. When the geological prior information is believed to be reliable, it can be incorporated through the parameterisation in which case the history matching would search through geologically plausible realisations. The Karhunen-Loeve expansion, also known as the Principle Component Analysis (PCA), is an effective parameterisation approach based on the spectral decomposition of the prior model covariance matrix. In this method, the eigenvectors of the covariance matrix form a basis and their coefficients are independent parameters. Only a few vectors usually are retained for the basis according to the largest eigenvalues. In the earliest application of the method in petroleum engineering by *Gavalas et al, 1976*, pressure data from multiple wells were matched using simple synthetic reservoir models. The authors found that including the prior information reduced the error in the estimates of porosity and permeability and also improved the convergence. In a more recent work, *Floricich et al, 2005* applied the PCA to reduce the dimensionality of the problem of determining pressure and saturation changes in the reservoir from multiple 4D seismic attributes. *Sarma et al, 2006* applied the KL-parameterisation for a problem of optimization of net present value (NPV) in the case of water-flooded reservoirs using synthetic models. Although the KL-parameterisation can provide accurate characterisation of complex geological models, the computational cost of its application in history matching is too high making it impractical for some large-scale problems. This problem of the standard KL method is alleviated in its extension, called a kernel principle component analysis (KPCA). *Sarma et al, 2007* demonstrate applications of KPCA for history matching of synthetic and real field models. The authors note that the method is capable of representing geological models characterised by complex multi-point statistics and that the computation is highly efficient.

Because the KL-expansion methods are based on the prior covariance matrix, bias can be introduced when the prior information is erroneous. *Khaninezhad and Jafarpour, 2014* proposed a hybrid parameterisation scheme which aims to balance the effect of prior with information specific to the calibration data. The scheme combines basis vectors from the KL expansion with some prior-independent basis functions such as the discrete cosine transform (DCT) basis. The DCT scheme itself was earlier applied by *Jafarpour and McLaughlin, 2009* for history matching and showed high efficiency. DCT originates in the field of image compression (part of JPEG standard), it can describe a dataset of arbitrary structure with a set of basis vectors and their coefficients.

Another approach which combines the information from prior model with the information about the data resolution is presented in the work by *Bhark et al, 2012*. In this work, a two-stage history matching is demonstrated which aims to update the geological model at a range of scales from coarse to fine. The first stage employs the spectral representation of the prior model as basis for parameterisation. The algorithm performs history matching initially with a small number of parameters (frequency modes) to adjust the coarsest spatial details of the model first. This step is then repeated several times, each time increasing the number of parameters which corresponds to matching finer spatial details of the model. The process is stopped when adding finer details does not improve the match quality. The authors note that this process yields a model commensurate with the data resolution. The second stage of history matching is using the streamlines generated on the final model of the first step to perform the generalized travel-time inversion. This stage results in conditioning the fine scale local heterogeneities to calibration data and thus further improving the data match.

The gradual deformation method (GDM) provides a suitable framework for modelling complex geological realisations. *Roggero et al, 2007* applied the method in history matching of the Girassol field model in which both production and 4D seismic data were assimilated. The authors note that in order to assimilate the significant amount of spatial information from 4D seismic data, a flexible parameterisation was required for which the GDM method well suited. Model flexibility was further enhanced by extending the GDM with so called facies proportion calibration method in which facies proportions and variograms, usually constant inputs for the GDM, also become variable. Figure 3.12 demonstrates how model updates by different methods minimize the objective function. Reduction of the misfit throughout the steps of history matching indicate the increase in degrees of freedom that the model gained by combining the facies proportion method with GDM.

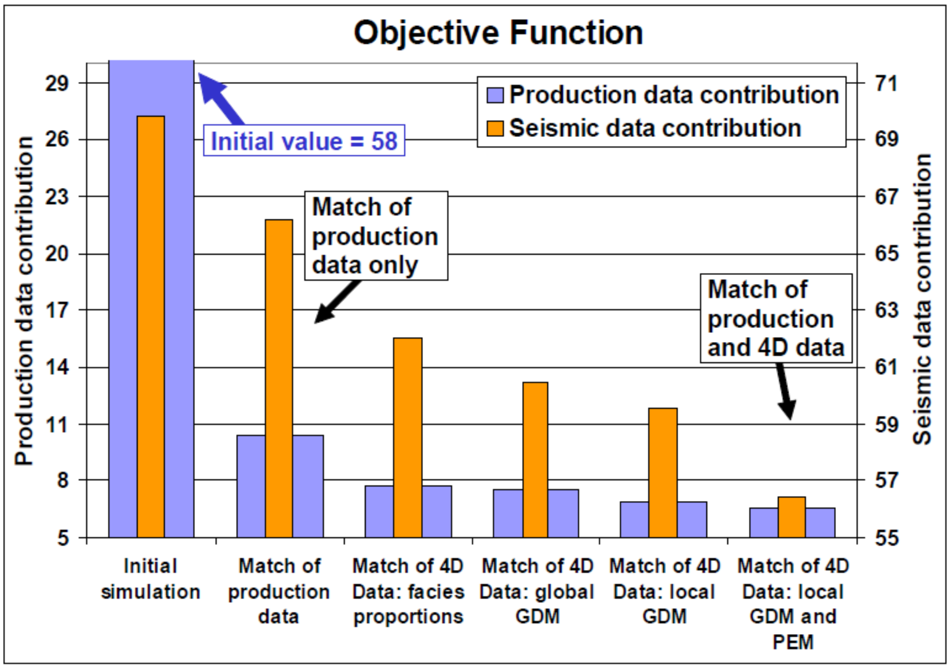

**Figure 3.12. Objective function minimization using different parameter. After *Roggero et al, 2007***

*Ding and Roggero, 2009* extended the GDM method to allow continuous change of geostatistical realisations without being bounded to the grid-block based domains of the usual gradual deformation method. The parameterisation also is capable of varying the geometrical sizes of the deformation domains.

*Choosing a parameterisation consistent with data resolution*

Too many potential parameters exist in a simulation model so that the amount of observed data is not enough for calibrating all of them. As a result, practical history matching problems are ill-posed which means that many realisations of the model exist that fit the data. If a solution (a model estimated by history matching) is highly non-unique, its future predictions are unreliable. Parameterisations aim to reduce the dimensionality of the problem and to narrow down the range of solutions. At this point, the prior assumptions that accompany a chosen parameterisation become important as these will form a part of the solution determining future model predictions. If a parameterisation leaves too few parameters for calibration and fixes the rest of the model to some prior values, then the chance of obtaining a unique solution is high but the solution will be mostly defined by the fixed part of the model which will induce prediction errors (*Hunt et al, 2007*). *Moore and Doherty, 2006* and *Hunt et al, 2007* argue that the simplifications required to obtain that uniqueness create a form of a “structural noise” (*Cooley, 2004; Cooley and Christensen, 2006*) which is in most cases higher than the measurement noise. Another problem with such a model is not so much the error of its forecast but the uniqueness of it which creates overly confidence in parameter estimates (*Oliver and Chen, 2011*). An alternative approach to reducing the non-uniqueness of solutions is to leave many parameters for calibration but apply some kind of a regularisation which will narrow down the range of solutions to smoother and simpler ones (*Hunt et al, 2007, Oliver and Chen, 2011*). It can also be argued that using many parameters with regularisation better agrees with the principle of model parsimony (Occam’s razor) than the case with too few parameters. Indeed, regularised solutions with many parameters are simpler and smoother which means that sparse data constrain only low frequency property trends rather than a highly detailed geological model. On the other hand, the solutions with too few parameters are not simpler, their fixed parts will most likely produce discontinuities (as in zonation) or other form of structural noise.

The regularisation can be explicit such as the prior term in the objective function, or it can also be implicit. *Le Ravalec-Dupin and Hu, 2007* did not use the prior term in their objective function as they believed that the combined pilot point-gradual deformation parameterisation provided the necessary regularisation by restricting the solution space. In another example by *Dickstein et al, 2010*, strong regularisation effect is reported when adding 4D seismic data to the dataset. The solution space is now restricted by the data itself which is more useful.

An alternative perspective but with similar meaning is presented by *Jafarpour and McLaughlin, 2009* and *Khaninezhad and Jafarpour, 2014*. They discuss parameterisations consistent with data resolution in terms of the balance between the prior-dependent (such as from PCA) and prior-independent (such as from DCT) basis functions in a parameterisation scheme. The hybrid scheme proposed in the latter work aims to reduce the influence of errors in prior when it is uncertain.

## 3.4 Problems of history matching specific to the integration of 4D seismic data

This section describes the differences in the history matching workflow, considerations and problems occurring when adding 4D seismic data. The major reason for concerns when reconciling reservoir simulations and 4D seismic data is that they belong to different domains in terms of the physics that cause these responses (and hence modelling approaches), scale of models, and errors in data. The coverage of history matching studies given here reflects the major questions discussed in publications. This means that there are of course questions that can be important but not included here as they are not widely discussed.

### *3.4.1 Objective function*

In an early work on history matching with 4D seismic data, *Waggoner et al, 2002* used a correlation function as a measure of match between the model-predicted and observed seismic data. However, the least-squares formulation of the objective function (eq. 2.2 in Theory chapter) remains the most popular amongst the history matching studies. Members of 4D seismic and production datasets are characterised by their own noise statistics as described by the corresponding covariance matrices. These weight the importance of pieces of data in the objective function. It is therefore convenient to consider the following form of the objective function with seismic and production data in separate terms (a version without the prior term is given, after *Aanonsen et al, 2003*):

$$J(m) = (s(m) - d_s)^T C_S^{-1}(s(m) - d_s) + \left(p(m) - d_p\right)^T C_P^{-1}\left(p(m) - d_p\right), \tag{3.1}$$

where *s(m)* and *p(m)* are seismic and production data predicted by model $m$, $d_s$ and $d_p$ are observed seismic and production data, $C_s$ and $C_p$ are seismic and production covariance matrices. *Aanonsen et al, 2003* discuss the importance of properly characterising the correlations in data to avoid wrong solutions in history matching. They propose a method for estimating the covariance matrix for seismic data based on fine scale variations in the data. This includes calculating the covariance function on the data after subtracting larger scale trends and normalisation. Also, authors note that production data probably will not be correlated if sampled at intervals exceeding 10-20 days, for example, monthly. In another study of joint history matching to production and 4D seismic data by *Stephen et al, 2006*, the signal and noise in both seismic and production data were separated in frequency domain using the Weiner filter. Also, the correlations in seismic data were estimated along the directions of inlines and crosslines. In the context of seismic inversion, *Sambridge, 1999*, following the method described in *Gouveia and Scales, 1998*, estimated the covariance matrix using realisations of noise receiver function.

In addition to the noise in observed data, modelling errors obscure comparison of model predicted and observed data. In a history matching study by *Stephen et al, 2006*, modelling errors were associated with approximate predictions by the streamline simulator which was used for faster history matching. For a subset of representative models, simulation was repeated with the finite difference simulator, and the difference in predictions gave the modelling error estimates. Similar modelling error issue is described by *Stephen et al, 2007* where approximation of predictions was caused by upscaling. Again, difference between predictions of fine and coarse scale models gave the error estimate.

If we were able to perfectly calculate the parameters of noise in data and modelling errors, then the seismic and production terms in the objective function could be balanced based on this information. However, estimation of noise statistics is difficult because data contains noise of different origins, inherited from different stages of data acquisition process and also added during the processing stage. We cannot estimate all modelling errors either, some of them are simply not known and for some, there are no means for calibration. It is for that reason that the important question of balancing the seismic and production terms remains open. *Johnston, 2013* (p.167) observe that at best, the balancing is currently done empirically.

An alternative approach to combining different terms in the objective function (different objectives) is offered by the multi-objective optimization (*Ching-Lai and Md Masud Abu, 1979*). Instead of combining different, often conflicting, terms, the optimization aims to find a variety of solutions which balance them. The terms are now called different objectives. The objectives are said to be balanced when no improvement in an objective is possible without a degradation of another objective. The final set of balancing solutions form a Pareto front in the space of the objective values. The optimization is performed using the principles of dominance of solutions and crowding distance. The first forces the algorithm to choose solutions with improved objectives (and thus tending to the Pareto front), and the second preserves the diversity of solutions by preferring less ‘crowded’ (in the solution space) solutions. *Park et al, 2013* applied the multi-objective optimization evolutionary algorithm to synthetic and real field problems where production and 4D seismic data were integrated. The results show that it is easier to obtain more diverse solutions with the multi-objective optimization approach than by using a single objective function with weighted terms because of supposedly more efficient exploration of the solution space in the former case. In a more performance-oriented work by *Christie et al, 2013*, the application of the multi-objective particle swarm optimization algorithm resulted not only in the better explored parameter space, but also on a gain in history matching speed.

The results of studies described above suggest that the multi-objective optimization is an efficient tool for obtaining diverse sets of solutions better describing the reservoir dynamics. The fundamental principle of the multi-objective optimization is the one of the equality of solutions on the Pareto front (given equal crowding). What the present work investigates however is how different levels of match of different data types (4D seismic and production data in particular) affect the quality of the resulting models, that is here the solutions are said to be non-equal (different levels of match of production and seismic data are discussed in Chapter 7).

### *3.4.2 Parameters for matching 4D seismic data*

Adding 4D seismic data naturally affects the choice of model parameters. With the new data constraint, we are now able to better estimate such parameters as location and extent of faults, baffles, other flow pattern controls, so these can make the new parameter set. At the same time, in addition to the simulation model parameters, there are now parameters that control prediction of seismic data itself, such as constants of the petro-elastic transform and parameters of time-depth conversion. These clearly do not affect the predictive capability of a simulation model but still can be included in the parameter set to improve the match of seismic data. In other words, changes to the parameter set reflect both the benefit and the cost.

In the work by *Stephen et al, 2006*, the initial set of parameters included both simulation model parameters such as permeabilities and fault transmissibilities and petro-elastic model parameters. Analysis of sensitivities reduced the number of parameters leaving parameters from both categories which stressed the importance of parameters in both categories (as well as the dependence of simulation model estimates on the uncertainty of a petro-elastic model). In general, there are numerous examples of using 4D seismic data to condition the spatial, grid-based distribution of the transmissibility (via grid-based permeability, transmissibility multipliers, etc.). The work by *Bhark et al, 2012* is one of the examples where a multiplier field at the grid-cell resolution was updated using the grid connectivity transform (GCT) to reduce the dimensionality of the problem. The size of the subspace of parameters in turn was iteratively adjusted to account for the spatial resolution of 4D seismic data.

The application of 3D seismic data traditionally is constraining the static descriptions of reservoir such as structural data, calibrated distributions of properties or property trends such as porosity and net to gross ratio, and lithology and fluid indicators (*Ødegaard and Avseth, 2004*). At the same time, useful applications can be found when 3D and 4D seismic attributes are combined for interpretation. *Andersen et al, 2006* integrated information from 3D and 4D seismic cubes to derive the information on probability of occurrence of sands. This was related to areas of gas- and water floods in the Oseberg field. *Johnston, 2013, p. 163* describes a situation where 4D seismic signal bears information about the occurrence of sands unavailable from 3D seismic data alone. As a result of saturation change, reservoir sands become detectable on 4D seismic data as the relationship between the impedance of reservoir and surrounding rocks changes. For this reason they are sometimes called ‘4D sands’.

### *3.4.3 4D seismic data in different domains*

Although there is a clear causal relationship between changes of reservoir pressure and saturation on one hand and 4D seismic signature on the other, these data reflect different physical quantities and belong to different domains from the modelling perspective. Petro-elastic modelling and seismic forward modelling are required to predict seismic data from simulation results. For this reason, predicted and observed data in seismic history matching cannot be directly compared but rather need to be transformed to some common domain. *Gosselin et al, 2003* described the options available for seismic history matching as comparison of data in the seismic domain, petro-elastic domain and the pressure and saturation domain. In order to compare in the seismic domain, seismic data need to be predicted for each realisation of the simulation model. For comparison in petro-elastic domain, observed seismic need to be converted to petro-elastic properties. Similarly, in pressure and saturation domain, observed seismic need to be converted to these properties.

The domain of petro-elastic properties has been the most popular option amongst publications on seismic history matching (*Waggoner et al, 2002; Gosselin et al, 2003; Aanonsen et al, 2003; Mezghani et al, 2004; El Ouair et al, 2005; Stephen et al, 2006; Roggero et al, 2007; Dong and Oliver, 2008; de Brito et al, 2010*). *Gosselin et al, 2003* point out that using the data in the elastic domain avoids the inclusion of seismic forward modelling in the history matching loop which saves the CPU time. It also avoids the inversion to pressures and saturations which can introduce errors due to pressure-saturation ambiguity in 4D seismic signal, and moreover, the results of this inversion are not independent of the reservoir model used for the inversion. *Landa and Kumar, 2011* and *Tillier et al, 2011* compared data in time domain in their history matching studies. The authors argue that comparison in time domain is preferable because there is no need for time consuming and error-prone inversions which means that the data is available for history matching earlier after acquisition. In an earlier history matching example applied to the Bay Marchand (Gulf of Mexico) field, *Vasco et al, 2003* used 4D amplitude change peaks (21 points in total) as observed data. In another study by *Landa and Kumar, 2011* the differences of seismic traces together with production data are used in a joint probabilistic inversion. The authors note that for their synthetic case, comparing observed and predicted seismic data in traces is simple, whereas in practical applications, one might rather consider 4D seismic attributes because of the noise in data and errors of seismic modelling. Data in pressure and saturation domain were compared in a synthetic study by *Davolio et al, 2011* for which 4D *P*- and *S*-impedance data were inverted for pressures and saturations.

In a work on assisted history matching of production and 4D seismic data by *Walker et al, 2006,* observed and predicted seismic data are compared using different physical quantities (different domains). The subject of study, Harding reservoir, demonstrated strong saturation dominated 4D effect while the influence of pressure was minimal. For this reason the authors chose to compare the simulated saturation change map directly to the observed impedance change map (Figure 3.13) using a correlation function as measure of match.

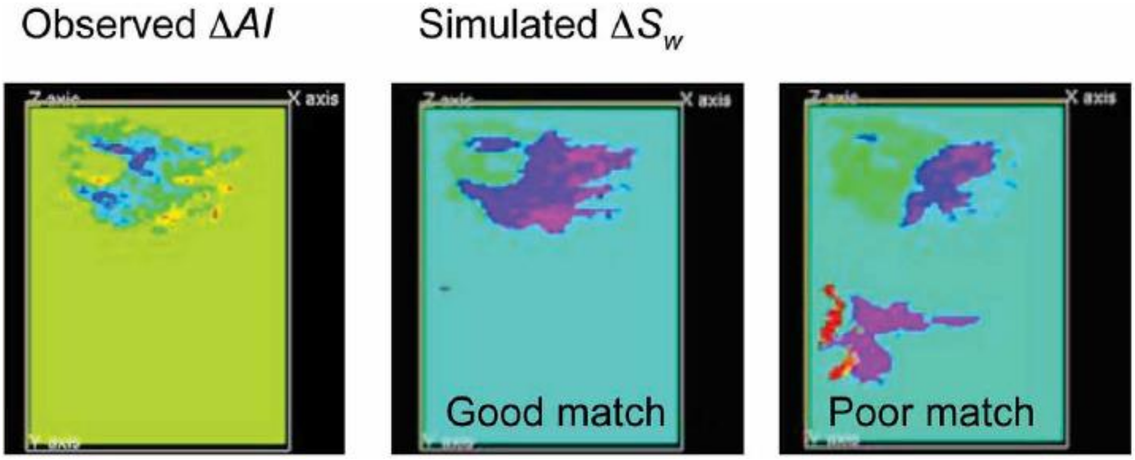

**Figure 3.13. Example of matching simulated water saturation change ($\Delta S_w$) to the observed 4D impedance change ($\Delta AI$) for Harding reservoir. After *Walker et al, 2006***

The study focused on the relationship between the quality of history data match and the quality of future forecasts. In particular, the results show that a subset of models history matched to production data only show unsatisfactory forecast quality (Figure 3.14, a, called “prediction quality” in figure annotation). On the other hand, adding 4D seismic constraint fully excluded the models with bad predictive capability (Figure 3.14, b). Noteworthy is that the constraint by 4D seismic data has been effective despite the difference between the domains of the compared (observed versus predicted) seismic data. This suggests that the data error (difference between the domains of water saturation map and impedance map) is of lower order of importance here compared to the information common to the two domains – spatial 4D signature.

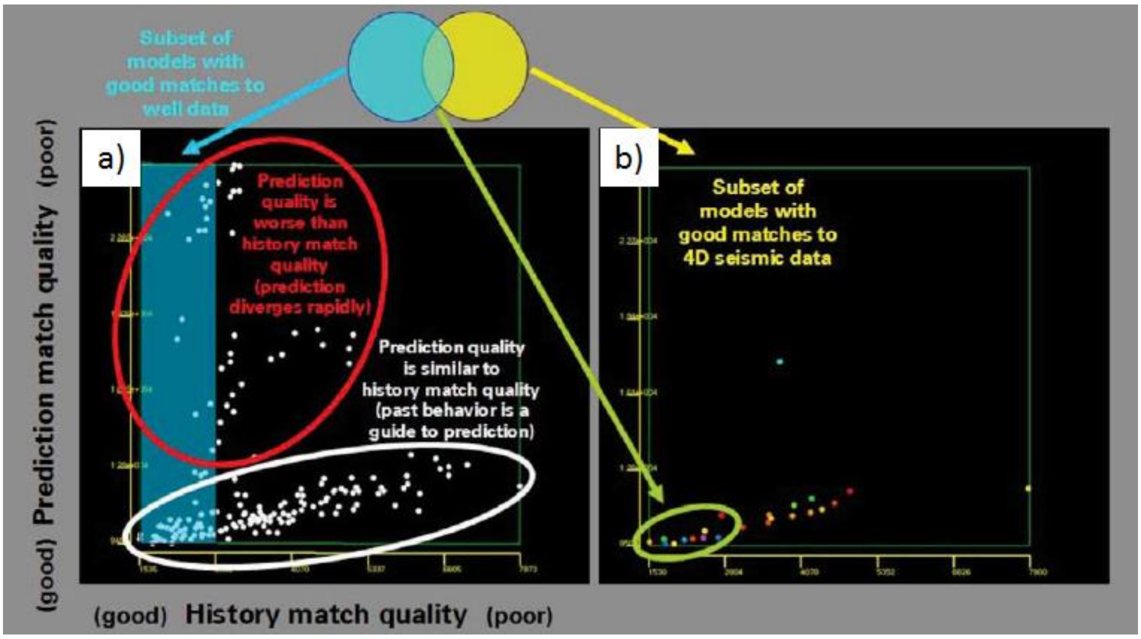

**Figure 3.14. Cross-plots of production forecast quality versus history match quality: a) matching well production data, b) matching 4D seismic data. After *Walker et al, 2006***

Overall, the experience of published history matching studies suggests that 4D seismic data need to be transformed to some attribute which makes it a more robust source of information as errors will be minimized. On the other hand, inversion to pressures and saturations seems to be an error-prone process due to the ambiguity in inferring these two properties. Although the domain of petro-elastic properties is also accessible through inversion, no significant problems are reported regarding the change of information content of seismic data due to the inversion itself. The most likely reason for this is that other factors affect the information content much more. For example, using a single seismic attribute versus a combination of attributes, or using a map- or volume-based attributes. These factors are discussed in the following section. Most likely, seismic attributes including those in the petro-elastic domain were chosen in the majority of studies for their robustness, intuitive interpretability, and the availability of certain seismic attributes for their studies. Also, the last example demonstrates the spatial 4D signature can be more important than the difference between the domains.

### *3.4.4 4D seismic attributes*

Often, not a single elastic property but a combination of attributes is used as observed data for history matching. *Gosselin et al, 2003* used inverted acoustic impedance and Poisson’s ratio, *Roggero et al, 2007* used the acoustic impedance with added $\Delta V_p/V_p$

attribute serving as a low frequency 4D component. Using several data types undoubtedly provides a better constraint for the model parameters. In the context of 4D seismic though, we can be more specific about this aspect. If *P*-impedance data is complemented with *S*-impedance (or any derivatives like the Poisson's ratio), the dataset will be more sensitive to different production related effects as this combination ($I_p$-$I_s$) is used as a basis for pressure and saturation discrimination (*Cole et al, 2002; Andersen et al, 2006,* also see Figure 3.1, b). As for the time strain, $\Delta V_p/V_p$, or time shift attributes, their addition partly restores the low frequency component of the 4D signal. As noted by *Johnston, 2013,* the results of the 4D inversion seem to be more limited in the low frequency part than the 3D seismic data. Therefore, the addition of these attributes provides a constraint in the low frequency part.

Where the structure and stratigraphy of the reservoir is simple, map-based attributes can provide sufficient level of details for adequate interpretations (*Johnston, 2013*). In these reservoirs, the signal is not obscured by interference from other layers, the reservoir is relatively thin, and also, if there is a reservoir compaction, the overburden effects will be small.

An example of a map-based 4D seismic interpretation is monitoring the water sweep at Hoover field (Figure 3.15). The seismic response of the reservoir in this field is a single cycle, tuning to subtuning thickness, trough-peak event with a strong hydrocarbon leg response (*Helgerud et al, 2011*). The actual 4D seismic map in Figure 3.15 shows hardening of the reservoir due to water displacing oil (shown in blue). The circled area over the actual 4D seismic map indicates an area above the OWC that is unswept, suggesting that there may be a baffle. Including the baffle in the simulation model improved the predicted 4D seismic map, leaving only a question about its transmissibility which was subsequently answered by well pressure analysis.

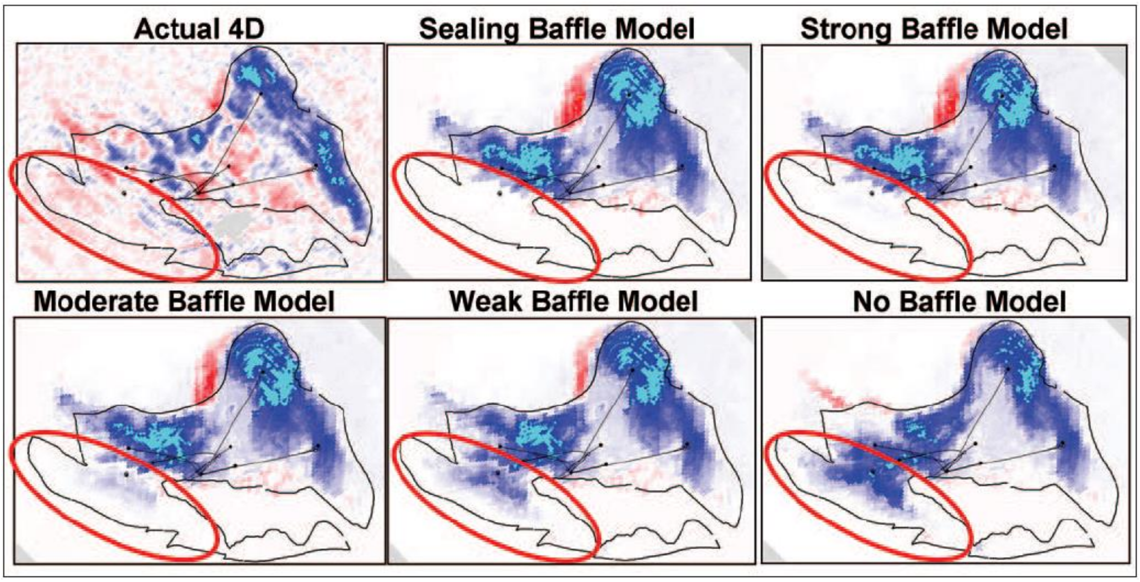

**Figure 3.15. Maps of observed and predicted 4D signal showing different scenarios of the baffle transmissibility. After *Helgerud et al, 2011*.**

Another example of using seismic maps is found in a work by Stephen et al, 2006. This time, 4D seismic data is used quantitatively, within an automatic history matching workflow (with NA algorithm) applied to the UKCS Schiehallion field. The maps of predicted acoustic impedance are compared to the observed seismic attributes (sum of negatives of coloured inversion) using two time-lapse differences: after one year of production, and after another year of production (Figure 3.16).

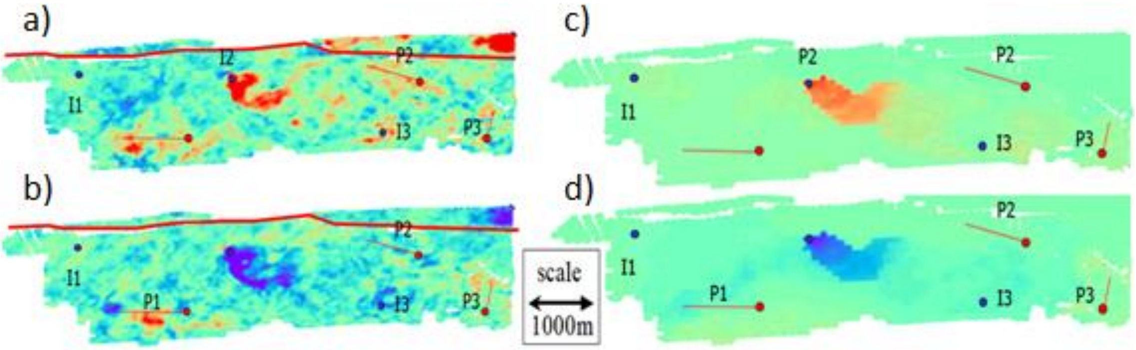

**Figure 3.16. Comparison of observed and predicted 4D attribute maps: a) observed time-lapse difference map after one year of production, b) observed map after another year of production, c)-d) same as (a)-(b), but predicted maps. After *Stephen et al, 2006*.**

Strong 4D signal is observed around the injector well I3 which is attributed to building up the pressure. There are more signals over the map but those were interpreted as noise or, if they were above the horizontal red line representing a sealing fault, not modelled. 12 faults, 10 pilot points, and 6 parameter of the petro-elastic model were adjusted in the assisted history matching resulting in good predictions of the 4D signals as shown in Figure 3.16, c and d.

In stacked and thick reservoirs however, interpretation of maps only can be ambiguous due to complex seismic response from multiple layers. An example of stacked reservoirs is a thick, complex, multi-cycle Miocene channel-levee system comprising a West African field (Figure 3.17). The production here is maintained by several depletion mechanisms: solution-gas drive with limited aquifer support, gas injection for storage, and water injection for pressure maintenance. Tracking the respective 4D effects can be ambiguous on a map due to vertical overlap and thickness. Figure 3.18 illustrates the problem. Figure 3.18, a and b show maps of amplitude of quadrature (-90° phase shift) time-lapse difference. Red area in the northern part of the field (Figure 3.18, a) corresponds to gas injection and critical gas saturation, while the red signal in the southern part is misleading as there is no gas injection there. Similar situation is shown in Figure 3.18, b. Water is injected in the southern part only, so the map in the north is inconsistent with production data. The ambiguity is resolved as shown in Figure 3.18, c where volumetric geobodies are derived by applying cut offs on the quadrature difference data. Blue and red geobodies are shown as clearly separated in space.

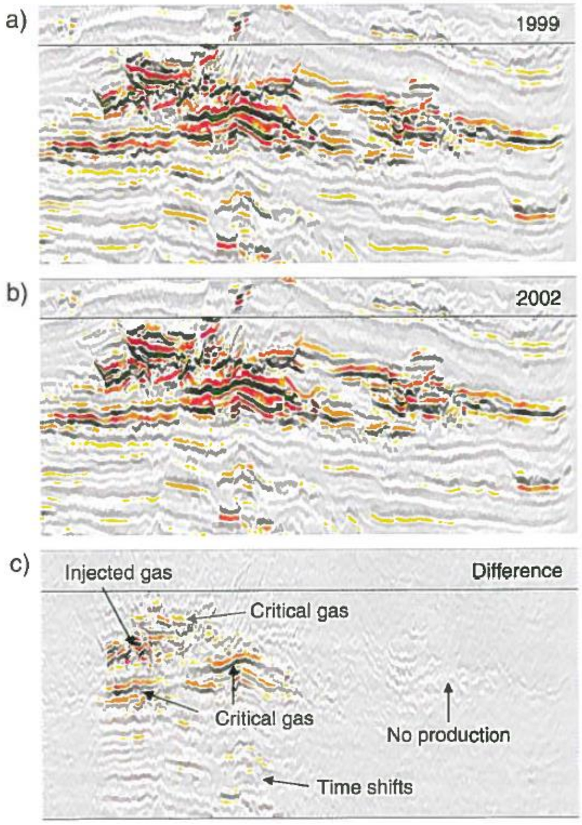

**Figure 3.17. Seismic cross-sections for a West African field: a) pre-production baseline survey, b) monitor survey, c) time-lapse difference. After *Johnston, 2013***

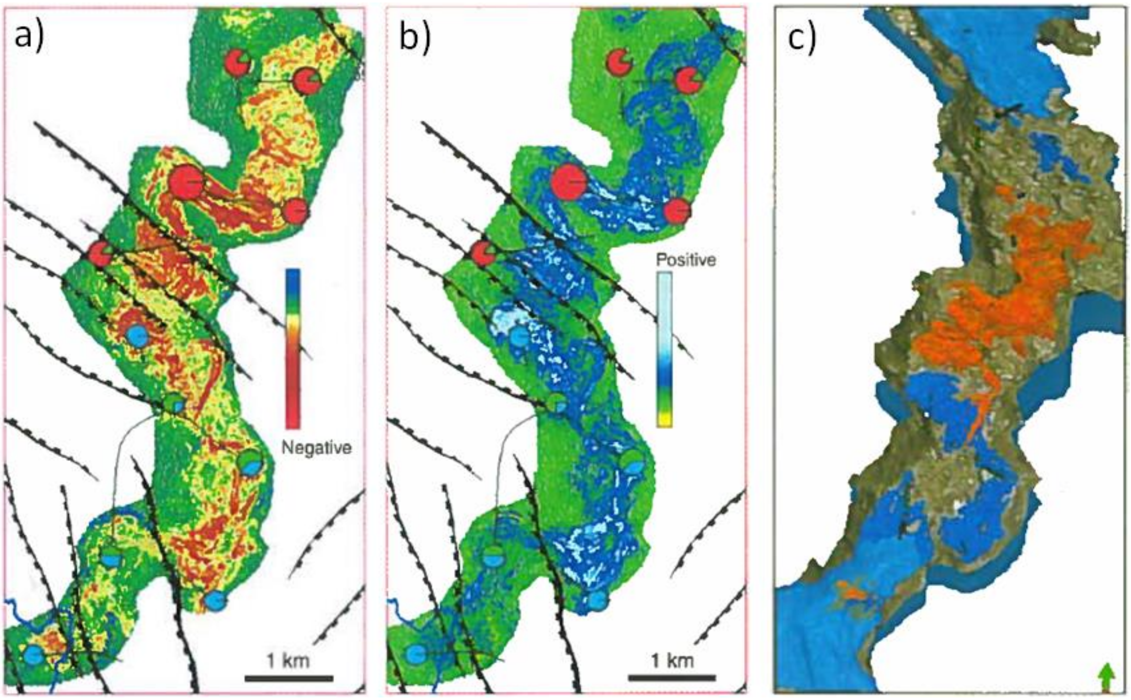

**Figure 3.18. Comparison of map-based and volumetric attributes: a) reservoir interval map of maximum negative amplitude of quadrature (-90° phase shift) difference indicating softening of rocks by red, b) map of maximum positive amplitude of quadrature difference indicating hardening of rocks, c) volumetric geobodies from cut-offs on quadrature difference data showing water saturation increase in blue and gas saturation increase in red. After *Johnston, 2013***

Another example of using the volumetric attributes is given in *Roggero et al, 2007*. The Girassol field has very similar reservoir architecture to the previous example being composed of Oligocene channel-levee complexes, stacked elementary channels and associated levees. In this history matching study predicted and observed data were compared using volumes of *P*-impedance time-lapse differences. Comparison of volumes was needed in order to use the high (compared to well data) spatial resolution of 4D seismic data. The model itself was made more flexible by parameterization (see the parameterisation section) which allowed the authors to reproduce volumetric details of the 4D signal (Figure 3.19).

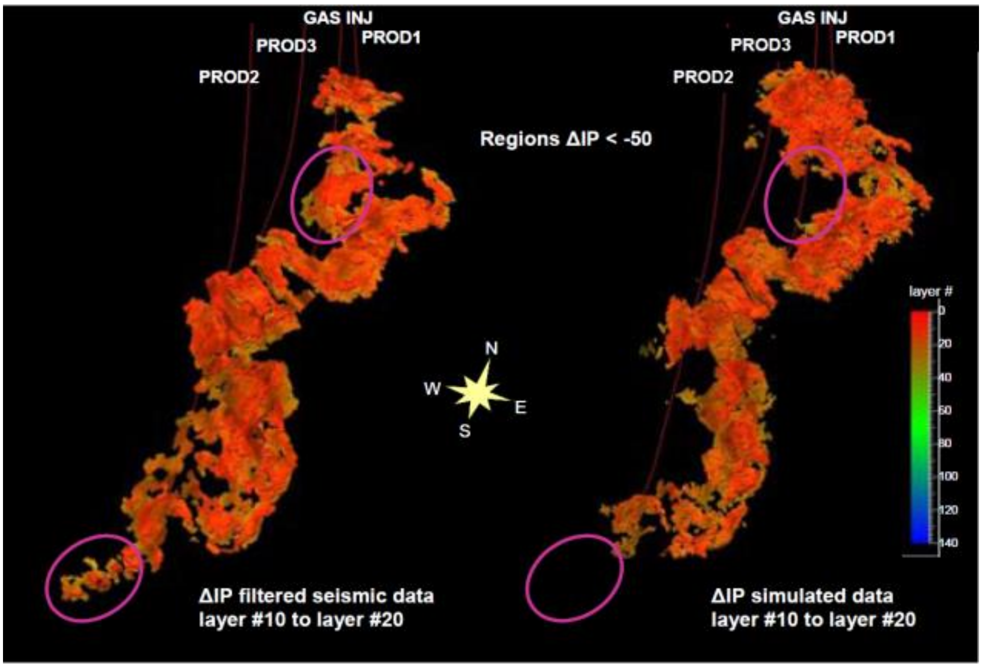

**Figure 3.19. Comparison of observed (left) and predicted (right) 3D geobodies visualising highly negative values of 4D *P*-impedance differences. After *Roggero et al, 2007*.**

Although the volumetric attributes provide finer details for reservoir characterisation, care should be taken fitting them as they have more chances to be noise than coarser, but sometimes more robust, map attributes. Authors in *Roggero et al, 2007* note that errors of the final model prediction can be due to fitting the data in 3D pixel by pixel while a better representation of uncertainties might be required.

Even more informative, quantitative characterisation of rock properties such as compressional and shear velocity and density is possible by employing the full waveform inversion (*Tarantola, 1986*). This is a method of seismic depth imaging which yields velocity models of high resolution. Full azimuth multi-component seismic data from seabed seismic sensors (such as ocean-bottom cables or, even better, ocean-bottom sensors, see *Beaudoin and Ross, 2007*) particularly suits as input for full waveform inversion because of its high quality. In the work by *Andorsen et al, 2013*, the method allowed improving the velocity model significantly which subsequently led to improved 4D images of the water front as part of the water flood monitoring program in Valhall. Figure 3.20 demonstrates the change in the 4D seismic map (specifically around injector G18) achieved due to applying the inversion.

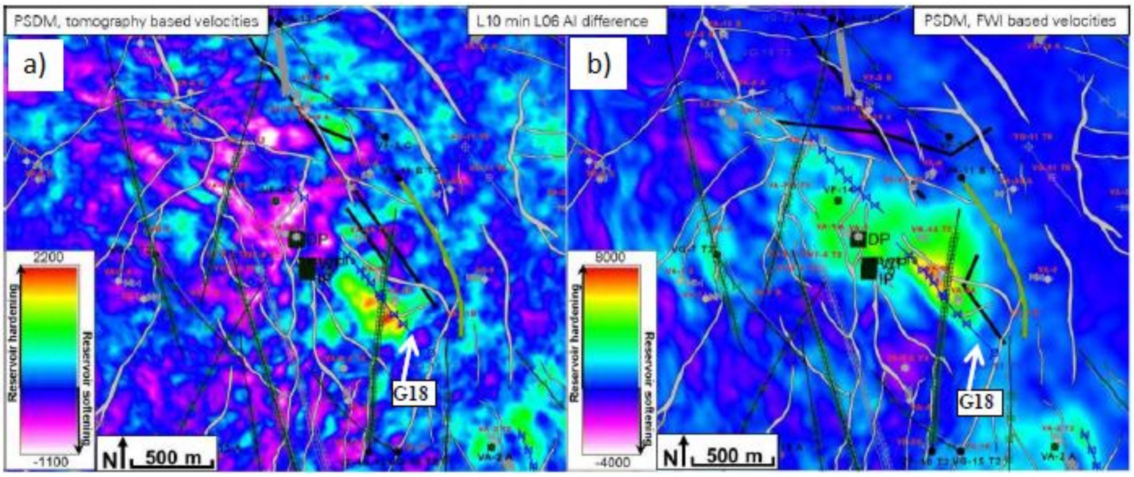

**Figure 3.20. Time laps acoustic impedance difference in Valhall field: a) 4D map with ray tomography based velocity model, b) 4D map with full waveform inversion velocity model**

In another work on Valhall by *Yang et al, 2013,* the inversion directly to the time-lapse changes of properties is discussed. The authors compare two approaches to the time-lapse full waveform inversion. In the first, the inversion is applied on baseline and monitor surveys separately, while in the second they are inverted jointly. The results of the second method appeared to be cleaner and more localised which lead to the conclusion of superiority of the second approach. The last example by *Queißer and Singh, 2010* does not use the data from seabed sensors but still demonstrates a successful application of the inversion for monitoring of $CO_2$ sequestration. Compressional velocity models resulting from the inversion allowed the authors to calculate $CO_2$ saturations in the Sleipner aquifer leading to a conclusion that the method is suitable for quantification of free gas during the $CO_2$ sequestration.

### *3.4.5 Scale of model and data*

There is a scale difference between the results of reservoir simulation and observed seismic data. Areally, simulation model grid is discretized with about 100x100m cells, whereas the seismic bin size is 12.5 m. Vertically, the seismic resolution is coarser but smaller scale heterogeneities may still affect seismic predictions as described by *Sengupta et al, 2003*. The authors found that replacing smooth saturation outputs of the simulator with a more realistic patchy distribution leads to predictions of petro-elastic properties quantitatively comparable to the observations. The authors suggest that the simulation results should be downscaled to a finer grid for which the petro-elastic transform is more suitable. These considerations were applied in history matching works by *Enchery et al, 2007, Roggero et al, 2007,* and *Tillier et al, 2011*. An alternative approach for reconciling observed 4D seismic data and simulator’s output is upscaling 4D seismic data to the simulation grid (*Stephen et al, 2006*) which seems to be a more robust solution because of the inherent ambiguity of the downscaling process.

Scale is an important consideration when combining different data types and the model responses too. Because of the inherent uncertainty and difference in scale of data sources, coupling them provides more robust description of reservoir processes compared to using a single data type. An example of coupling different data types for reducing the uncertainty in planning the development strategy is given by the Magnus field study (*Erbas et al, 2014*). Magnus field is in production since 1983, the high productive plateau period ended in 1995, and now is developed using tertiary recovery – water alternating gas (WAG). The main reservoir unit, Magnus Sandstone Member (MSM), is formed by stacked turbidite sandstones (sand lobes, 2-7 m thick) which are separated by shales of varying thickness and lateral extent (*MacGregor et al, 2005, Moulds et al, 2005*). The shales represent barriers to areal and vertical sweep and have been a source of uncertainty for the development planning since the earliest stages of production (*Atkinson, 1985*). Unswept oil lenses of 5-10 metres were found behind the water flood front adjacent to the fully swept sands (*King et al, 1998*). Gas injection started in 2002 particularly aimed at the remaining oil after the secondary water flood. Despite the efficiency of WAG scheme, it required optimization due to suboptimal areal and vertical sweep (*Erbas et al, 2014*). The MSM reservoir, initially assumed a single unit for WAG scheme, was required further vertical separation into MSM-G, MSM-E and MSM-E lobes and their subunits. By analysing primarily the PLT (production log tool), 4D seismic data, and material balance in combination, the development strategy was adjusted by redirecting the flows in the reservoir. In particular, the units MSM-G, MSM-E and MSM-E were seen separated, MSM-E was found to be unaffected by gas injection, MSM-A was found to have low WAG efficiency. Figure 3.21 shows injected gas extent in reservoir units. 4D image of the unit MSM-E shows absence of gas while PLT indicated otherwise and would be misleading if interpreted individually. Gas balance calculations were in agreement with 4D seismic though which means gas finds its way out of MSM-E in proximity of the well. This example demonstrates that coupled analysis of data allowed tacking the uncertainty caused by ‘invisible’ shale barriers. Although the barriers cannot be mapped using the seismic data (due to low thickness of the lobes), 4D signal gives information which helps to handle their effect.

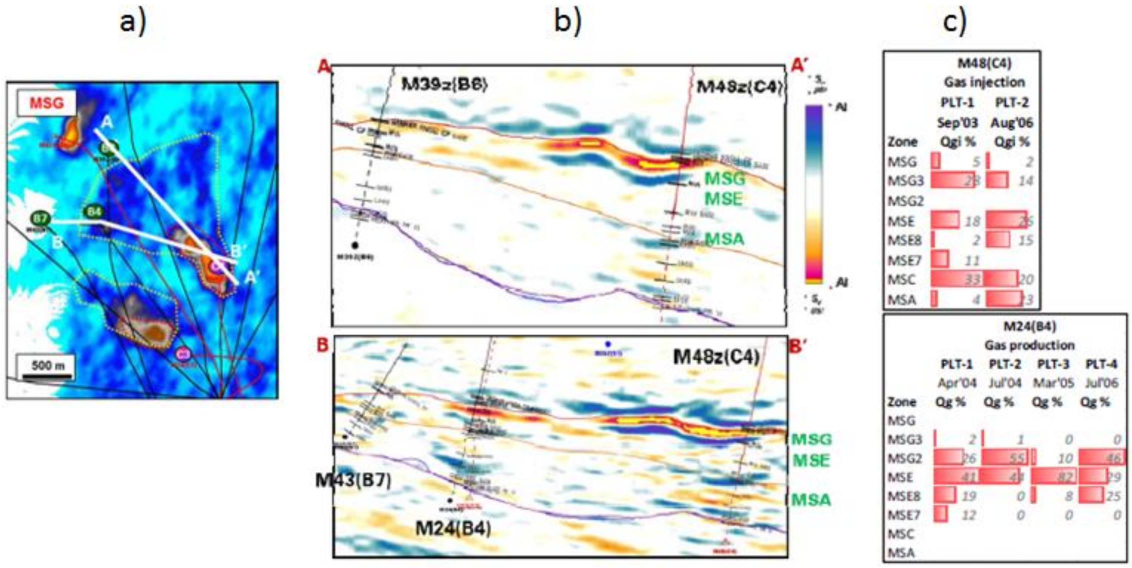

**Figure 3.21. Gas injection monitoring using 4D seismic and PLT data: a) map of Sum of Negatives attribute of 4D amplitude change along MSG lobe, b) cross-sections along lines AA' and BB' showing 4D inverted impedance change where red means reservoir softening and blue - hardening, c) PLT logs showing relative injection and production to(from) reservoir units. After *Erbas et al, 2014***

*Illustration of scale relationship in the template Schiehallion reservoir*

The template Schiehallion reservoir and the corresponding model used in this work are described in Chapters 5 and 6, while here only the necessary parameters are given for calculations. In the following, scales of the model are related to the timing of 4D surveys in order to illustrate the expected information content in 4D seismic data. Following the actual 4D survey timing in Schiehallion field, 4 years interval between the baseline survey and the monitor is considered in this work. Given the water saturation change is the main 4D seismic effect, the area affected by the water-flood is where 4D seismic data will effectively provide information about the reservoir. Therefore, the advance of the water front by the time the monitor survey is shot is equivalent to the depth of investigation of the 4D seismic method. One of the simplest methods to estimate the position of the water front is by using the Buckley-Leverett frontal advance equation (*Buckley and Leverett, 1942*):

$$xf = \frac{Qt}{A\phi}\left(\frac{dF_w}{dS_w}\right)_f, \quad (in\ SI\ units) \tag{3.2}$$

where $Q$ is flow rate, $t$ is time, $A$ is cross-sectional area, $\phi$ is porosity, $S_w$ is water saturation and $F_w$ is water fractional flow given by

$$F_w = \frac{1}{1 + \frac{k_{ro}}{\mu_o}\frac{\mu_w}{k_{rw}}}, \tag{3.3}$$

in which $k_r$ is relative permeability, subscripts $o$ and $w$ signify oil and water respectively.

The quantity $\frac{dF_w}{dS_w}$ in equation 3.2 can be estimated for a particular value of water saturation using the fractional flow curve in turn obtained from relative permeabilities as shown in Figure 3.22. In this case, the value of water saturation of 0.56 is used because it is shown (see section 5.3) to give at least 3% of 4D impedance change which is on lower margin of detectability (*Johnston, 2013*).

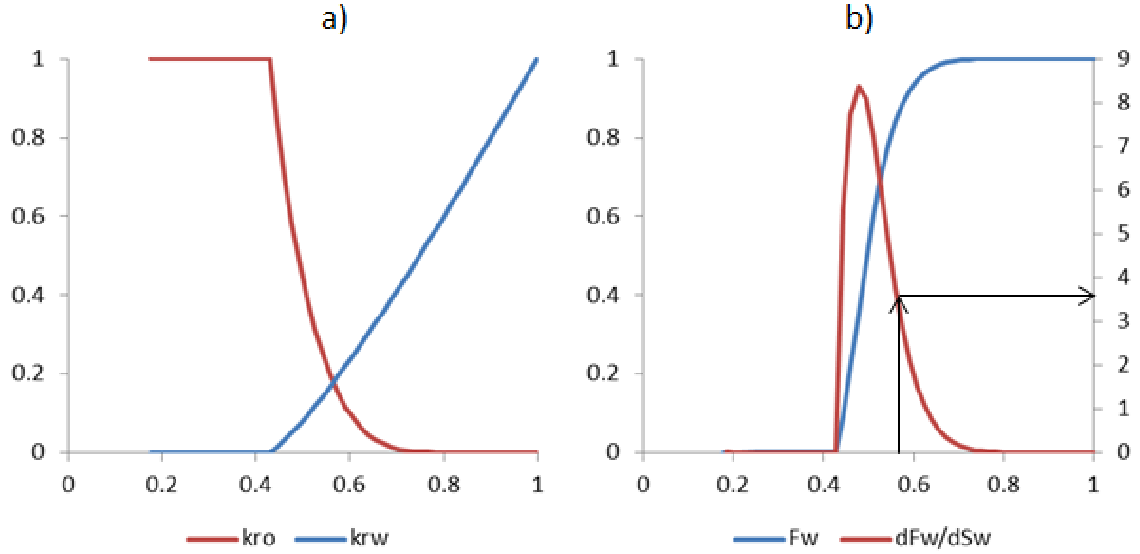

**Figure 3.22. Calculation of dFw/dSw for Buckley-Leverett front advance formula.**

Table 3.1 summarizes parameters used for calculation of the position of the water front, *xf*. The resulting value of the front position (2700 ft) is illustrated in Figure 3.23 together with the simulated water saturation distribution. As expected, the simulated water saturation extends further due to the reservoir heterogeneity while the Buckley-Leverett calculation assumes none. The figure shows that the 4 years interval between the seismic surveys allows the water front to cover the most of the inter-well space so that the information on that area should be reflected in the seismic data. The wells on the other hand will not be reached within the first 3 years of production given the shortest distance between the producer and the injector being 2000 ft (calculated using the equation 3.2). This lowers the information content of the well data regarding the water flood pattern. Although not directly seeing water, the wells will still have information about the pressure change. The pressure wave from the injector will reach a producer within 15 days according to the transient pressure wave travel time given by (see for example, *Stewart, 2011, p. 41*):

$$tp = \frac{\phi \mu c_t r^2}{4k}, \quad (in\, SI\ units) \tag{3.4}$$

where $\mu$ is fluid viscosity, $c_t$ is total compressibility, $r$ is radius of pressure wave front, $k$ is permeability. This can be used for absolute permeability calibration, however, this work focuses on the spatial patterns of property change so the pressures are not used here.

**Table 3.1. Parameters of the template Schiehallion reservoir used for calculation of Buckley-Leverett front progression and pressure wave propagation distance**

| Parameter | Symbol | Unit | Value |
|---|---|---|---|
| Porosity | $\phi$ | fraction | 0.28 |
| Net to gross | *ntg* | fraction | 0.49 |
| Permeability | $k$ | mD | 490 |
| Viscosity | $\mu$ | cp | 3.06 |
| Total compressibility | $c_t$ | 1/psi | 1.32E-05 |
| Liquid rate | $Q$ | bbl/day | 17000 |
| Time between 4D seismic surveys | *tss* | years | 4 |
| Well spacing | *xw* | ft | 4000 |
| Reservoir cross-sectional area | $A$ | ft$^2$ | 817320 |
| | | | |
| **Buckley-Leverett front advance for tss** | ***xf*** | **ft** | **2660** |
| **Time for the front to reach wells** | ***tw*** | **years** | **3** |
| **Pressure wave travel time from injector to producer** | ***tp*** | **days** | **15** |

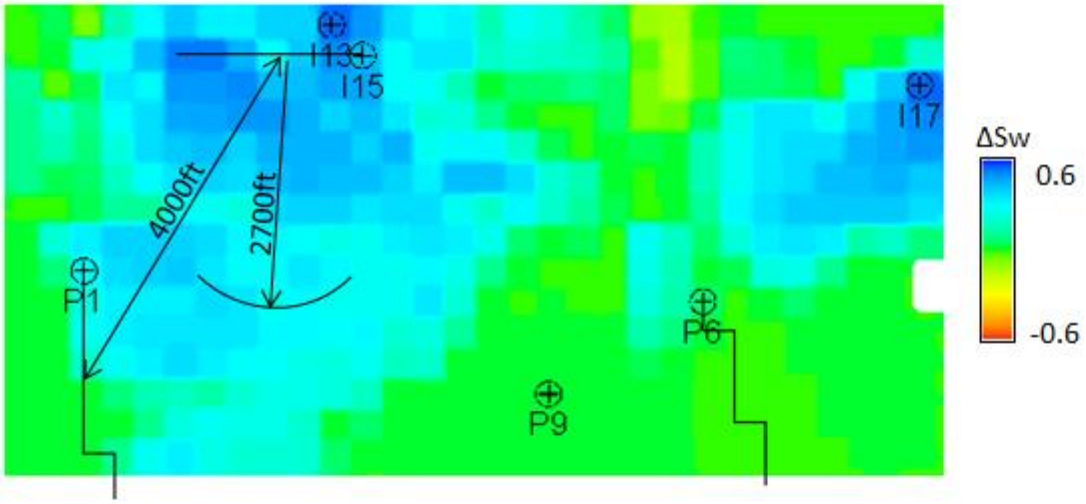

**Figure 3.23. Scheme of well placement with characteristic distances shown on the map of average water saturation for the template Schiehallion reservoir (T31a only, see Chapter 6 for more details). The simulation time is 4 years.**

## 3.5 Summary

It is commonly recognized that the addition of 4D seismic data in the integrated reservoir characterisation studies improves the quality of the final models. It happens so because the spatial information from 4D seismic attributes complements the production data from wells. 4D seismic data has been a tool helping in reservoir management decisions by indicating the extents of water movement, pressure compartments, and bypassed hydrocarbon areas. In the last 15 years however this information has also been used to build better reservoir models.

In the context of history matching, 4D seismic interpretations and quantitative measures are combined with engineering judgement to improve reservoir models manually or within automatic (assisted) history matching workflows. Usually, seismic attributes such as maps and volumetric attributes derived from either seismic traces or inverted impedances or velocities are used as observed data. Map-based attributes provide averaged views on seismic effects and as such are more robust, whereas volumetric attributes can resolve more details and are better suited for stacked reservoirs. Using multiple seismic attributes improves the information content significantly. There is no definite understanding though on how to balance the seismic and production terms in an objective function. Weights are assigned to pieces of data based on calculated error statistics but these are uncertain.

The choice of optimization algorithm depends on the complexity of the problem, more specifically, on the smoothness of the objective function. Combined dataset of production and 4D seismic data usually produces more complex shapes of the objective function for which stochastic, rather than deterministic algorithms, can be more suitable. Stochastic algorithms are designed for global search avoiding local minima. They also better handle the forward problem treating it as a “black-box”, that is no assumptions are made about the structure of the objective function and its differentiability. Particle swarm optimization stochastic method has been shown to work effectively on history matching problems including those with 4D seismic data. The deterministic, most often gradient-based, algorithms on the other hand converge faster. In cases where efficient calculation of sensitivities such as by the adjoint method is possible, the gradient algorithms can be used with large numbers of parameters. Ensemble Kalman filter is an effective method for history matching, especially with production data. Research is undergoing for improving its applicability for 4D seismic history matching.

The parameterisation is another important consideration in a history matching problem. The best strategy here is to find a right balance between the parameters exposed to calibration by the dynamic data, and the imposed prior knowledge. Using too few parameters can results in unique models bearing a significant bias from the structural noise. Using more parameters is preferable if there are means of regularizing the solutions. It was shown that the regularising effect occurs when the solution space is restricted by adding 4D seismic data.

# Chapter 4. Methodology

## 4.1 Introduction

In this chapter we will discuss the realization of the seismic history matching workflow. As discussed in Theory chapter, history matching is an iterative process where model predictions are calculated at every iteration via forward modelling such as reservoir simulation and seismic modelling. These are compared to the observed data in the domains of production data and seismic attributes. The comparison evaluates the goodness of current models and the updated models are suggested by the optimization algorithm. The process repeats until acceptable models (that is fitting data within predefined error level, and also meeting certain conditions on the parameter values such as deviation from prior) are found. These steps are schematically illustrated in Figure 4.1. The focus of the present work is optimizing the integration of 4D seismic data into the history matching process which requires customizing this workflow. In particular, forward modelling of seismic attributes includes calculating of seismic attributes which in this case are represented by the 'coloured inversion' procedure. Both construction of models and preparation of observed seismic dataset require applying the model based inversion which is also implemented here. The process of the automatic history matching is driven by an optimization algorithm which in this case is the particle swarm optimization (PSO) algorithm. Implementation of these processes will be discussed in the subsequent sections.

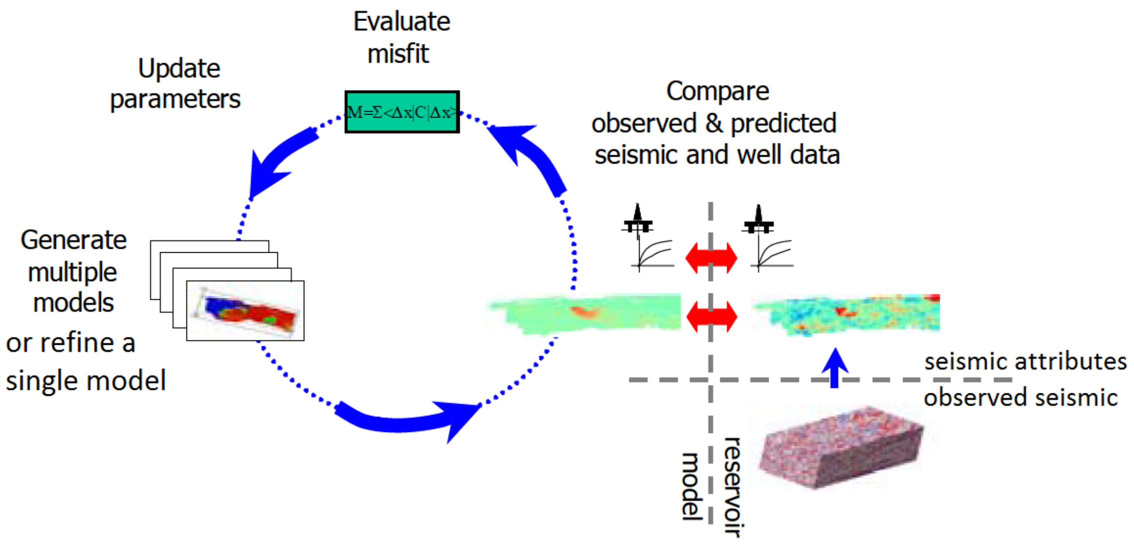

**Figure 4.1. History matching workflow. After *Stephen et al, 2006***

## 4.2 Particle swarm optimization

Both the model based inversion and the history matching workflows are implemented in this work using the particle swarm optimization (PSO) algorithm. PSO is a versatile stochastic algorithm that it is easy to implement and control with only a few parameters. Case studies discussed in the literature review suggest that stochastic algorithms better suit optimization problems where the objective function is more complex as in cases where 4D seismic is combined with production data in history matching. Stochastic algorithms are also capable of global search thus avoiding local minima. The PSO algorithm has many similarities with other population-based techniques such as the Genetic algorithms. However, PSO has demonstrated higher efficiency in many cases when applied to the problems of history matching and seismic inversion (see the literature review). In the following sections, we will discuss the implementation details specific to the present work, illustrating them with examples of application.

### *4.2.1 The algorithm*

The task of history matching (as a process) is finding values of parameters that minimize the objective function. Particular set of values of $n$ parameters can be viewed as a point in $n$-dimensional space (model space). To describe the PSO algorithm, we will call such point a particle $p$ which stochastically moves in the model space with tendency to the best regions. The goodness of a region in the model space is determined by the value of the objective function ($J$) in it – the lower the value, the better the region. The algorithm operates with a population, or a swarm, of such particles. Throughout the life of the swarm, each particle visits a series of locations and always remembers the best visited so far. This quantity is called a local best and is denoted $x_{pbest}$. The best position out of best positions of this particle and of all of its neighbours is called a global best and denoted $x_{gbest}$. Neighbours for any given particle are defined by the topology as described later.

The algorithm starts with initialisation of the swarm by distributing particles randomly in the model space. Subsequently, at each iteration $i$ positions of particles $x_p$ are updated according to their velocities $v_p$:

$$x_p[i] = x_p[i-1] + v_p[i], \tag{4.1}$$

where a velocity $v_p$ is determined by the random function of the distances of the particle from the global best point $x_{gbest}$ and the local best point $x_{pbest}$:

$$v_p[i] = v_p[i-1] + c_1\varphi_1\big(x_{pbest}[i-1] - x_p[i-1]\big) + c_2\varphi_2\big(x_{gbest}[i-1] - x_p[i-1]\big) \tag{4.2}$$

In the above two equations, $i$ is the current iteration, $i-1$ is the previous iteration, $c_1$ and $c_2$ are constants controlling traction to the local best and the global best points, $\varphi_1$ and $\varphi_2$ are realisations drawn from the uniform distribution of random numbers from 0.0 to 1.0. Iteration is defined as a single update of velocities and positions of all particles. It is the philosophy of the PSO algorithm that the particles are being driven at the same time by the intelligence of individual particles (local best) and the population (global best). The former force facilitates exploitation, while the latter – exploration. The balance between exploitation and exploration in the behaviour of the particles is controlled by the parameters $c_1$ and $c_2$ in the above velocity equation. Typical values for the parameters are 2 and 2. Higher $c_1$ will make the algorithm search different places more thoroughly (particles are more independent), while higher $c_2$ will result in faster convergence. Values of these constants do not depend on the range of $x$ (which is, in turn, problem specific) because they express fractions of change of that same $x$.

The above formulation of the velocity equation allows the particle swarm to explode with time as the velocities grow and the oscillations become wider. Different techniques are applied therefore for damping the velocities and keeping the swarm in the "box" such as limiting the maximum velocity or "stopping" at the model space boundaries ($X=X_{max}$, $V=0$ when a particle tries to fly beyond a boundary). The velocity calculation may also be modified. *Shi et al, 1998* proposed using inertia to control the influence of the previous velocity by multiplying it by a time variant constant $w$. The resulting velocity equation becomes:

$$v_p[i] = v_p[i-1]w[i] + c_1\varphi_1\big(x_{pbest}[i-1] - x_p[i-1]\big) + c_2\varphi_2\big(x_{gbest}[i-1] - x_p[i-1]\big) \tag{4.3}$$

The multiplier $w$ linearly decreases with iterations (usually from 0.9 to 0.4). Decreasing $w$ makes the search more exploitative and thus prevents the swarm from exploding. Another method for controlling the level of oscillations is using the constriction coefficient (*Clerc and Kennedi, 2002*). Usually it is a multiplier (0.7-0.8) applied to the final value of the velocity which may improve the social behaviour of the particles. In this work, both the inertia and stopping at boundaries are used.

As mentioned before, topologies are used to assign neighbours for each particle $p$ in the swarm. A global best $x_{gbest}$ for each $p$ is then found by querying its neighbours for their local bests and choosing the best of them. In this way, different $p$ in general will have different $x_{gbest}$ as different $p$ have different neighbours, but since particles are connected, the information about the best of $x_{gbest}$ will eventually spread across the swarm. Neighbours are assigned prior to the run and do not change. Different topologies used in PSO are shown in Figure 4.2. In the circle topology (Figure 4.2, a) any given particle is connected to all other particles but through its two (or more) neighbours. This way the information is transmitted at a slow rate. The information is transmitted fast in the star topology (Figure 4.2, b) which also is called the global best topology. In this case for any given particles, the rest of the swarm will be its neighbours. Too many connections in the star topology may reduce the exploitative ability of the swarm, while too few connections in the circle topology may result in a slow convergence (but usually a better chance of finding the global minimum). The random neighbour topology (Figure 4.2, c) may offer a compromise in terms of the rate of information transmission. For each particle $p$, its neighbours are assigned randomly. The probability of any other particle to become a neighbour of $p$ depends on the desired approximate number of neighbours $Nn$ (chosen by experimenting based on the algorithm performance) and is given by:

$$t = 1 - \left(1 - \frac{1}{Np}\right)^{Nn}, \tag{4.4}$$

where $Np$ is the number of particles in the swarm.

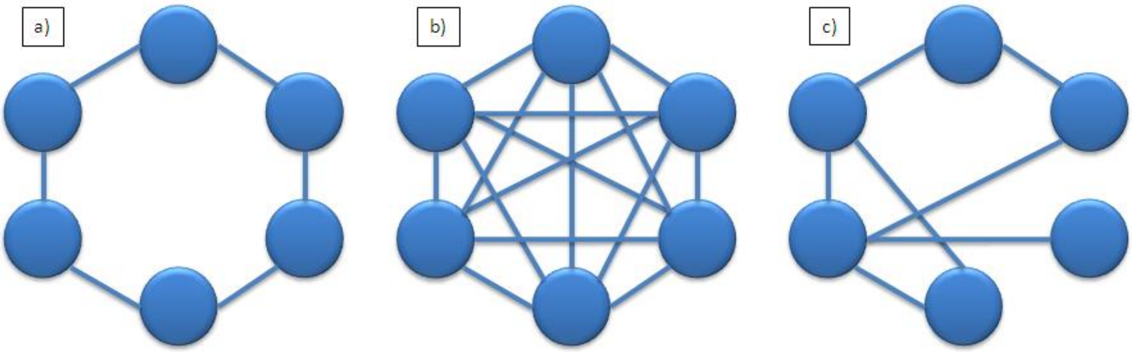

**Figure 4.2. Neighbourhood topologies used in PSO: a) circle, b) star, c) random neighbours**

### 4.2.2 Benchmark case

The following example will demonstrate how the choice of parameters for the PSO algorithm affects its performance. For this example, we will take a typical function which is among others used for benchmarking optimization algorithms, the Griewank function given by:

$$f_G(x) = \left(1 - \prod_{i=1}^{Nd} \cos\left(\frac{mx_i}{\sqrt{i}}\right)\right) + \frac{1}{4000}\sum_{i=1}^{Nd}(mx_i)^2, \tag{4.5}$$

where $m$ is a scaling factor which can be adjusted so that the function's argument spans the representative range of values while keeping $x$ in the interval from -1 to 1. Here $m$ equals 40. The function has multiple local minima modelled by the cosine elementary functions in the first term and a global minimum at $x$=0. The 2-dimensional Griewank function is visualised in Figure 4.3.

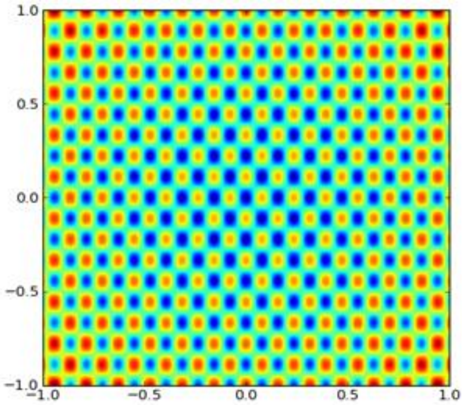

**Figure 4.3. Griewank function in 2 dimensions.**

In the first test, we will examine how the balance between the exploration and exploitation affects the performance of the algorithm. We will use the Griewank function in 2-dimensions (Figure 4.3) to be able to visualise the resulting response surface.

Exploration inclined behaviour is modelled by increasing the parameter $c_2$ relative to $c_1$ so that a traction to the global best point prevails. The exploitive behaviour on contrary is caused by a larger $c_1$ so that the particles are mostly guided by their own experience rather than taking knowledge from the rest of the swarm. Figure 4.4 demonstrates the effect of shifting balance between exploration and exploitation. The parameters $c_1$ and $c_2$ are assigned as follows: (a) $c_1$=0.5, $c_2$=2.0; (b) $c_1$=2.0, $c_2$=0.5; (c) $c_1$=2.0, $c_2$=2.0. Star topology is used in all three cases. Number of particles is 50, number of iterations is 100 (the number of iterations is defined by the convergence of the slowest scenario as discussed below). The values of the misfit function from the resulting ensembles of particles of the three cases, sorted in descending order, are plotted in Figure 4.5. The results in Figure 4.4 and Figure 4.5 are representative examples of the many runs performed in each experiment to make sure the results are not biased by a single stochastic realisation.

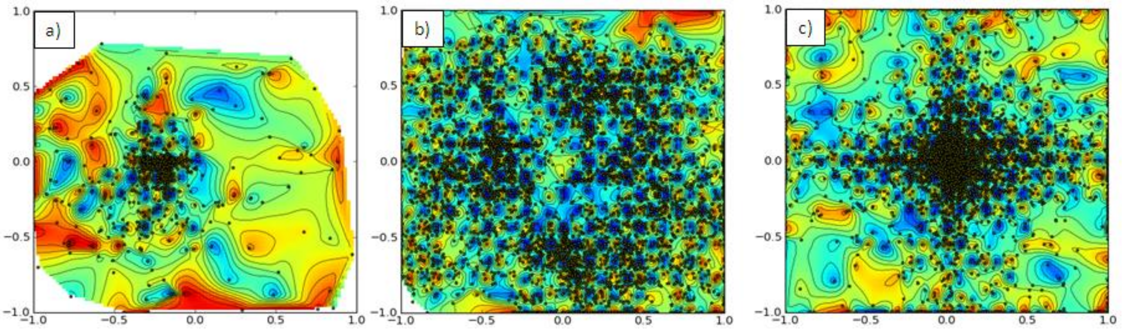

**Figure 4.4. PSO swarms used to find minima of the 2-dimensional Griewank function. A) Exploration inclined, b) exploitation inclined, c) balanced. The coloured map on the background of the particles is built by interpolating values of the misfit function read from the particles themselves, so it represents a response surface. The global minimum is at (0,0).**

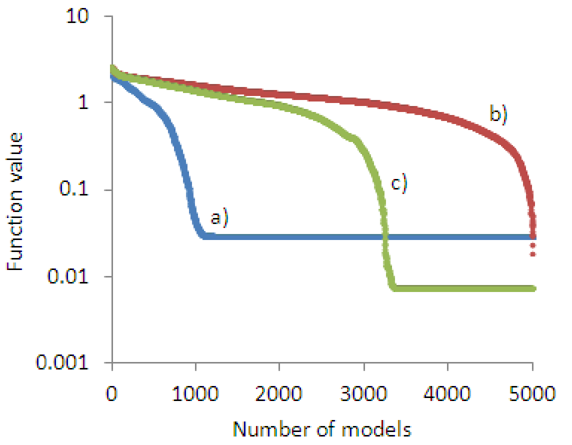

**Figure 4.5. Convergence of the PSO algorithm for the three scenarios shown in Figure 4.4.**

In the exploration inclined case the ensemble of particles converged very quickly to one of the minima minimizing the presence of particles around the map (Figure 4.4, a). The convergence is fast in this case, but not the best solution is found (Figure 4.5). In the next case the particles preferred to follow their own best points, so the swarm could find much more details of the function around the map as shown in Figure 4.4, b, but the convergence rate was too low (Figure 4.5). Balancing the two forces in the third case allowed finding the best solution although more iterations was required than in the explorative case.

The next test demonstrates the importance of the particles' neighbourhood topology in the PSO algorithm. For this test the 40-dimensional Griewank function was chosen because the algorithm demonstrates more stable convergence rates for different topologies in this more complex case. Here we compare the results for the three topologies: star, circle, and random. In each of these runs, the number of particles is 100, the number of iterations is 100, $c_1$=$c_2$=2.0. In the star topology the number of neighbours equals to the number of particles, in both the circle and random, the number

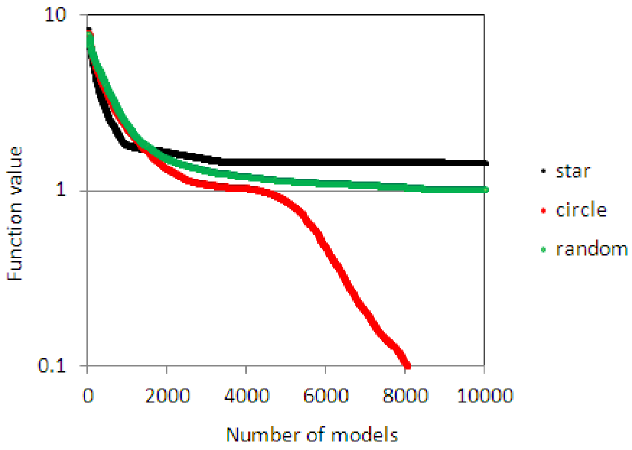

**Figure 4.6. Convergence of the PSO algorithm minimizing the 40-dimensional Griewank function using three topologies: star, circle and random.**

of neighbours is 20. For the circle topology this number of neighbours gave the best result in this case, so the number is used here. In general, the best number of neighbours is problem specific. The values of the objective function were again sorted and plotted for the three cases as shown in Figure 4.6. As mentioned earlier, in the star topology the information about the global best point is transmitted immediately to all the points which adds to the explorative character of the swarm's behaviour. As a result, it converges faster in the beginning, but fails to find the best solution (Figure 4.6, black curve). The circle topology shows the best result here being able to find a solution very close to the global minimum (the values of the objective function are higher in 40D). The random topology shows the result in the middle.

## 4.3 Reservoir simulation

Reservoir simulation was carried out using ECLIPSE100 black oil simulator. The scope of modelling included 3 phase flow in the model reservoir, no surface network constraints were modelled.

## 4.4 Parameterisation of history matching problem

Two types of parameterisation are used in history matching experiments of this work. The first type is based on transmissibility regions formed by geobodies and the second is a method similar to the pilot points method (*Marsily et al, 1984*). The two very different parameterisation schemes are chosen intentionally. As discussed in Chapter 6, the 'geobody' bears a significant amount of prior information which is encapsulated in the shapes of the deterministic objects (geobodies) while the pilot points offer an unbiased modification to the permeability field which relies on the calibration data only (see also section 3.3.2 for a discussion of the balance between the prior information and that from the calibration data).

In the parameterisation based on transmissibility regions, transmissibility multipliers are applied to the transmissibility field either inside the regions or between them. This parameterisation is inspired by using geobodies derived from seismic data as a major heterogeneities controlling the flow in the reservoir (*Martin and Macdonald, 2010*). Such framework of geobodies can incorporate a significant amount of prior information for history matching the simulation models. An example of geobodies distribution is shown in Figure 4.7. When the transmissibility multipliers are applied within the regions, such parameterisation becomes similar to the trivial zonation approach (Literature review, section Parameterization). However, multipliers applied between the regions can effectively model any structural or stratigraphic flow barriers such as faults or shale baffles.

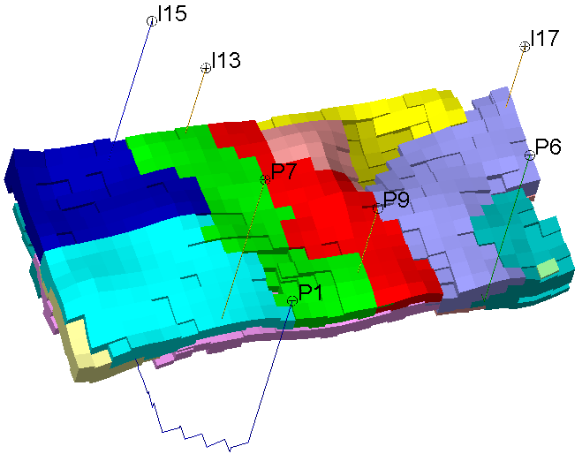

**Figure 4.7. Example of geobodies that serve as transmissibility regions in history matching parameterisation. The colours of the regions signify different indices.**

The second parameterisation scheme aims to modify the permeability field of the model directly. In order to reduce the number of parameters, the property updates are applied at sparse points from which they are interpolated in the volume of reservoir. This method is similar to the well-known pilot point method (*Marsily et al, 1984*). The classical pilot points however use kriging for interpolation while in this work the interpolator is based on the exponential smoothing function because no prior assumptions are made about the statistics of the resulting permeability fields. Because of the obvious similarity of the methods and intuitive perception of the pilot point method, the parameterisation in this work will be called the pilot points throughout the rest of the thesis.

The interpolating function has the following form:

$$k(r) = \sum_{i=1}^{Npp} P_i e^{-\left(\frac{(r-r_i)}{a}\right)^d}, \tag{4.6}$$

where *k(r)* is permeability at a location in space given by the two-component vector *r=[x,y]*, same value of *k* is then applied for the whole thickness of the specified interval (reservoir layers are thin in the examples of this work, so the vertical variation of permeability is modelled by using a separate set of points for, say, lower reservoir), *Npp* is the total number of pilot points, $P_i$ is an individual pilot point located at $r_i$, a is the radius of influence of pilot points, and *d* is decay power controlling smoothness of interpolation.

## 4.5 Petro-elastic modelling

The sequence of rock physics calculations aims to convert the time-lapse changes in pressure and saturation resulting from the reservoir simulation into the changes in seismic velocity and density of rocks. The modelled impedance values can be compared with the results of the seismic inversion in a seismic history matching workflow. Modelling the impedance and seismic velocities of rocks also is a part of the seismic forward modelling process as the variation of the elastic properties defines the reflection coefficients for the seismic waves. The fundamental equations of rock physics used to model the elastic properties are discussed in Theory chapter (section Rock physics foundation of the 4D seismic method). Here we will discuss the computational sequence of modelling the petro-elastic properties in the context of the synthetic seismic modelling. The sequence of rock physics calculations implemented here follows the algorithm presented in *Mavko et al, 1998* and *Mavko et al, 2009*. The choice of this algorithm was inspired by its successful application in works of *Stephen et al, 2006, Edris et al, 2008* and *Kazemi et al, 2010*.

The reservoir rocks are composed of different lithologies, permeable and impermeable, and different fluids saturating them. Modelling elastic properties of such composite media requires rules for calculating their effective properties as the compositions are very complex. In our case, the effective modulus of a combination of different rock types is calculated using the Backus average, the effective bulk modulus of a mixture of fluids by Wood's law, and finally, the effective bulk modulus of the saturated rock is calculated using the Gassmann's equation.

The sequence of the petro-elastic modelling steps as it is implemented in the present work is the following:

*1. Calculate the bulk modulus and density of pore fluids*

Bulk modulus of a fluid mixture $K_f$ is given by the Reuss average (Woods law) (eq. 2.11 in Theory chapter):

$$\frac{1}{K_f} = \frac{S_w}{K_w} + \frac{S_o}{K_o} + \frac{S_g}{K_g}, \tag{4.7}$$

where $K_w$, $K_o$, and $K_g$ are bulk moduli of water, oil and gas respectively and $S_w$, $S_o$, and $S_g$ are saturations of these fluids. Density of the fluid mixture $\rho_f$ is a saturation-weighted average of densities of its constituents (eq. 2.12 in Theory chapter):

$$\rho_f = S_w\rho_w + S_o\rho_o + S_g\rho_g, \tag{4.8}$$

where $\rho_w$, $\rho_o$, and $\rho_g$ are densities of water, oil and gas respectively. The calculation of $K_w$, $\rho_w$, $K_o$, $\rho_o$, $K_g$, $\rho_g$ follows the sequence given in *Mavko et al, 2009*, pages 340-343. The formulae were taken from the source without modifications and therefore are not repeated here.

*2. Calculate the pressure effect on bulk and shear moduli of rock frame.*

Various laboratory measurements indicate the exponential relationship between the rock's moduli and the differential pressure (Theory chapter, section Pressure dependence of reservoir rocks). In this work the following expression for the bulk and shear moduli of rocks is used after *MacBeth, 2004* as shown in *Stephen et al, 2006*:

$$m_{dry,r} = \frac{m_{dry,r,inf}}{1 + E_{v,r}e^{-P_{eff}/P_{v,r}}}, \tag{4.9}$$

where $m_{dry,r}$ is bulk or shear modulus of dry rock $r$. $m_{dry,r,inf}$ is bulk or shear modulus of dry rock $r$ at standard temperature and pressure, $Ev,r$ and $Pv,r$ are the excess compliance present in the rock $r$ as a result of geological or mechanical processes and the stress sensitivity respectively (index $v$ means these are different for bulk and shear moduli), $P_{eff}$ is the differential pressure.

*3. Calculate the saturated sand bulk modulus using Gassmann's formula.*

With the values of fluid's bulk modulus $K_f$ and dry sand (permeable rock) bulk modulus $K_{dry}$ calculated as shown above, the bulk modulus of saturated sand $K_{sat}$ is obtained using the Gassmann's equation (eq. 2.10 in Theory chapter):

$$K_{sat} = K_{dry} + \frac{\left(1 - \frac{K_{dry}}{K_0}\right)^2}{\frac{\varphi}{K_f} + \frac{(1-\varphi)}{K_0} - \frac{K_{dry}}{K_0^2}}, \tag{4.10}$$

where $\varphi$ is porosity and $K_0$ is bulk modulus of mineral grains of sand.

*4. Calculate the effective modulus of the composition of saturated sand and shale.*

For a thin (compared to the seismic wavelength) laminated layer of rock consisting of sand and shale and the seismic wave propagating normal to the layer, the effective modulus $M_{eff}$ is given by the Backus average (*Backus, 1962*):

$$\frac{1}{M_{eff}} = \frac{NTG}{M_{sand}} + \frac{1 - NTG}{M_{shale}}, \tag{4.11}$$

where NTG is net to gross ratio calculated in an element of volume, $M_{sand}$ and $M_{shale}$ are moduli of sand and shale (permeable and impermeable rocks), defined by

$$M_r = K_r + \frac{4}{3}\mu_r \tag{4.12}$$

with $r$ denoting sand or shale. In the last expression, $K_r$ and $\mu_r$ bear the effect of pressure calculated in step 2, and $K_{sand}$ also accounts for the saturation effect from step 3.

*5. Finally, calculate the effective density, velocity and impedance of the composite rocks.*

The effective density $\rho_{eff}$ of a composite rock consisting of saturated sand with porosity $\varphi$ and shale in ratio given by NTG is calculated as a weighted average:

$$\rho_{eff} = NTG\left(\rho_{0,sand} + \varphi\rho_f\right) + (1 - NTG)\rho_{shale}, \tag{4.13}$$

where $\rho_{0,sand}$ is density of mineral grains of sand, $\rho_{shale}$ is density of shale, $\rho_f$ is density of fluid mixture calculated as shown in step 1.

The compressional velocity $V_p$ of seismic waves in effective medium with modulus $M_{eff}$ and density $\rho_{eff}$ is given by:

$$V_p = \sqrt{\frac{M_{eff}}{\rho_{eff}}}, \tag{4.14}$$

from which the $P$-impedance is calculated as:

$$I_p = \rho_{eff} V_p \tag{4.15}$$

The values of petro-elastic parameters used in this work are given in Table 4.1.

**Table 4.1. Values of petro-elastic parameters (after *Stephen et al, 2006* and operator's dataset)**

| Parameter | Value |
|---|---|
| $K_0$ | 37 GPa |
| Oil gravity | 25 API |
| Brine salinity | 0.018 |
| Temperature | 58° |
| $K_o$ | 1.17 GPa |
| $K_w$ | 2.58 GPa |
| $K_g$ | 0.04 GPa |
| $K_{dry,inf,sand}$ | 7.17 GPa |
| $\mu_{dry,inf,sand}$ | 4.51 GPa |
| $K_{dry,inf,shale}$ | 18.09 GPa |
| $\mu_{dry,inf,shale}$ | 5.16 GPa |
| $E_{v,sand}$ | 1.0 |
| $P_{v,sand}$ | 4.0 MPa |
| $E_{v,shale}$ | 1.0 |
| $P_{v,shale}$ | 4.0 MPa |

## 4.6 Seismic modelling

The seismic modelling is used in this work to predict the seismic response of the reservoir simulation models. The result of seismic modelling is interpretable seismic attributes which are then related to the effects of lithology variation and also the dynamic effects of the pressure and saturation change. AVO (amplitude versus offset, see *Yilmaz, 2001*) effects are not modelled in this work because a) the modelling of

AVO adds complexity to the workflow which requires closer reference to the field data, and b) an extra uncertain modelling step will only add unknowns to the relationship between the simulation model details and those in seismic attributes which is the subject of this study (studying such seismic-related effects is an interesting topic on its own and is seen as one of the ways of extending this work).

The seismic forward modelling is based on 1D convolution model (more details in Theory chapter). The Earth's impulse response is viewed as a sequence of reflection coefficients *r(t)* which is convolved with the seismic wavelet *w(t)* to obtain the seismic response *x(t)*:

$$x(t) = w(t) \otimes r(t) \tag{4.16}$$

The time series *r(t)* represents a sparse sequence of spikes $R_{i,i+1}$ separated by zeros. Each spike has a magnitude of a reflection coefficient calculated at the boundary of media *i* and *i+1* with contrasting impedance. In an assumption of normal incidence of the seismic wave, the reflection coefficient is given by:

$$R_{i,i+1} = \frac{I_{i+1} - I_i}{I_{i+1} + I_i}, \tag{4.17}$$

where $I_i$ and $I_{i+1}$ – P-impedances of media *i* and *i+1*. The distributions of P-impedance and P-velocity are calculated using the petro-elastic model as shown in the previous section. The positions of spikes on a reflectivity series *r(t)* correspond to points where a normal incidence seismic ray intersects cell boundaries of the simulation grid as shown in Figure 4.8. The term seismic ray is an abstraction for illustrating how a point belonging to a spherical front of the seismic wave travels through the Earth. All seismograms of a seismic survey are modelled as being recorded by zero offset receivers, i.e. as if the

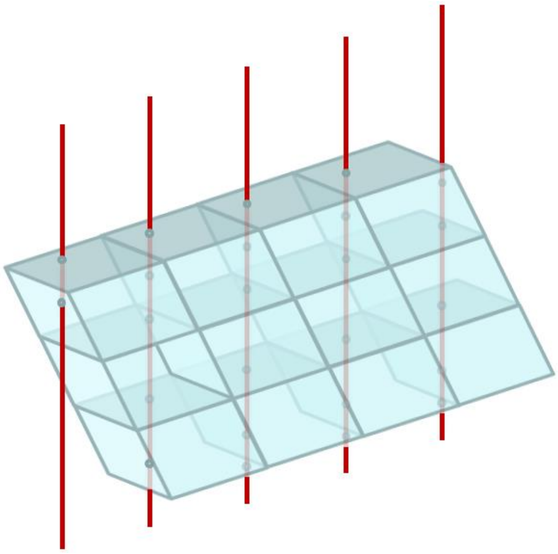

**Figure 4.8. Rays of normal incidence crossing the simulation grid. Coordinates of reflectivity spikes on the rays are given by blue points of intersection.**

source and the receiver for each trace were located at the same point. The subsequent modelling steps are illustrated in Figure 4.9. Using the points of intersection from the previous step, values of impedance and velocity are read from the simulation grid. These are used to calculate the reflection coefficients and position them onto the trace *r(t)* according to the two way time (TWT) coordinate of each point, given by

$$TWT_i = \sum_{j=0}^{i} \frac{2 * \Delta z_j}{V_j}, \tag{4.18}$$

where $TWT_i$ is the TWT coordinate of the $i_{th}$ simulation layer with $TWT_0$ being the coordinate of top of the grid defined by $\Delta z_0$ – depth of the grid top, and $V_0$ – velocity in overburden, $\Delta z_i$ is the distance between two vertical points in the grid. The resulting trace *r(t)* finally is convolved with the seismic source wavelet *w(t)*. In this work the wavelet is modelled by the Ricker formula which gives an approximation to the explosive seismic source (*Yilmaz, 2001*):

$$w(t) = (1 - 2\pi^2 f^2 t^2) e^{-\pi^2 f^2 t^2}, \tag{4.19}$$

where *f* denotes seismic dominant frequency which is taken as 30 Hz here.

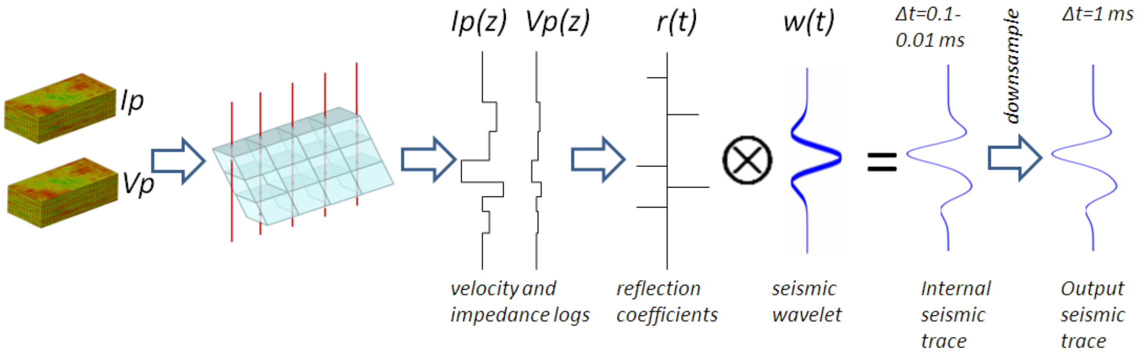

**Figure 4.9. Sequence of steps for seismic forward modelling based on 1D convolution model.**

We should not forget that it is important to ensure fine enough time step between the samples in *r(t)*. The problem is that the distance between the spikes in *r(t)* is measured in discrete samples while they are in fact separated by time intervals of continuous length. If the time distance between the two successive spikes is less than the sample time step, the two (or more) spikes will fall onto the same sample. Because the spikes are recorded sequentially, only the last one will survive. The net result will be losing spikes as illustrated in Figure 4.10, a. The reflections in this section are rather chaotic because the spikes are lost regardless of their magnitude – large spikes can be as well ‘eaten’ by even the tiniest ones if they happen to follow them. The problem is resolved when finer sampling is used as shown in Figure 4.10, b.

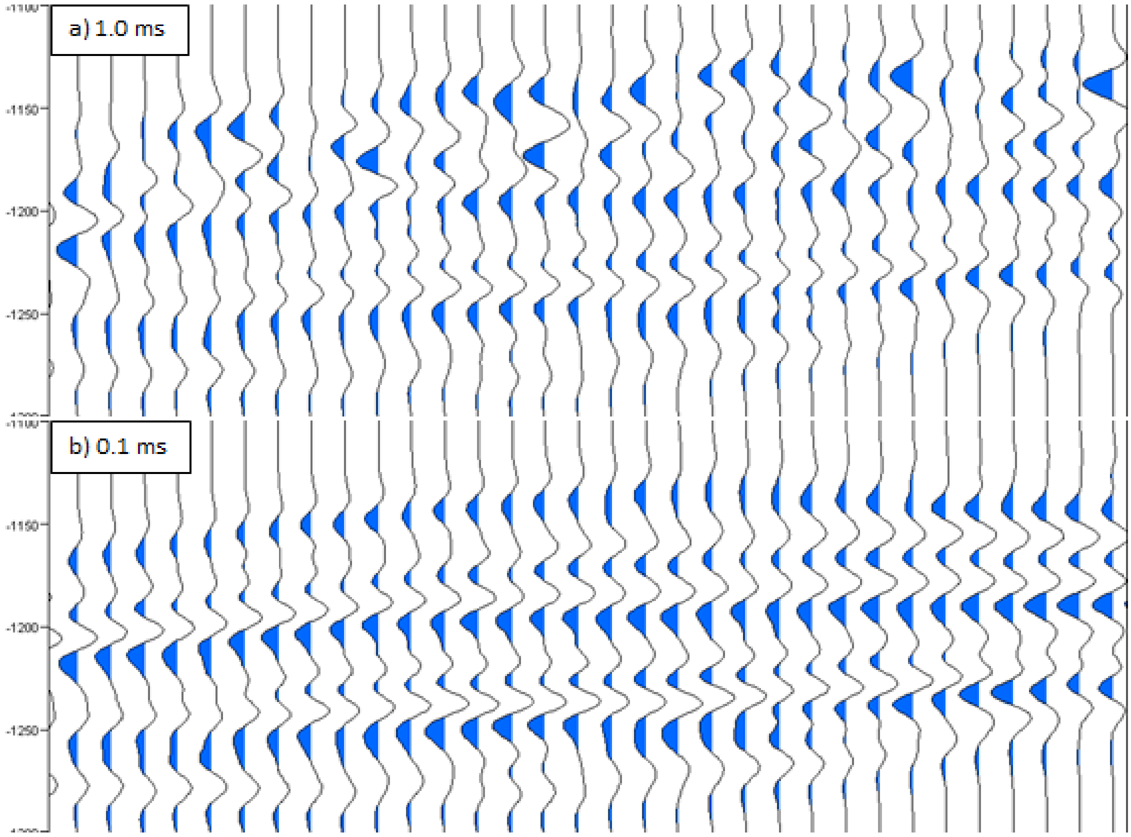

**Figure 4.10. Two seismic sections modelled with different time resolutions of *r(t)*: a) 1.0 ms, b) 0.1 ms.**

After the *r(t)* trace is convolved with the seismic wavelet, it can be downsampled back to typical sampling rates of seismograms recorded in the field (1-2 ms) as shown in Figure 4.9.

## 4.7 Seismic inversion

The seismic inversion is used to estimate elastic properties of rocks such as, in simpler cases, acoustic impedance or relative impedance. These can be compared to predictions of impedance change by simulation and petro-elastic models in the course of history matching which is a focus of the current work. Different options exist for the seismic inversion as described in Theory chapter. Here, we will use the coloured inversion algorithm and a model-based stochastic inversion driven by the particle swarm optimization algorithm.

### *4.7.1 Coloured inversion*

The coloured inversion procedure results in shaping the spectrum of seismic data to match that of the impedance logs, and also in a constant phase shift of -90° (Theory chapter). This can be achieved by convolving the seismic traces with a specifically designed filter *h(t)*. The first step is calculating the amplitude spectrum of the filter, *H(f)*. The multiplication of *H(f)* with the spectrum of seismic traces, *X(f)*, should give the shape of spectrum of impedance logs, *I(f)*. This is equivalent to multiplying a normalised spectrum of seismic data by the spectrum of impedance logs. *X(f)* can be normalised by the average spectrum of all traces in the survey, $\overline{X(f)}$ . This will result in an estimate of the 'coloured inverted' seismic spectrum $X_{CI}(f)$ of the following form:

$$X_{CI}(f) = \frac{X(f)}{\overline{X(f)}} * I(f), \tag{4.20}$$

from which the spectrum of the filter *H(f)* is:

$$H(f) = \frac{I(f)}{\overline{X(f)}} \tag{4.21}$$

The amplitude spectrum of impedance logs can be characterised by a single parameter $\alpha$ from the approximate relationship $I(f)=f^{\alpha}$ (*Lancaster and Whitcombe, 2000*). This parameter characterizes the impedance distribution of rocks in a particular field and should be estimated from the analysis of well logs. An example of estimation of the parameter $\alpha$ is illustrated in Figure 4.11. Three impedance logs were taken at arbitrary locations in a synthetic impedance model (Figure 4.11, a), and their spectra were plotted on log scale (Figure 4.11, b). The slope of a best fitting line gives the parameter $\alpha$.

With the above power law approximation of the impedance spectrum, the spectrum of the filter finally reads:

$$H(f) = \frac{f^{\alpha}}{\overline{X(f)}}. \tag{4.22}$$

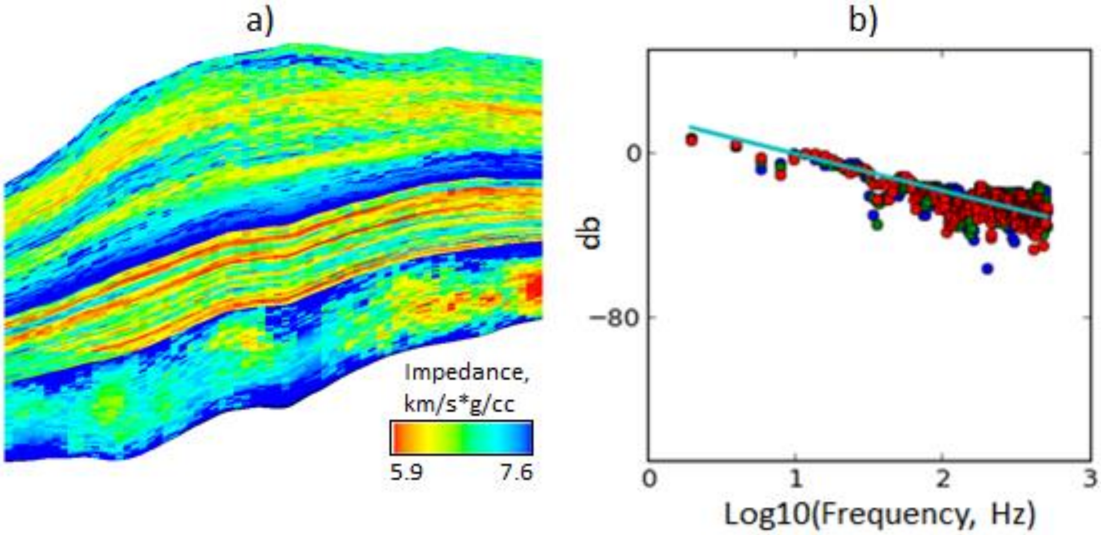

**Figure 4.11. Estimation of parameter *α* from values of spectrum of impedance logs: a) impedance distribution in synthetic model, b) spectra of three (marked by red, green and blue dots for distinction) impedance logs from arbitrary locations in synthetic model. db indicates attenuation in decibel (db=20lg(A), where A is displayed quantity).**

The simplest option for the implementation of our filter *h(t)* with the required frequency response *H(f)* will be designing a finite impulse response filter (finite duration, no feedback) by the window method (*Parks and Burrus, 1987; Ifeachor and Jervis, 2002*). The main steps of the method are following:

1. Define the desired frequency response $H_D(\omega)$
2. Calculate the ideal infinite impulse response $h_D(t)$
3. Multiplying it by a window function to get a finite impulse response coefficients *h(t)*.
4. Verify if the frequency response of *h(t)* satisfies the requirements.

The notation *D* in the above means desired or ideal which will differ from the actual outcome as further explained.

Following the steps of the method, we will set $H_D(\omega)$ to the spectrum we need (the last expression for *H(f)*). In order for our filter to be real valued, its spectra must be conjugate symmetric. In particular, the positive and negative parts of the imaginary part of the spectrum must be antisymmetric. We also want our filter to give -90° phase shift which means it has to be a filter of type 4 – even number of samples, antisymmetric (*Parks and Burrus, 1987*). The second step is the analytical calculation of the infinite (defined on $-\infty<t<\infty$) impulse response of $H_D(\omega)$. In cases like ours, the analytical expression for $h_D(t)$ can not be obtained because $H_D(\omega)$ is of arbitrary form. In such cases we have to use an approximate calculation using the inverse discrete Fourier transform (IDFT) (*Ifeachor and Jervis, 2002*). The third step is the essence of the window method. If we just took the infinite signal $h_D(t)$ and truncated it (or just took the output of IDFT), we certainly would get a finite version of the filter but that would have had very bad frequency response. The reason for it is the Gibbs's phenomenon which we will demonstrate by calculating the frequency response of the truncated filter.

Truncating the infinite signal is equivalent to multiplying it by a rectangular window with ones inside the window and zeros outside, so that the finite impulse response becomes:

$$h(t) = h_D(t)w(t), \tag{4.23}$$

where $w(t)$ is a window function. If we now calculate a frequency response of $h(t)$, we get the following expression in the frequency domain:

$$H(\omega) = H_D(\omega) \otimes W(\omega), \tag{4.24}$$

because multiplication in the time domain is convolution in the frequency domain. This shows why the notation $D$ was used: the desired ideal response $H_D(\omega)$ is different from $H(\omega)$ as the former is inevitably convolved with $W(\omega)$ – frequency response of the window making the filter finite. $W(\omega)$ for the rectangular window is known to be the classic sinc function. Convolving the sinc function with the $H_D(\omega)$ adds ripples to the latter as illustred in Figure 4.12.

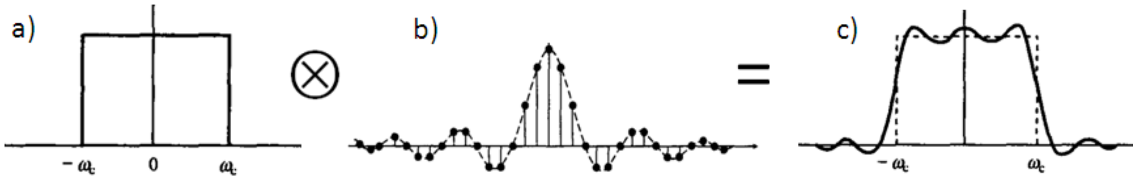

**Figure 4.12. Illustration of the Gibbs phenomenon: a) frequency response of ideal low pass filter, b) frequency response of rectangular window function, c) frequency response of finite (truncated by the rectangular window) low pass filter. After *Ifeachor and Jervis, 2002***

The idea of the window method is to replace the rectangular window by a window without sharp edges at its ends. Kaiser window (*Kaiser, 1966*) is an example which has tapered ends with a shape controlled by a single parameter $\beta$ (Figure 4.13). Tapered ends of the window reduce side lobes of its frequency response which reduces the ripples at the expense of the width of the transition zone though. This is illustrated in Figure 4.14 – the frequency response of a 10-80 Hz band pass filter has ripples when it is truncated by a rectangular window (Figure 4.14, a). These are removed when it is multiplied by the Kaiser window instead of the truncation (Figure 4.14, b), and the resulting response is slightly wider. The Kaiser window is chosen because it provides a parameter (*β*) for balancing the amount of ripples (side lobes level of its frequency response) and width of the transition zone (main lobe level).

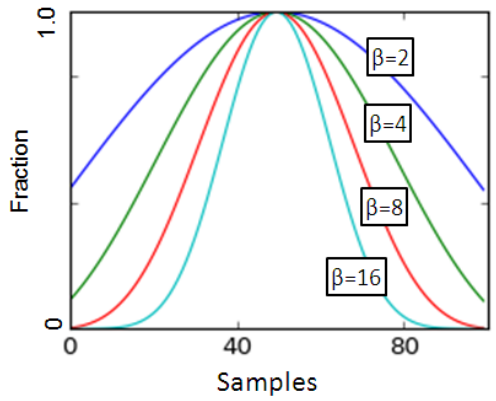

**Figure 4.13. Kaiser windows with different β**

The filter coefficients *h(t)* were calculated by applying the IDFT on $H_D(\omega)$ and multiplying the result by the Kaiser window. *h(t)* is shown in Figure 4.15, a and its frequency response in Figure 4.15, b. The frequency plot shows that the actual spectrum of the resulting filter (shown in green) is very close to the one we requested (blue), that is the one given by *H(f)* above.

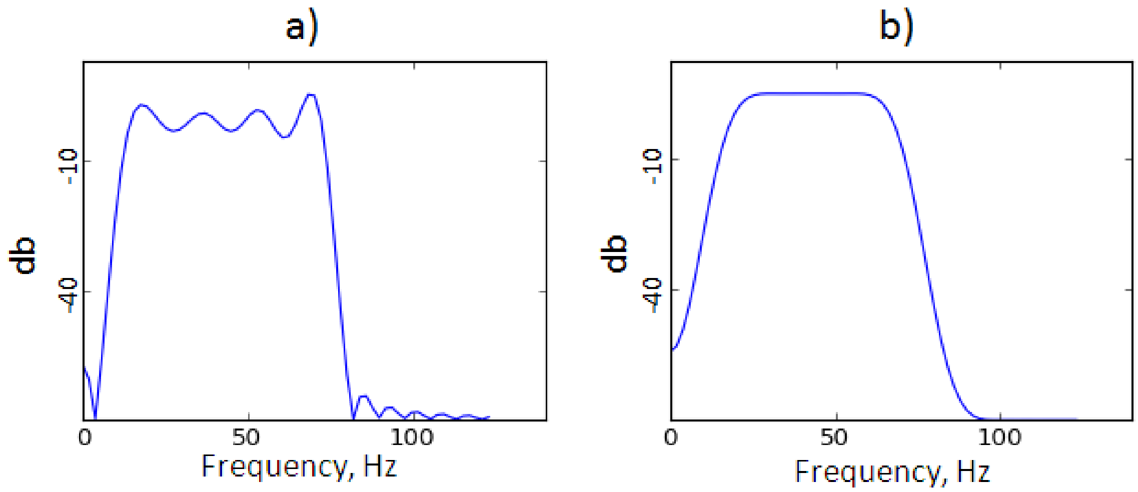

**Figure 4.14. Frequency response of finite 10-80 Hz band-pass filter: a) filter truncated in time by a rectangular window, b) Kaiser (β=8) window used instead of the rectangular. db indicates attenuation in decibel.**

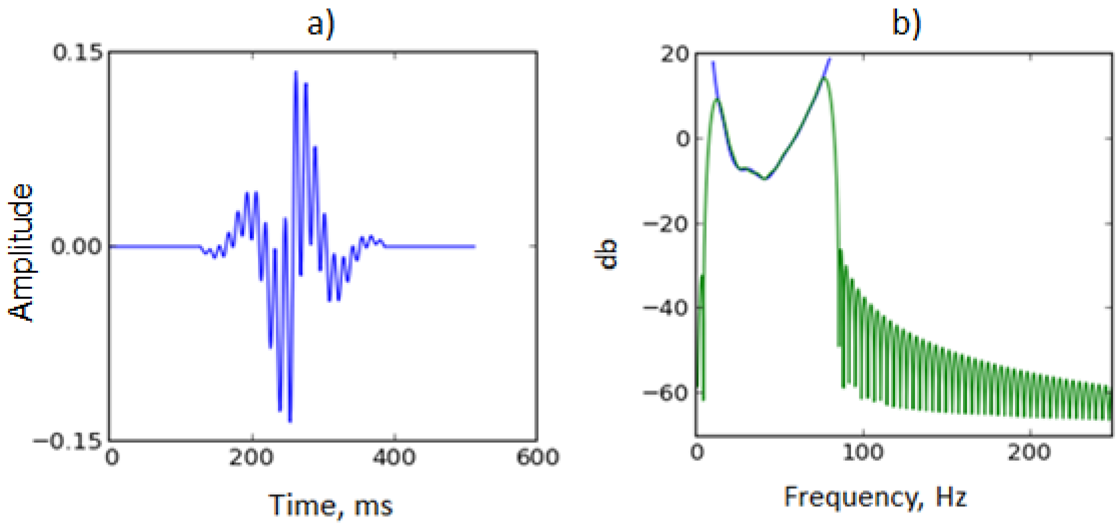

**Figure 4.15. 'Coloured inversion' operator: a) filter *h(t)* in time domain, b) frequency response of *h(t)* in green and the desired frequency response $H_D(\omega)$ in blue. db indicates attenuation in decibel.**

As follows from the filter specifications, its application leads to -90° constant phase shift and shaping the spectrum of seismic data to match the impedance spectrum. This does not alter the frequency content of data but it does change its visual appearance making the section easier to interpret by human. Coloured inversion and a quadrature amplitude (-90° constant phase shift only) attributes has been useful in reservoir characterisation and interpreting 4D seismic data (*Johnston, 2013*). Figure 4.16 compares the seismic section (a) calculated with the impedance model from Figure 4.11 with the band-limited version of that impedance (b) and the coloured inversion (c). The band-limited impedance is calculated by applying 10-80 Hz filter with frequency response shown in Figure 4.14, b. The purpose of this comparison is to illustrate the effect of applying the coloured inversion by operating with the following terms: section (a) is the observed seismic data, (b) is the ideal or reference solution for impedance against which the coloured inversion results (c) are compared; (c) is calculated from (a); (b) is not calculated from (a) but rather (b) is a source for (a). In a real situation, the section (b) obviously is not available as we do not know the precise impedance. It is the goal of seismic inversion to get an estimate of it. As the results show, although the coloured inversion technically does not calculate the impedance values, it does enhance the look of the seismic section so that it can be used as an estimate of the band-limited impedance for fast track interpretations.

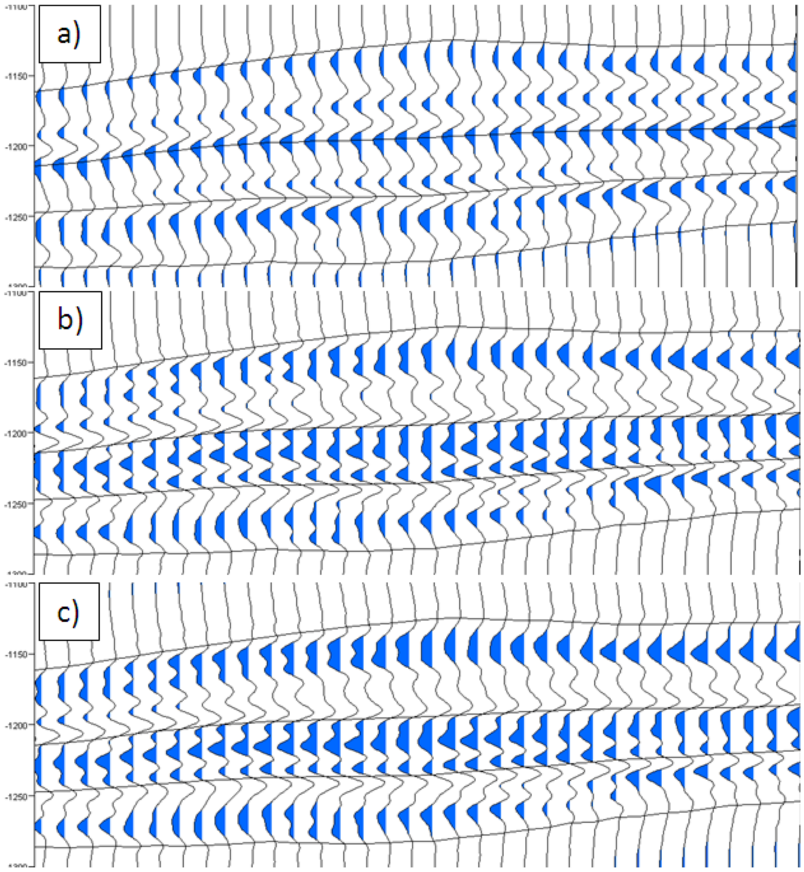

**Figure 4.16. Comparison of (a) seismic section, (b) band-limited impedance, and (c) coloured inversion calculated using the impedance in Figure 4.11. The lines trace boundaries of formations which in the model (in depth) correspond, from top to bottom, to formations T35/T34, T31a, and T31b of the Schiehallion field which is described in Chapter 5.**

### *4.7.2 Model-based inversion*

Model based inversion performs search through models of a certain type to find those fitting the data. The models reflect our assumptions about the reservoir architecture such as blocky layers of impedance or minimal structure modelled by sparse spikes (see Theory chapter, section Seismic inversion for more details). In any case, the aim of introducing models to the model-based seismic inversion process is reconciling the band-limited information from the seismic data with components from other sources of information and a priori knowledge. The results of the inversion are impedance models which can be compared to the simulation model predictions in the seismic history matching workflow. Also, by inverting the baseline survey, we can infer the NTG distribution. These are the reasons for implementing the inversion in this work.

The target of the inversion in this work is distribution of NTG or 4D impedance change models consistent with data. We will use a stochastic algorithm because it is a better choice for finding different realisations of models fitting the noisy data. One common way of parameterizing the inversion is dividing the model into a number of layers, so that the inversion parameters are *P*- and *S*- velocities, density and time thickness of each layer (*Cooke and Cant, 2010*). This approach has drawbacks for using in our problem as further explained. If several steps are taken in the inversion, such as inverting for velocity and density properties in time and then rescaling them onto the simulation grid, then errors are introduced due to the finite discretization of the latter. Here, an alternative scheme is used therefore. The seismic data are inverted for the NTG property (NTG inversion) or impedance and *P*-velocity properties (4D impedance inversion) on the simulation grid directly. This takes away the need for a time to depth transform in the future. The result is a model of NTG or impedance and *P*-velocity in depth which fits the data as much as possible. *S*-velocity inversion is not performed as shear velocity usually is noisy and poorly constrained by the seismic data (*Johnston, 2013*), moreover, excluding it from the process simplifies the calculations (*Cooke and Cant, 2010*).

The parameters of the inversion (values of NTG or 4D impedance depending on the inversion type) cannot be just assigned to all of the simulation layers because different regions of the model require different number of parameters if any at all. Therefore, the parameters are assigned according to a layering which is defined (for example interactively) as an integer property of the simulation grid and used as an input for the inversion algorithm. This way, any deterministic information can be incorporated into the model such as impermeable streaks, pinch outs, different numbers of layers per parameter, etc.

Two types of inversion are used in this work: inversion for NTG and inversion for 4D impedance change ($\Delta I$) in each layer. These take different approaches:

In the case of NTG inversion, NTG values are parameters. They are assigned to the grid cells according to the parameter index property described above. Then petro-elastic and seismic models are run to determine the data fit.

In the case of 4D impedance inversion, density is taken as being a linear function of velocity. *Gardner et al, 1974* demonstrated a linear relationship between these quantities which is often used in inversions because the density itself is poorly constrained by the seismic data *(Cooke and Cant, 2010*). Using the values of impedance update (4D impedance change) $\Delta I$, velocity at base survey, $V_0$, and the proportionality constant linking the density and velocity, $k$, a velocity update $\Delta V$ is obtained by:

$$\Delta V = \Delta I \frac{k}{2V_0} \tag{4.25}$$

In the derivation of the above expression, the second order velocity change is neglected.

The calculated updates of impedance and velocity are added to the base survey's impedance and velocity (which are calculated with inverted NTG) to obtain the values of these properties at the monitor survey time. Finally, the seismic forward models are calculated from both surveys and differenced to obtain the 4D seismic difference cube. The 4D difference traces are compared with observed data to obtain the misfit value to proceed to the next iteration with a new update $\Delta I$. The algorithm used for the inversion is the particle swarm optimization algorithm (discussed in more details in the next section). This way the inversion essentially is looking for suitable updates for the existing (base survey) impedance rather than an independent solution. It is not independent because the seismic difference depends not only on $\Delta I$ but also on the underlying geology. However, we will examine how sensitive it is to NTG later.

### *4.7.3 Effect of the prior term*

The effect will be demonstrated on an underdetermined inversion where 32 parameters are estimated from a 40 ms seismic signal. Figure 4.17 compares the results of the inversion without prior term (panels a and b) and with prior term (panels c and d). The panels a and c show how far the inverted solution is from the true impedance, and the panels b and d show how the final models' predictions fit the data. The prior term is the square of the difference between the current solution and the prior solution. The latter is constant 0, that is no 4D impedance change.

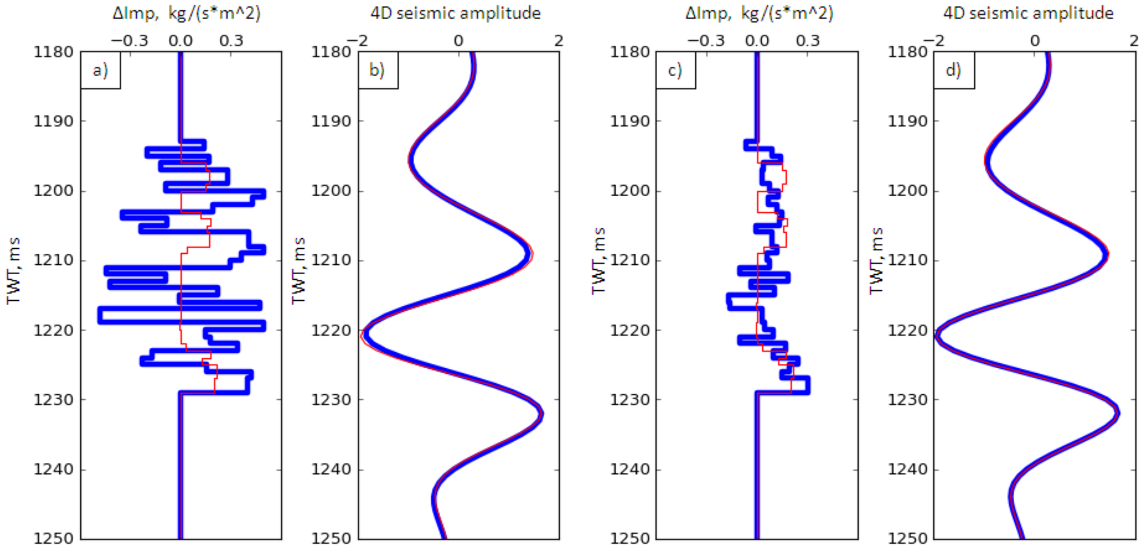

**Figure 4.17. Comparison of inversion without prior (panels a and b) and with prior (panels c and d). Panels (a) and (c): true ΔImp in red and inverted ΔImp in blue. Panels (c) and (d): observed 4D seismic trace in red and predicted by the inversion final model 4D seismic trace in blue.**

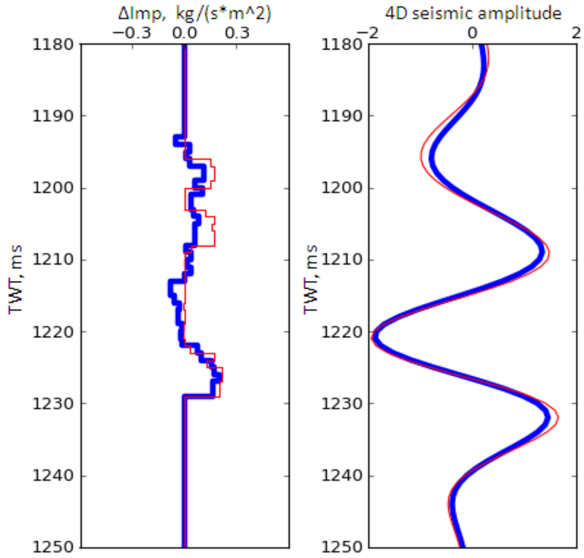

**Figure 4.18. Results of inversion with more weight given to the prior term. Notations are same as in Figure 4.17.**

Clearly, the prior term has improved the solution as shown in Figure 4.17, c. It has done so by forcing the algorithm to choose the minimal and smoothest solution out of many fitting the data. Should we wish to go further with smoothing the solution, at some point, we will have to sacrifice the data fit as shown in Figure 4.18. When fitting the real noisy data though, the remaining misfit is determined by the level of noise, which means in practice we will opt for a smoother solution and imprecise data fit to avoid fitting the noise.

### *4.7.4 The common in coloured inversion and model-based inversion*

In the previous example, the need for strong regularisation was caused by the large number of parameters which could not be independently resolved from 4D seismic data alone due to their scale. Then how complex a model should be in order to take advantage of the information from seismic data? The answer depends on the target model. If we want our model to obey certain geostatistical laws, flow simulation constraints, or to end up in any other desirable form then the complexity of the model (number of parameters estimated in the inversion) most likely will be determined by other factors than the seismic resolution. On the other hand, if the target of the inversion is an interpretable impedance model on its own then we would choose fewer layers in that model, e.g. 10-20 ms per layer. In either case, we would like to illustrate the scale of the impedance changes which is determined by the seismic data which can be done by filtering the impedance in the seismic bandwidth as shown in Figure 4.19. Panel (a) shows the full bandwidth true and inverted impedances, and panel (b) shows the band-limited versions of these (red and blue curves). In addition, the coloured inversion curve is shown for comparison. It is easier to see this way that the differences between true and inverted impedances in panel (a) are only in high frequencies, whereas the band-limited versions of them agree very well (Figure 4.19, b). Another observation is that the coloured inversion provides an adequate estimate of the band-limited impedance without the complications of the model-based inversion process.

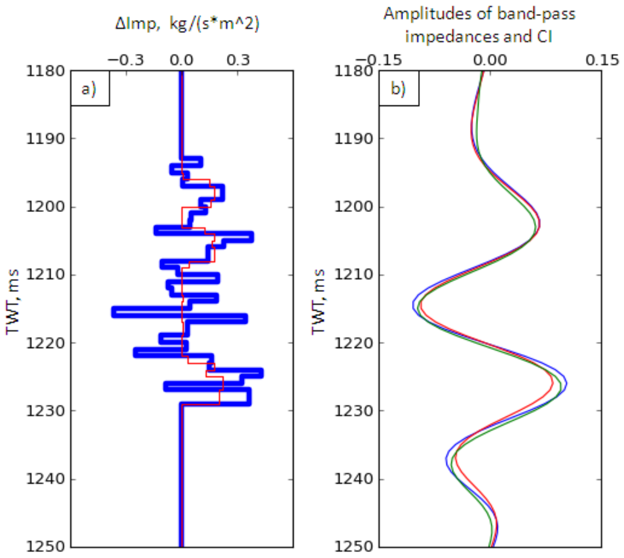

**Figure 4.19. Full bandwidth impedances (a) and band limited impedance estimates (b). A) true ΔImp in red and inverted ΔImp in blue, b) band-limited versions of true ΔImp in red and inverted ΔImp in blue, result of coloured inversion in green.**

## 4.8 Parallel computation

It is the characteristic of stochastic algorithms that many evaluations of the objective function may be required in order to find an acceptable solution. Each function evaluation is a forward modelling run such as reservoir simulation and seismic modelling in history matching or just modelling of a seismic trace in seismic inversion. Whether a single function evaluation is costly (in terms of the computation time) or not, parallelizing the computations on the entire ensemble of models can provide a significant gain in efficiency.

In a problem where a stochastic optimization algorithm is used, the parallelization can be adopted at different levels, of which we will discuss two used in the present work. The first is parallel computation of the individual models during the history matching. In the context of the PSO, each particle evaluates the function at every new location as it stochastically moves in the model space, so the ensemble of such particles can be divided between the computational units of a parallel system. Within one iteration of the PSO algorithm, the particles are fully independent. They need to exchange information when moving to the next iteration though – the value of the global best point is needed to update the velocities. Here, we have two options. The first is to synchronize at the end of each iteration so that the global best is calculated over the entire ensemble and communicated to all the computational units. The second option is for the computational units to proceed with global best available so far without waiting for the slower units to complete their iteration. This option may provide a speed gain but at a cost of added complexity of the implementation and imprecise global best, which is why the first option was chosen in this work.

The second level for parallelization is used for the model-based seismic inversion problem in this work. Because the inversion algorithm used here operates on a single seismic trace at a time, the inversion of all the traces in a seismic cube can easily be parallelized. This way the PSO algorithm is applied on each trace and all the particles are calculated by a single computation unit within a reasonable time as the forward modelling of one seismic trace is not expensive using the 1D convolution method. There is no need to communicate the results of inversions between the units, so they can be stored on the disk and combined in the end of the process.

Parallelization of computations is implemented using the Message Passing Interface (MPI) because it provides the ability to operate with distributed memory systems which is convenient for parallelization on the level of entire models such as simulations of seismic forward models. MPICH2 (on Windows PC) and OpenMPI (on Linux cluster) implementations of MPI were used. The libraries are linked to the main program using the C++ header “mpi.h”.

The MPI functions facilitate communication between processes which in turn need to be physically created and run in parallel to achieve the goals of parallelisation. This part was implemented by using a multi-core processor (on Windows PC) or a cluster of processors (Linux cluster). In the latter case, a cluster of 40 processors was available for this study. As described above, the particles of the PSO algorithm were spread across the available processors for individual computation in the case of history matching. In the case of seismic inversion, each processor performed a complete PSO run on designated seismic traces.

# Chapter 5. Seismic response study

## 5.1 Introduction

Seismic modelling creates a link between reservoir simulation studies and 4D seismic data analysis. As such it is used in predicting 4D seismic effects in 4D feasibility studies before the survey, as well as in interpretation of the results of those surveys. Model-based interpretation of the 4D seismic signature is based on our understanding of the geology, rock physics and the underlying processes in the reservoir. Therefore, regardless of the application of the seismic modelling, we should understand the resolution limits of the seismic attributes controlling whether or not the production related effects that we study are detectable on the seismic data. For this purpose, a range of models and scenarios of pressure and saturation changes with their seismic responses are studied in this chapter. The outcomes of this study will be used in the forthcoming chapters for interpreting the results of seismic history matching.

The method used for this study is similar to that applied in 4D feasibility studies. These aim to predict the chances of success of 4D surveys based on the expected magnitudes of changes of the petro-elastic properties and the resulting 4D signatures. The usual input for such seismic modelling studies is rock physics data, properties of fluids, production data and seismic survey parameters (e.g. timings). In this work these data are borrowed from the Schiehallion field dataset used here as a template field. Using data from the template field dataset will create a modelling framework facilitating a feasible problem set up to model a variety of scenarios of hydrocarbon displacement.

## 5.2 Schiehallion field overview

The Schiehallion field is a deepwater offshore field situated on the Atlantic margin of UKCS, approximately 175 km to the west of the Shetland Islands in the North Atlantic Ocean (Figure 5.1). It was discovered in 1993, and oil production commenced in July 1998. The peak production achieved at 190 mb/day. The water injection scheme has operated from the start of development. Total recoverable reserves of the Schiehallion field together with the Loyal satellite are 350-500 million barrels.

Net sand distribution in the reservoir was mapped using the amplitude attributes and inversion products of the 3D seismic data. First 3D seismic survey was acquired in 1993 which was followed by a second higher specification survey acquired in 1996. 4D monitor surveys were shot in 1998, 2000, 2002, 2004, 2006, and 2008. 4 years interval between the baseline survey and the first monitor (1998-2002, the pair processed together) allows the water front to progress and be effectively detectable as discussed in section 3.4.5.

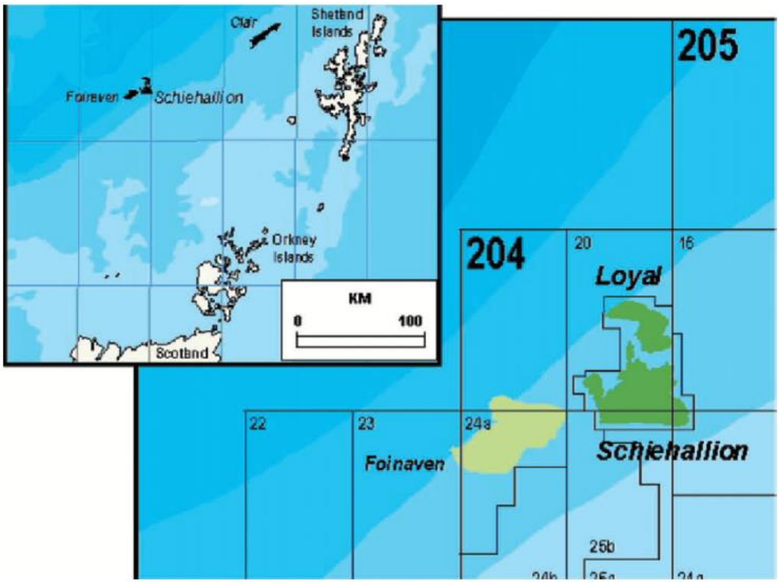

**Figure 5.1. Location of the Schiehallion field.**

Hydrocarbon reserves are associated with a Palaeocene deep marine complex of channelized sands T25/T28, T31, T34, and T35 (in age) with the unit T31a accounting for 60% of hydrocarbon volume. The reservoir sands are mostly noncemented, fine to medium grained with high porosity (23-32%) and permeability (600-1600 mD). The reservoir is compartmentalised and heterogeneous consisting of stacked turbidite channel sands 10-50 m thick (Figure 5.2). The reservoir depth is 5905-6772 ft. The geometry of channels varies across the field with smaller, more confined channels with poorer connectivity situated in the eastern part, broad channels in the middle, and sheets of sands in the western part. Poorer than expected connectivity of the reservoir and limited aquifer support made the injection levels insufficient to support the reservoir pressure in early stages of the development. The resulting pressure depletion caused gas liberation from the oil with the bubble point pressure close to the initial pressure. The period 1998-2003 of production therefore is marked by high GOR values, and also, the 4D seismic data bear clear signature of gas effects.

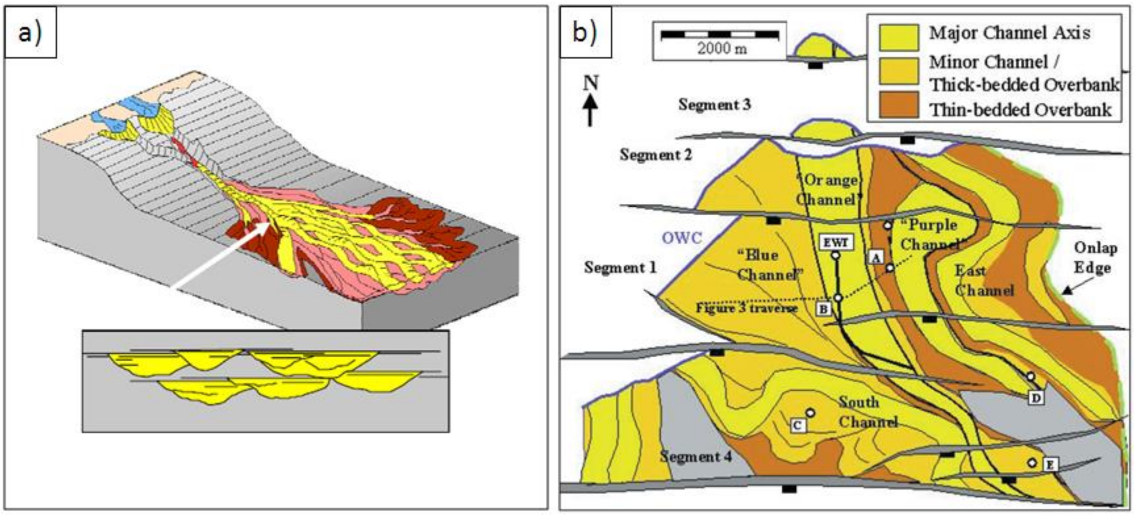

**Figure 5.2. Conceptual geological model of turbidite sands of the Schiehallion reservoir (a), and facies map of the T31a sand above the oil-water contact (b). After *Leach et al, 1999, Govan et al, 2006*.**

The bubble point pressure is close to the initial reservoir pressure of 2907 psi at datum depth of 1940 m TDVSS. The oil is medium oil with gravities of 22-26 API, viscosities in the range of 1.5-4.5 cP due to high wax content, and gas oil ratios of 340-380 scf/bbl (*Leach et al, 1999; Richardson et 1997; Govan et al, 2006, Dijksman et al, 2007*).

Geological and simulation models built by the field's operator benefited from the good quality of seismic data well imaging the shallow (2000 m) reservoir sands. These models together with the additionally available PVT data and rock physics measurements were used in the present work as templates for studying the seismic response for a range of development scenarios and geological settings.

## 5.3 Petro-physical model

Using the template data of the Schiehallion field we will study the magnitudes of 4D seismic effects occurring in hydrocarbon production scenarios. The approach we will take is similar to that of 4D feasibility studies where the time-lapse seismic response to changes in rock and fluid properties is forward modelled using the rock physics equations. The sequence of rock physics calculations is described in Methodology chapter (section Petro-elastic modelling). The parameters of the hydrocarbon displacement scenarios and corresponding changes in elastic properties and seismic amplitudes are listed in Table 5.1. These calculations use rock and fluid properties from the Schiehallion dataset, and the results are in agreement with the published results of the rock physics studies (*Meadows et al, 2005*).

**Table 5.1. Estimation of time-lapse changes in impedance, reflectivity and travel time for different development scenarios.**

| | Sw | So | Sg | P-velocity (km/s) | Density (g/cc) | P-wave impe-dance (km/s* g/cc) | P initial (psi) | P final (psi) | Impe-dance change (%) | Reflec-tivity change (%) | Travel time change (ms) |
|---|---|---|---|---|---|---|---|---|---|---|---|
| Preproduction | 0.17 | 0.83 | 0 | 2.62 | 2.46 | 6.44 | 2907 | 2907 | **0.0** | **0.0** | **0.0** |
| Water swept | 0.83 | 0.17 | 0 | 2.73 | 2.49 | 6.79 | 2907 | 2907 | **5.4** | **-31.8** | **-1.1** |
| Gas swept | 0.17 | 0 | 0.83 | 2.47 | 2.33 | 5.76 | 2907 | 2907 | **-10.5** | **65.9** | **1.6** |
| Pressure up | 0.17 | 0.83 | 0 | 2.45 | 2.47 | 6.04 | 2907 | 5500 | **-6.2** | **38.0** | **1.9** |
| Pressure down | 0.17 | 0.83 | 0 | 2.61 | 2.45 | 6.39 | 1500 | 2907 | **-0.7** | **4.1** | **0.1** |
| | | | | | | | | | | | |
| Overburden | | | | 3.35 | 2.27 | 7.60 | | | | | |
| Underburden | | | | 3.35 | 2.27 | 7.60 | | | | | |

| Reference parameters | |
|---|---|
| Porosity | 0.28 |
| NTG | 0.85 |
| Rs, Mscf/stb | 0.36 |
| Average reservoir thickness, m | 35 |

Figure 5.3 illustrates time-lapse changes in elastic properties for the production scenarios of Table 5.1: oil displacement during the water flooding (a), oil displacement by gas or gas exsolution (b) and variations of reservoir pressure (c). In the case of water displacing oil both seismic velocity and density of saturated rock increase with increasing water saturation which causes impedance change of around 5% and the amplitude change of around 30% for the full displacement (for water saturation change from 0.17 to 0.83, see Table 5.1). This is above the usual rule of thumb threshold for 4D seismic detectability of 3-4% of impedance change *(Johnston, 2013)* which means that the effect of water saturation change can be a basis for 4D seismic interpretation in this field. A different character of the impedance change is observed in the process of gas displacing oil or gas exsolution as a result of pore pressure depletion (Figure 5.3, b). A small amount of gas in the oil-gas mixture causes a rapid drop in seismic velocity and impedance of the saturated rock. After the initial drop, the velocity starts to increase with gas saturation which is a consequence of the relationship between the velocity, modulus and density, with density being in the denominator:

$$Vp = \sqrt{\frac{K + \frac{4}{3}\mu}{\rho}} \tag{5.1}$$

In terms of the 4D seismic signature it means that the appearance of gas in oil will cause a strong 4D anomaly but further increase of gas saturation will see much weaker variations of 4D amplitude. While this effect is a good indicator of the presence of gas, it may shadow pressure and water saturation effects which will be demonstrated later.

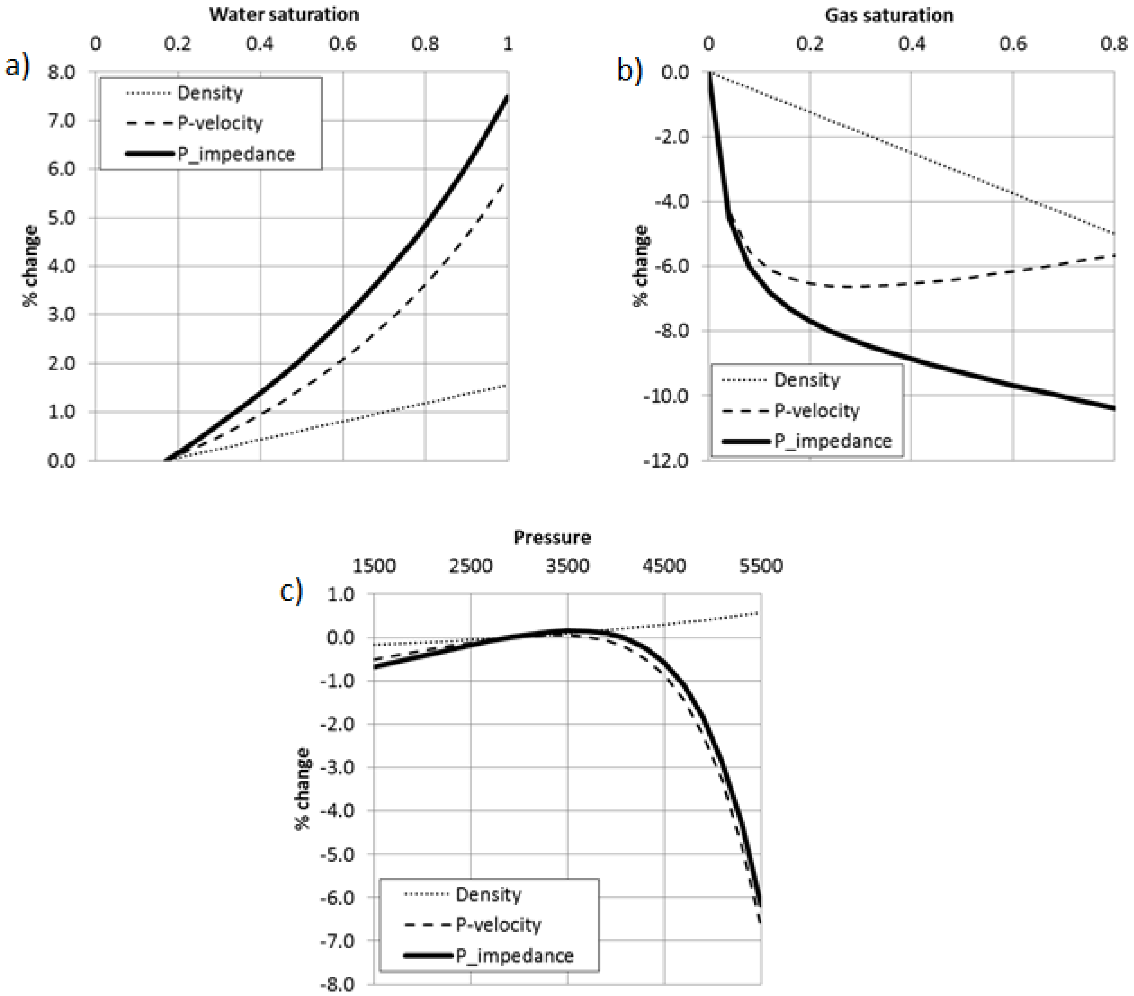

**Figure 5.3. Time-lapse changes of density, P-velocity, and P-impedance of reservoir rocks as a result of changes in: a) water saturation, b) gas saturation, and c) pressure.**

A strong pressure effect, up to 6% of impedance change and 38% of amplitude change, can be observed in high pore pressures (Figure 5.3, c). This is a result of the exponential relationship between the rock frame's modulus and pore pressure as discussed in Theory chapter (section Pressure dependence of reservoir rocks). A good example of the pressuring up effect is 4D signal around injectors which may suggest insufficient communication across the reservoir. Pressure drop below the initial pressure of 2907 psi causes less than 1% of impedance change and can not be normally detected by the 4D seismic method unless the pressure depletion results in gas coming out of solution. In fact, the evolution of free gas and its strong 4D signature can be used to interpret pressure depletion in compartmentalized reservoirs as shown in reservoir management studies on the Schiehallion field (*Govan et al, 2006*). The small decrease in impedance of saturated rock with pressure depletion (Figure 5.3, c) is caused by the fluids compressibility. Due to the insufficient thickness of the reservoir the time shifts are small (1-1.5 ms, Table 5.1) to be confidently detected in the presence of tuning effects.

Figure 5.4 shows the same scenarios modelled with varying NTG. Notably, the saturation effects strongly depend on the NTG while the pressure effect is almost unchanged for different NTG levels. Shaly reservoirs with low NTG contain less fluid (shale is assumed impermeable in this model) so the effect of saturation change is diminished in them. The pressure effect on the other hand is dominated by variations in rock's modulus regardless of saturation. The figure shows that the detectable changes of saturation are higher in shaly reservoirs which reduces their detectability using the 4D seismic data.

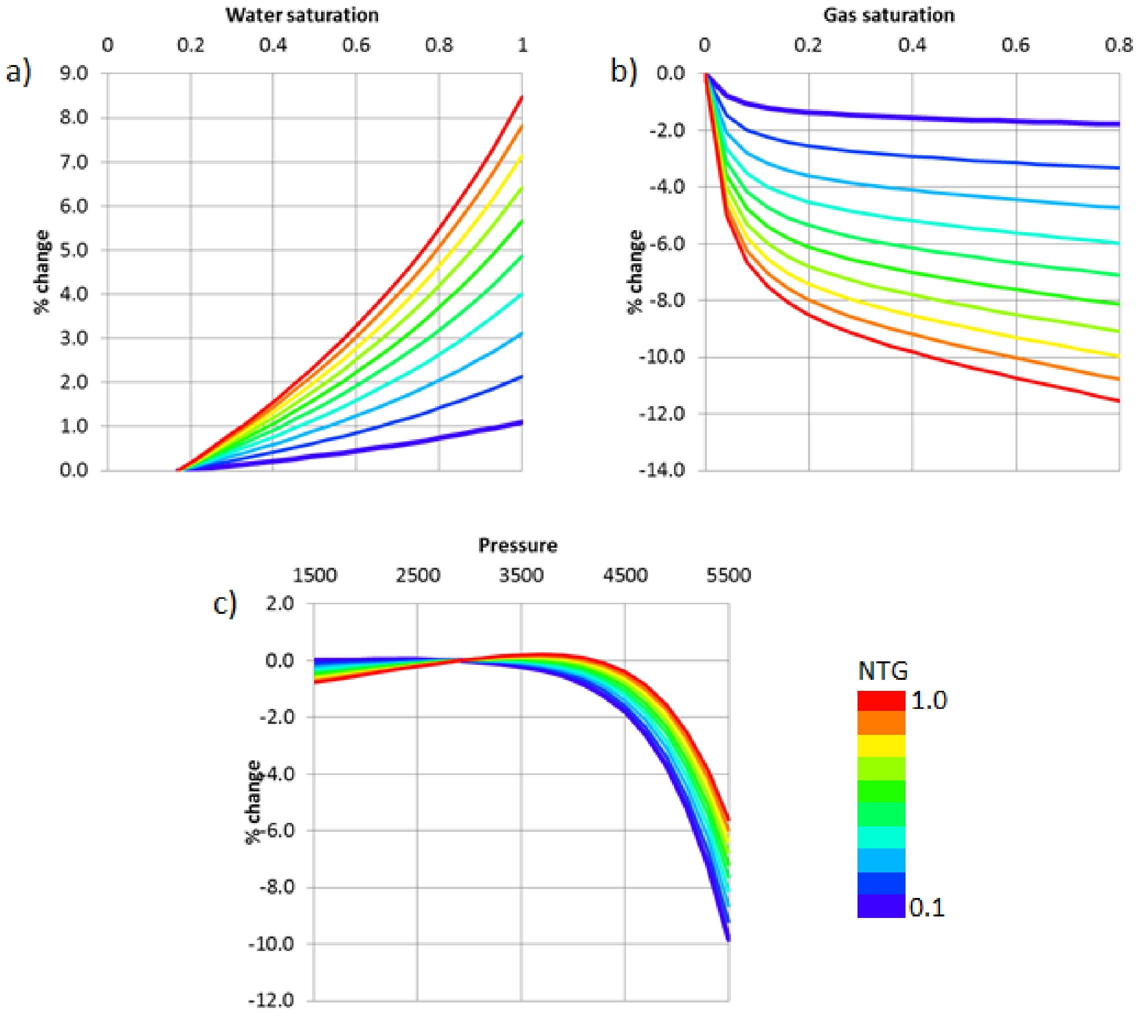

**Figure 5.4. Time-lapse changes of P-impedance of reservoir rocks with different NTG ratios as a result of changes in: a) water saturation, b) gas saturation, and c) pressure.**

## 5.4 Model-based interpretation of 4D seismic effects

In this section we will use the simulation model of the Schiehallion field (Segment 1 of it) in order to study the 4D seismic responses to pressure and saturation changes occurring in realistic scenarios of field development using the seismic forward modelling. This will help to understand the variety of the 4D signals and the ability of seismic attributes to image certain production-related effects. Throughout the study of the 4D seismic effects, we will use different seismic attributes including the cross-sections through the modelled seismic cubes and maps. By their definition (see Introduction), seismic attributes are chosen with a view to emphasizing certain information in the data such as the signal energy on a map to track the effective properties of the reservoir, or the waveforms to understand the heterogeneity of a cross-section. In that sense, an important seismic transformation is the 'coloured inversion'

(CI) which can enhance the appearance of the target objects on the seismic data as discussed in Theory and Methodology chapters (in both, section Coloured inversion). This will be further examined here using the seismic attributes based on the CI data. The applicability of map- and volume- based attributes for the history matching purpose will be discussed in the next chapter.

Imaging of the seismic cross-sections can be improved if the underlying properties are shown on the background of the seismic traces. To achieve it, the properties of the simulation grid are mapped into the time coordinate. This is done by using the virtual seismic traces intersecting the simulation grid as described in Methodology chapter (section Seismic modelling), with the velocity model resulting from the rock physics modelling. The examples shown in this section will be accompanied by the combined cross-sections produced in this way.

The first example in our study demonstrates the seismic response to the conflicting effects of water and gas saturation increases. According to the rock physics analysis of the previous section, appearance of a small amount of gas in oil causes acoustic softening of the rock, while the water saturation increase causes an increase of impedance which alone can result in up to 30% variation of the seismic amplitude. However the combined effect of appearance of gas in the reservoir and water influx is a destruction of the 4D seismic amplitude. Figure 5.5 shows the seismic response to the changes in the reservoir saturation and pressure after 4 years of production (base survey at 0th year and the monitor at 4th year). The map of the seismic attribute (Figure 5.5, a) is dominated by the effects of gas saturation increase due to massive gas exsolution in the period of pressure depletion as discussed in the field overview section. The area marked by the red rectangle in the attribute map lacks any signal though. The absence of signal is not easy to interpret: it can be that there is no change in the reservoir, or there can be no reservoir (*Johnston, 2013*). In our case, examining the time-lapse impedance and water saturation properties in the cross-sections (Figure 5.5, b and c) helps explain the effect. A thin layer of rock softening at the top of the reservoir indicated by the impedance decrease (Figure 5.5, b) is the free gas cap. At the same time, a massive water influx is observed the lower part of the reservoir (Figure 5.5, c). The two effects cause opposite 4D seismic amplitudes which cancel preventing us from seeing them. An important point is that we are missing the chance of observing a significant water influx from the injector I16 because of the presence of small amount of gas on top of the reservoir.

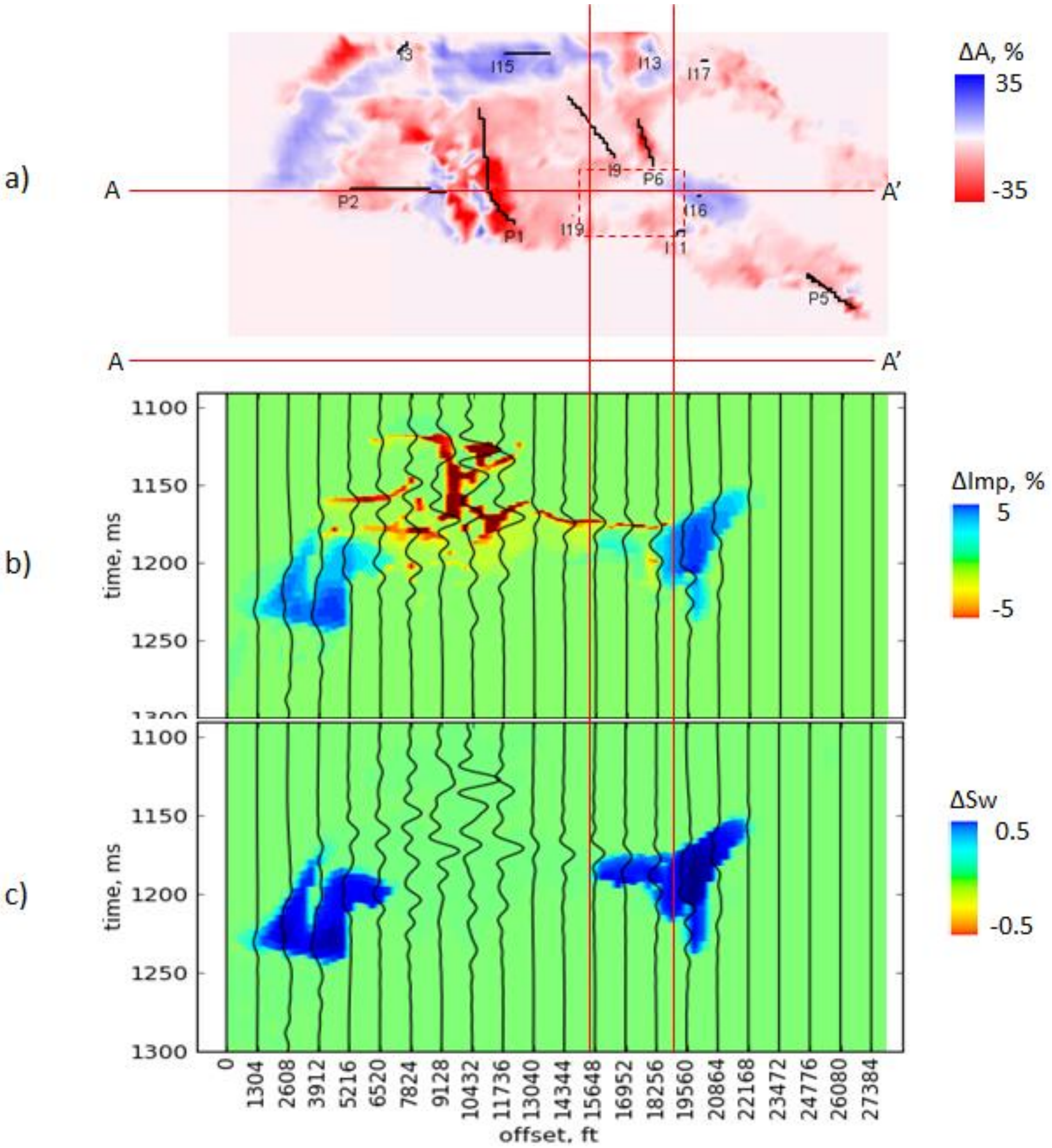

**Figure 5.5. Combined effect of water and gas saturation change. A) map of seismic attribute (average amplitude on CI), b) cross-section along the line AA' showing differenced CI traces and the time-lapse impedance difference on the background, c) same as (b) but the background is water saturation change. The time-lapse differences are at 4 years of production. Red rectangle shows where gas and water responses interfere.**

The next figure, Figure 5.6, shows the same properties and the attribute map after another year of production (base survey at $0^{th}$ year and the monitor at $5^{th}$ year). This time, the gradual increase of water saturation and decrease in gas saturation compared to the previous year makes the water effect more visible, but the signal may be obscured by the non-repeatability noise which makes the water influx hard to detect in this area.

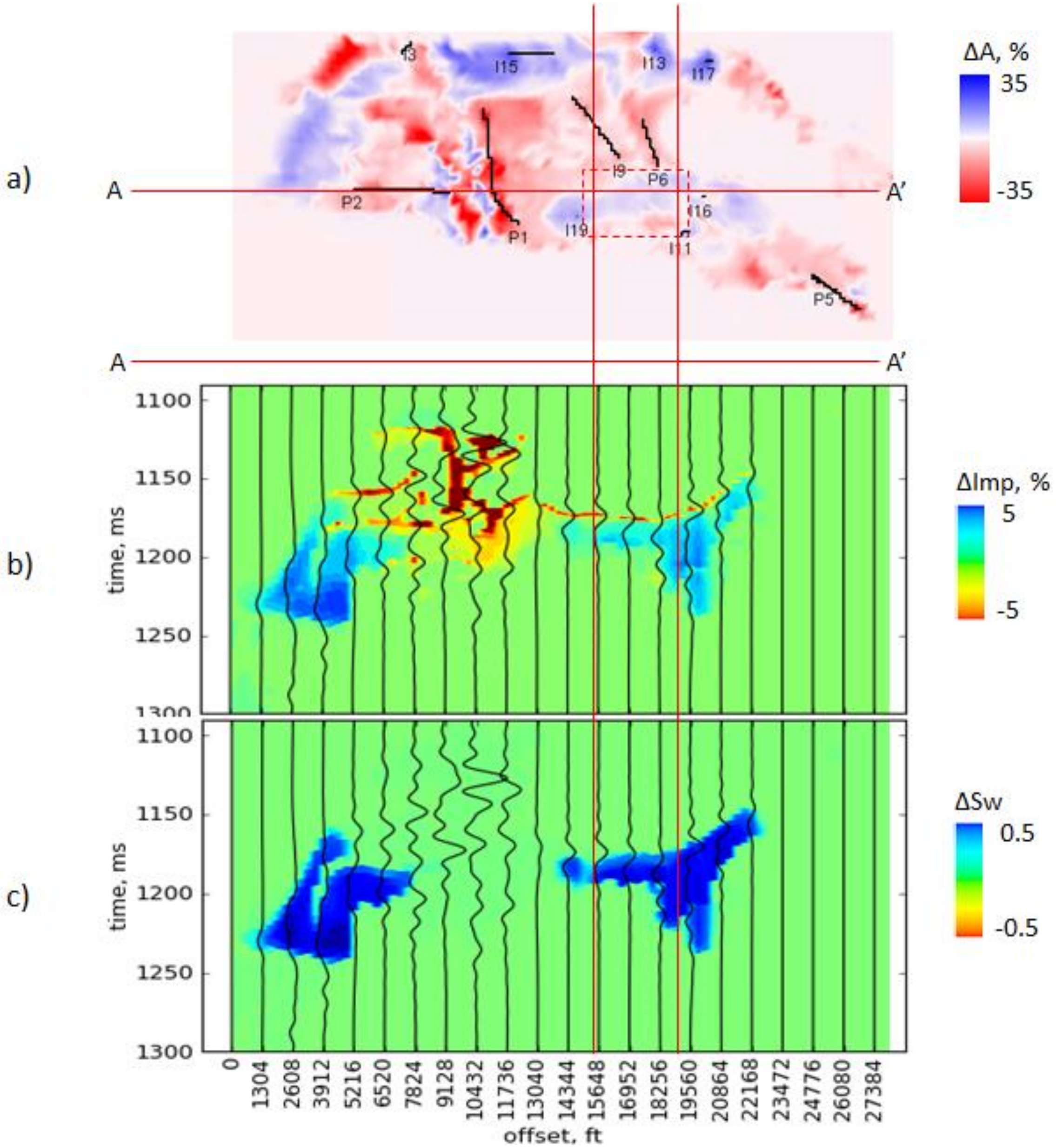

**Figure 5.6. Same as Figure 5.5, but the time-lapse differences are at 5 years of production.**

Stronger 4D anomaly is observed in the northern part of the model as shown in Figure 5.7. This is related to the water saturation increase as a result of the water injection by the wells I15 and I3. This shows the true water saturation effect as it is observed in the 4D seismic data for our template dataset. An interesting effect can be observed in the same Figure 5.7. In the bottom of the reservoir, the impedance decreases (Figure 5.7, b). Usually, we would relate this to e.g. pressuring up since it is not at the top to be a gas effect. This time however, the water saturation cross-section shows (Figure 5.7, c) that the water saturation in the original water leg decreases which is a result of oil being pushed down in the water zone.

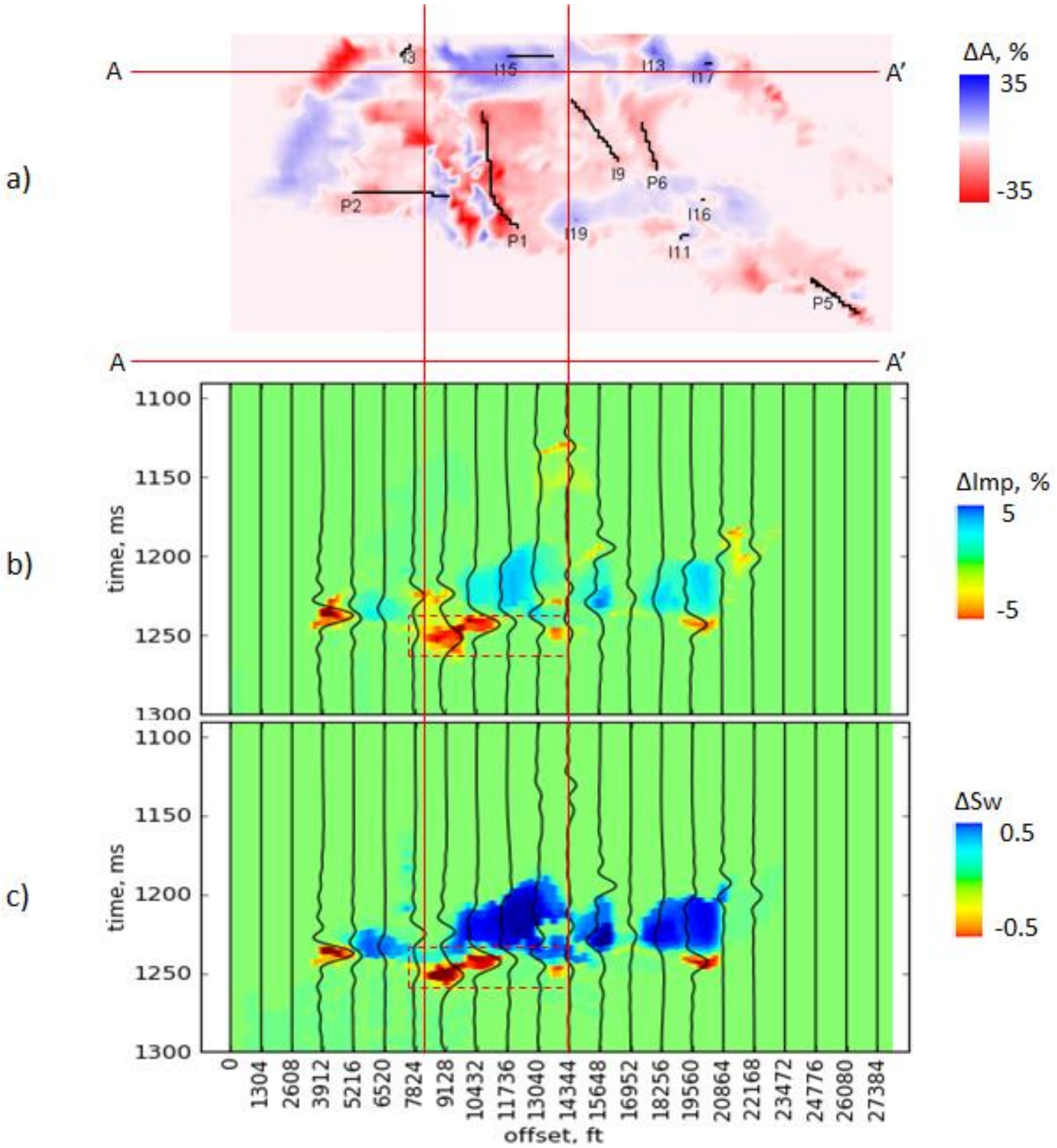

**Figure 5.7. Effects of variation of water saturation. Annotations are the same as in Figure 5.5. The time-lapse differences are at 4 years of production. Red rectangle shows the decrease of water saturation.**

The next example demonstrates the combined effect of pressuring up and water saturation increase occurring around the injector I11 (Figure 5.8). The volume of water injected in this well at the start of the injection period causes increase in pore pressure up to 5000 psi due the limited connectivity of the reservoir. At the same time, the oil is substituted by water around this injector. We showed in the rock physics section (Table 5.1), the pressuring up above 4500 psi and the water sweep cause 4D effects of similar magnitude but in opposite directions. Similar to the previous example, the conflict of the two effects in this case causes reduction in their detectability as illustrated in Figure 5.8. The anomalies falling into the lines AA' and BB' are very weak and are of opposite signs. By comparing the water saturation and pressure changes in Figure 5.8 we can see the different signs of the 4D signal are caused by the dominance of the pressure effect in the cross-section BB’ and stronger effect of water sweep in AA’.

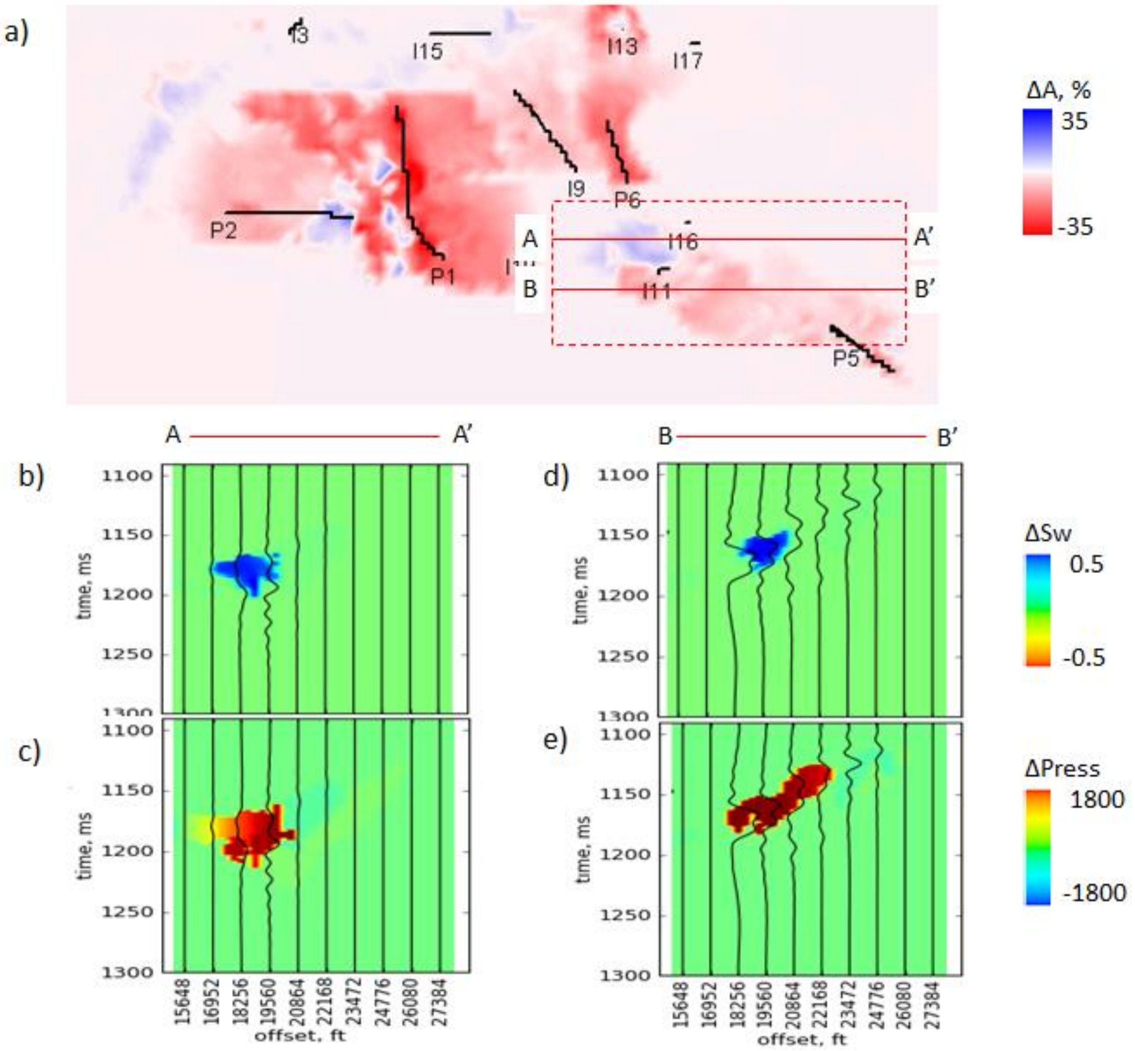

**Figure 5.8. Combined effect of pressuring up and water saturation increase. A) 4D seismic attribute (average amplitude on CI) map, b) cross-section along AA’: CI traces and the time-lapse water saturation in the background, c) as (b) but with the time-lapse pressure in the background, d) and e) as (b) and (c) but along the line BB’. Time-lapse differences are at 1 year of production.**

In the examples shown so far, we used maps of the seismic attribute to interpret the 4D effects. We assumed that changes of the impedance within the reservoir can be traced using the seismic attribute. However, due to the limited vertical resolution of seismic data, it can be difficult to localise seismic signals caused by the reservoir properties in a particular interval. The reflections from different layers interfere which may lead to ambiguous interpretations of the maps. Indeed, the tuning thickness (assuming velocity of 3000 m/s and 30 Hz wavelet) is 25 m which means that at this separation from the underlying and overlying intervals there is maximum interference of reflections. We should expect this interference from the reflectors in the underlying and overlying interval T31b and T35 respectively which at times have only minimal separation from T31a.

An example of such limitation of the map attribute was given in Literature review chapter (see Figures 3.15 and 3.16) where volumetric attributes were preferred as a result. The conflicting 4D effects that we observed in this section can also be better resolved using the cross-sections (see Figure 5.7 for example). However, in order to assess how well the impedance changes are traced by the seismic attribute map, we will compare the maps of the impedance change with the maps of 4D seismic attributes (Figure 5.9).

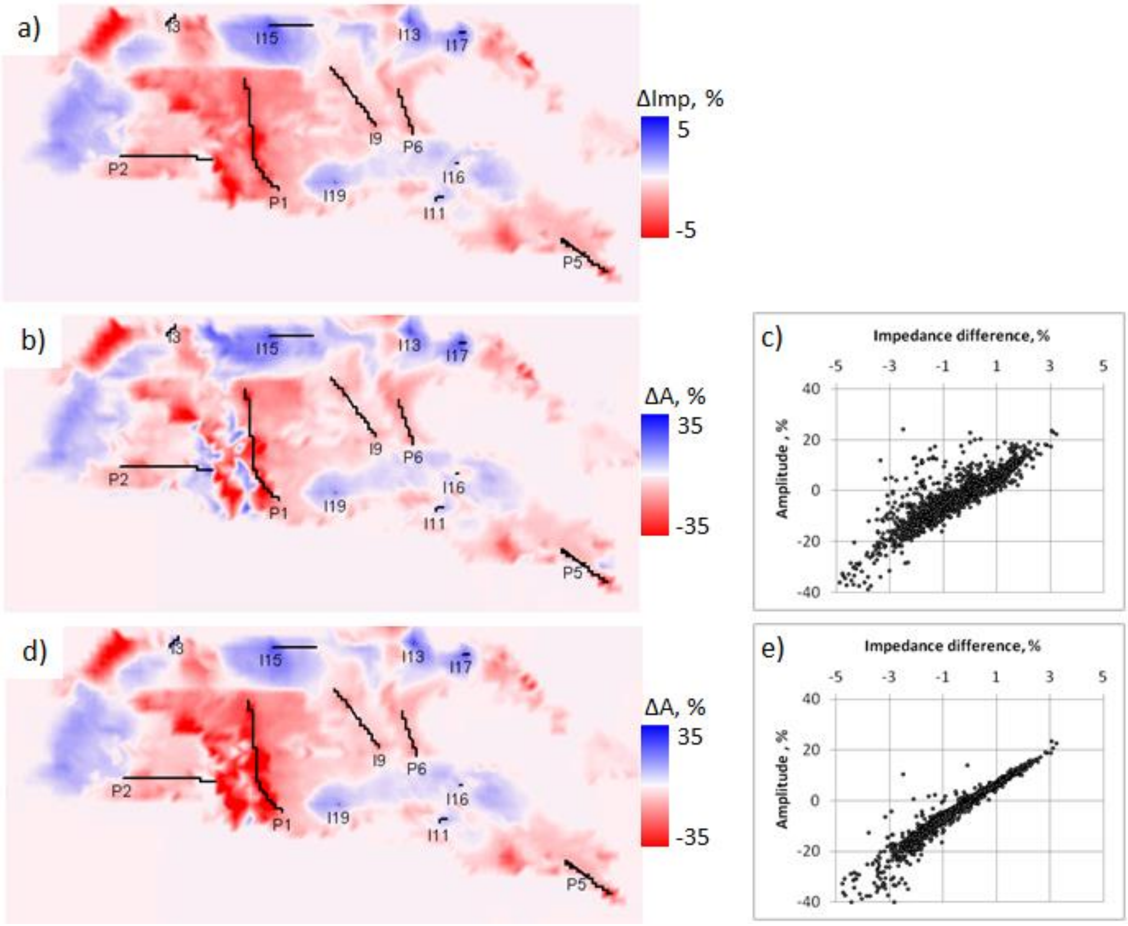

**Figure 5.9. Comparison of maps of impedance change in the reservoir T31a and 4D seismic attributes. A) map of impedance change (depth average impedance), b) 4D seismic attribute (average amplitude on CI) map, c) cross-plot of sample from the maps in (a) and (b), d)-e) same as (b)-(c) but for a model without pressure and saturation change outside of reservoir. Time-lapse differences are at 5 years of production.**

Let us compare the average map of the impedance change (panel a) with the map of 4D seismic attribute (panel b). The principal features of the impedance change can be easily traced on the seismic attribute map. However, the area around well P1 shows discrepancy between the maps. This is where the reservoir T31a is overlaid by the producing reservoir T35. It is the 4D response to the production changes in the overlying (T35) and the underlying (T31b) reservoirs that interfere with the useful signal distorting it. To verify that, let us set all the impedance changes outside of the reservoir T31a to zero and recalculate the seismic response. The resulting seismic attribute map is shown in Figure 5.9, d. Notably, the artefacts around the producer P1 are largely removed and the correlation between the attribute and the impedance change improved as indicated by the cross-plot in Figure 5.9, e, although some of the scatter remains. This is associated with the factors other than just the signals foreign to the reservoir which includes the reservoir geometry and the tuning effects (constructive and destructive interference of amplitudes). In the following section, these factors will be investigated using the specifically designed models and scenarios of pressure and saturation change.

## 5.5 Seismic response and factors affecting it: a detailed study

The examples we studied using the Schiehallion model demonstrated a range of 4D seismic anomalies occurring in the course of the field development. It was shown that the detectability of the pressure and saturation changes is limited by the resolution of the seismic data. The interference of the signals from the different stratigraphic layers prevents us from getting a pure seismic signal related to the properties of interest. In this section, we will study the variety of seismic responses together with the factors affecting them using the tailored synthetic models. We will start our discussion with a generic tuning effect, then consider the seismic response to the variations of static and dynamic parameters in turn.

### *5.5.1 Tuning effect*

The tuning effect (*Yilmaz, 2001*) is usually visualised using the classical wedge model (*Widess, 1973*) similar to that shown in Figure 5.10. The wedge-shaped reservoir in that figure has lower impedance than the surrounding rocks (6.1 km/s·g/cc and 7.6 km/s·g/cc respectively), so the upper boundary of the reservoir is marked by the negative amplitude and the lower boundary by the positive amplitude. At the thick end of the model, both the reservoir top and base can be separated by the seismic amplitude picks. As the reservoir pinches out, the seismic reflections start to interfere with the resulting amplitude being a sum of the two reflections. Depending on the thickness of the wedge, the combined amplitude increases if the wavelets interfere constructively and decreases if destructively. The variation of the amplitude with the reservoir thickness is called the tuning effect and is illustrated in Figure 5.11. The thickness of (in this case) the maximum amplitude is called the tuning thickness which is determined by a quarter of wavelength of the seismic wavelet. As shown in the Figure 5.11, the tuning occurs not only in the base and monitor surveys but also in their 4D difference.

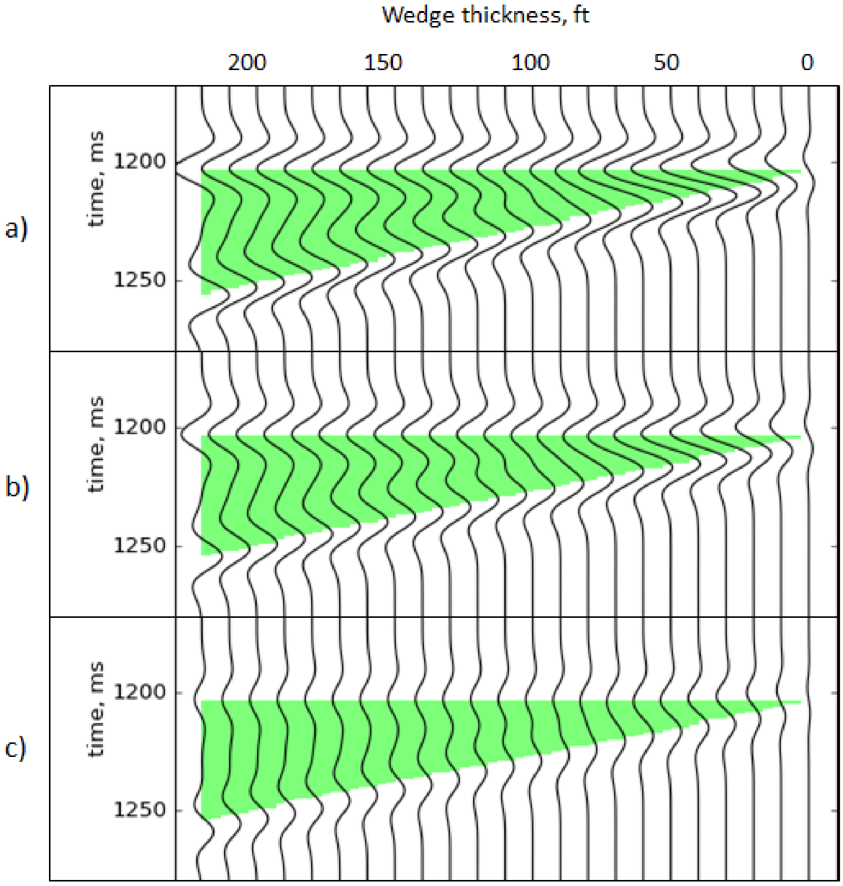

**Figure 5.10. The seismic amplitudes are subject to the tuning effect due to variation of the reservoir thickness: a) base survey amplitudes, b) monitor survey amplitudes, c) time-lapse seismic difference.**

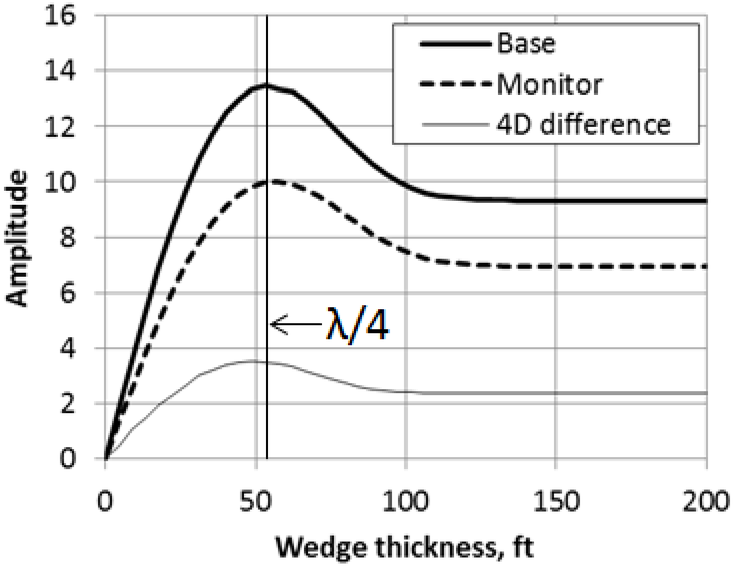

**Figure 5.11. Variation of the seismic amplitude with the thickness of the reservoir (assuming seismic velocity of 6562 ft/s or 2000 m/s and 30 Hz seismic wavelet). Maximum of amplitude is observed at the layer thickness corresponding to the quarter of seismic wavelength λ.**

### *5.5.2 Grid for the synthetic model*

In the following discussion we will study the seismic response to variation of static and dynamic properties in the model. In order to optimize the calculation time which for the dynamic properties includes reservoir simulations, a subgrid was extracted from the Schiehallion simulation grid as shown in Figure 5.12. The subgrid presented in this figure will be a basis for the synthetic models used in this chapter and in some examples of the following chapter. As shown in Figure 5.12, b and Figure 5.13, a, the subgrid includes the same stratigraphic layers as the original grid: T35/34, T31a and T31b. The interval T31a will constitute the producing reservoir for the synthetic model. The map-based seismic attributes will be calculated over the interval T31a. The area for the subgrid is chosen with a view to include the varying thickness of the reservoir as shown in Figure 5.13. The number of cells in the original Schiehallion grid is 106x41x42. The subgrid is regridded to produce a coarse and a fine versions of it with dimensions 24x34x42 cells in the first, and 48x68x168 in the second. We will apply the fine version of the grid to model different NTG distributions to create a reference seismic response. The coarse version will be applied in the cases requiring reservoir simulations. Also, in the following discussion of the seismic responses to variation of static and dynamic properties, a flattened version of the grid will be used (for example see Figure 5.15).

This is done to isolate the effects of the properties variation from the effects of the reservoir geometry.

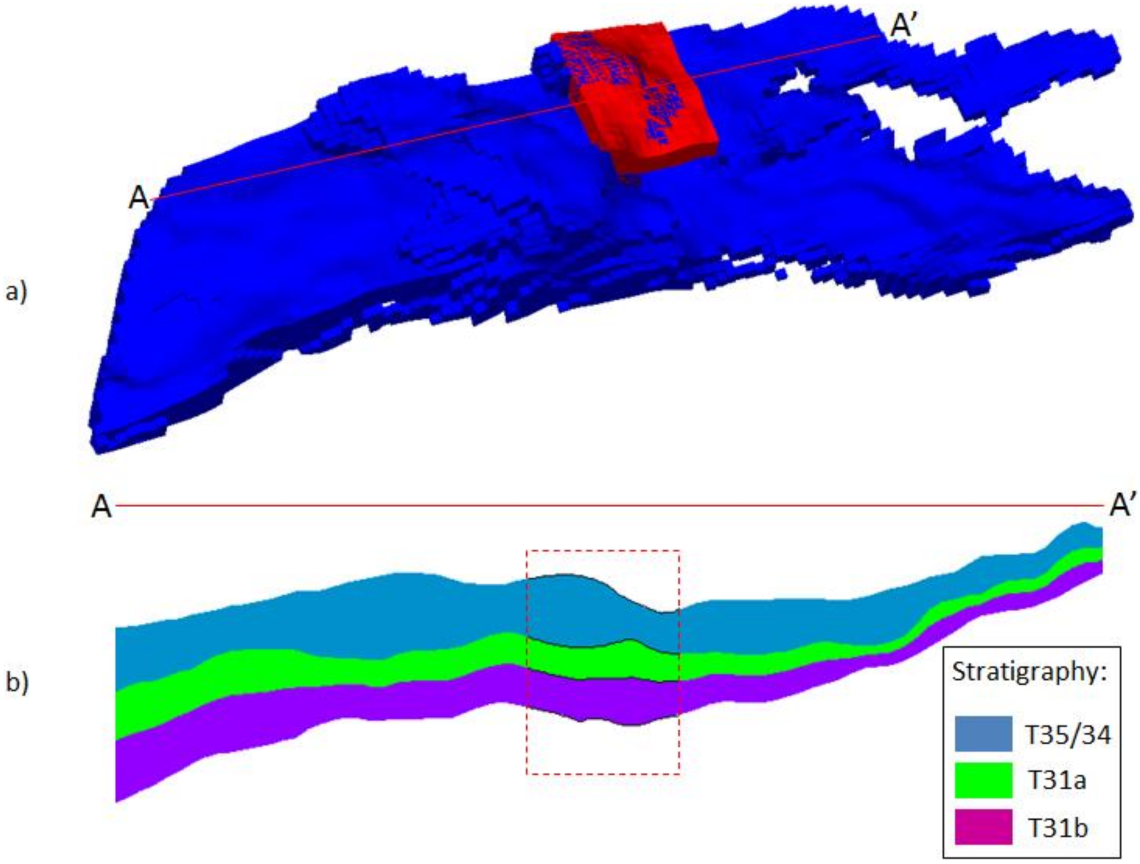

**Figure 5.12. Extracting a subgrid from the Schiehallion (Segment 1) simulation grid for synthetic modelling. A) 3D view of the grids: Schiehallion grid in blue and the subgrid in red, b) cross-section along AA' showing the stratigraphic layers in the model, the red rectangle shows the extent of the subgrid.**

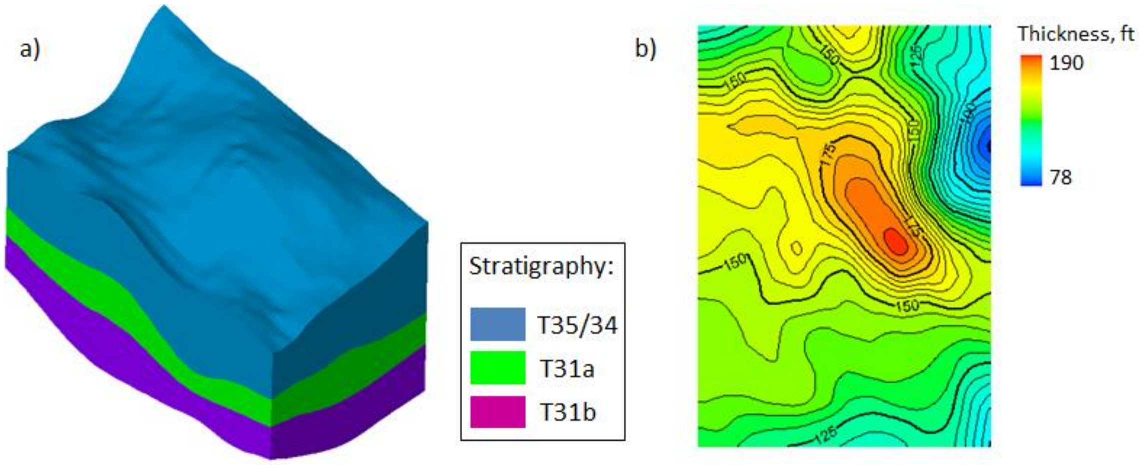

**Figure 5.13. A) 3D view of the subgrid with the stratigraphic intervals, b) thickness map of the interval T31a.**

### 5.5.3 Variation of static properties: NTG

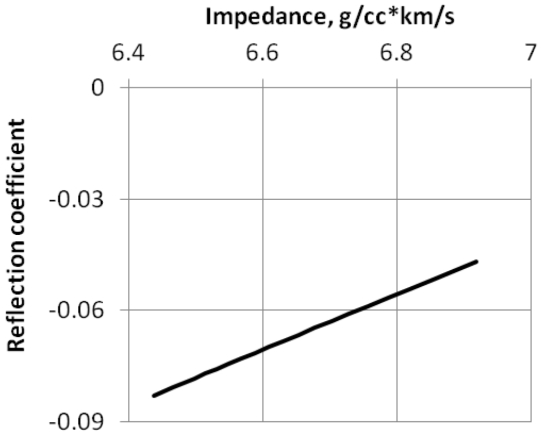

**Figure 5.14. Function of reflection coefficient on impedance. Impedance of overburden and underburden is 7.6 g/cc·km/s**

The function of the reflectivity on the impedance of a layer is non-linear generally but has an extensive linear part which allows us to think of the amplitude as being proportional to the impedance. Figure 5.14 illustrates the relationship between the reflectivity of the reservoir layer and a range impedance values corresponding to changing water saturation in a water sweep. However, the relationship between the average impedance of the layer and the amplitude of the seismic response can be more complex as more reflections than just the top and base of the reservoir appear in the sequence. In the following model realisations we will attempt to model different reflection sequences.

The first test investigates the effect of reflections within the target reservoir and in the enclosing rocks, overburden and underburden. The impedance contrasts can be modelled by varying the NTG ratio of the rocks as shown in Figure 5.15. Three models are shown in the figure: a) a model with high NTG of the enclosing rocks, b) a model with NTG of enclosing rocks reduced by a factor of 0.3, and c) a model with constant zero NTG of enclosing rocks. The first case models a situation where the reservoir is not contrasting with the enclosing rocks by its impedance which occurs when the reservoir is a part of a stack of sands but is isolated hydrodynamically. Normally, we would expect the reservoir to have contrast with the surrounding layers to be able to delineate it in seismic by tracing its reflection. But even in that case, sands from underlying or overlying reservoirs may appear somewhere immediately below or above the horizon obscuring the interpretation. An example of the stacked reservoir was given by the Schiehallion case where along the main reservoir T31a, we encountered patches of reservoirs T31b and T34/T35 immediately below or above it. The second model in Figure 5.15 is a more conventional scenario where the reservoir is softer than the surrounding rocks, e.g. sand reservoir in shales. The third case is similar to the second but the impedances of the overburden and underburden are constants (equal to that of shales) in order to isolate the effect of seismic interference with those layers. The three scenarios are compared in terms of their seismic response (Figure 5.16), similarity of the RMS attribute maps to the map of average impedance (Figure 5.17 a, b, and c compared to d), and the correlations of those maps (Figure 5.18).

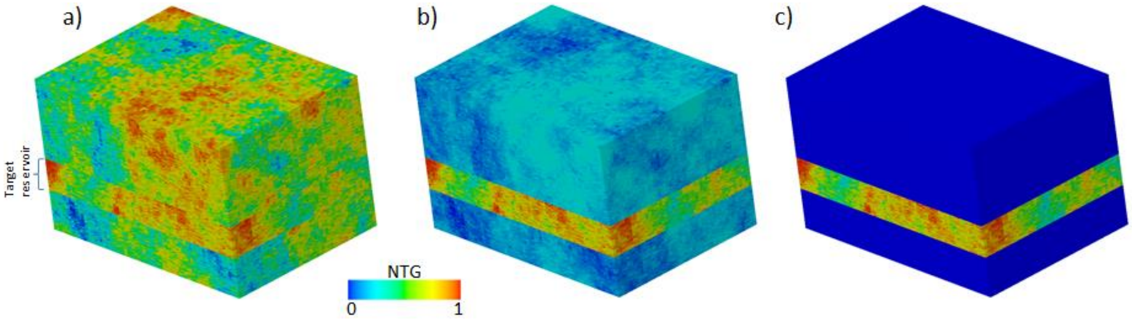

**Figure 5.15. Models of NTG distribution with different level of NTG in the enclosing rocks: high NTG (a), NTG reduced by a factor of 0.3 (b) and NTG is constant zero (c).**

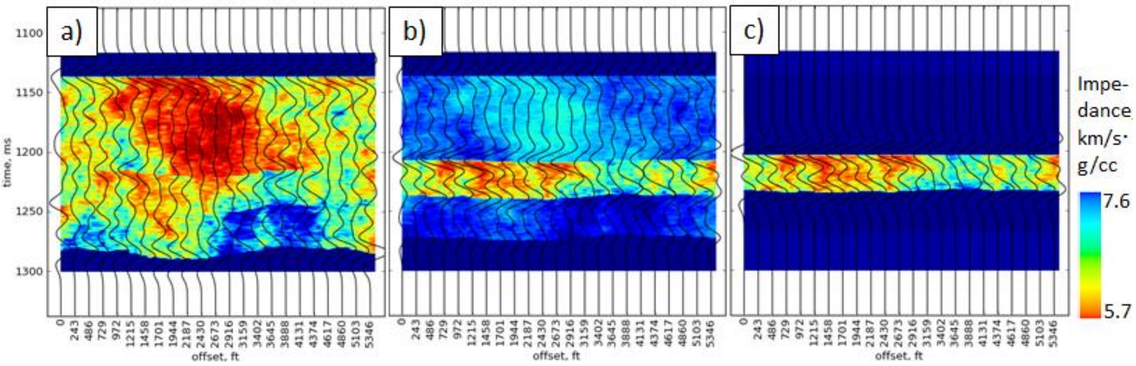

**Figure 5.16. Cross-sections of impedance models imaged in time together with their seismic responses. The models a, b, and c are the same as in Figure 5.15.**

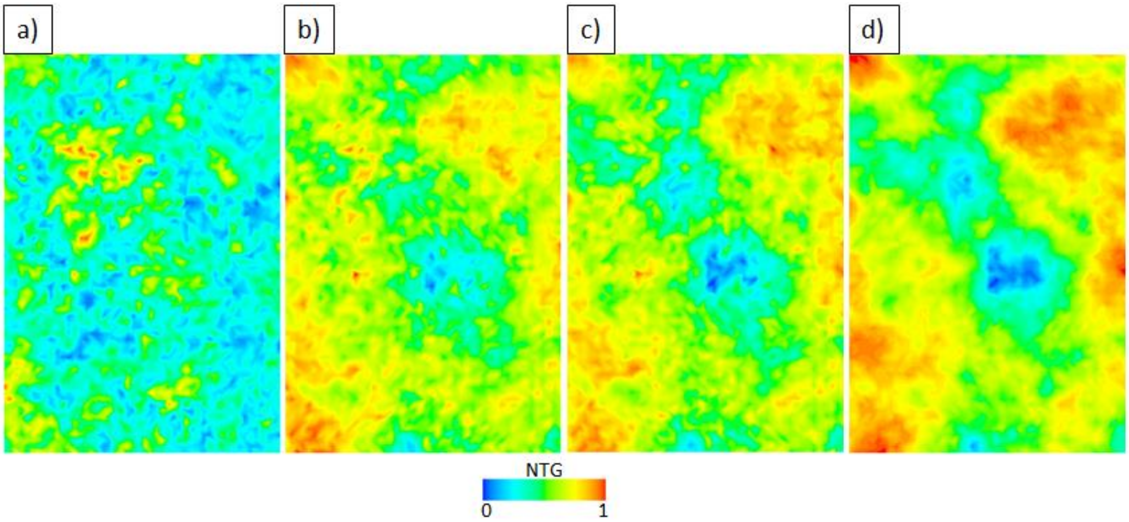

**Figure 5.17. RMS attribute maps for the three models (a, b, and c) shown in Figure 5.15 and the map of average impedance over the producing interval (d).**

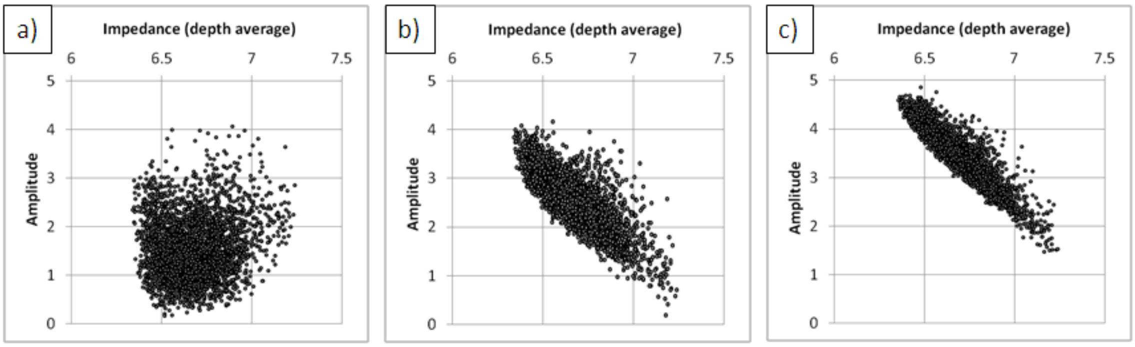

**Figure 5.18. Cross-plots of samples from the maps of average impedance and RMS attribute calculated for the three cases (a, b, and c) shown in Figure 5.15.**

High NTG of the enclosing rocks in the first model causes a complex seismic waveform within the producing interval from which it is difficult to derive the impedance of this interval uniquely (Figure 5.16, a). As a result, the RMS attribute map calculated from these seismic traces over the producing interval has little in common with the map of average impedance (Figure 5.17, a and d). Low levels of NTG in overburden and underburden of the other two models (Figure 5.15, b and c) reduce the variation of the signals in the surrounding rocks and the seismic amplitude is controlled predominantly by the impedance of the producing interval. This naturally increases the correlation between seismic attributes calculated over the producing interval and the average impedance of that interval as shown in Figure 5.17, b and c and Figure 5.18, b and c. The major features such as the areas of high and low impedance correlate very well with the true impedance on these maps (the correlation of the map in Figure 5.17, b is somewhat weaker due to the remaining signal from the overburden and underburden) However, the correlation of both maps Figure 5.17, b and c is distorted by some higher frequency noise. This originates from the more abrupt nature of the RMS attribute map compared to the map of (first order) average impedance as a result of amplification of large values by the second order RMS operator.

The other attribute that we consider here, sum of negatives (SoN), is equivalent to a first order average operator which results in smoother maps than the RMS attribute. But as the name of the attribute suggests, the seismic amplitude should be negative over the reservoir interval, that is we can not apply it on the seismic section for the model in Figure 5.15, a. Figure 5.19 shows the map of SoN comparing it with the RMS attribute. It turns out that the correlation of the SoN attribute with the average impedance is even weaker than that of the RMS attribute (Figure 5.19, c). The reason for it is the way the seismic attribute is used. In case of the SoN attribute only the negative half of the seismic wavelet is used (see Figure 5.16, c), while the entire wavelet bears more information. Hence, the SoN map has wider areas of low signal (blue, in Figure 5.19, b).

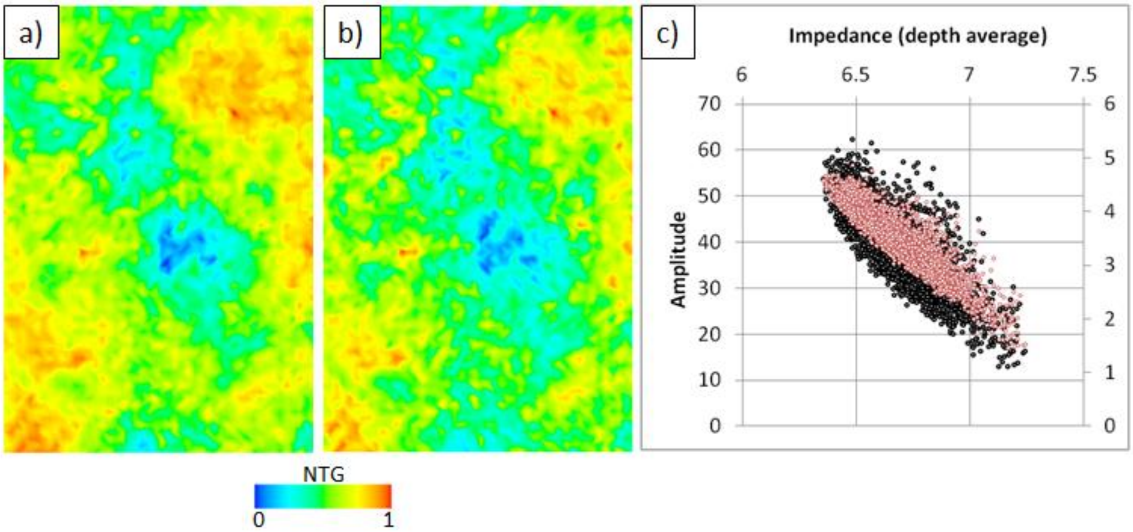

**Figure 5.19. Maps of seismic attributes and their correlation with the average impedance for the model with NTG(enclosing rocks)=0. A) Map of RMS attribute, b) map of SoN attribute, c) cross-plot of average impedance against RMS attribute (red dots) and SoN attribute (black dots).**

This is where a -90° constant phase shift (sometimes referred to as quadrature-phase) transformation is useful as it turns the negative amplitude at the reservoir top and the positive amplitude at the reservoir base into a wavelet of a single polarity (negative in this case) within the reservoir with energy concentrated inside the reservoir rather than on its borders. The ‘coloured inversion’ (CI) is an example of such transformation as discussed in Theory and Methodology chapters. The seismic traces before and after the CI transformation are compared in Figure 5.20 using the same model with constant zero NTG of the overburden and underburden. In this case, the amplitude has constant polarity so the entire interval of the seismic trace can be used for the SoN calculation.

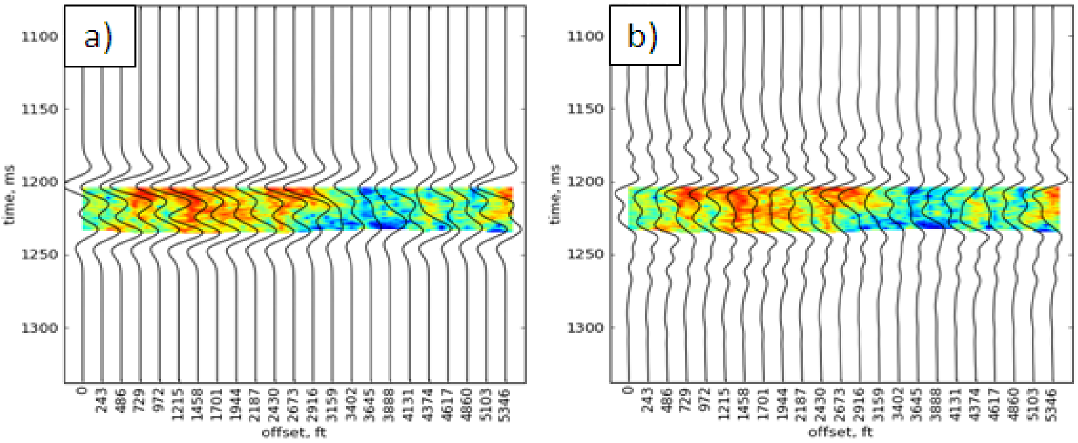

**Figure 5.20. Cross-section of the impedance model with NTG(enclosing rocks)=0, together with (a) seismic traces and (b) seismic traces after coloured inversion.**

The SoN attribute map calculated on the seismic traces after the CI transformation is compared with the average impedance map in Figure 5.21. The two maps look very similar and their cross-plot shows that they are nearly proportional. This shows that the area below the CI curve is proportional to the average impedance of the interval for this reservoir (characterised by its thickness and the impedance contrast).

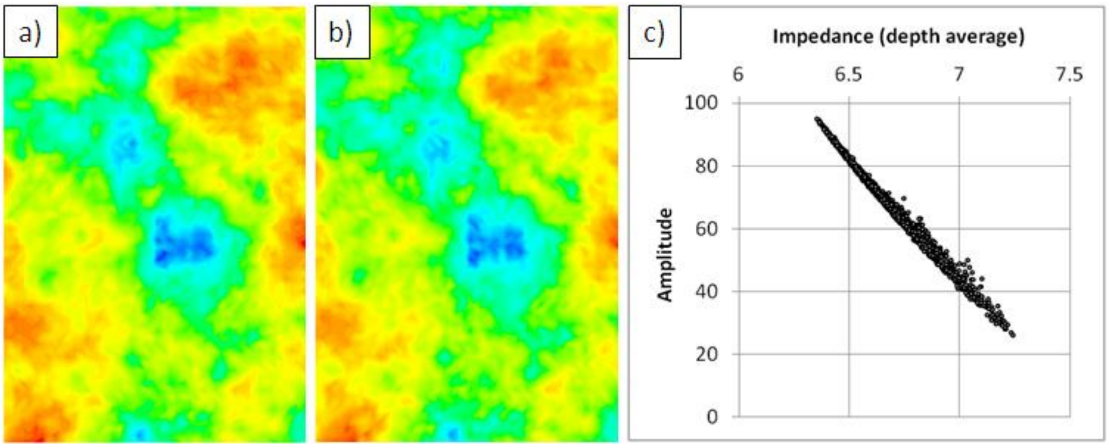

**Figure 5.21. Correlation of the SoN attribute calculated on the seismic traces after the 'coloured inversion' (CI) with the average impedance. A) average impedance map, b) SoN on CI, c) cross-plot of the samples from the two maps.**

We showed that the SoN attribute together with CI transformation can be a good estimate of the average impedance for a single reservoir. In the case when the impedance of the overburden and underburden is not constant (model with NTG of enclosing rocks reduced by a factor 0.3) there will be interference with the reflections from outside of the reservoir as discussed before. Calculating the SoN attribute on CI transformed seismic data still provides better correlation with the average impedance than the RMS attribute on the raw seismic traces as shown in Figure 5.22.

The seismic response is defined by the reflections created by impedance contrasts which occur due to the heterogeneities of rocks such as different lithology or different saturation. We will further study the effect of such heterogeneities on calculation of the seismic attributes by generating a model as shown in Figure 5.23. In this model, the vertical correlation length of the NTG distribution is significantly smaller than in the previous model which creates more impedance contrasts along the seismic ray path. Again, we will only consider a model where the reservoir contrasts from the enclosing rocks (Figure 5.23, b).

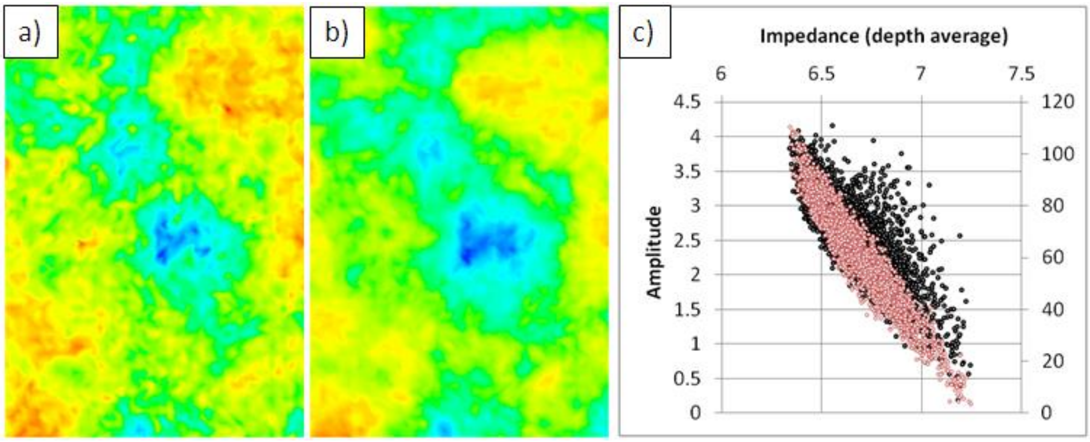

**Figure 5.22. Correlation of RMS and SoN seismic attributes with the average impedance for the model with NTG of enclosing rocks reduced by a factor 0.3. A) Map of RMS attribute, b) map of SoN on CI, c) cross-plot of average impedance against RMS attribute (black dots) and SoN on CI attribute (red dots).**

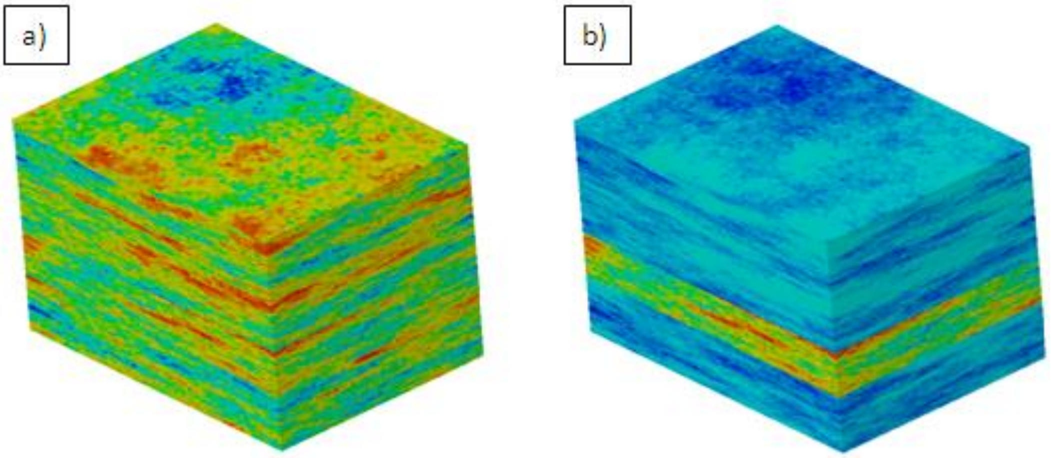

**Figure 5.23. Model of NTG distribution with reduced vertical correlation length. A) original model, b) same model but with NTG of enclosing rocks reduced by factor 0.3.**

The same maps of seismic attributes as in the previous case were generated for this model and compared to the map of the average impedance (Figure 5.24). Unlike the previous case, the difference between the seismic attributes is beyond the minor high frequency signals but spans the major features as well. Overall, the similarity of the RMS attribute with the average impedance map is very low while the SoN on CI reproduces the average impedance quite well which is also demonstrated by the cross-plots in Figure 5.25. To understand the reasons for these differences, we will investigate the seismic response to the impedance variation in the model. Red rectangle in Figure 5.24 shows the area where the signal is reversed in the RMS attribute compared to the impedance map. The cross-section along the line AA’ (Figure 5.26) shows that a lens of shale (low NTG, high impedance) is a situation within this interval which creates a strong impedance contrast. This leads to high seismic amplitude with high RMS values as shown in the RMS attribute. The average impedance on the other hand is not that high since the sand thickness is smaller in this interval, hence the discrepancy between the attributes. The RMS attribute is first of all a measure of impedance contrast which for the thinner reservoir correlates with the impedance of reservoir. In this case however, the SoN on CI attribute has better correlation with the average impedance in the interval.

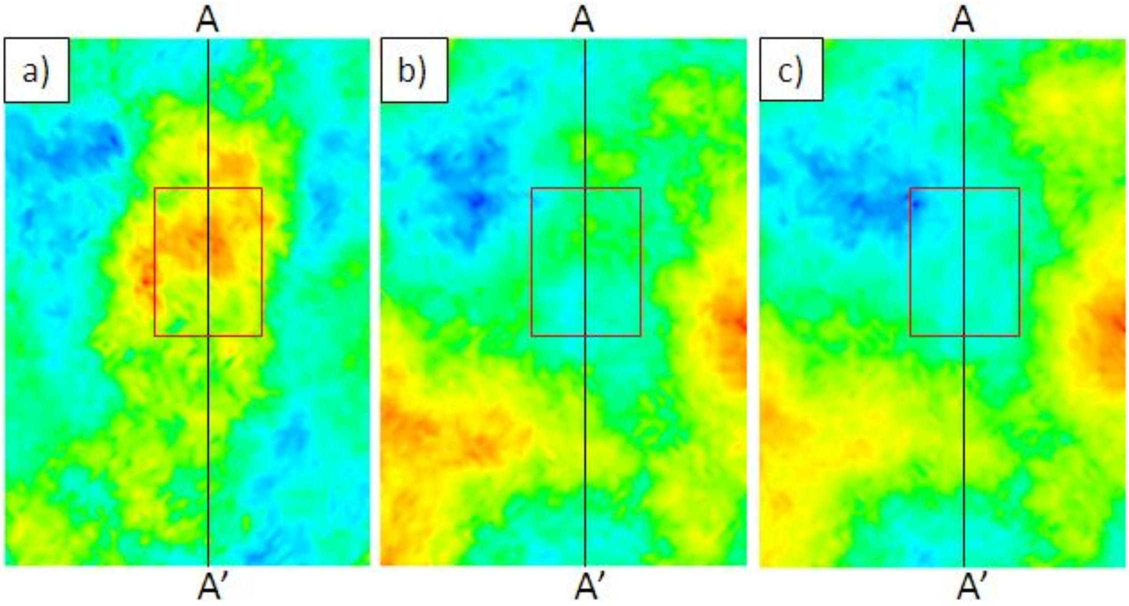

**Figure 5.24. Maps of seismic attributes compared to the average impedance map: a) map of RMS attribute, b) map SoN on CI, c) average impedance map. Red rectangle shows the area of difference. Cross-section AA' is shown in Figure 5.26.**

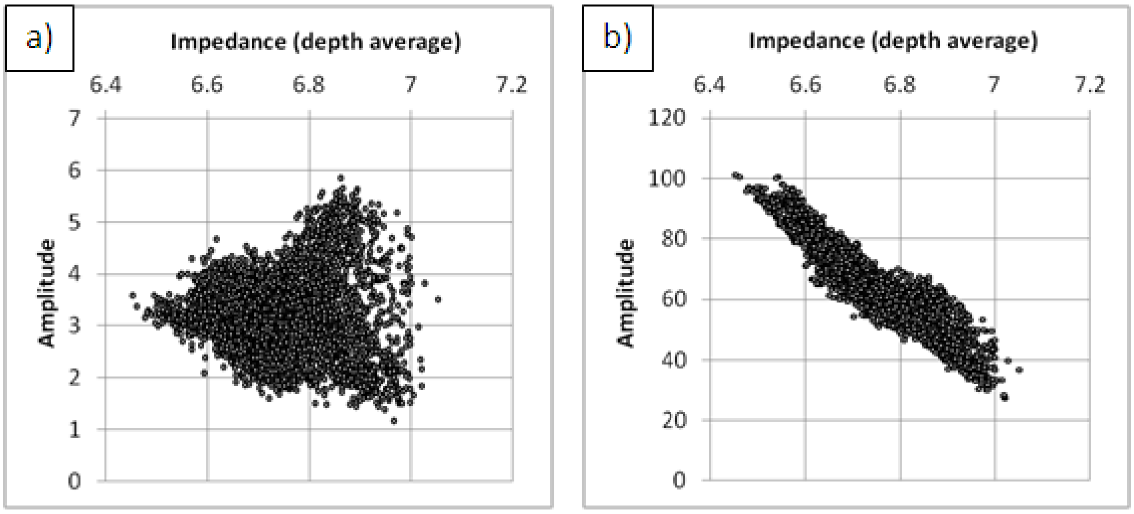

**Figure 5.25. Cross-plots of samples from the maps of (a) RMS attribute, and (b) SoN on CI against the average impedance.**

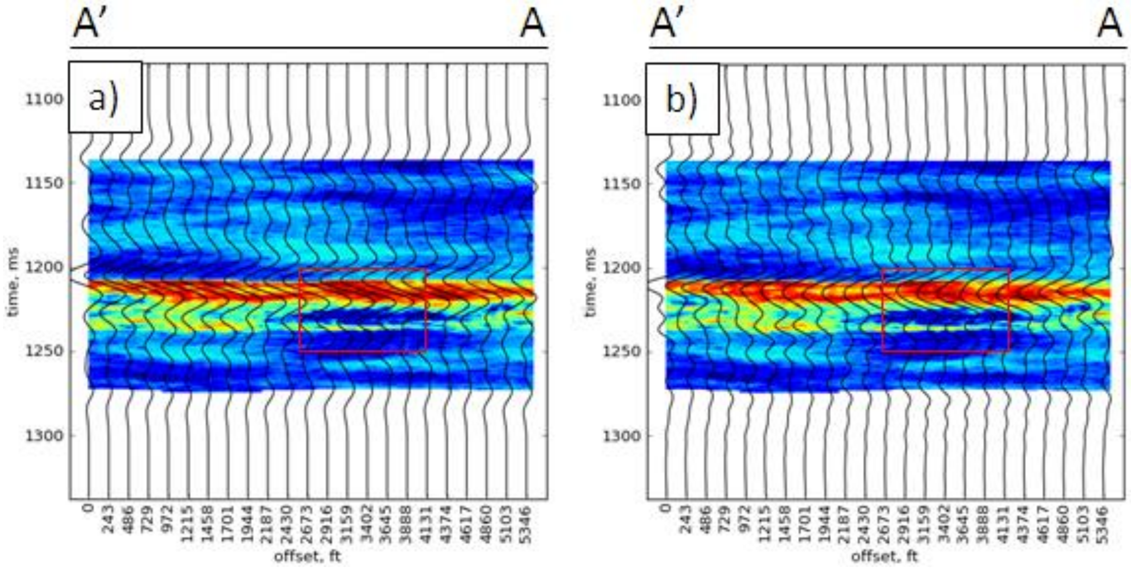

**Figure 5.26. Cross-sections along AA' (see Figure 5.24) of the impedance model, together with (a) seismic traces and (b) seismic traces after coloured inversion. Red rectangle shows where the maps of RMS and SoN on CI differ.**

The grid sector used so far for the models was obtained by flattening the surfaces of the Schiehallion grid as described earlier. Here, we will return to the original geometry of the Schiehallion grid in order to assess the impact of the varying thicknesses of layers on the seismic response. The fragment of the Schiehallion grid with the original geometry is shown in Figure 5.27, a. The distribution of the NTG property is the same as for the model in Figure 5.23 where the NTG of overburden and underburden rocks is reduced by a factor 0.3 (high contrast reservoir).

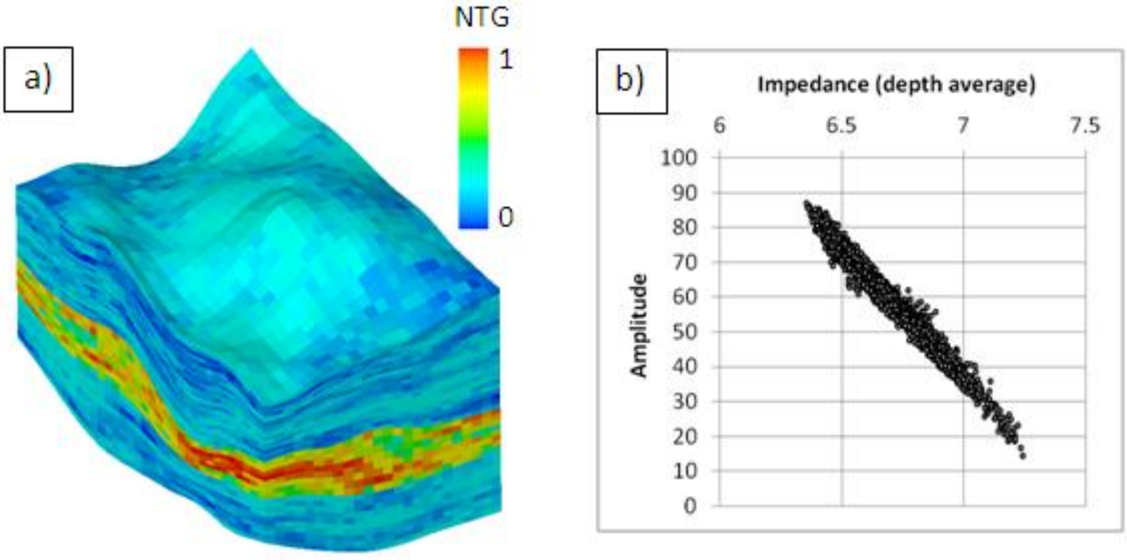

**Figure 5.27. A) NTG model on the part of Schiehallion grid without flattening, b) cross-plot of samples from the maps of SoN on CI against the average impedance.**

SoN on CI seismic attributed was calculated over the producing interval and compared to the average impedance as shown in Figure 5.27, b. The cross-plot shows that variation of thickness of the layers did not change the character of the relationship between the impedance and the seismic attribute maps.

## 5.6 Seismic response to pressure and saturation changes

In the previous section we studied the seismic response to variation of the elastic properties of rocks modelled by different distributions of the NTG property. The basis for the 4D seismic method though is changes of pressure and saturation in the reservoir accompanying the processes of hydrocarbon displacement or gas injection for storage. In this section we will study how these effects are resolved in the seismic attributes.

In section 5.4, examples of simulated pressure and saturation changes were studied in connection with the corresponding 4D seismic response of the models. These illustrated what production effects can be expected in a reservoir setting (reservoir geometry, rock and fluid properties and petro-elastic model) such as the one found in Schiehallion field. The aim of this section is to study the seismic responses to a range of pressure and saturation effects for which a fast method for generating them is required. The fastest way of modelling the variety of pressure and saturation realisations is assigning the values of the pressure and saturation directly to the grid cells of a simulation model rather than obtaining them via simulations. We took similar approach when modelled distributions of NTG in the previous section. However, the 4D seismic signal is caused by time-lapse changes in pressure and saturation (ΔPr,ΔSat) rather than their instant values (Pr,Sat). One way of modelling it is directly assigning the changes of pressure and saturation (ΔPr,ΔSat) to the grid cells and calculating the 4D seismic response from them. This would require a linear relationship between ΔPr,ΔSat values and 4D seismic signal. The linearity of this relationship is invalid in general, so making such assumption would harm the modelling results. Therefore, instead of modelling random Pr,Sat or random scalar ΔPr,ΔSat, we will model random initial values of Pr,Sat, and random vectors of ΔPr,ΔSat defined by a direction in Pr,Sat space and a magnitude. In other words, we will model realisations of evolutions of pressure and saturation. To get the time lapse seismic response for the variety of pressure and saturation changes, we can calculate the base survey with the grid cells at their initial values of Pr,Sat and the monitor with the final values given by Pr+ΔPr,Sat+ΔSat. Moreover, we can define any intermediate Pr,Sat state by adding only a fraction of ΔPr, ΔSat to the initial pressure and saturation. This can be viewed as moving along the ΔPr, ΔSat trajectory and parameterized with just one parameter – the fraction value between 0 and 1. Overall, the advantages of this approach compared to studying pressure and saturation distributions from a simulator are in the following. Firstly, simulations are slower. Secondly, and this is the most important reason for choosing the trajectories approach, is the ability to model the full range of possible pressure and saturation evolutions. Reservoir simulator does not provide this ability, at least with a reasonable effort, because of the way pressures and saturations are constrained: we can only control the input parameters for the simulator while the output is a narrow set of pressure and saturation realisations which is difficult to vary in a controllable manner.

As long as our aim is to get a seismic response (a seismic trace) for each value of ΔPr,ΔSat, one value of ΔPr,ΔSat should be assigned per column of cells (one trace is assumed to penetrate a single column of cells) within one reservoir, rather than to each cell or in any other way. Therefore, we will use the term trajectory to name a single ΔPr,ΔSat per column of cells within one reservoir, while there can be more than one reservoir. An example of ΔPr,ΔSat realisation is given in Figure 5.28 for which the trajectories are depicted in the Pr,Sat space as shown in Figure 5.29. The modelling approach used here does not include any interaction or dependence between the columns of cells, so they can be viewed as independent 1D models of pressure and saturation change. However, these will be shown in 3D grids for the following reasons. Firstly, the grid used in this section was established before from the Schiehallion model, it has known geometry so the transition from the previous section with NTG variation to the current section is natural. Secondly, it is easier to model and interpret cases such as gradual rise of oil-water contact (see Figure 5.32) when the realisations are on a single grid rather than on separate columns. And thirdly, the whole reason for taking the trajectories approach was optimizing the process of generating realisations of seismic responses in terms of the (modelling process) performance. Performing calculations on a 3D grid facilitates achieving this goal.

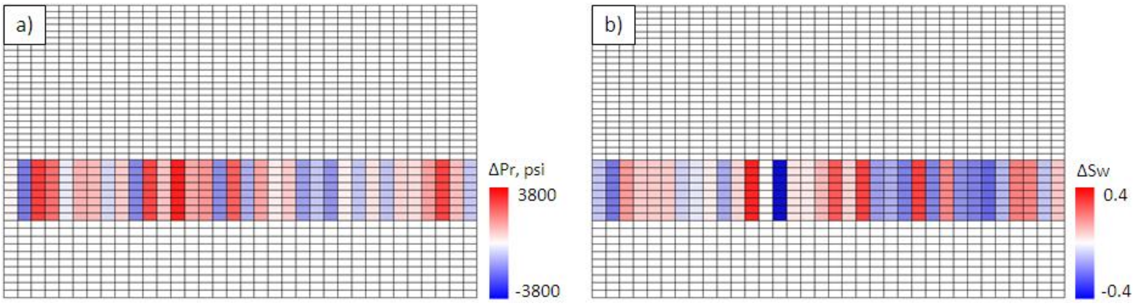

**Figure 5.28. Realisation of random ΔPr (a) and ΔSat (b) in a model of one reservoir.**

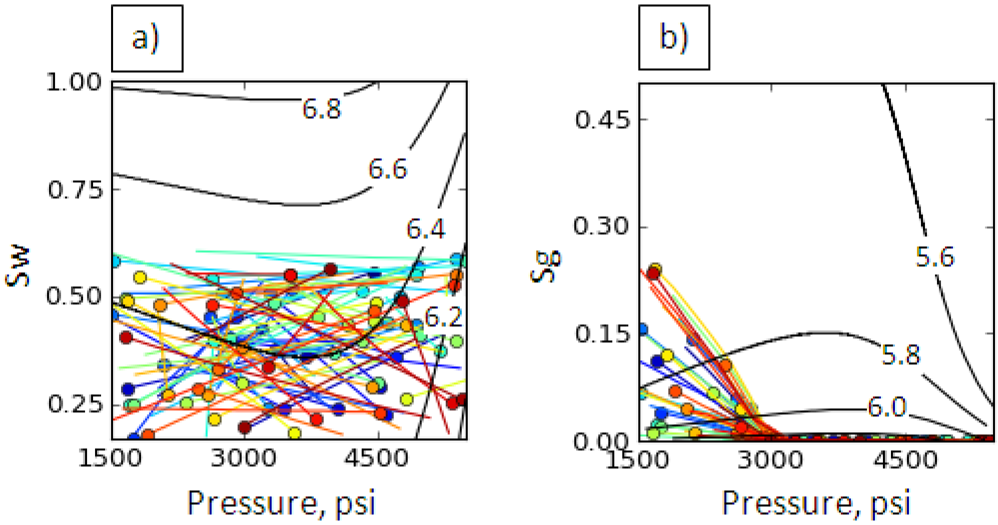

**Figure 5.29. Random trajectories of pressure and saturation change in (a) pressure-water saturation and (b) pressure-gas saturation coordinates. Only 80 trajectories are shown out of 816 defined on the grid of the model. Lines begin with dots indicating the start of the trajectory. Different colours are used for the lines to improve the visibility. Numbers on the contours are impedance values in km/s·g/cc.**

The plots show that the trajectories start at random locations and have random directions and magnitudes. However, since these represent changes in pressure and saturation occurring in natural displacement processes, some constraints need to be imposed on them. The following constraints were applied in this case. The first eliminates the appearance of gas when the reservoir pressure is above 3000 psi (slightly above the bubble point pressure from the Schiehallion example), and sets the volume of gas in a column of cells to be proportional to pressure drop below the bubble point. This assumes the process of gas exsolution with pressure decrease widely observed in the Schiehallion example. Although changes in gas saturation generally are not limited to this case (e.g. gas injection can lead to pressure increase), here we will model just this effect for clarity without losing the range of variation of seismic responses (whether we lost the range of the variation can be checked by simply removing this constraint).

Another constraint is applied to the way water and gas are distributed vertically. Because of their densities they tend to occupy lower and higher cells respectively (effect of buoyancy). This is modelled by filling the cells from bottom (top) with values of water (gas) until they reach $S_{wmax}$ ($S_{gmax}$), and moving to the next cell when the saturation of the previous is above critical. $S_{wmax}$=0.74 and $S_{gmax}$=0.5 in this case to match observations from the Schiehallion model. An example of distributions of water and gas constrained this way are shown in Figure 5.30. Hydrostatic pressure variation is small and ignored here. An important remark should be made about the way the pressure and saturation distributions are modelled with the constraints. Here, we do not have to model accurate states of the three phase fluid saturation and pressure. The aim is to span the range of the combinations of their values to study the corresponding range of seismic responses. This assumes that feasible combinations of the pressure and saturation changes are included in the modelled range. In the subsequent sections we will see that the conclusions about the seismic responses are not affected by this factor. The conclusions hold true even without using the constraints mentioned here so they can be viewed as only improving the presentation of pressure and saturation changes.

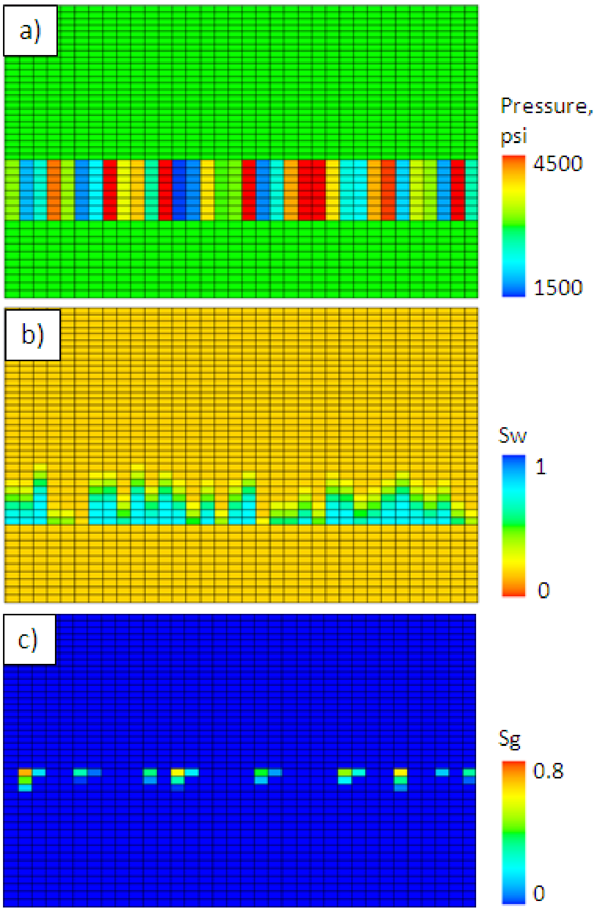

**Figure 5.30. Distributions of (a) pressure, (b) water saturation, and (c) gas saturation corresponding to the initial pressure and saturation state of the reservoir. Cross-sections of the model grid are shown.**

Similar to the previous section, we will study the seismic response by calculating the maps of the seismic attributes over the reservoir interval. The maps themselves will not be visualised here because, with the random trajectories in the adjacent cells, no information can be gained from their visual inspection. Instead, the values from the maps will be used in cross-plots.

### 5.6.1 *Correlation of 4D seismic attribute with impedance change subject to NTG variation*

In this subsection we will investigate the effect of the interference of the seismic signals from different layers within the reservoir and in the surrounding rocks. In particular, we will check if different vertical sequences of NTG property will affect the relationship between the values of impedance change and the 4D seismic attribute.

In the previous section it was shown that the interference of the signals from different layers makes the relationship between the average impedance of the reservoir and seismic attributes more complex. The correlation between the impedance and the seismic attributes was reduced when the impedance contrast of the reservoir (compared to the enclosing rocks) was weaker. Similar test for the 4D seismic attribute is done in this section using the cross-plot of the impedance change between the base and monitor surveys versus the 4D seismic attribute given by a difference of base and monitor seismic responses.

Again, we will choose two models of NTG distribution, with high NTG of overburden and underburden (low contrast reservoir) and reduced NTG of the enclosing rocks (high contrast reservoir) as shown in Figure 5.31.

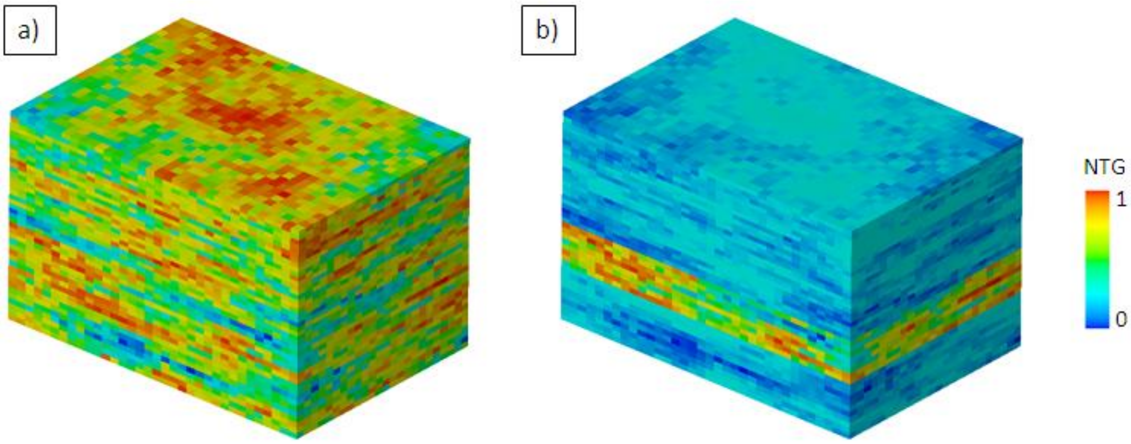

**Figure 5.31. Models of NTG distribution used for modelling the 4D seismic response: a) NTG of enclosing rocks is as high as in the reservoir (low contrast reservoir), b) NTG of enclosing rocks is reduced by a factor of 0.3.**

First of all, using the model in Figure 5.31, b, we will check how different seismic attributes compare with the impedance change. For this purpose a simple scenario of Pr,Sat change is chosen in which the water saturation increases systematically in the reservoir as in a bottom water drive (Figure 5.32). Figure 5.33 shows corresponding ΔPr, ΔSat trajectories – a line in the Pr,Sw coordinates and only a point in the Pr,Sg coordinates indicating no change of pressure and gas saturation. In this and the subsequent experiments, modelling the Pr,Sat change (moving along the red line in Figure 5.33) is done is 10 steps by adding one tenth of the ΔPr, ΔSat to the current Pr,Sat state. At each step, the seismic data are predicted from the current model from which the maps of the seismic attributes are compared. In this case, each column of cells in the 3D grid gives one point on the attribute map. The value of the attribute at this point changes with time (in 10 steps). This way, we get 816 (number of points on the map 24 x 34 = 816) time-variables for each map of seismic attributes or impedance. The correlation between the variables on different maps can be studied by cross-plotting them. Figure 5.34 shows cross-plots of the variables from different seismic attributes versus ones from the impedance map. Each cross-plot contains 816 curves, with each curve showing the change of a seismic attribute with the change of impedance.

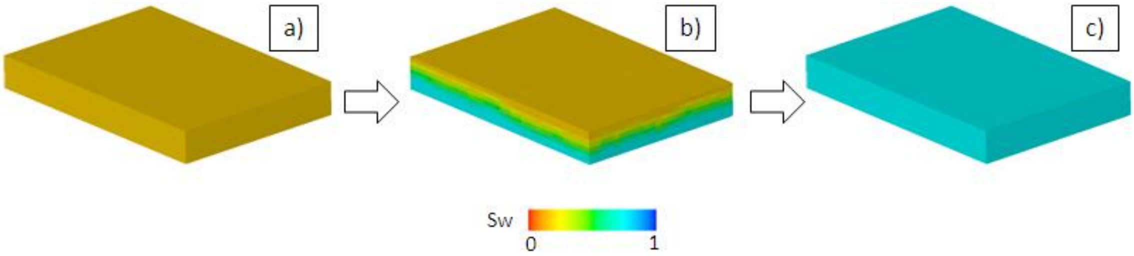

**Figure 5.32. Modelling of increasing water saturation as a bottom water drive: a) initial water saturation (Sw=0), b) intermediate level of oil-water contact, c) water swept reservoir (Sw=0.75). Only the producing reservoir interval shown. Slight variation of the oil-water contact depth in (b) is due to the way Sw is distributed accounting for the NTG variation. This variation (of Sw) does not affect any of the results presented here.**

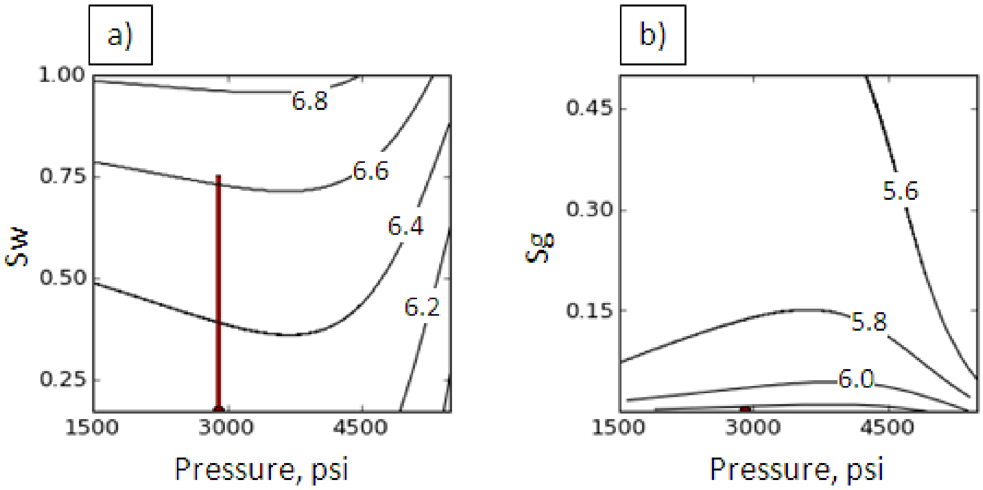

**Figure 5.33. Trajectories of pressure and saturation change in a) pressure-water saturation and b) pressure-gas saturation coordinates. The format of the figure is the same as in Figure 5.29.**

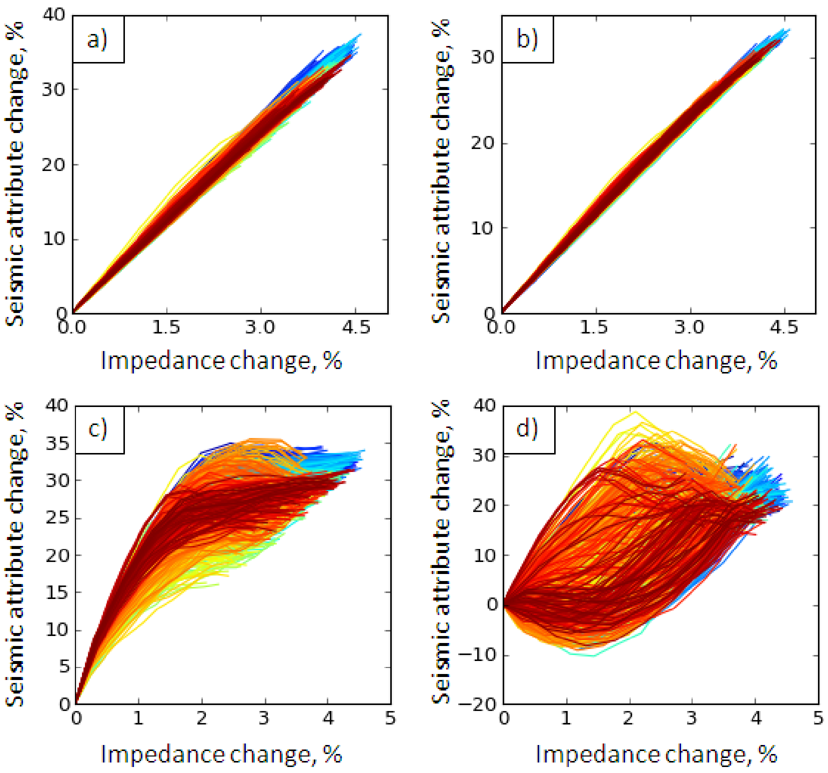

**Figure 5.34. Cross-plots of different 4D seismic attributes versus impedance change: a) (1st order) average of difference of CI-transformed seismic, b) difference of maps of average of CI-transformed seismic traces, c) as (a) but RMS instead of first order average, d) as b but each map is RMS of seismic traces.**

Since in our model, the average water saturation changes similarly in each column of cells, the differences between the curves of any cross-plot in Figure 5.34 are due to the NTG distribution (the grid is flat, so no geometry effect in this case). In this figure, we compare 1st and 2nd order average attributes and also maps of differences and differences of maps. The 1st order average attribute is defined as a sum of amplitude samples from the specified interval divided by the number of samples. The 2nd order average attribute (RMS attribute) is defined as a square root of a sum of squares amplitude samples divided by the number of samples ($RMS = \sqrt{\frac{1}{n}\sum_{i=1}^{n} A_i}$, where $A$ is amplitude, and $n$ is the number of samples). In general, the choice of attributes is dictated by the need to highlight certain geological information from the raw seismic data. In our case, the choice is based on the correlation of the seismic attribute with the underlying impedance changes. In particular, using the 1st order average here is inspired by the results of the previous section where the SoN attribute (first order average) had better correlation with the impedance change. We replace the SoN by the simple average because we are dealing with differenced seismic traces which have varying polarity. The SoN attribute can still be used for individual (base and monitor) surveys, and then the maps differenced. The SoN attribute used this way will be compared with the average attribute in the later discussion.

Figure 5.34 shows that in case of the first order attributes, they track the impedance change very well (panels a and b). Also, the two attributes, the difference of the maps and the map of difference show similar agreement with the impedance. In the case of RMS, taking the attribute of the differenced seismic trace seems preferable, but due to the amplification of the higher values, we can see that the curves depend on NTG more strongly and are nonlinear. Overall, the first order attributes look preferable because they are less affected by the NTG variation.

Since we have defined the preferable attributes, we can study the issue of the low contrast of the reservoir – when the NTG of enclosing rocks is as high as that of the reservoir (Figure 5.31, a). In the previous section, we found that such a case of low contrast reservoir was devastating for the seismic attributes because the seismic amplitude is proportional to the impedance contrast. Lack of contrast caused poor detectability of the reservoir sands (see Figure 5.17, a). Here, a similar test was conducted comparing the time-lapse impedance change with the change of the seismic attribute (average of differenced seismic traces) for the models with low (Figure 5.35, a) and high (Figure 5.35Figure 5.31, b) contrast reservoir. The percentage of the impedance and the seismic attribute change are in agreement with the data from our rock physics analysis presented in Table 5.1. The high percentage of 4D attribute in Figure 5.35, a is due to the effect of low base – the amplitude of the base survey (the denominator) is low due to the low contrast.

The result shown for the 4D attribute in Figure 5.35 suggests that it is not the contrast of the reservoir that determines the 4D signal but the pressure and saturation change. In other words, the effect of NTG variation is largely swept away by the differencing. We should stress however, that the effect of NTG here means the effect on the relationship between the impedance and the seismic attribute. Of course, the NTG variation still affects the impedance change itself (more on this in the later discussion).

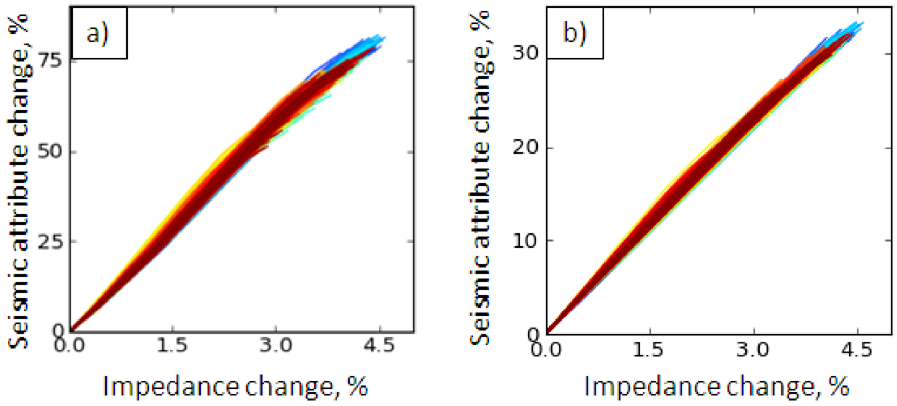

**Figure 5.35. Cross-plots of 4D seismic attribute (average of seismic difference) versus impedance change for the case of systematic increase in water saturation. A) model with high NTG outside of reservoir b) model with low NTG outside of reservoir.**

In the next test, we will compare the models with high and low reservoir contrasts when not just the water saturation changes in the reservoir but the full spectrum of possible changes of pressure and saturation occur. This is modelled using the random trajectories as discussed before. Figure 5.29 visualises a subset of trajectories which illustrates the concept. Similar to the previous test, each step (out of 10) of moving along the trajectories gives a map of time-lapse impedance change and the 4D seismic attribute for the current state of the reservoir. These are then cross-plotted as shown in Figure 5.36. The result confirms the findings of the previous test where only water saturation changed. Again, the presence of the high NTG overburden and underburden did not affect much the relationship between the time-lapse impedance and 4D attribute.

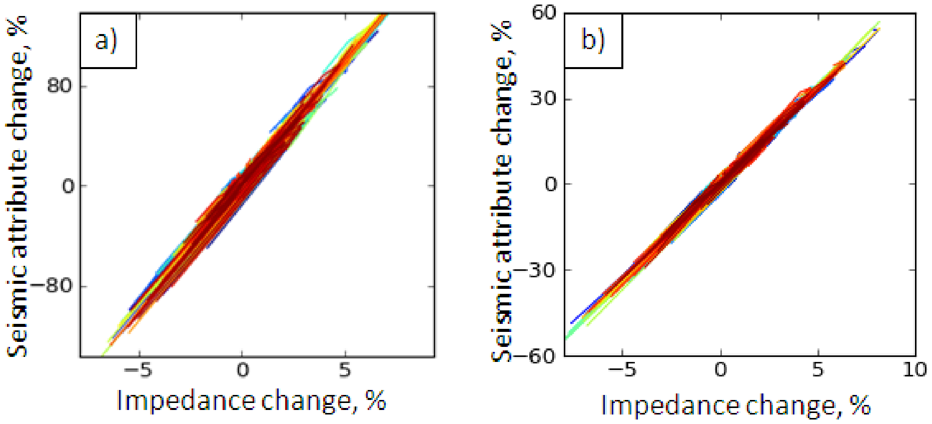

**Figure 5.36. Cross-plots of 4D seismic attribute versus impedance change for the case of random trajectories. A) model with high NTG outside of reservoir b) model with low NTG outside of reservoir.**

### *5.6.2 Interference of the 4D signals in the stacked reservoirs*

The effect of the NTG was reduced in the differenced seismic data because it mostly the static part of the signal. On the other hand, if the signal outside of the reservoir is also a time-lapse, then we should expect a greater interference. This is studied in the following test where we use a model with two reservoirs as shown in Figure 5.37, a. The seismic attribute is calculated over the upper target reservoir while the underlying reservoir is a source of the interfering signal. Similar to the last test, the trajectories of pressure and saturation change are random both in upper and lower reservoirs, but are independent of each other in the two reservoirs. The rest of the experiment set up is the same as in the previous tests with the result presented in a form of a cross-plot (Figure 5.37, b). This time we can see that the curves representing the seismic responses of separate columns of cells are different functions, not lines of a (nearly) same slope as in the previous tests. This result tells us that a strong interference occurs if the underlying reservoir is also producing. In particular, this illustrates the weakness of the map based attribute in application to the stacked reservoirs, also discussed in Literature review chapter (section 4D seismic attributes).

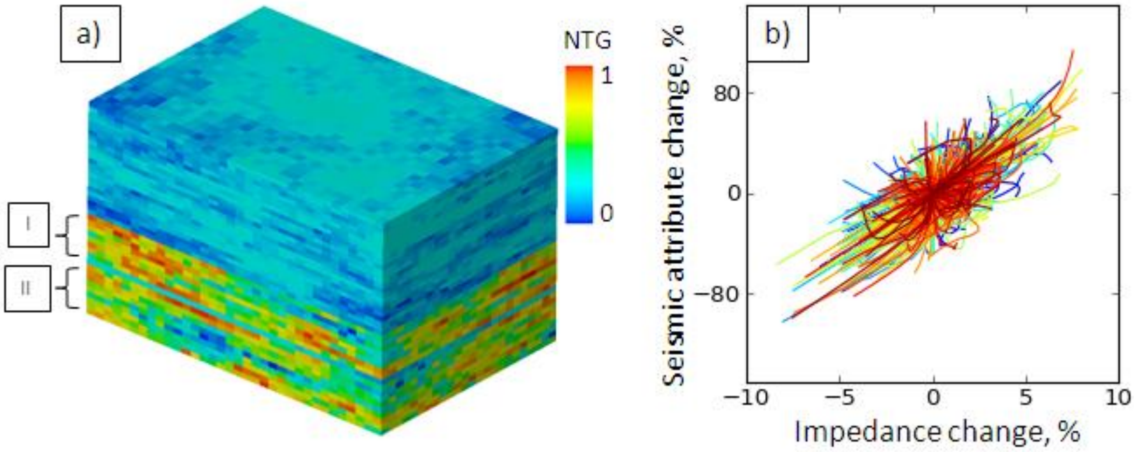

**Figure 5.37. A) model with two reservoirs, target reservoir I and the underlying reservoir II, b) cross-plots of the 4D seismic attribute and the average impedance change calculated over the target reservoir.**

### *5.6.3 Effect of the reservoir geometry on the seismic response*

The time-lapse seismic responses modelled so far using the flattened grid showed good correlation with the impedance changes provided there are no pressure and saturation changes in the surrounding rocks (outside of the seismic attribute time window). In this we will return to the original geometry of the grid to assess the effect of the thickness variation (Figure 5.38, a). Only the systematic change of water saturation (trajectories are shown in Figure 5.33 and the evolution of the water saturation in Figure 5.32) is modelled to ease the examination of the resulting cross-plot. The rest of the experiment is the same as in the previous cases with a single high contrast reservoir. The resulting cross-plots of the seismic attribute (1st order average of CI amplitudes) change versus the impedance change for all 816 points on the map are shown in Figure 5.38, b. Notably, the curves are still nearly linear, similar to the ones shown in Figure 5.35. At the same time, their slopes are different and the difference depends on the thickness of the reservoir layer: the amplitude is higher in thinner parts and lower in thicker due to the tuning effect (constructive interference of the amplitudes).

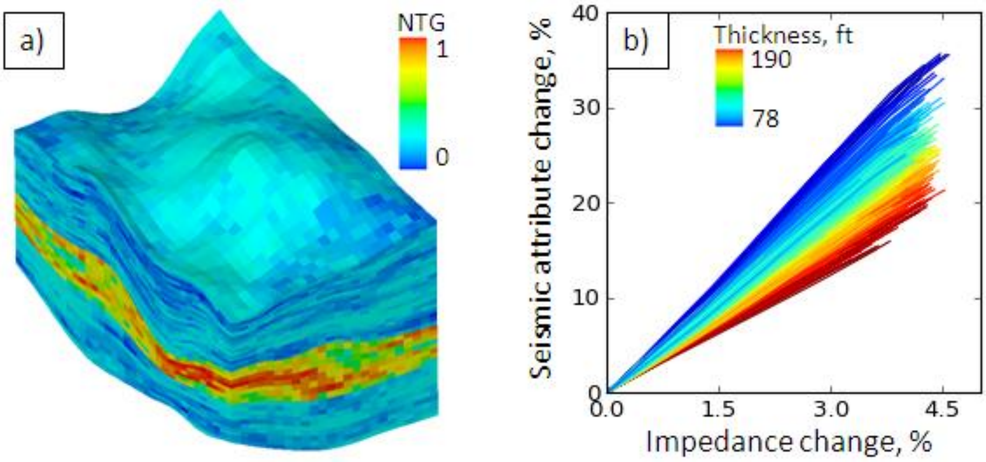

**Figure 5.38. A) NTG model on the part of Schiehallion grid without flattening, b) cross-plot of 4D seismic attribute (1st order average on CI) versus impedance change. Line colours correspond to reservoir thickness.**

We have shown that the seismic attribute detects the impedance changes well, but the character of the relationship is still conditioned to the layer thickness. The practical implication of this conclusion is that the quantity of interest, which is impedance in this case, is better determined by the observed data and affected less by the secondary factors such as distributions of static properties or nonlinearities. These factors cannot be fully captured by our imprecise models so their reduced role is advantageous. The thickness of layer is easier to model though.

### *5.6.4 Variation of 4D seismic response due to the ‘wrong’ NTG model*

In the previous sections we studied how well the seismic attributes estimate the average impedance of the reservoir interval. At the same time, the interpretation of the 4D seismic data aims to reveal the pressure and saturation changes behind the 4D anomalies, not the impedance by itself. In this context, another type of question can be posed. How would the 'static' factors (e.g. NTG distribution) affect the seismic response if we get them wrong? After the analysis made in the previous sections, we know that the relationship between the impedance change and the 4D seismic response isn't affected much by the NTG distribution, however, the 4D impedance values themselves certainly will be different for a different NTG model (see Figure 5.4 in the Petro-physical model section above). As a result, a different NTG model will give a different 4D seismic response. Again the reason for the difference lies in the rock physics model now, not in the seismic domain, nevertheless this constitutes the effect of wrong NTG in our model on the seismic response. The effect is illustrated in Figure 5.39, where a simple experiment, similar to the one in subsection 1 with the systematic increase in water saturation, was conducted with two different NTG models. The time-lapse seismic responses for the two models are then compared in a cross-plot (Figure 5.39, c). These seismic responses are obtained with the same dynamic parameters (ΔSw) but different static parameters (NTG). The cross-plot shows the expected difference between the seismic responses due to the NTG substitution.

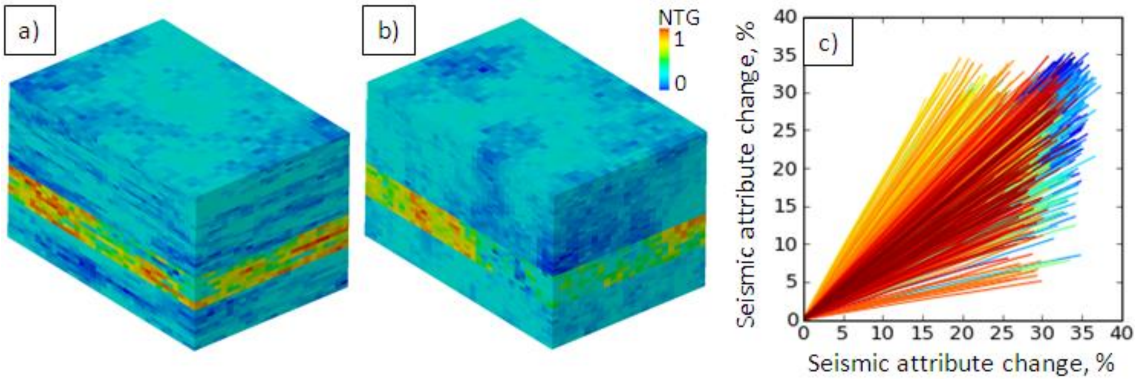

**Figure 5.39. Comparison of seismic responses from two different NTG models. A) first NTG model, b) second NTG model, c) cross-plot of seismic responses. Different colours of the lines correspond to indexes of cell columns and applied to ease distinguishing the lines.**

The spread of the curves (lines) in the cross-plot above shows the error we would get if we tried to invert the observed seismic data for the water saturation changes using the wrong NTG model. However, this applies to inversion of the individual points only. In other words, if the number of constraints (or observations in this case) is small then the external factors such as the wrong static properties can cause arbitrarily large errors. In reality, when we are inverting seismic data for the reservoir parameters, there are at least two factors that stabilise our solution: using more seismic data (and other data types in general, but here just more points of the seismic attribute will do) and choosing the solution out of a predefined solution set. The first point is demonstrated in the following test (Figure 5.40) where the maps of the seismic attributes are still generated on each step (out of 10), but instead of using all 816 points from the maps, they are randomly grouped by 24 cells giving 34 curves for the cross-plot (Figure 5.40, c). The cross-plot shows that the grouped seismic attributes change similarly for the two NTG distributions. This result is expected. Different points of the attribute map (before grouping) had the same value of the dynamic property ($\Delta S_w$) at each step but different values of NTG. So, grouping several observations allowed to us to filter out the variable part and determine the property of interest – $\Delta S_w$.

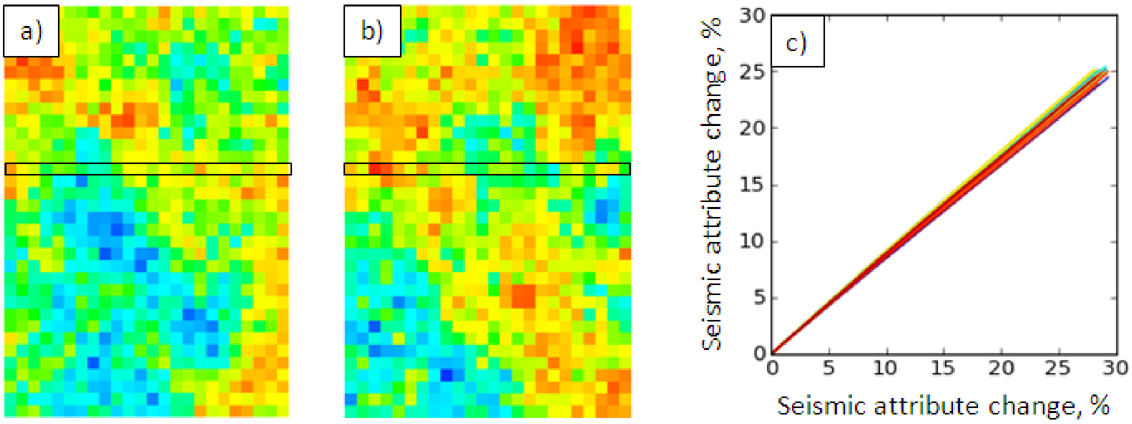

**Figure 5.40. Comparison of seismic responses from the models shown in Figure 5.39, calculated in groups of 20 cells. A) first NTG model, b) second NTG model, c) cross-plot of seismic responses. Top views of producing intervals are shown for the NTG models, 3D views are given in Figure 5.39. The black rectangle shows groups of 20 cells within which the seismic response is calculated and averaged.**

The second point in stabilising the inversion results is discussed in more details in the following chapters. Briefly, the predefined set of solutions determines the form of the final solution, and as such is a way of incorporating our requests of a desired result and a limiting factor at the same time. For example, the inversion for impedance on a simulation grid as described in the Methodology section, limits the results to the piecewise-constant (blocky) distributions. We will never get, say, a smoothed vertical impedance distribution (not that we would usually need them) but we are guaranteed to stay within a class of impedance distributions on the grid of which we will find the one giving the best data fit. Another example is the inversion for pressure and saturation changes versus the seismic history matching (inversion for parameters affecting the flow – e. g. permeability). Clearly, the history matching case is more restrictive than the inversion for Pr,Sat in terms of the resulting distribution of Pr,Sat because in history matching, we will only get distributions that the simulation model can generate. Again this ensures that the distributions will probably be spatially smoother in the history matching case and also that they are feasible given the current model. At the same time, this can be a limitation or an example of overly restrictive prior because the limits imposed by the simulation model are as correct as the model is. The uncertainty of the resulting Pr,Sat distribution will be underestimated in that case.

## 5.7 Conclusions

We studied 4D seismic signatures occurring as a result of a range of production-related changes in the reservoir. According to the rock physics analysis the effects of water sweep, gas coming out of solution, pressuring up are confidently detectable using 4D seismic attributes for the chosen template dataset of the Schiehallion field. We can use corresponding 4D anomalies to constrain the simulation models in seismic history matching studies of the following chapters.

Map-based seismic attributes are affected by interference of the seismic signals and difficulties in localising the signature of target properties. Superposition of the reflections leads to constructive and destructive summation of the amplitudes and accounts for the amplitude cancellation and nonlinearities in the seismic response. These factors reduce the detectability of the pressure and saturation changes. In a high contrast reservoir however, the variation of reservoir impedance is detectable by the seismic attributes. It was shown that the first order average of amplitudes correlates well with the impedance.

Effect of NTG on the relationship between the average impedance and the seismic attribute is largely reduced after 4D differencing. However, the interference occurs if the underlying or the overlying reservoir is producing. This is the reason why the volumetric attributes can be preferred in stacked reservoirs.

# Chapter 6. Problems of incorporating seismic interpretations in simulation models

## 6.1 Introduction

Increased computer power and advances in data acquisition and processing techniques result in more complex geological models available today. For example, integrated analysis of seismic and other data types allow us interpreting channels, inter-reservoir shales, and other sophisticated details of the sediments bedding and reservoir architecture which are then represented in reservoir models as distributions of facies, NTG, porosity and permeability properties. *Miranda, 2007* and *Martin and Macdonald, 2010* present studies on building models of the Schiehallion reservoirs using interpretations of high resolution seismic data. In the latter study, a framework of geobodies was extracted from the 3D seismic images which was then incorporated into the simulation model to define transmissibility regions. This allowed the authors to achieve good pressure matches on the wells. However, the main question regarding the deterministic objects incorporated in a simulation model is whether it is compatible with the dynamic data and what bias it will produce. If such inclusions result in areas of fixed properties in the simulation model then this becomes a particular case in a class of underparameterized problems. *Hunt et al, 2007 and Oliver and Chen, 2011* point out that insufficient parameterisation leads to more unique but also more biased models. The bias from the fixed part of the model (not varied in history matching) is recognised as "structural noise". As discussed in Literature review chapter (section Choosing a parameterisation consistent with data resolution), *Jafarpour and McLaughlin, 2009* and *Khaninezhad and Jafarpour, 2014* stress the importance of balance between the controlling factor of the prior information incorporated though the parameterisation and the ability of the model to assimilate the information from the dynamic calibration data (observed data in history matching).

In this chapter, the problems associated with integrating the deterministic interpretations such as geobodies into simulation models are discussed. The examples chosen here are largely influenced by the Schiehallion model (described in Chapter 5) and its parameterisation with the seismically derived geobodies.

## 6.2 Unrealised variability in a controlled experiment

We started our discussion in this chapter by naming some problems of insufficient parameterization such as the bias of the deterministic part of the model and associated difficulty in studying the range of model responses. A good example where we may face these problems is when conducting a history matching experiment in which a model is fitted to the known synthetic truth. The synthetic truth is a simulation model with certain distribution of properties and giving some response – well rates, BHPs, 4D seismic images. The response of the truth, or of the reference model, is then taken as observed data which is to be matched by another, variable model under investigation. After the 'observed' data for the experiment is found, the next step is building a model that would match the reference response through a history matching process. In this situation, it seems logical and is in fact straightforward to re-use the reference model instead of creating a new one, with only a part of it made variable by designating parameters. However, depending on the purpose of the history matching study, this approach is not without pitfalls. In particular, the fixed part of the model gives constructive bias to the model response in that it is of course fixed to the true values. If the purpose of history matching is studying how the variable parameters are resolved by the data then incorrect estimates can result from such a study because it is not known a priori what the balance between the variable and fixed parts of the model is in defining the model response. We may find that the variable parameters converge to their true values in history matching too easily even though they are not fully resolved by the data. Continuing this reasoning, two pieces of data with different information content (e.g. of different type or quality) are likely to lead to similar values of the variable parameters in that experiment if the response is already mostly defined by the fixed part of the model leaving us with no clue on the difference between those data pieces. The consequence of using an inflexible model from this perspective is the excessive confidence in the estimated parameters not warranted by the data.

In the following sections, we will run history matching experiments comparing the models with different levels of flexibility to demonstrate the scope of the problem of the reduced variability of predictions in the overly fixed settings. Our approach will be based on generating multiple realisations of history matched models as opposed to using a single best model as it does not give an insight into the sensitivity of parameters. Generally speaking, once the history matching algorithm has converged to the best model, we declare that a solution to the parameter estimation problem is found. The solution alone, especially if it coincides with the true values (in a synthetic setting, of course), does not tell how hard it was to find it, whether the objective function in the vicinity of it was steep or flat, in other words, how well the solution is determined by the data or what is the uncertainty of the solution being correct from the data perspective. Although methods exist that quantify the uncertainty of parameter estimates, e.g. those based on sampling the response surface or analysing the sensitivity matrix, calculating the associated probabilities involves many assumptions about the measurement and model errors. This is why dealing with any numerical estimates of uncertainty is avoided here in favour of direct comparison of the ranges of predictions (production forecasts) in the counter-cases – the fixed models and more flexible models.

The following two sections compare two scenarios: over-determined models and less determined models. In the first, too few parameters are used for calibrating the models to the dynamic data. As a result, the variance of the resulting realisations of history matched models is mostly determined by the prior knowledge embedded in the parameterisation itself rather than information in the data. In the second scenario, the parameterisation (pilot points) is not so restrictive (more flexible). This allows the data to determine the variability of model estimates.

### *6.2.1 Over-determined models*

In the first experiment, we will model a situation where the prior knowledge about spatial distribution of heterogeneities is incorporated in the parameterisation (connection of prior information and parameterisations is discussed in the literature review, section Parameterization). Zonation is known to bear such spatial information when the extent of the zones is fixed prior to history matching. Closest adaptation of zonation to seismic history matching is a parameterisation where transmissibilities of seismically-derived geobodies are varied. In either case the volume of reservoir is divided into regions to control the flow pattern in a reservoir with a reduced number of parameters. In this section, the regions will be referred to as deterministic channels to stress that their geometry is defined prior to history matching. Figure 6.1 shows the channels used here. Transmissibilities of those channels on the other hand will constitute the history matching parameters. In line with the spirit of over-determined models, the reference and the variable models (reference and variable models are defined in the beginning of 6.2) share all the properties including the geometries of the channels, and only the transmissibility multipliers are not known in the variable models so these will be estimated through history matching.

For the history matching experiments the models are used with the grid described previously in the Chapter 5 (section Grid for the synthetic model). Only the interval called the producing interval in Chapter 5 is used here because at the moment, we are not interested in the effect of impedance variation in the overburden and the underburden rocks on the seismic response, that is the seismic map calculated within the reservoir interval. The active part of the grid has 24x34x8 cells with approximate sizes of 160x160x20 ft. Two history matching scenarios are considered here which are called "Model 1" and "Model 2" cases. The differences between the cases are the different well placements and slightly different channel geometry as shown in Figure 6.1 and Figure 6.2 and also different values of transmissibilities in their reference models. Transmissibilities in the models are set using 7 parameters – transmissibility multipliers applied within and between the regions (channels). The location of the parameters is shown in Figure 6.1 and Figure 6.2.

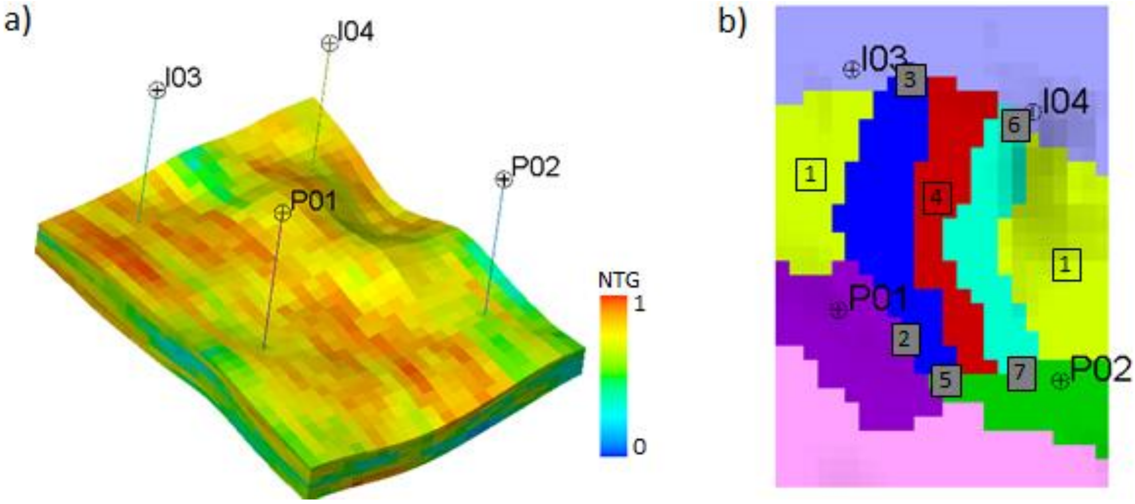

**Figure 6.1. Model 1 case: a) NTG distribution, b) distribution of deterministic channels that act as transmissibility multipliers. Different colours of regions signify different indices of the regions. Numbers in boxes are numbers of history matching parameters. Inter-region multipliers are in grey shaded boxes, and within-region multipliers are without shading.**

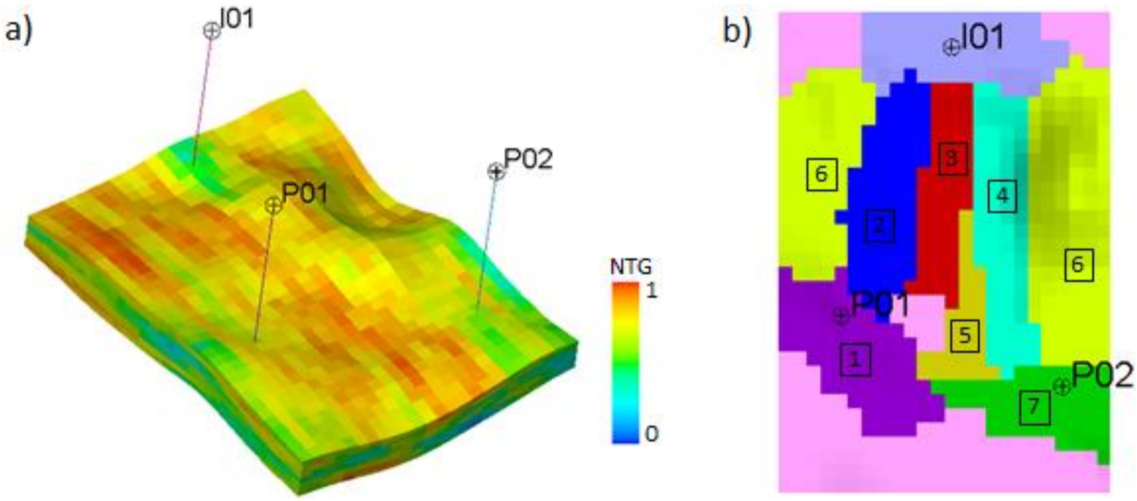

**Figure 6.2. Same as Figure 6.1 but for Model 2 case.**

As discussed before, historic data in these experiments are obtained from reference models. Reference models for cases Model 1 and Model 2 are defined by setting particular values for the transmissibility values described above. Table 6.1 summarises the values of parameters set in reference models (‘true’ values) and also the parameter ranges set for the subsequent history matching experiments. Prior to any adjustments to the transmissibility field by transmissibility multipliers or permeability modifications via pilot points, the permeability of all the models, including the reference one is constant, equal to 1000 mD. This is the case in this (6.2.1) and in the following (6.2.2) sections. Moreover, models with the constant permeability are considered base case (or starting) models for history matching scenarios. Predictions of the base case models are compared with predictions of the history matched models in order to highlight the effect of tuning the parameters in each of the history matching scenarios.

**Table 6.1. ‘True’ values of history matching parameters for Models 1 and 2.**

| parameter number | Model1 | | | Model2 | | |
|---|---|---|---|---|---|---|
| | 'true' value | minimum | maximum | 'true' value | minimum | maximum |
| 1 | 0.05 | 0.005 | 2 | 1 | 0.2 | 2 |
| 2 | 0.01 | 0.005 | 2 | 0.2 | 0.005 | 2 |
| 3 | 0.5 | 0.005 | 2 | 0.05 | 0.005 | 2 |
| 4 | 0.7 | 0.2 | 2 | 0.7 | 0.005 | 2 |
| 5 | 1 | 0.005 | 2 | 0.05 | 0.005 | 2 |
| 6 | 0.01 | 0.005 | 2 | 0.1 | 0.005 | 2 |
| 7 | 0.05 | 0.005 | 2 | 1 | 0.2 | 2 |

Setting the parameters to the 'true' values listed in Table 6.1 results in distributions of pressure and saturation in the reference models as shown Figure 6.3 and Figure 6.4. These distributions are obtained after simulating two years of production (Aug 1998-Aug 2000). Seismic responses corresponding to these states of pressure and saturation are shown in Figure 6.5. For characterising 4D seismic response, mean of coloured inversion attribute was chosen as discussed in Chapter 5 (section Seismic response to pressure and saturation changes) where the procedure for calculating the attributes is described too. Parameters of added noise shown in Figure 6.5, b and Figure 6.5, d will be explained later.

The reference 4D seismic maps show 4D effects of water displacing oil in the areas around injectors I01, I02, and I03 and also the effect of gas exsolution near the producers P01 and P02. As shown in Figure 6.1 and Figure 6.2, producing wells P01 and P02 are located in distinct geobodies with limited connection with the neighbouring geobodies and ultimately with the injectors from which the pressure is supported. The resulting pressure depletion causes gas liberation – analogous to the effects observed in the Schiehallion case (Chapter 5, section Model-based interpretation of 4D seismic effects).

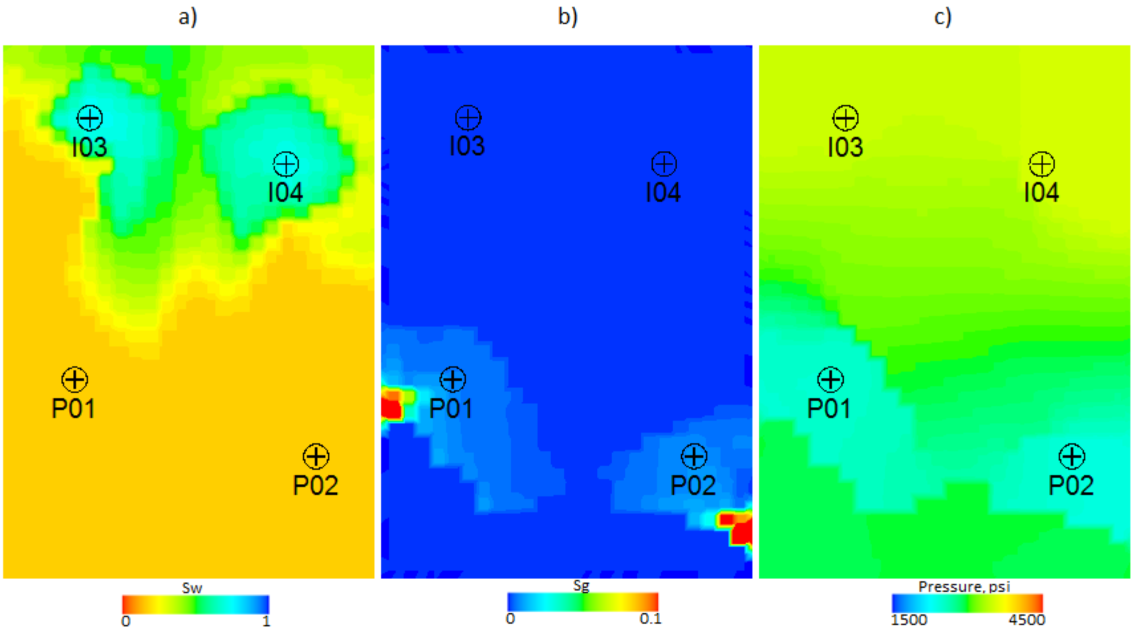

**Figure 6.3. Average maps of reference pressure and saturation for Model 1 for Aug 2000 (after 2 years of production): a) water saturation, b) gas saturation, c) pressure. Averages calculated over the reservoir thickness.**

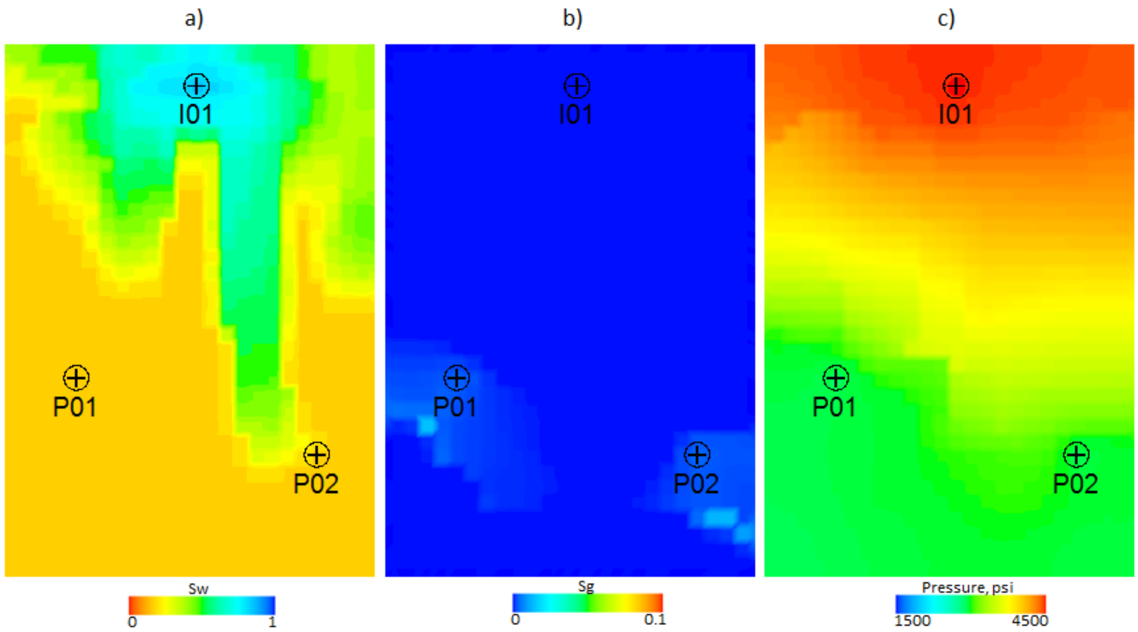

Figure 6.4. Same as Figure 6.3, but for Model 2.

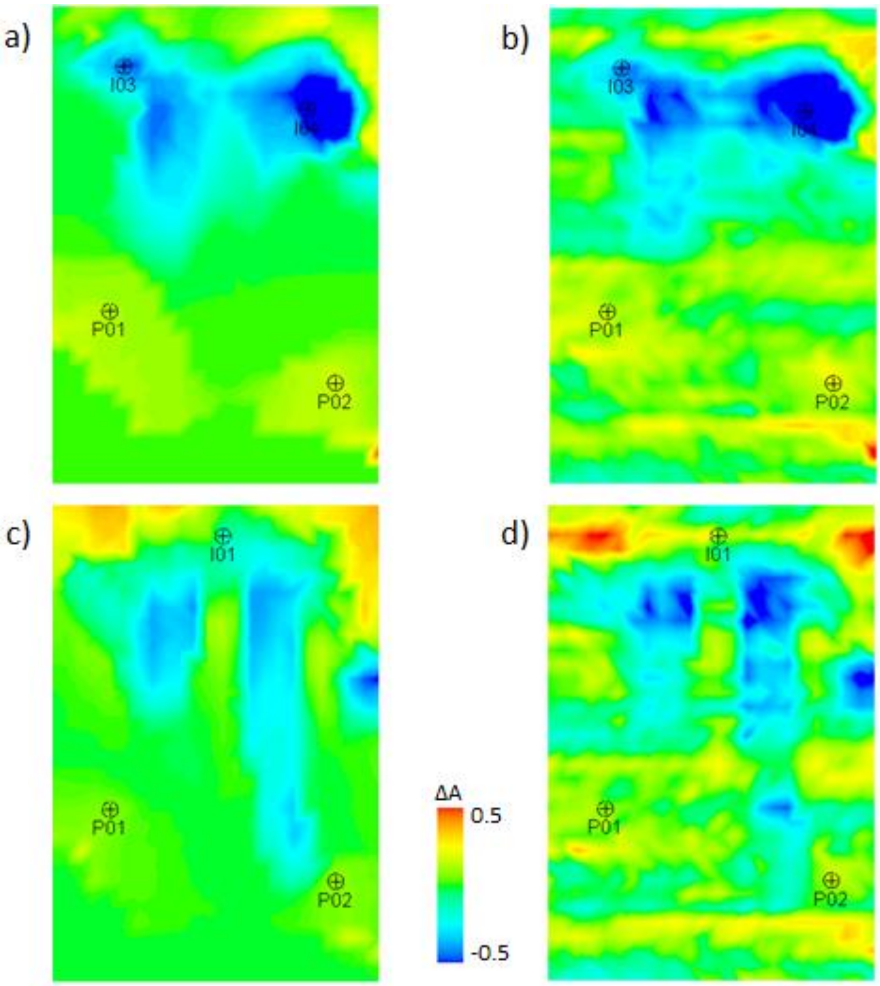

Figure 6.5. Reference 4D seismic response used as observed data in history matching experiments: a) seismic response of Model 1, b) as (a) but with added correlated noise, c)-d) as (a) and (b) but for Model 2. Noise in (b) and (d) is the same.

4D seismic maps presented above (specifically, the noisy versions) are used as observed data for the history matching experiments conducted here. Moreover, the observed dataset consists of those seismic maps only, no production data are used for model calibration because no water cut is observed in wells within the 2 years of production. Although it is shown in Chapter 7 that it is difficult to constrain production forecasts effectively by history matching to seismic maps only, in this rather synthetic case with only few parameters, this constraint can be effective enough provided a map has enough information. In particular, the map for Model 2 has more constraining information than that of Model 1 because the water front progressed further in Model 2 due to the specific parameter values (both models simulated 2 years though). Different information content in Model 1 and Model 2 is intentional and is required for comparison of parameterisations as discussed before (beginning of section 6.2).

Adding noise to the observed data as shown in Figure 6.5, b and Figure 6.5, d is important for this synthetic case. Indeed, when the number of parameters is not large, there is a chance for the history matching algorithm to converge to the true values exactly. This would nullify our attempts of studying the range of forecasts resulting from multiple realisations of calibrated models. Adding noise on the other hand will move the solutions somewhat away from the true values allowing more equiprobable solutions. The next question about adding the noise is what type should be used. As described in Theory chapter, different types of noise exist in field measured seismic data such as multiples or strong coherent ground-roll with the random incoherent noises usually suppressed during the seismic processing. In this case, correlated noise with the following characteristics is chosen: strength of 40% of maximum amplitude of the seismic data, correlation length of 500 ft along the flow (NS) and much longer than the model dimensions across it (EW). The noise is chosen to be correlated in the direction across the flow to ensure it does not interfere with the parameter estimation with the channels (parameters) oriented along NS direction in the first scenario (section 6.2.1). On the other hand, it can interfere with the useful signal in the second scenario (section 6.2.2) with pilot points which is in line with the increased flexibility of the parameterisation there.

History matching was carried out using the PSO algorithm with 40 particles and 25 to 30 iterations. The sorted values of the objective function for history matching of Model 1 and Model 2 cases are shown in Figure 6.6. The objective function contains data errors without correlations, with error level set to a constant. The absolute value does not matter here because all the cases uses similar seismic attribute so are perfectly comparable.

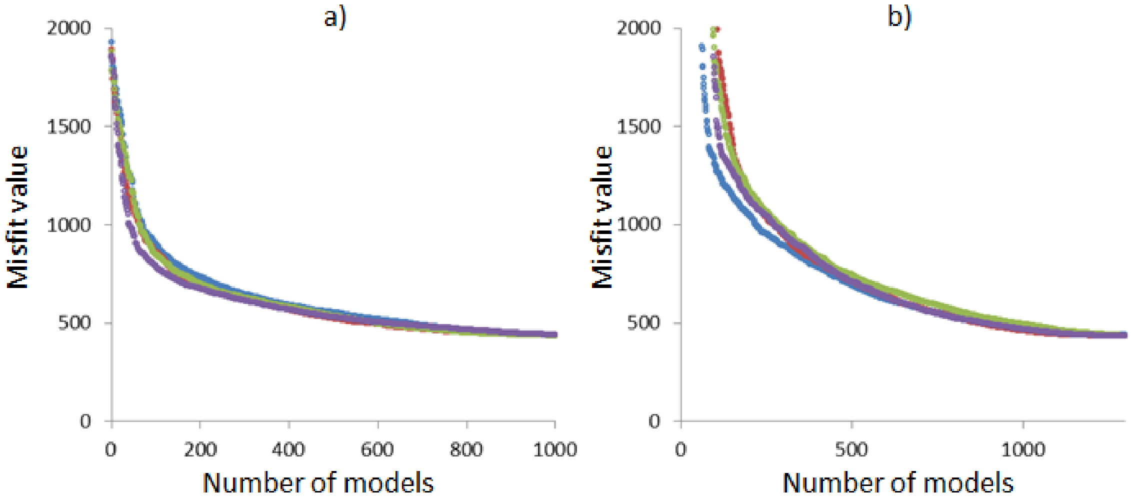

**Figure 6.6. Misfit reduction with the number of models for four history matching runs for a) Model 1 and b) Model 2. The function is obtained by sorting the misfit functions of individual particles in descending order. Some of the initial misfits (b) were truncated.**

The observed dataset consisted of seismic maps shown in Figure 6.5, b and Figure 6.5, d only. The added noise in these data allowed solutions to be obtained that are slightly different from the true case for different realisations. Predicted data were the same seismic attributes as observed data. Figure 6.7 and Figure 6.8 show, out of the ensemble of realisations, predictions of 2 history matched models for each of Model 1 and Model 2. The figures compare the predictions of history matched models with the original predictions of the reference models shown without added noise for clarity although the noisy versions were used in history matching. Also, the seismic prediction of the base case model is shown for comparison (plot (b) of each figure). The base case model is the one without transmissibility barriers, that is all transmissibility multipliers are set to 1. As expected, the historic maps were well repeated by the predictions of the history matched models. Because these models fit the data equally good, they can be treated as equiprobable realisations of history matched models given the data (only data fit defines probability here as there is no preference in terms of values of parameters). The variability of these realisations will be studied using their production forecasts as shown below.

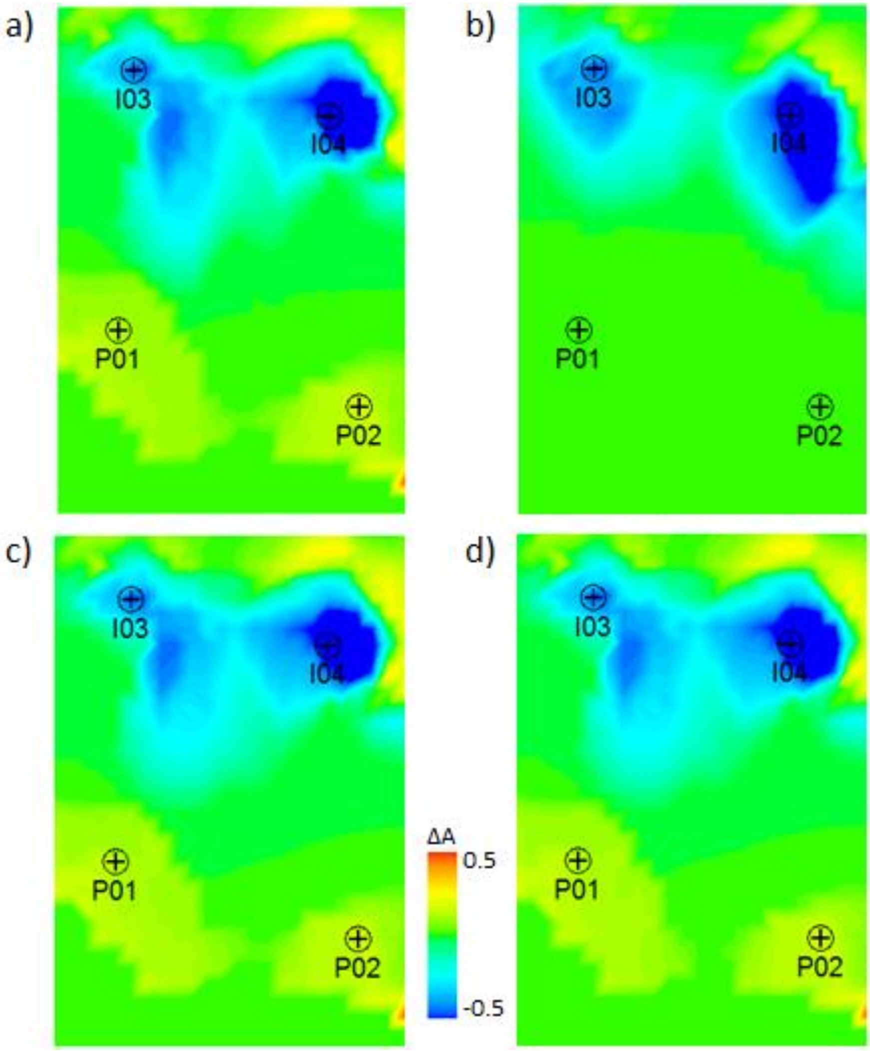

**Figure 6.7. Results of history matching using the seismic maps as data and the deterministic channels as parameters: a) noise-free seismic prediction from the reference model, b) prediction of the base case model, c)-d) predictions of two (picked randomly) realisations of the history matched model. Model 1 case.**

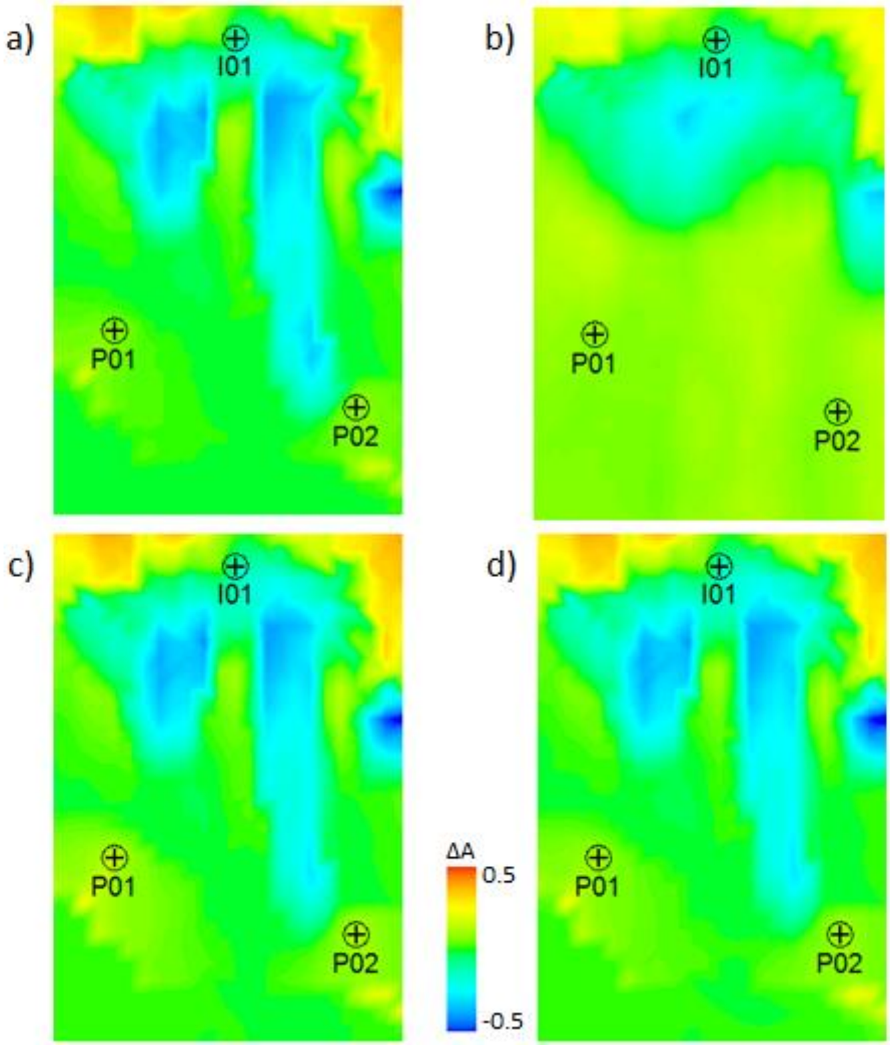

**Figure 6.8. Same as Figure 6.7 but for Model 2 case.**

Figure 6.9 shows water and oil forecasts of wells P01 and P02 for realisations of history matched models Model 1 and Model 2 (4 realisation of each). It can be seen that the variance of predictions among realisations is very small – they predict almost similar data in both cases, Model 1 and Model 2. In particular, Model 1 case (Figure 6.9, a) does not show greater spread of predictions compared to the Model 2 case (Figure 6.9, a) despite the information content in data used to constrain Model 1 is lower. This means that other information apart from that in the data also contributed to finding these close realisations. This information is the prior knowledge embedded in the parameterisation itself – we knew the geometry of channel prior to history matching, so finding their transmissibilities was an easy part. This could be done even with such poorly constraining data as in Model 1. In the next section (6.2.2), we will not use that prior knowledge about the channel geometry (as we are switching to pilot points) to demonstrate the constraining power of the data itself.

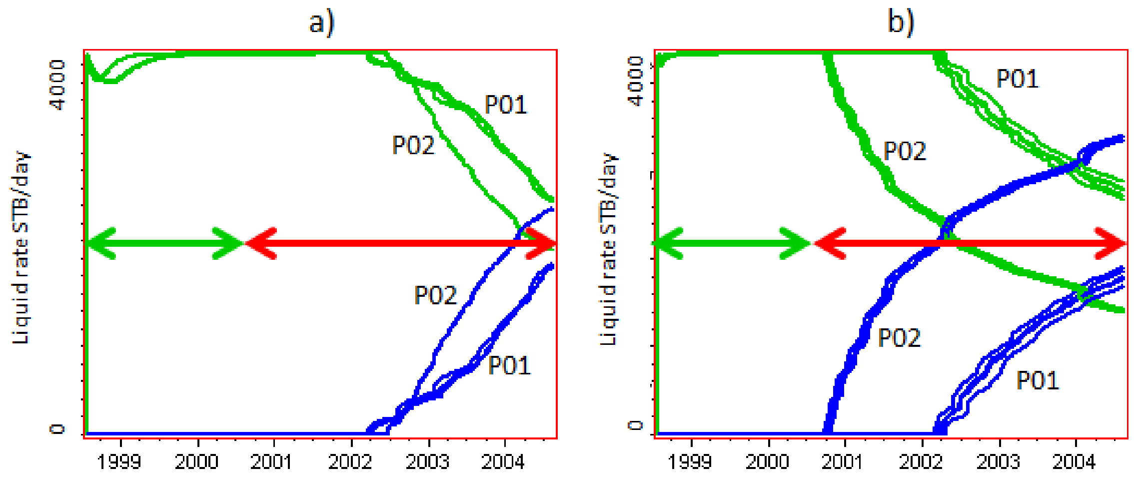

**Figure 6.9. Forecasts of water (blue curves) and oil (green curves) rates in wells P01 and P02 by history matched models in case of: a) Model 1, and b) Model 2. Green arrow indicates the history matching period (only seismic data used for history matching), and red arrow – forecasting period. Four realisations of each model are shown.**

### *6.2.2 Less determined models and the role of information in the data*

The goal in this section is obtaining realisations of history matched models constrained by the data only. In particular, the constraining effect of any prior knowledge embedded in the model such as geometry of heterogeneities (as in the previous case, section 6.2.1) should be minimized. For this reason, the pilot point parameterisation is chosen this time (see Methodology chapter for particular implementation of pilot points in this work). The distribution of points used in the present case is shown in Figure 6.10 together with the deterministic channels from the previous case for comparison. Total number of points is 25. The radius of influence for all points, 500 ft, is chosen based on the distance between the points, 600-800 ft. The power of influence decay is 4. Pilot points control the permeability. The permeability values in the range 10-2000 mD, sampled on the logarithm scale are assigned to the points and interpolated during the history matching. In this setting, no information about the channels is present in the models being history matched (except for the rose coloured non-reservoir area below wells P01 and P02 which is assumed known to be non-reservoir and does not affect the flow anyway), and the flow pattern is formed by the permeability point only. The observed data in this case are the seismic responses of the same reference models (same observed data as in the previous case). This means that we will try to match flow patterns created by deterministic channels (in reference models) by those in models with smooth permeability fields.

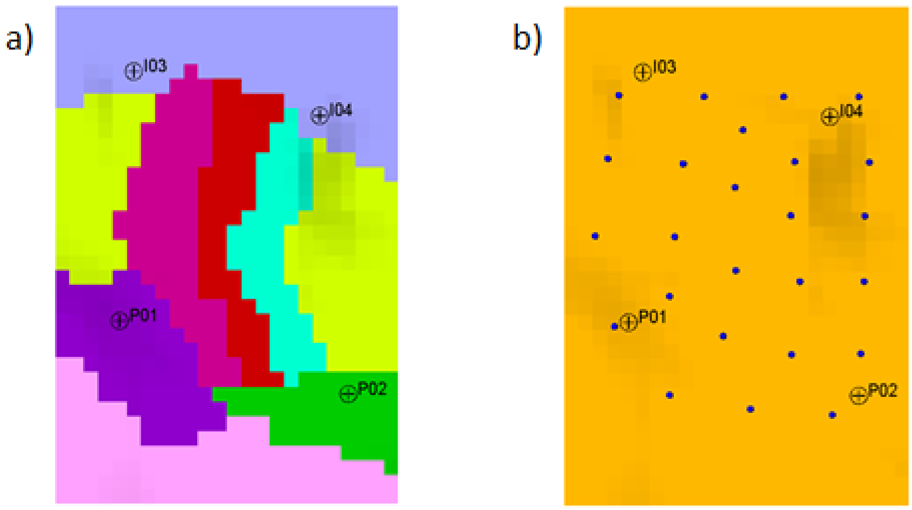

**Figure 6.10. Parameterisations: a) by deterministic channels (section 6.2.1), and b) by pilot points (this section).**

The history matching runs were repeated with the new parameterisation method. Since there are more parameters here (25) compared to the previous case (7), more particles are needed for effective search by PSO. In this case 80 particles were used through 45 iterations. The sorted values of the objective function for history matching of Model 1 and Model 2 cases are shown in Figure 6.11. The final value of misfit in Figure 6.11 is determined by two factors: noise in the observed seismic and the fact that it is not possible to replicate the reference transmissibility field exactly using sparse pilot points (although the match is still good as shown in the following figures).

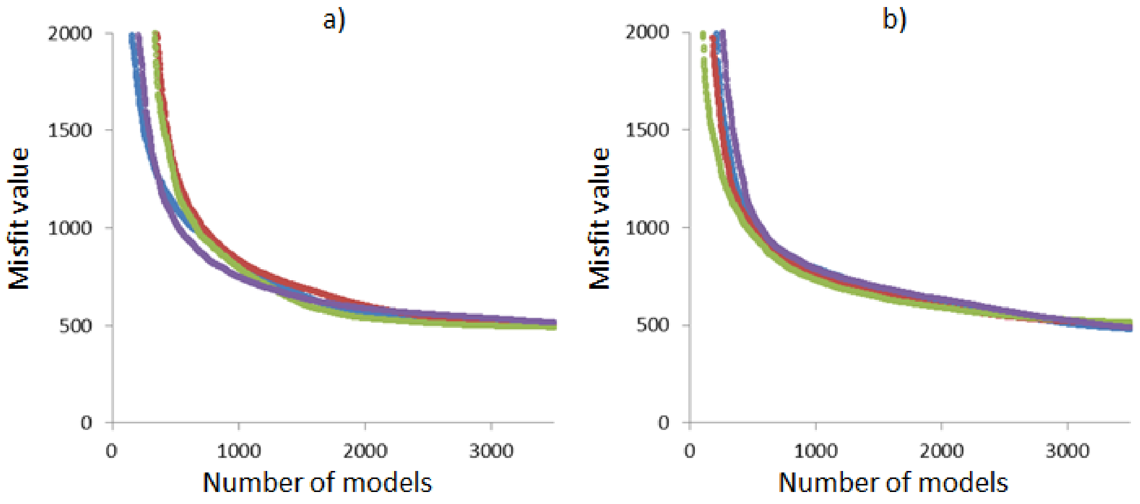

**Figure 6.11. Misfit reduction with the number of models for four history matching runs for a) Model 1 and b) Model 2. The function is obtained by sorting the misfit functions of individual particles in descending order. Misfits of the initial models are several orders of magnitude higher, so truncated.**

Seismic responses of two (out of 4 realisations) history matched models are compared to the prediction of the reference models and the base case model in Figure 6.12 and Figure 6.13. The maps of the reference and the base case models are the same as in the previous section (6.2.1).

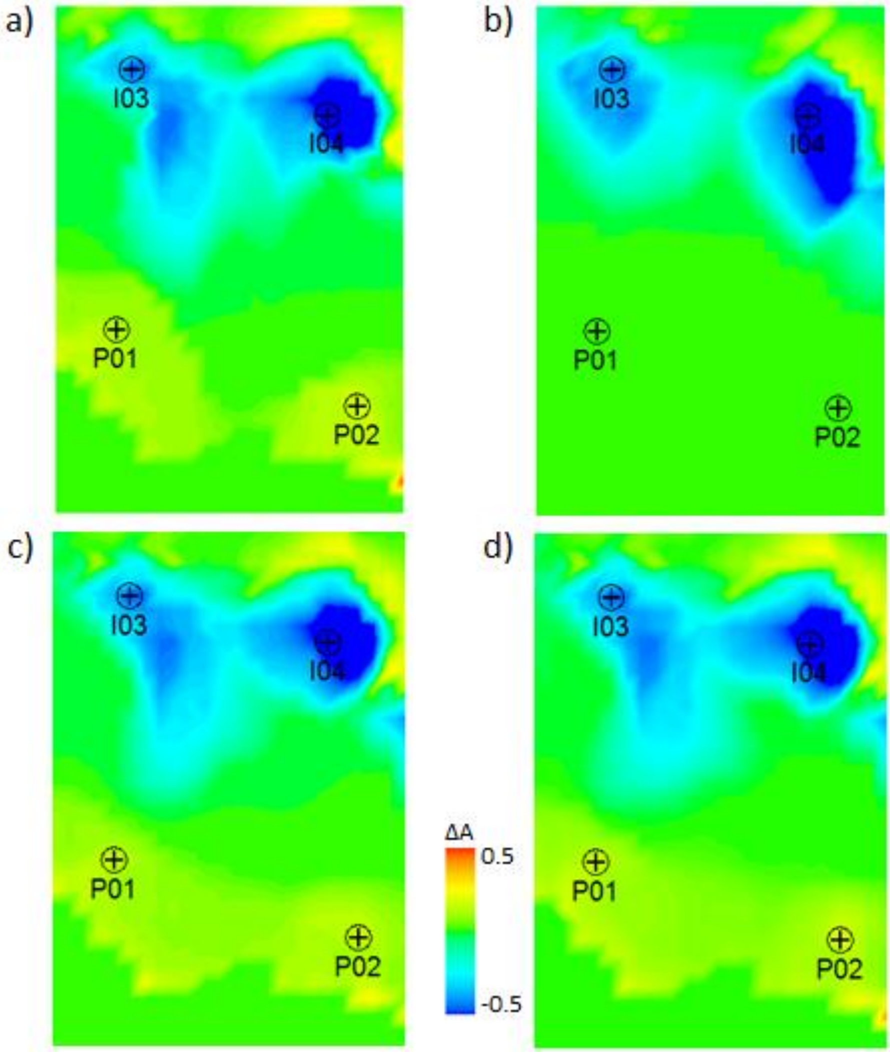

**Figure 6.12. Results of history matching using the seismic maps as data and the pilot points as parameters: a) noise-free seismic prediction from the reference model, b) prediction of the base case model, c)-d) predictions of two (picked randomly) realisations of the history matched model. Model 1 case.**

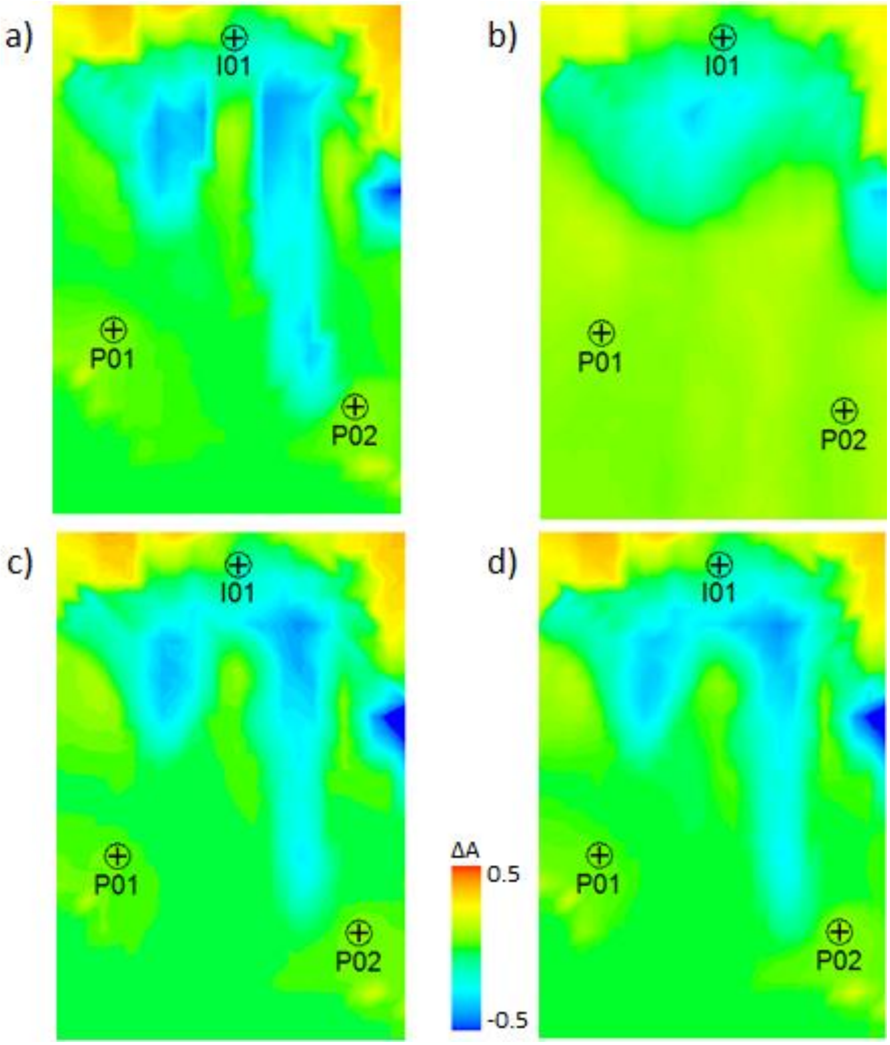

**Figure 6.13. Same as Figure 6.12 but for the case of model2.**

By comparing the results of history matching with the responses of the reference models and with that of the base case model, we can see that quality of the match is good and that the models improved compared to the base case model. Unlike the previous case with fixed channels, the boundaries of the channel are smoother here, especially in Figure 6.13. This is understandable given the limited resolution of a smooth permeability field constructed with sparse pilot points. In this case again having the models which fit the data allows us to study the variation of underlying properties and associated predictions of non-calibration data (production forecasts) to understand the data-sensitivity of the parameters. Figure 6.14 shows the forecasts of water and oil rates produced by the history matched models for Model 1 and Model 2 cases.

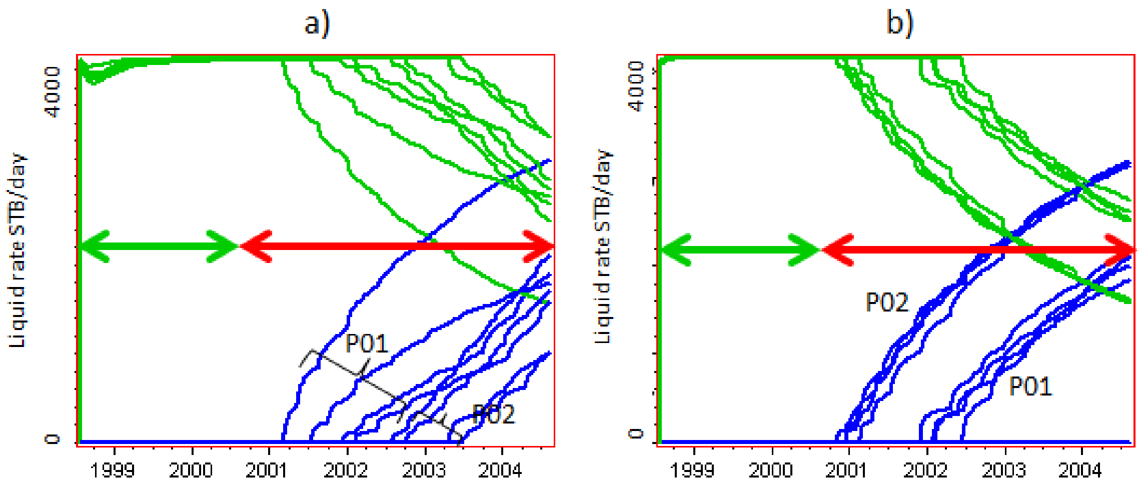

**Figure 6.14. Forecasts of water (blue curves) and oil (green curves) rates in wells P01 and P02 by history matched models in case of: a) Model 1, and b) Model 2. Green arrow indicates the history matching period (only seismic data used for history matching), and red arrow – forecasting period. Four realisations of each model are shown.**

Two important observations can be made from Figure 6.14: 1) there is now a spread of predictions in Figure 6.14, a, and 2) the spread greatly reduces in Figure 6.14, b. Given that all the models in the ensemble of history matched models reproduce the calibration data (seismic maps) well, we can say that the constraint provided by the calibration data is not enough to uniquely determine the values of all the history matching parameters in Model 1, while the parameters in Model 2 are better determined by the calibration data. This concludes the comparison of two parameterisation cases: 1) deterministic channels with unsupported by data, overly constraining prior information about geometry of heterogeneities in the reservoir and 2) neutral pilot points which do not make any assumptions about the underlying reservoir and as such fully depend on the data. It is important to stress that the goal of this comparison by no means is comparison of the parameterizations themselves, but it is a demonstration of the effect of whatever prior information is embedded (and fixed) in the model. This prior knowledge masked the information deficit in the observed data of Model 1 and contributed to easily finding good models in the history matching. In a real situation though, deterministic inclusions of this kind will act as strong but their contribution will not be as constructive since such prior knowledge is imprecise. In the following section, we will investigate the effect of using the deterministic parts in the variable models in history matching. Geological features interpreted in the seismic data are the example of such elements.

Before moving on to the next section, let us analyse permeability distributions resulting from history matching with the pilot points. The following figures (Figure 6.15 and

Figure 6.16) are interesting because they demonstrate the variety of permeability fields occurring as a result of fitting the response of the reference model. To remind the reader, the reference model is parameterized with deterministic channels, so it is impossible to obtain exactly the same transmissibility field by varying permeability via sparse pilot points. What we get instead is a range of models that are equally good in terms of fitting the calibration data (seismic maps in this case). To illustrate the fact that the transmissibility field of the reference model is unreachable by the pilot point models, equivalent permeability fields were generated (for illustration purposes only) for the reference models Model 1 and Model 2 (Figure 6.15, a and Figure 6.16, a) using the following procedure. The initial permeability value of 1000 mD was multiplied by whatever regional transmissibility multipliers existed at any given location. If multipliers were applied between the regions (channels) then barriers were set at the boundaries and coloured accordingly (note the extra grey scaled legend in Figure 6.15, a). Finally, we can say that Figure 6.15, a and Figure 6.16, a show the reference permeability distributions. It is now clear that in no circumstances can these be found by history matching a model parameterised with pilot points. This illustration is also important for subsequent analysis in the rest of this thesis where all the history matching cases will match responses of reference models with unreachable properties. This setting is useful as it emulates the real history matching framework: the real object under investigation (a reservoir) can never be accurately described with approximate discrete models.

Also, two conclusions can be made from observations made in Figure 6.15 and Figure 6.16. Firstly, since models in plots (b)-(d) are different in terms of permeability but similar in terms of data match, the objective function is multimodal, so the solutions in individual (local) minima are important. The second conclusion relates to Figure 6.16, that is the case of Model 2. Here the permeability distributions are again different, but the production forecasts from those models are similar (Figure 6.14, b). This suggests that models in general cannot be effectively compared in terms of their permeability because it is too difficult to relate a permeability pattern to the actual performance of a model, especially if the permeability in question is one of realisations remotely approximating the truth case.

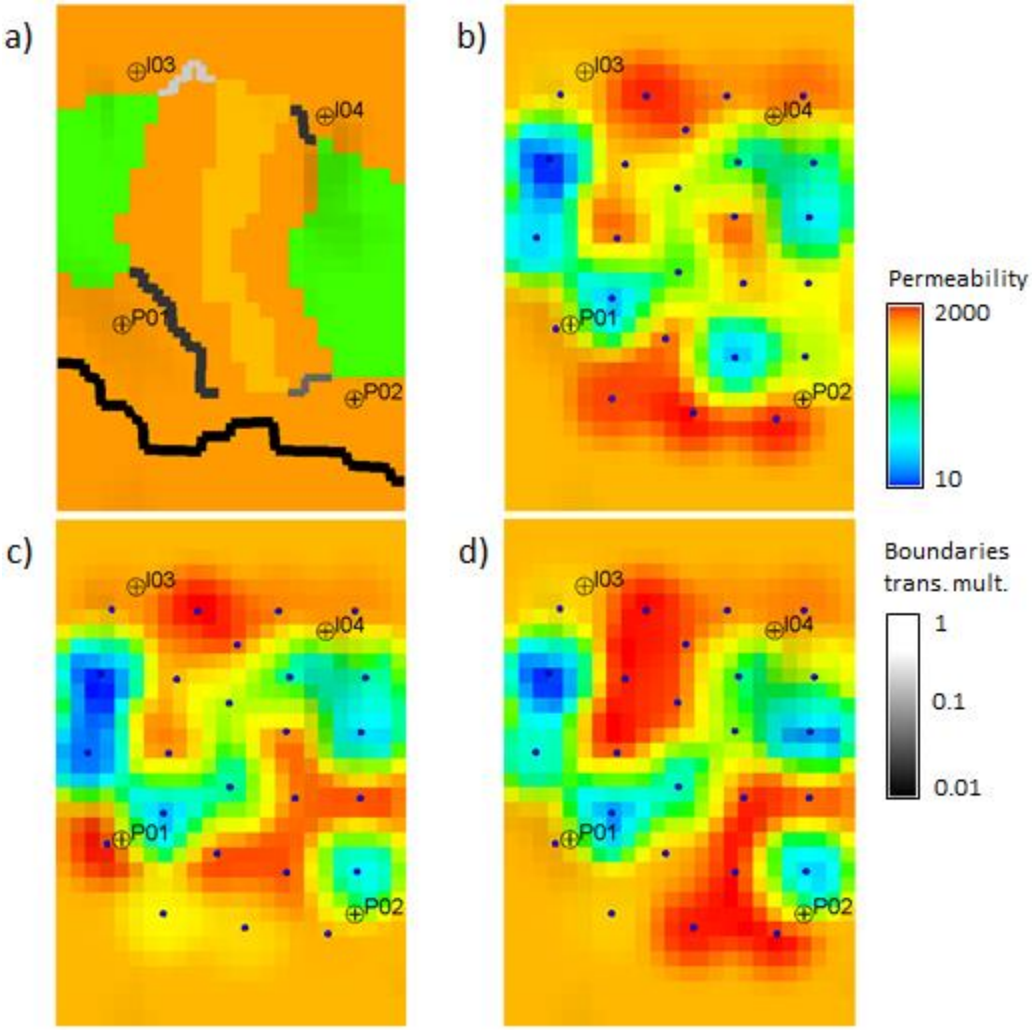

**Figure 6.15. Comparison of a) (equivalent) permeability in the reference model, and b-d) permeability distributions estimated from the data by history matching in a series of realisations. Model 1 case. The extra grey scaled legend reflects the transmissibility multipliers applied to the barriers in (a).**

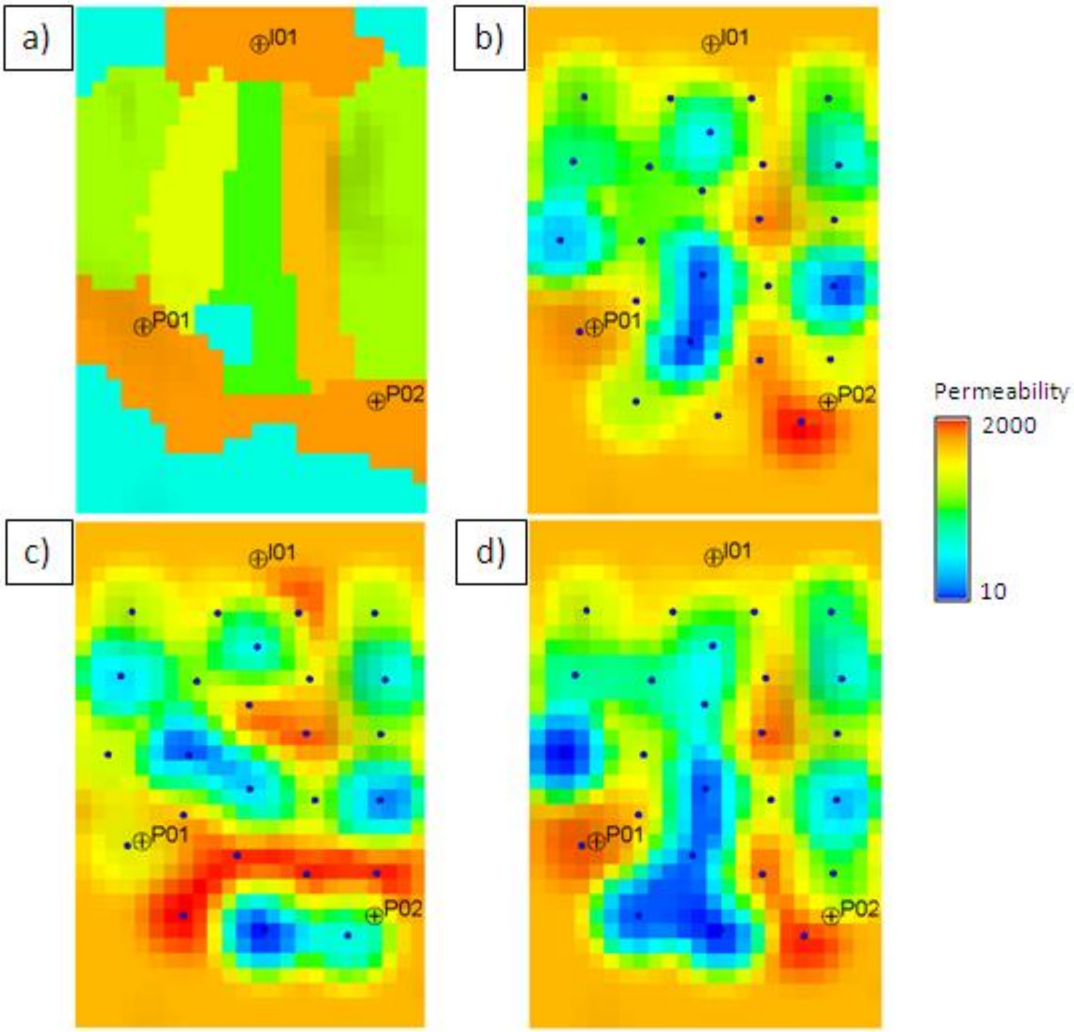

**Figure 6.16. Same as Figure 6.15, but Model 2 case.**

## 6.3 Including seismic interpretations in the simulation model

In the previous section we dealt with a model where the problem of parameter estimation was made over-determined by fixing a massive part of the model. As a result a unique history matched model was obtained. This uniqueness was not supported by the data though which was demonstrated be a counter-example with pilot points. In this section, we will continue discussing the bias from the fixed part of the model, and the fixed part will not be perfect this time. The bias will originate from deterministic inclusions in the model – geobodies interpreted from seismic data. We will also relate the bias to the complexity of model represented by its parameters.

### *6.3.1 Models for history matching*

In this section, a new more realistic and detailed reference model is introduced which will also be used throughout the rest of the thesis. Using a more sophisticated model will facilitate better understanding of the questions of combining production and seismic data and learning from the complexity of the model responses depending on the model representation. Using the details of the Schiehallion model built from the field data will ensure that we are not missing the critical details for the useful conceptualisation of the parameter estimation aspects. And again, this history matching study requires thousands of simulation runs for which the only feasible option given the resources constraint is using smaller models with significantly reduced run times. Extracting a part of the Schiehallion model preserving the original horizontal wells and properties therefore seems to be a reasonable compromise between the details and usability. Shown in Figure 6.17 is the place of our submodel in the bigger Schiehallion Segment 1 model. The submodel dimensions are 9740x4846x330 ft and 30x15x42 cells. The area covered by the submodel is substantial, including the producer wells P1, P6, P7 and P9. Out of the wells active in the period 1998-2002 (the history matching period), only the producers P5 and P2 are not included. Also included are the injectors I13, I15 and I17 providing the pressure support in the area. The southern boundary of the submodel coincides with the major, mostly sealing fault dividing the eastern part of the Segment 1 into two regions. No flow is allowed through the boundaries of the submodel, but the material balance in the volume of reservoir is maintained through the production and injection levels. Overall, the submodel realistically represents the range of (characteristic to fewer wells) responses of the bigger model because of its multi-well pattern, two-layers producing interval T31 (T31a and T31b), combination of water and gas saturation -induced 4D seismic effects. For the rest of our discussion, the submodel will be the subject of our study, so we will simply call it the model, and the bigger, original Schiehallion model will be called the original model when a reference needs to be made to it.

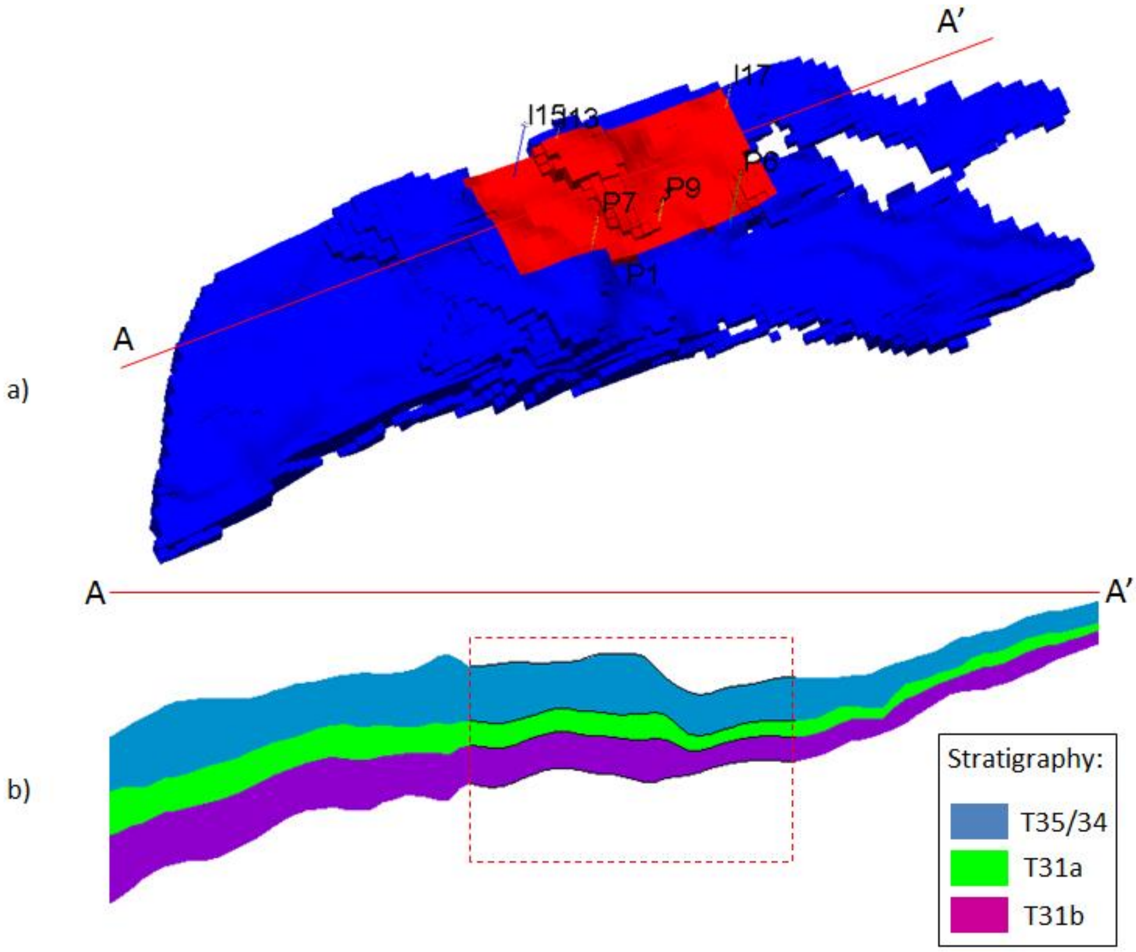

**Figure 6.17. Extracting the subgrid from the Schiehallion (Segment 1) simulation model. A) 3D view of the grids: Schiehallion grid in blue and the subgrid in red, b) cross-section along AA' showing the stratigraphic layers in the model, the red rectangle shows the extent of the subgrid.**

As shown in Figure 6.17, the model consists of the following stratigraphic layers: T35/T34, T31a and T31b. No wells are completed within the interval T35/T34 and it is mostly isolated from the underlying interval T31. Also, the pore volume in T35/T34 is small due to the large non-reservoir areas as shown in Figure 6.18. It is for these reasons that it was made hydraulically isolated from the rest of the model and made inactive at the simulation stage to save some simulation time, but used again when calculating the seismic response. The division of the layer T31 into T31a and T31b is rather nominal because the two sublayers amalgamate in places where the thin shaly layer between them pinches out, particularly in the eastern end of the model (Figure 6.18, b). As described in the previous chapter, the reservoir of the Schiehallion field is comprised of stacked channels of varying width. This is illustrated by the maps of the NTG property in Figure 6.19 where we can see a significant lateral variation of reservoir quality characteristic for the heterogeneous turbidite settings.

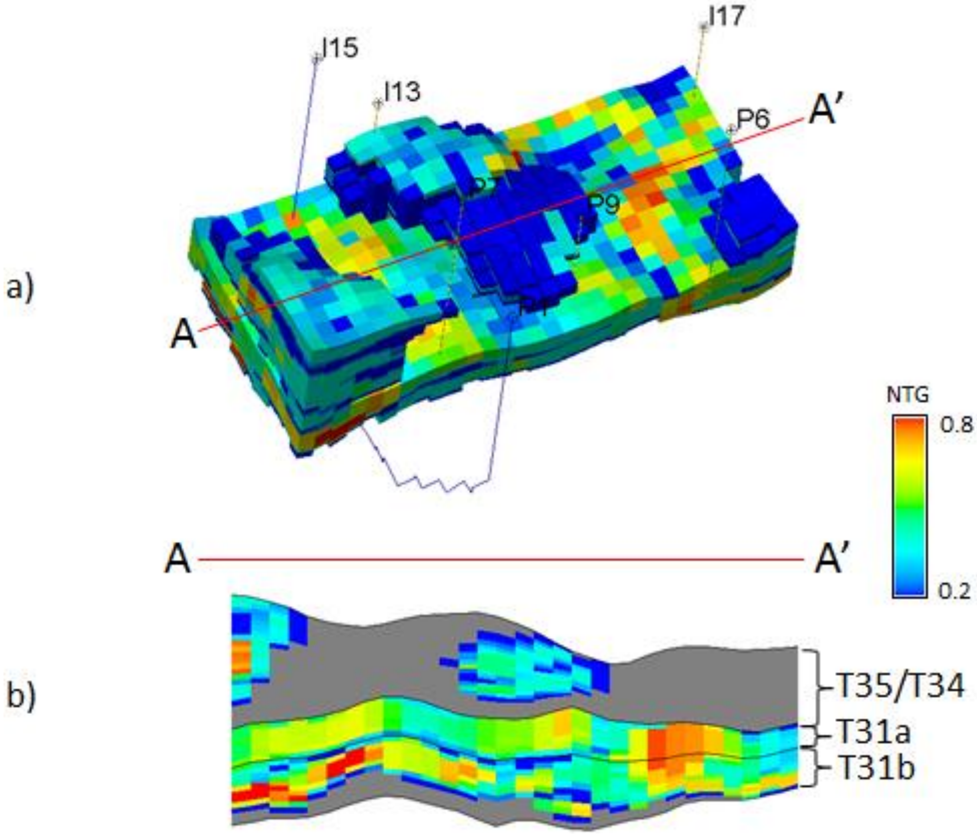

**Figure 6.18. NTG distribution in the model. A) 3D view, b) cross-section along AA' line.**

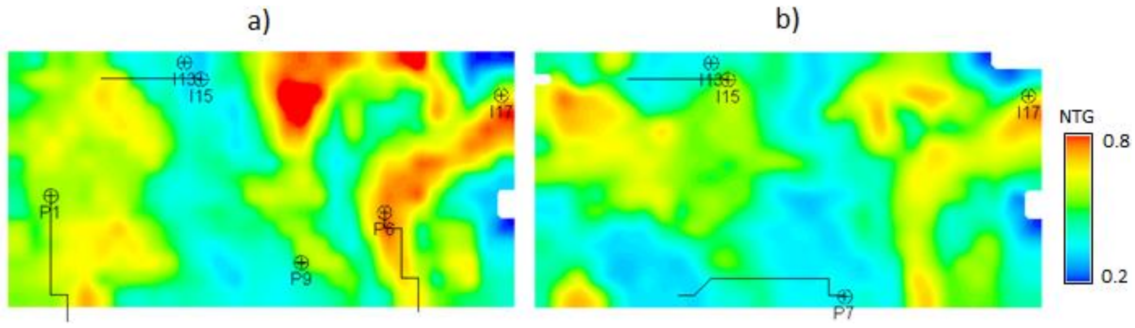

**Figure 6.19. Map of average NTG property within the interval: a) T31a, b) T31b.**

In the highly heterogeneous channelized Schiehallion reservoir the connectivity has been a major uncertainty for the field development (see Chapter 5). Limited connectivity is associated with the compartmentalisation created by the channel stacks. Therefore, realisations of the transmissibility model can conveniently be created if the reservoir volume is divided into regions coinciding with the distinct geological bodies. This was done by the operator in the original Schiehallion simulation model based on seismic interpretation. The transmissibility regions, together with other properties of the original model, are copied over to our model as shown in Figure 6.20.

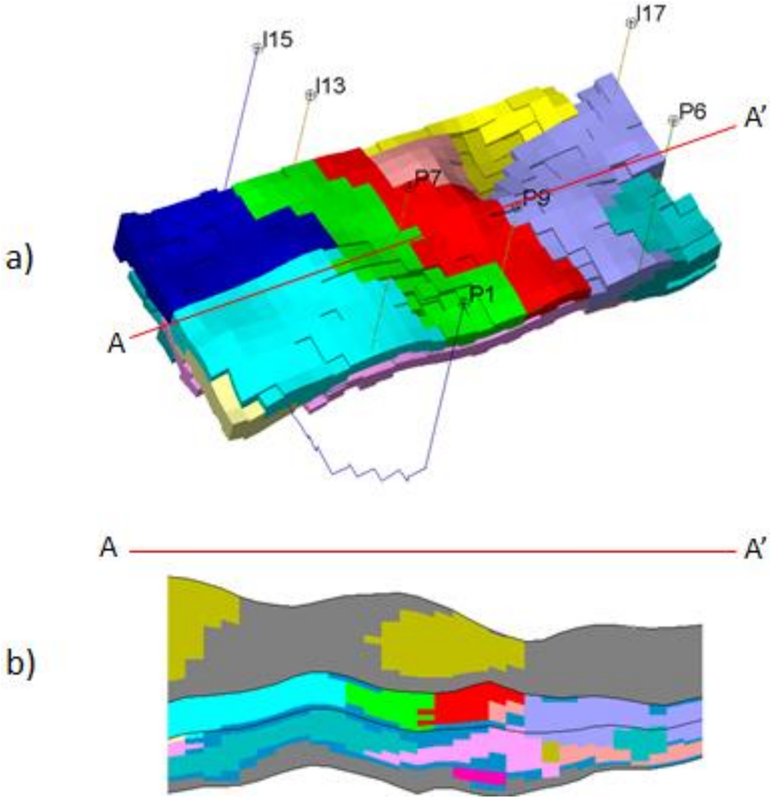

**Figure 6.20. Transmissibility regions derived from seismic amplitudes: a) 3D view (T31 only), b) cross-section along the line AA'.**

The initial state of the reservoir is characterised by the initial pressure of 2907 psi at the datum depth of 6365 ft TDVSS. OWC depth is 6772 ft so the model initially contains a water zone (Figure 6.21) but no gas cap. The water injection is maintained through the wells I13, I15 and I17 located downdip in the off-channel area (I13 and 15) and in the 'snake' channel (I17).

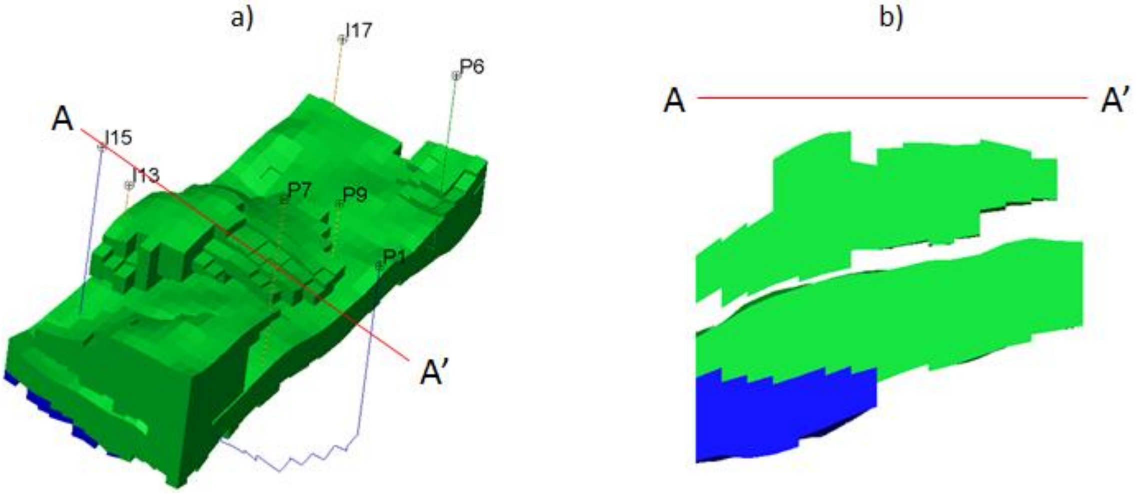

**Figure 6.21. Initial saturation distribution in the model: a) 3D view, b) cross-section along the line AA'. Green signifies oil, blue-water. OWC depth is 6771.7 ft. No free gas is present initially in the reservoir.**

The intended use of the reference model is of course calculating its response to be used as the historic data to condition other models in history matching. The model response in our case consists of well rates (Figure 6.22) and a 4D seismic attribute map (Figure 6.23). Similarly to the previous section, the seismic attribute is mean of coloured inversion calculated over the interval T31a only (calculation of seismic attributes is discussed in Chapter 5). Wells are made to produce at constant liquid rates: P1 20000 stb/d, P6 8000 stb/day, P7 4000 stb/day, P9 4000 stb/day. These levels correspond to the actual rates of the wells in the period between 1998 and 2002. The actual well rates could as well have been used as historic data, but this seems to have no advantage in the context of our controlled experiment, that is where the 'truth' is known precisely but is not necessarily achievable by the variable model. In other words, we are borrowing well regimes from the actual data in the form of approximate levels rather than the variable rates which are controlled by the well and surface network that is out of our modelling scope anyway.

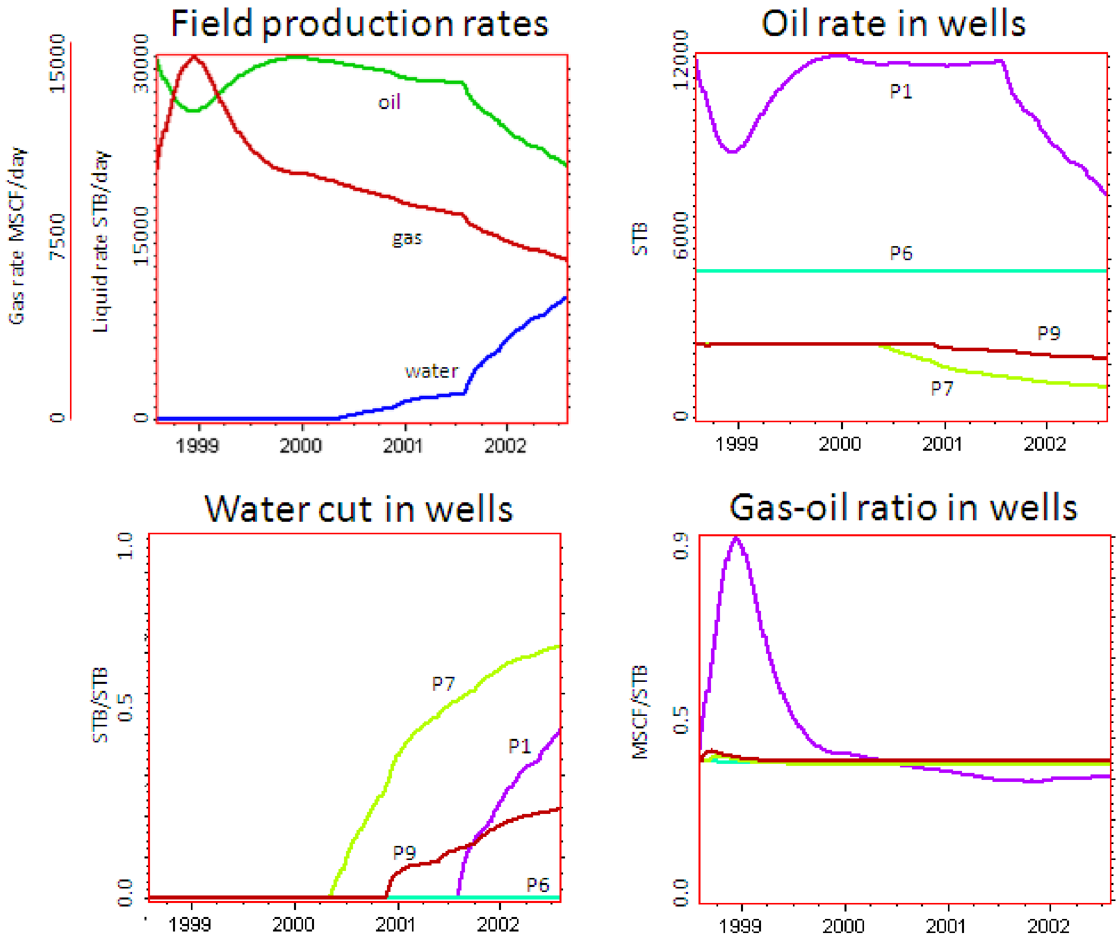

**Figure 6.22. Production profile of the reference model.**

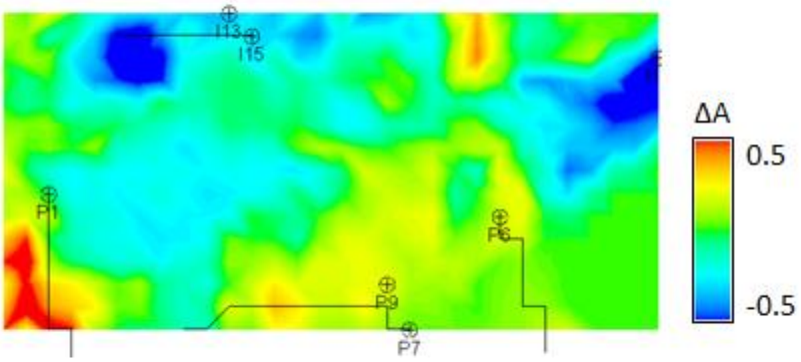

**Figure 6.23. Map of 4D seismic attribute calculated with the reference model: 'historic' seismic data. Red indicates (acoustic) softening of rocks, and blue indicates hardening.**

With the well liquid rates set to the constant values, we still have control on whether we will see the water cutting in wells, gas break outs and how the fluid displacement front is distributed in the reservoir. These effects are related to the information content in the predicted data (which will be the 'observed' data for other models). Therefore, an attempt was made to include the effects normally observed during the development of the Schiehallion field in this area. Some of this behaviour is described in the previous chapter and consists of interpretable movements of the water front and 4D seismic anomalies due to the gas exsolution. Observable on the production profile in Figure 6.22 is that all the wells except for P6 have seen the water cut, and that the production from well P1 begins with high GOR values. 4D seismic anomalies (Figure 6.23) are well understood when examined together with the maps of pressure and saturation change shown in Figure 6.24. The blue areas in the seismic map are associated with water invasion, the red area around the producer P1 is the gas break out.

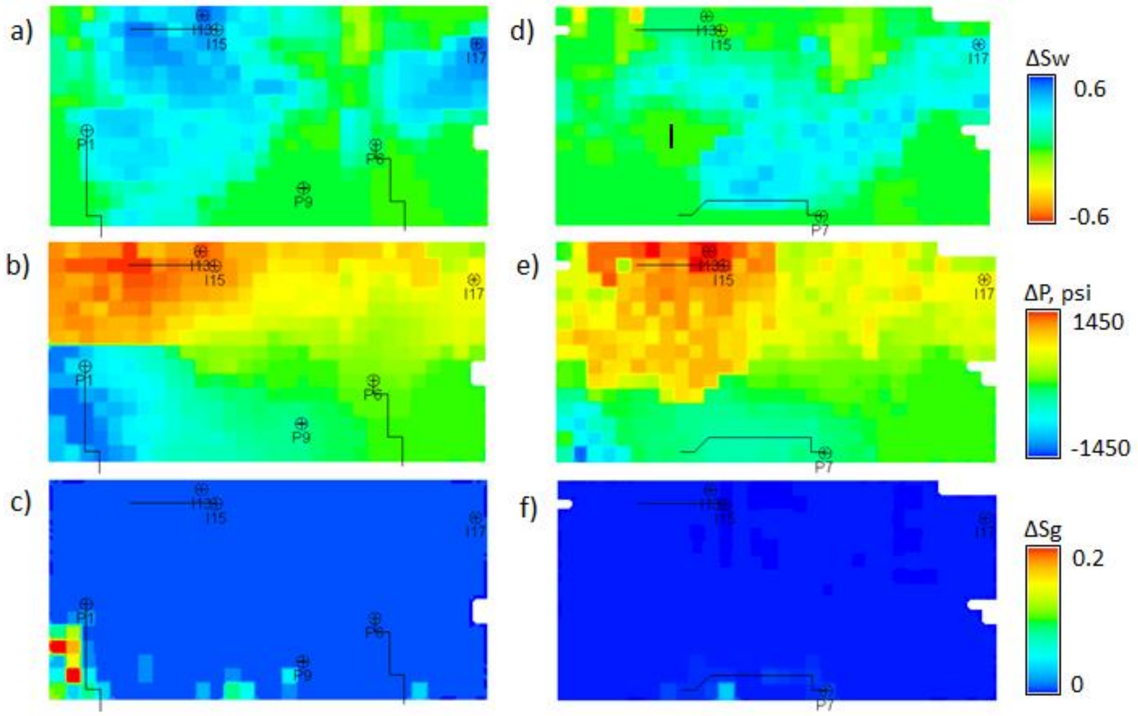

**Figure 6.24. Maps of pressure and saturation differences between the values on 01/08/2002 and on 01/08/1998: a) water saturation difference in T31a, b) pressure difference in T31a, c) gas saturation difference in T31a, d-f) same as (a)-(c) but for T31b.**

*Summary of Schiehallion field data used in this work*

From geological and simulation models:

- Structural surfaces
- NTG, porosity, permeability distributions
- Distribution of geobodies
- Initial pressure, OWC, GOC, relative permeability functions, compressibility, PVT properties of fluids
- Well trajectories, completion intervals

From operator’s dataset:

- Observed well rates (although only relative levels of well rates were taken)

Data that could potentially be used:

- Actual well rates. These data were not used but relative production and injection levels were used instead as the variability of the actual rates would not affect the concept of matching areal saturation distribution.
- Bottom-hole pressures. These data produce extra constraint, particularly on the absolute permeability levels. Although these were not necessary to illustrate the concepts of this work, including these data in the experiment is seen as a future work recommendation.
- Field seismic data. Using field seismic data is highly advantageous in general as these contain a significant amount of details belonging both to the response of complex geology and to the acquisition and processing artefacts. Therefore, seismic history matching will have to take into account these specifics which should be carefully studied separately from the conceptual study of this work. For this reason, testing the result of this work using the field seismic data is seen as a future work recommendation.

### *6.3.2 Model parameterisation based on seismic interpretation*

The reference model prepared as described above supplies the ‘historic’ data for our history matching experiment in which it will be matched by the predictions of another, variable model. Similar to the previous section, the variable (that is updated in history matching) model is derived from the reference model but the transmissibility distribution will be left free to vary. This is because the transmissibility distribution (not necessarily tied to the regions) has major influence on the process of hydrocarbon displacement and, consequently, on the quantities comprising what we call the model response – oil, water and gas rates and 4D seismic signal. Other model parameters such as the reservoir geometry and fluid properties affect the model response too but we will limit our analysis to just some of the parameters in order to maintain focus on the objectives of our study. The reason for choosing the transmissibility lies in the support of different parameters by field data: reservoir geometry and fluid properties are well conditioned usually by the seismic and well data, as well as laboratory measurements, while the transmissibility of the reservoir on a larger scale is the major uncertainty in a field development.

The 4D seismic data interpretation that is included in the simulation model in our case defines the transmissibility regions. These are the geological objects that cause distinct seismic anomalies, and mainly are traced by the discontinuities of the signal. Often, the discontinuities are associated with the flow boundaries in which case the corresponding geological objects form compartments in the pore space with different level of connectivity. For example, fluvial and turbidite settings combine highly permeable channel sands with marginal and over bank deposits of low permeability. *Martin and Macdonald, 2010* improved the pressure prediction of the Schiehallion field simulation model by incorporating geobodies interpreted from 3D seismic data. In general though, if the distribution of the objects is confidently derived from high resolution seismic data then the connectivity of the regions is what usually remains uncertain. The geological objects can be modelled by using the transmissibility multipliers which reduces the problem of estimation of the transmissibility field to 'connecting' the regions. The history matching problem can be parameterised accordingly so that the transmissibility multipliers between the regions are varied.

In the following discussion, we will demonstrate the effect of the bias created by such deterministic inclusions in the simulation model on its predictions. In the first experiment, the transmissibility regions are copied from the reference model and the history matching algorithm is employed to estimate the transmissibility multipliers. This set up does not produce any destructive bias of course, but the purpose is to show that the history matching problem is feasible and we can match the ideal case before moving on to the approximate models. In the subsequent runs, the ideal regions will be replaced with the ones derived from the seismic data. Also, similar to the previous section, a comparison will be made with the parameterisation by the permeability points.

### *Using transmissibility regions from the reference model*

In this history matching run, the transmissibility regions are copied from the reference model and the multipliers between the regions are estimated. Because such a model is error-free in its fixed part, we can expect that matching the seismic data will lead to an improved match of production data even if the latter is not in the objective function, or at least we can say that the solution where both data types are matched exists. History matching has been completed therefore using only the seismic map as the observed data. All possible contacts between the geobodies shown in Figure 6.20 (the exhaustive list of contacts is obtained by an automated search) are taken to be the parameters (38 in total).

PSO algorithm was used as before with the following parameters: 80 particles and 65 iterations. The sorted values of the objective function are shown in Figure 6.25.

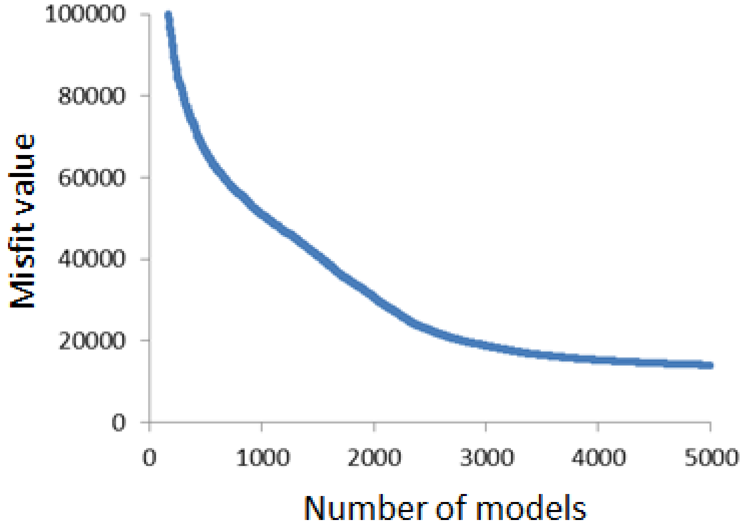

**Figure 6.25. Misfit reduction with the number of models. The function is obtained by sorting the misfit functions of individual particles in descending order. Initial misfits are too high, so truncated.**

Figure 6.26 compares predictions of the history matched model with observed data (the production data are shown only for comparison, it was not used to constrain the solution). It is easy to see that the history matched model reproduces both seismic and production data very well. The slight mismatch that is still present is caused by the unreachable lower limits of some of the parameters – lower limit of 0.001 is used for the parameters of history matching while some of the reference multipliers are exact zeroes, and the multipliers are varied in the logarithmic scale. Overall, this small perturbation to the problem input (due to not including zeroes) did not prevent the algorithm from confidently converging to a model matching also the production data. This is exactly the required result. The main purpose of this demonstration was establishing a benchmark case, that is where we are sure of the problem statement including the data, the parameters and the algorithm. This will make it easier to understand the errors in matching the data caused by certain ad-hoc parameterisations discussed in the following sections.

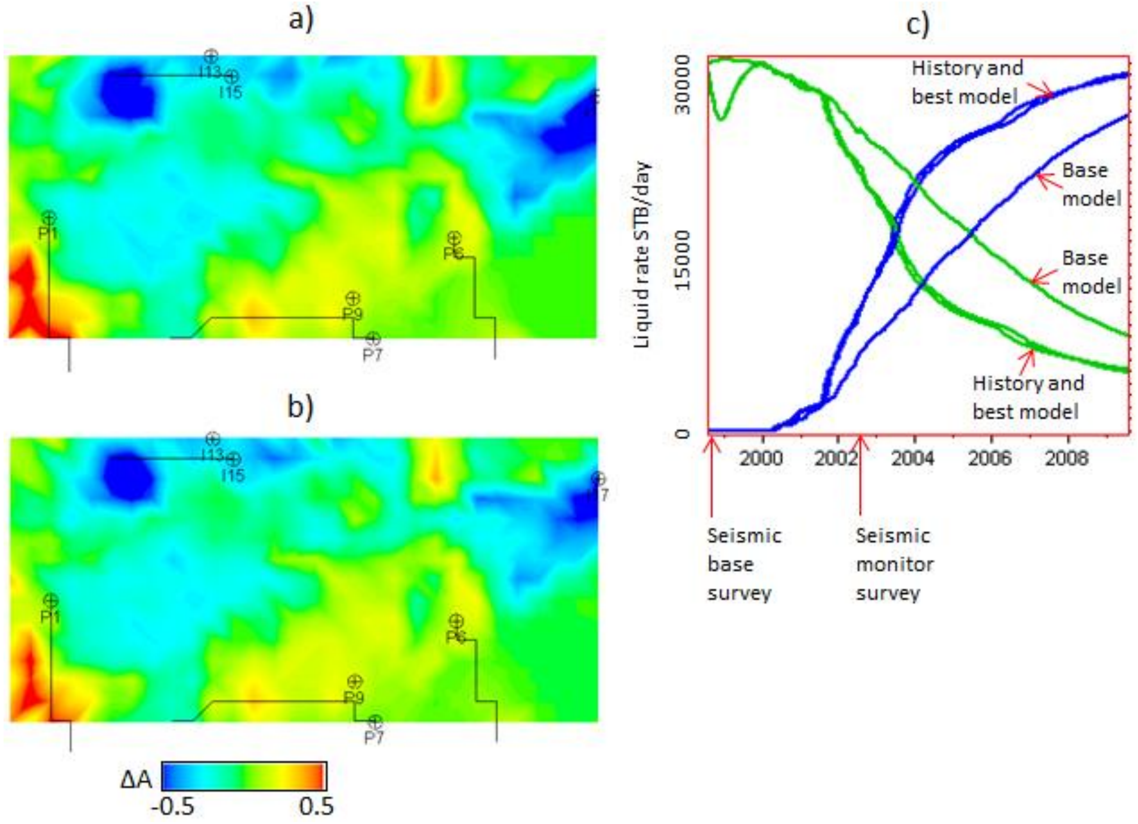

**Figure 6.26. Results of history matching of the model with transmissibility regions copied from the reference model: a) historic map of the seismic attribute, b) predicted map of the seismic attribute, c) field production rates for the reference model (labelled as 'history'), base model and the history matched model (labelled as 'best model'). Only seismic data are used in history matching in this case, production data are only given for comparison.**

*Using transmissibility regions from the data, based on seismic interpretation*

One may consider different options for extracting the spatial geological objects (geobodies) from the seismic data including amplitude thresholding, extracting volumetric attributes, delineation of the objects in the maps, or inverting the seismic data into a rock property to use for dividing the reservoir volume into regions. The common in all of these approaches is that we are looking for spatial discontinuities in the signal to relate them to the boundaries of regions. Importantly, certain approach is chosen to fit the specific purpose. The purpose in our case is to get approximate transmissibility regions supported by the data rather than copying them from the reference model. In this situation, we are not seeking any excessive details because building a model more complex than the reference model will negate the effect of the bias (from the fixed part of the model) – the model will always be too flexible. The optimal solution is regions of the same scale as in the reference model or larger, and then the approximation will be in their spatial distribution and extent. Therefore, maps will provide adequate level of details, but the maps of the rock property rather than seismic maps are preferred because of the stacked nature of the Schiehallion reservoir where the signal is affected by interference effects. As discussed in Theory chapter (section Seismic inversion), inverting for the NTG property resolves the compound signal, although in favour of a particular model as the inversion process is inherently non-unique. Again this satisfies our needs in a certain interpretation that fits the data (albeit one of many that are possible). Finally, the procedure followed here consists of inverting the seismic traces for the NTG property, calculating average maps of NTG for T31a and T31b, tracing the regions of high NTG and transferring them into the 3D grid as a new discrete property.

The methodology of the seismic inversion is detailed in Chapter 4. This is based on a simple idea. We try different distributions of NTG until the seismic prediction fits the observed data. The process is organised as an optimization loop using the PSO algorithm. It was shown in Chapter 4 that using a prior term in the objective function stabilises the solution. In this case, a piecewise constant prior is used which used vertically average NTG values in the intervals T31 and T35/T34 as shown in Figure 6.27, a. Another component of the problem statement is the parameters for the inversion distributed in space (Figure 6.27, b). In the non-producing interval T35/34 two to four simulation grid layers make up one parameter layer while in the main reservoir T31a a value of NTG is estimated in each simulation cell, and in T31b again the simulation layers are grouped by two. This results in 23 parameters in total which is more than uniquely determined from the seismic traces due to the thickness of layers, but a principle of regularised inversion is followed here – many parameters ensure flexibility in terms of the positioning effects (layer thicknesses are fixed) and the regularisation (the prior term) prevents the excessive oscillation of the solution. According to the prescribed workflow, 3D NTG property was estimated by the seismic inversion and the NTG maps were calculated from it. The resulting inverted NTG property is shown in Figure 6.28. The average map of the inverted NTG closely matches the reference NTG map as shown in Figure 6.29 (although the match of NTG is not necessary for the successful inversion as it is the solution not the data).

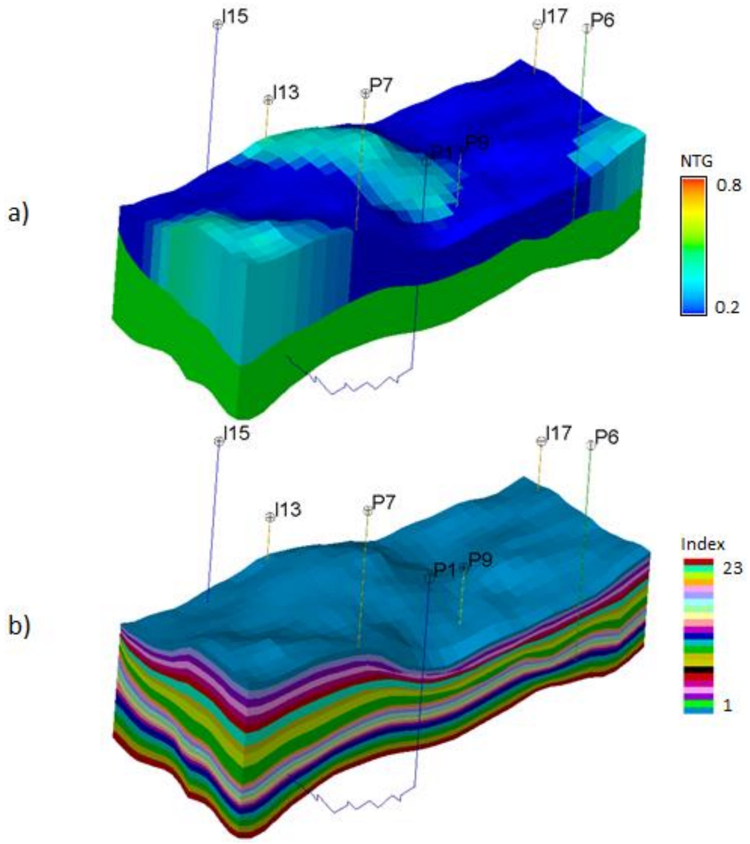

**Figure 6.27. Constituents of the input for seismic inversion: a) prior NTG model and b) distribution of the inversion parameters.**

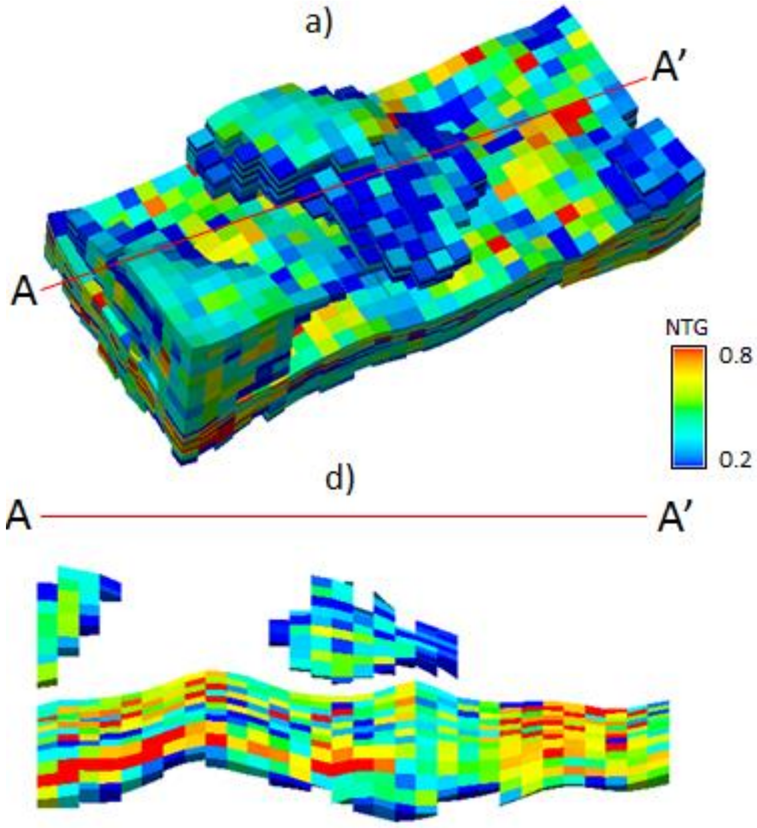

**Figure 6.28. Inverted NTG property: a) 3D view, b) cross-section along AA'.**

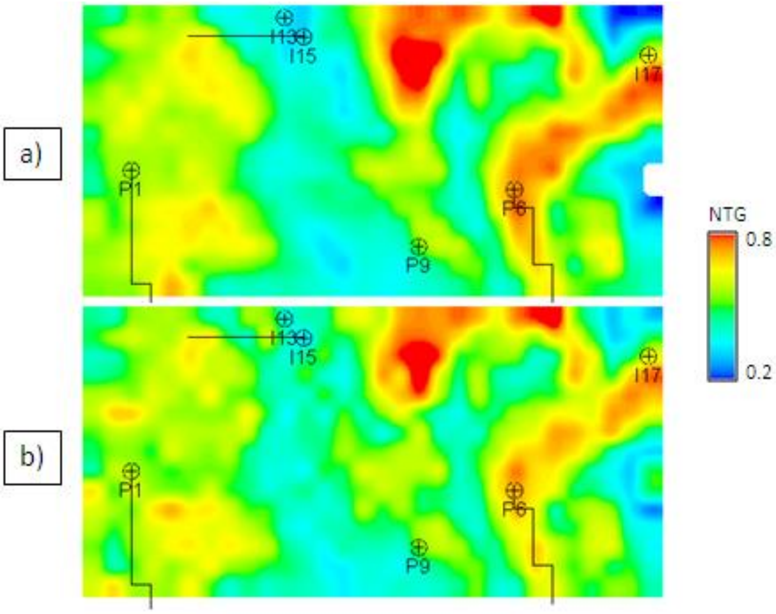

**Figure 6.29. NTG maps over T31a interval: a) reference model, b) inverted model.**

Being a product of seismic inversion, the NTG property is free from the seismic interference artefacts, so we can treat it as the true earth model representation and delineate the regions directly on the maps as shown in Figure 6.30, a and b. The boundaries of the interpreted regions then are converted into the discrete 3D property in the simulation model (Figure 6.30, c and d). Figure 6.31 compares the resulting interpreted regions with the regions in the reference model. This shows that interpreting the seismic data resulted in approximate regions in terms of their spatial extent as required in our problem.

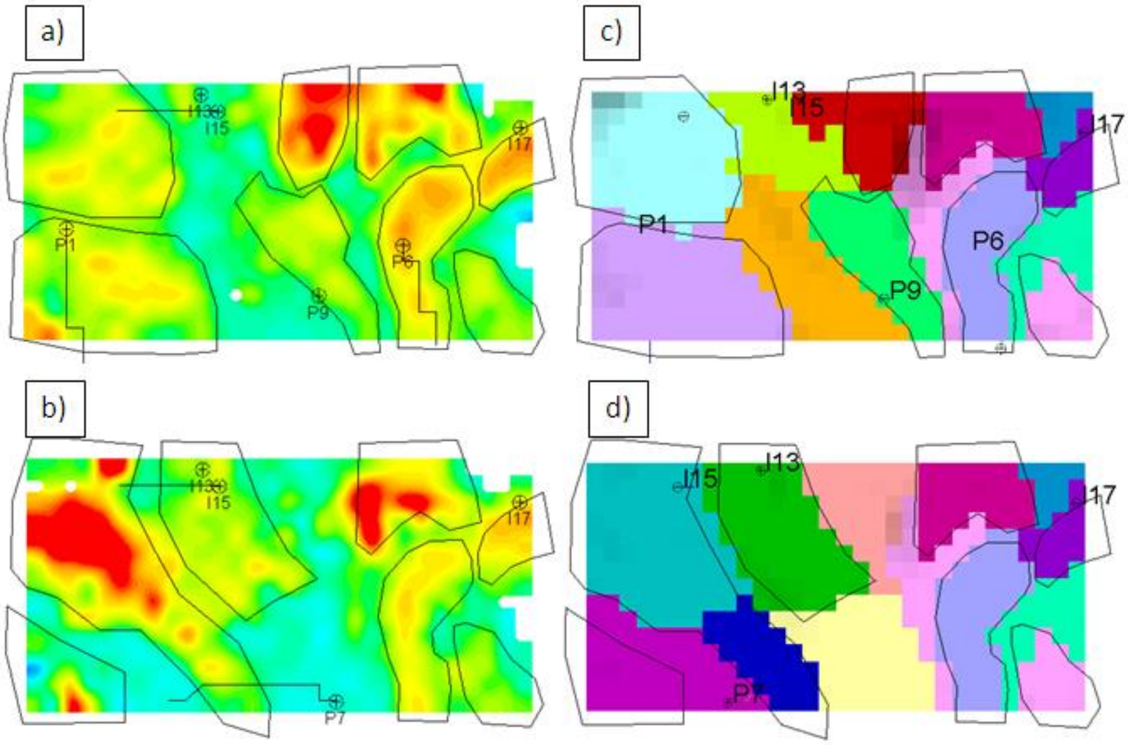

**Figure 6.30. Identifying transmissibility regions in the maps of inverted NTG: a) and b) the distinctive anomalies outlined as potential regions in T31a and T31b respectively; c) and d) the outlined boundaries are used to implement a discrete property of regions in the simulation model, T31a and T31b respectively.**

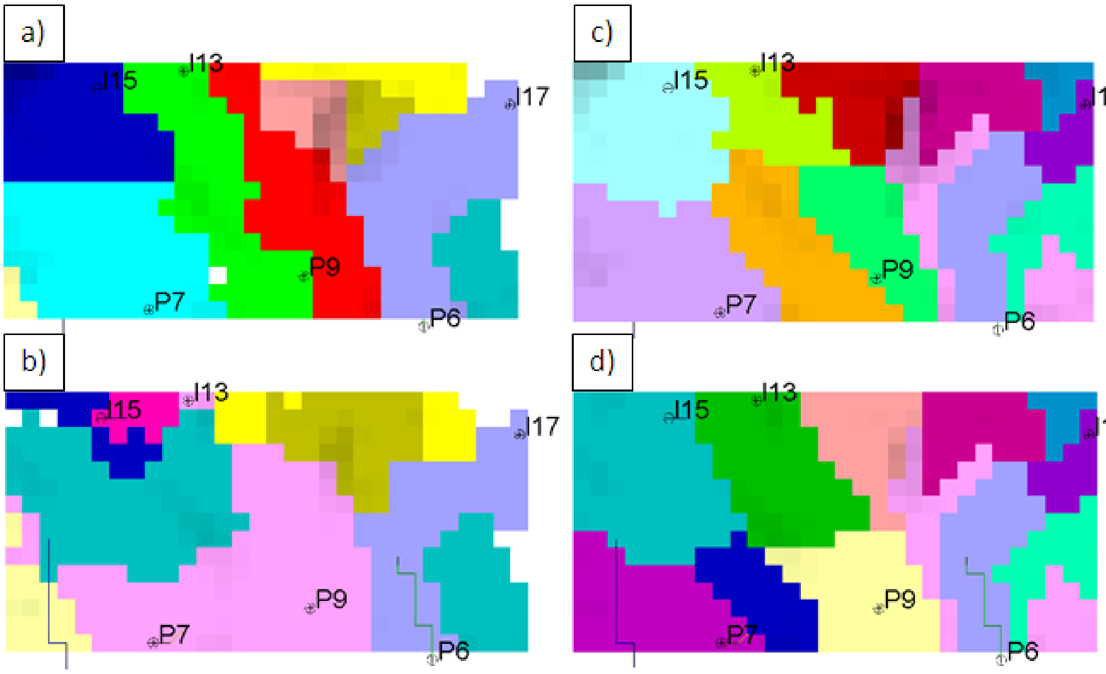

**Figure 6.31. Interpreted transmissibility regions compared to the ones from the reference model: a) and b) regions in the reference model, intervals T31a and T31b respectively, c) and d) interpreted regions, intervals T31a and T31b respectively. Different colours indicate indexes of regions.**

*Parameterisation bias*

In this section four cases with different parameterisations will be compared in terms of their ability to match 4D seismic data. In all four cases, history matching is performed using only the 4D seismic map as observed data. The cases are: approximate regions (Case 1), reduced approximate regions with indifferent fixed part (Case 2), reduced approximate regions with production matched fixed part (Case 3), and the pilot points (Case 4). Meaning of the cases will be explained in the following discussion.

We will start our discussion with the approximate regions case (Case 1) which uses the interpreted regions as described in the previous sections (see Figure 6.30). These regions and the transmissibility multipliers between them comprise the parameterisation in this case. Similar to the previous case, here all the possible contacts between the geobodies are found and made the parameters. The total number of parameters in this case is 45. History matching was conducted using 4D seismic map from the reference model as observed data. The resulting match of 4D seismic maps is shown in Figure 6.32 (the misfit function will be shown later).

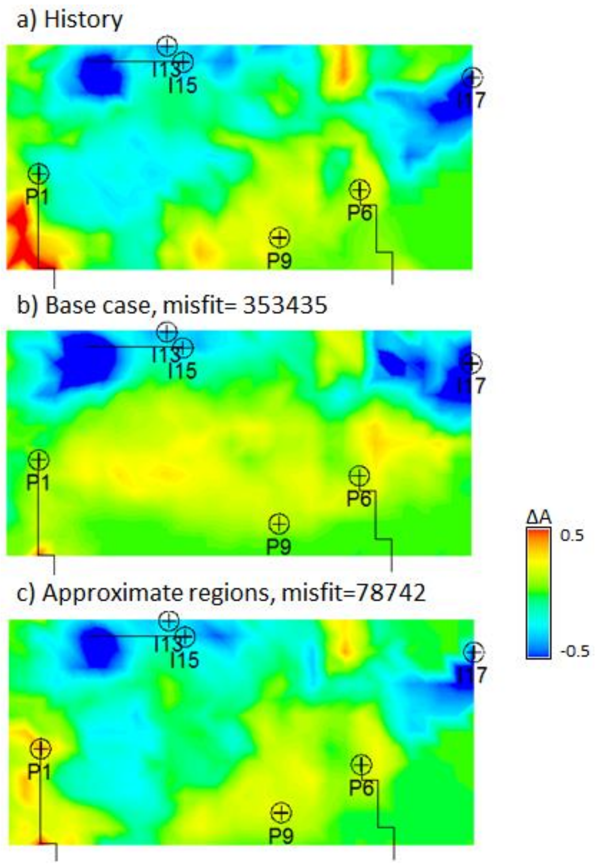

**Figure 6.32. Results of history matching using parameterisation based on approximate regions. 4D seismic maps are compared for a) reference model, b) base model, and c) history matched model.**

The results show that compared to the base model the match improved significantly. However, by comparing these results with the ideal case in Figure 6.26, we can conclude that replacing the ideal regions with the interpreted regions introduced an error due to the parameterisation. But we do not call this the parameterisation bias yet. It is not an attempt to attach some terminology labels here but it is that so far we are seeing an effect of different level than our ‘target’ bias. When we say that the fixed (to some erroneous values) part of the model creates a bias, we mean that it can be removed or significantly reduced when more parameters are added or the parameterisation is improved. However, it is difficult to do better than this result because the model that we are using is already even more complex than the reference model (45 parameters versus 38) and at the same time, the approximate regions are not far from their reference counterparts, at least we would not get better precision delineating regions when interpreting the real seismic data. In other words, this is the error that we got when we added a small perturbation to the regions, therefore, it is called irreducible in our case.

The situation here is that the history matched model is more complex than the reference model. The reality is known to be the opposite though: models should be simpler than the real objects they represent. To achieve it, we can change either the reference model or the variable model. There are advantages of the latter, that is making the variable model simpler in terms of number of variables. Firstly, we do not want to lose the current state where the match is achievable (even though not perfect) so when moving down in complexity we will know what simplification caused the bias. Secondly, the coarse scale reference model is limited in the ways of making it more complex.

One way of simplifying the variable model with interpreted regions (Case 1 model) is fixing a part of its 45 parameters. The rationale for this in the context of transmissibility multipliers is modelling an equivalent of lesser regions without redrawing them – as if we missed some of the objects during the interpretation. It is also equivalent to imposing some deterministic knowledge (because we are setting particular parameters to particular values) on the final model estimates. And finally, we may often opt for a history matching problem set up with fewer parameters due to the resource constraints, so here we show the implications. How to choose parameters for fixing and what values to assign to them? For consistency with the pilot points case (which will be explained later), it was decided to fix 17 parameters and leave the remaining 28 as parameters for history matching. Parameters to be fixed were selected randomly in order to avoid an extra selection bias. Next, for the values to be assigned to those 17 fixed parameters there are 2 options. The first is to assign some indifferent constant value, for example the midpoint value of the parameter range (in the case of log-scale it is 0.032). The second option is to try to compensate for the ad-hoc character of the fixed part and give it some reasonable values. For example, take the values for those 17 fixed parameters from the history matched version of Case 1 model. However, we cannot use the Case 1 history matched to 4D seismic map because it would be a pointless 28D version of Case 1, so we better borrow the values from Case 1 history matched to production data (assuming that solutions by matching seismic and production data are in many cases different as shown in Chapter 7). These two options describe the way the cases Case 2 and Case 3 were obtained. Because only 28 out of 45 parameters are left for history matching in those cases, they are called the reduced approximate regions cases here. Finally, what is left for the full characterisation of Case 3 is obtaining a version of Case 1 model history matched to production data. This was completed and the results are presented in Figure 6.33.

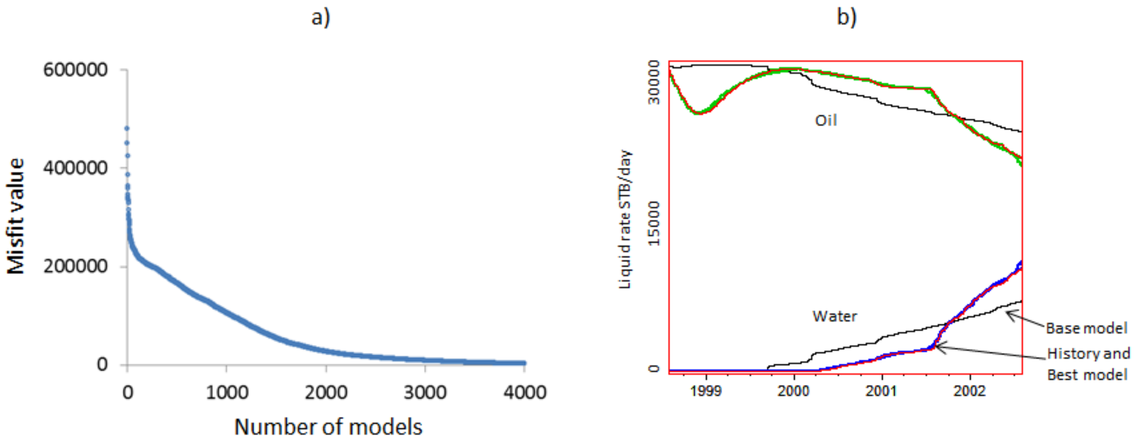

**Figure 6.33. Results of history matching of Case 1 model to production data: a) misfit reduction with the number of models sorted in the descending order, b) oil and water rates for the reference (red curve=history), base (black curve), and history matched (green curves for oil and blue curves for water) models.**

The two cases, Case 2 and Case 3, are expected to show the bias from their fixed parts, that is deterministic inclusions not supported by calibration data (sometimes called "structural noise", *Hunt et al, 2007*). In order to show that the bias comes exactly from fixing the parameters wrongly rather than reducing dimensionality (45D to 28D), we will consider the last case of the same dimensionality (28D), Case 4, based on pilot points. 28 pilot points are evenly distributed across the layers T31a and T31b as shown in Figure 6.34 (the distance between the points is approximately the production well spacing, hence the number 28 as mentioned before).

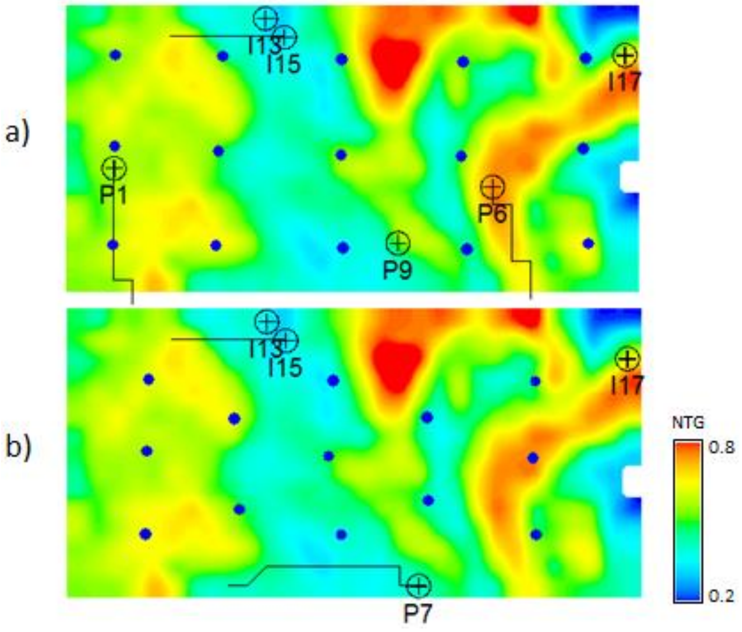

**Figure 6.34. Distribution of pilot points shown on top of NTG maps of the reference model: a) in reservoir T31a, b) in reservoir T31b.**

All the cases have so far been described so we are moving on to results of history matching using 4D seismic data. PSO algorithm was used here with the following parameters: 80 particles and 50 iterations. Figure 6.35 shows the misfit functions for the four cases. The objective functions in all cases use 4D seismic maps as data, and the error is set to a constant values (40% of amplitude of the reference seismic map), equal in all the cases which makes their misfits comparable. It is clear from the Figure 6.35 that for Cases 2 and 3 the misfit cannot be reduced below a certain level (higher than for other cases). This is the effect of the structural noise as mentioned before. Another 28-dimensional case, Case 4, uses pilot points that appear to be flexible enough to assimilate the details of the observed seismic map and result in a misfit as low as in the initial 45-dimensional Case 1. Another observation (although not as important here) from comparing the misfit functions is that the function for Case 1 falls faster than for Case 4 but then the reduction rate slows down and it levels with the one of Case 4. This behaviour (rapid initial decline followed by levelling) is characteristic for zonation-type method to which the parameterisation of Case 1 (regional transmissibilities) belongs.

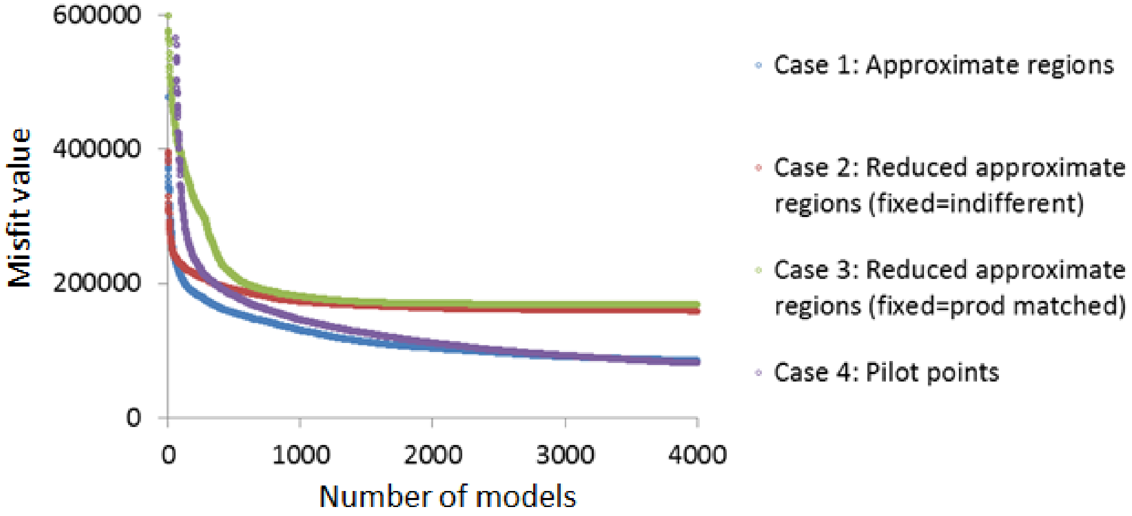

**Figure 6.35. Misfit reduction with the number of models for Cases 1-4. The function is obtained by sorting the misfit functions of individual particles in descending order. Some of the initial misfits were truncated.**

Finally, Figure 6.36 compares 4D seismic maps of the history matched models for Cases 1-4 with those of the reference and base cases. The misfit functions use consistent error values, so the misfit figures shown on top of the maps are comparable. Figure 6.36 demonstrates that the bias in Cases 2 and 3 prevents the models from reproducing the details of the observed data (misfits values above 150k). The match of Case 4 on the other hand is as good as the one of Case 1 despite the number of parameters is lower (both have misfit values around 80k). Improvement of cases 1 and 4 compared to 2 and 3 is approximately the same as of cases 2 and 3 compared to the base case (misfit value around 350k), that is a factor of 2 reduction of misfit values.

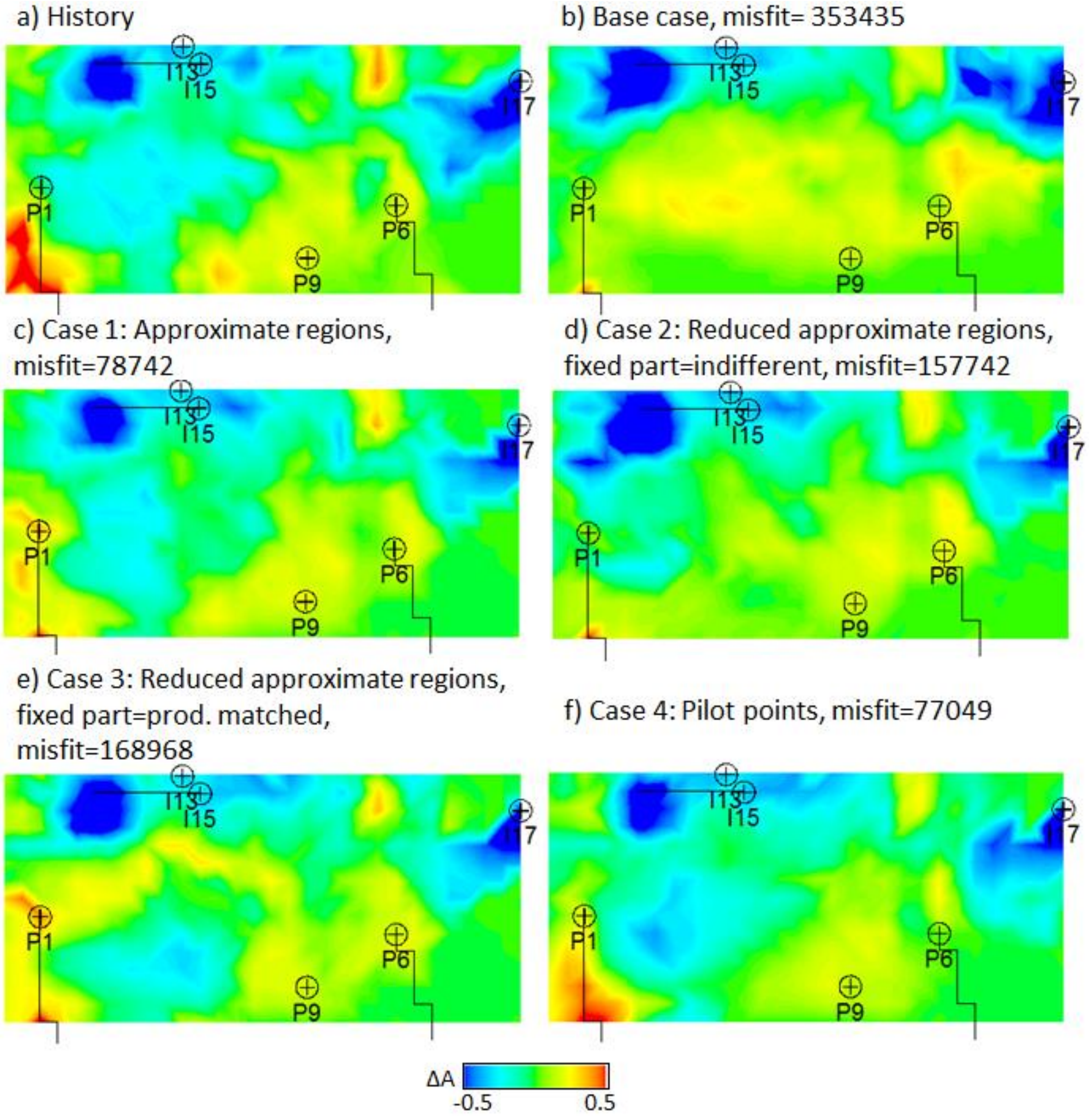
a) History

b) Base case, misfit= 353435

c) Case 1: Approximate regions, misfit=78742

d) Case 2: Reduced approximate regions, fixed part=indifferent, misfit=157742

e) Case 3: Reduced approximate regions, fixed part=prod. matched, misfit=168968

f) Case 4: Pilot points, misfit=77049

**Figure 6.36. Maps of 4D seismic attributed for a) reference model, b) base case model, and c-f) history matched models for Cases 1-4. The misfit figures shown are seismic misfits calculated with the same error value so are comparable.**

Figure 6.37 demonstrates the permeability solution obtained with pilot points (Case 4). This is just a generic model that happens to fit the data. An important remark needs to be made in connection with it. The comparison shown above by no means suggests superiority of the pilot points method over other parameterisations – too much valuable information is incorporated into those deterministic interpretations to be easily negated by a simplistic interpolation. However it shows that the specifics of the interpretations being incorporated into the simulation model can be incompatible with dynamic simulation data or be a reason for biased predictions. In that case, measures need to be taken to increase the flexibility of the parameterisation such as increasing the number of parameters or considering an alternative. As discussed in Literature review chapter (section Choosing a parameterisation consistent with data resolution), right balance between the prior information incorporated into the parameterisation and the flexibility of it to accept the details of calibration data maximizes the benefit of using these information sources.

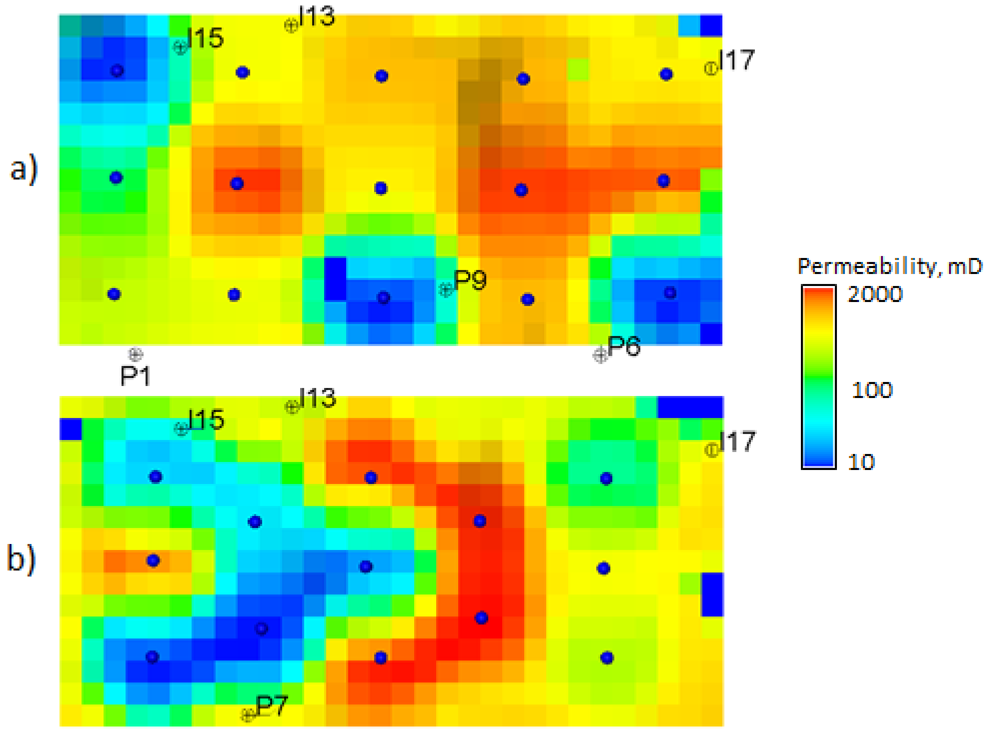

**Figure 6.37. Permeability distribution – solution for the history matching problem parameterized with the permeability points. Location of the permeability points is shown by the blue dots. The two panels show intervals T31a (a) and T31b (b).**

## 6.4 Conclusions

In this chapter, realistic scenarios of seismic history matching were considered in order to emphasize the problems of incorporating the deterministic distributions of properties into simulation models. The first example (section 6.2) was parameterized with deterministic channels of known geometry of which the transmissibilities were left to be estimated in history matching. However, the prior information that was supplied by means of distributing the channels in the model appeared to be defining enough for its predictive capability which in turn was not affected by history matching. Regardless of information density of the dynamic calibration data, the history matching resulted in the unique model. Replacing the parameterisation with pilot points removed that strong controlling effect of the prior knowledge and the real scale of dynamic constraint was now felt – we could not obtain a unique model by history matching anymore.

The second example (section 6.3) demonstrated an effect of so called structural noise on the history matching performance. Deterministic inclusions in the simulation model required more parameters to compensate for any incompatibilities with the dynamic data. Indeed, cases 2 and 3 can be viewed as models where certain assumptions were made about their fixed parts and the history matching was performed on a reduced parameter set (28 parameters). These assumptions (inaccurate prior knowledge) introduced a bias limiting the ability of models to match the dynamic data. Compared to those two cases (2 and 3), cases 1 and 4 performed better in history matching. In the former, the number of parameters was higher (45) while in the latter, the number of parameters was the same (28) but the structural noise was removed by replacing the deterministic regions with generic pilot points. This does not suggest a universal superiority of the pilot points, but stresses the importance of balance between the prior knowledge in a parameterisation and its flexibility to calibration with dynamic data.

# Chapter 7. Integrating data in seismic history matching: scale of constituents

## 7.1 Introduction

Using 4D seismic data in history matching of reservoir simulation models along with the traditional constraints that is the production data should result in better constrained model predictions because it provides extra information about the spatial distribution of pressure and saturation. The success of combining production and seismic data is reported in publications studying history matching with 4D seismic data as discussed in Literature review chapter. The extra spatial constrain of 4D seismic data definitely leads to more determined, more unique model estimates. However, 4D seismic data is not a direct simulation outcome, and moreover, the seismic modelling process often is controlled by uncertain parameters. This raises questions about the quality of constraint by 4D seismic data. In particular, what scale of details should be matched in the seismic data in order to maximize the benefit from this extra constraint? In this chapter, a series of history matching experiments is performed where the seismic signal (in 4D seismic map) is matched to different extents to understand the effective scale of seismic details providing the useful constraint for the simulation model. The resulting models are compared in terms of their pressure and saturation state and also by their forecasts.

It was shown in the previous chapter, that more flexible parameterisation reduces the bias from prior uncertainties in the final model estimates. In this chapter, we will continue using the 28-parameter pilot point scheme, and will also use a scheme with higher resolution, 77-parameter pilot points. These will be compared in terms of the parameter resolution required for fitting the seismic data. Also, it will be shown how much of this resolution is actually utilised when finding solutions effectively constrained by seismic and production data simultaneously. The effective resolution of the parameterisation is naturally determined by the scale of the signal in data that the model is trying to capture.

## 7.2 The history matching method

### *7.2.1 The experiment set up: model, data and parameters*

In this chapter we will follow the same approach as in previous chapters for inferring the internal characteristics of models from their responses and use predictions of a known reference model as observed data. This provides a fully controllable environment for the study and reduces the requirements for computational resources. Limitations associated with the synthetic nature of this approach do not reduce the practical value of the outcomes of the study because of its particular place among the studies of reservoir models. In particular, we focus on general concepts and decisions affecting the history matching results which is a necessary step and should precede case specific studies focused on real data. It is essential however that any models being used in a synthetic study are tied to the real geology and processes in order for the results to have practical meaning. In this study this is ensured by using models built from the real data (Schiehallion model). The background of the Schiehallion field and the analysis of modelled seismic effects are given in Chapter 5. The simulation model derived from the Schiehallion field model for the purposes of history matching experiments is described in Chapter 6 (section 6.3.1. Models for history matching). The image of the model grid with NTG property is repeated here in Figure 7.1 for clarity of the presentation.

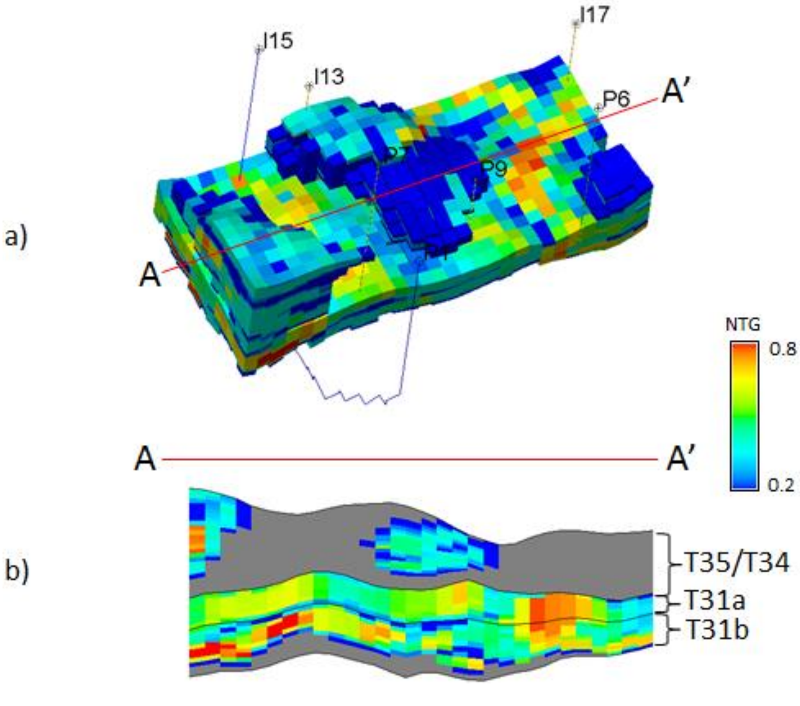

**Figure 7.1. NTG distribution in the model derived from the Schiehallion model for history matching experiments of the present study: a) 3D view, b) cross-section along AA' line.**

The model contains a reasonable balance between the grid size and associated computational requirements on one hand and abundance of geological details and variety of seismic signals on the other. As such this submodel is an optimal way of utilising the Schiehallion simulation model for a history matching study which involves many thousands of model runs.

The model includes 7 wells of which 4 are producers and 3 are injectors. These are active during 8 years of production history which includes periods of increased GOR and water cuts in some of the wells. The interpretable 4D seismic signal consists of gas breakouts and saturation substitutions due to the water front move. These are also slightly affected by the multiple layer interference which creates an extra amount of ambiguity in interpretation (see Chapter 6, section 6.3.1). In the Schiehallion field, reservoir T31a is the most significant in terms of the volume of hydrocarbons. It is penetrated by 3 of 4 producers, while the underlying T31b is penetrated by a single producer, P7. The upper layer, T35/34 is not producing in this model but is included for its effect on the seismic response.

The state of the reference model at which the historic data is generated is the same as in Chapter 6. This is set using the transmissibility regions as model parameters. The historic data includes oil and water rates in the wells, seismic maps, cube of seismic traces and inverted impedance property. Figure 7.2 and Figure 7.3 repeat the illustration from the previous chapter and shows the response of the reference model. Maps of pressure and saturation are repeated on Figure 7.4. Visualisation of seismic traces and of the inverted impedance is not given here as it does not add to the model description. These will be discussed later as they are used.

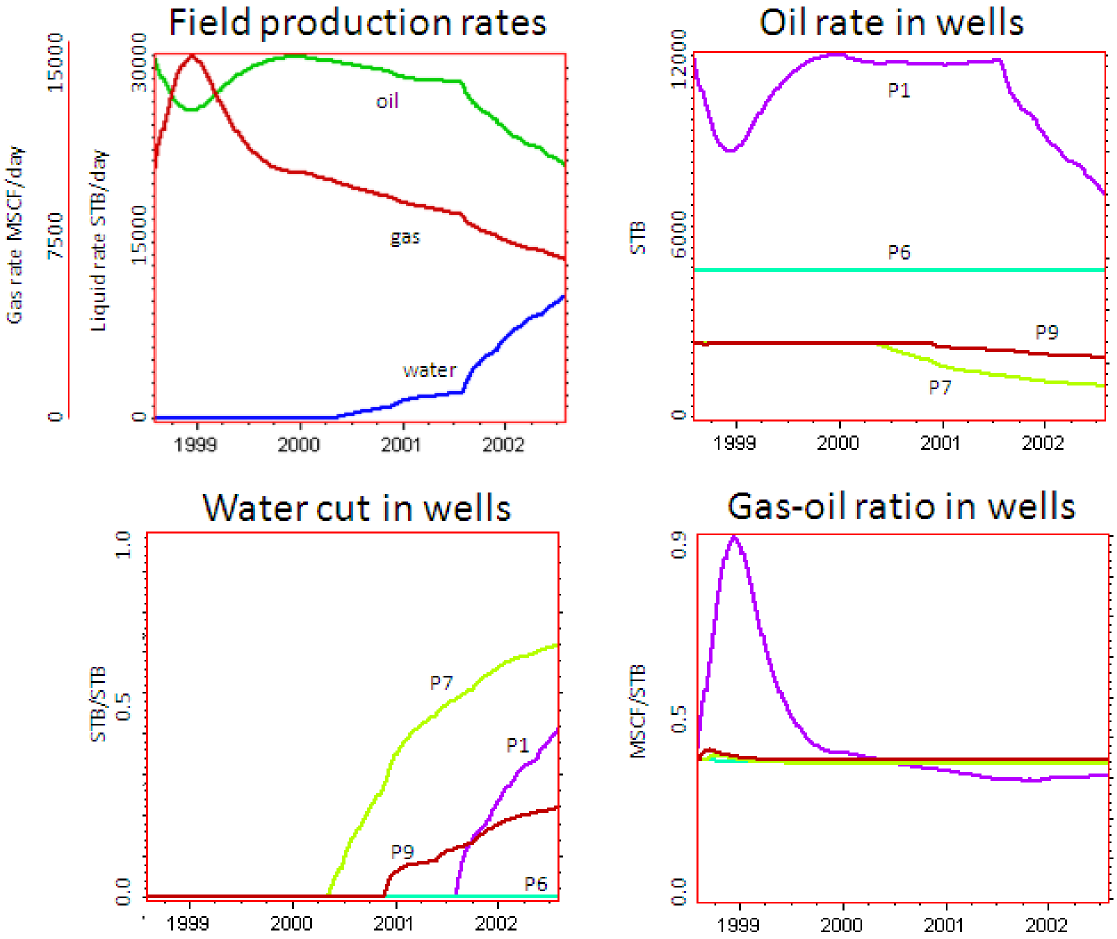

**Figure 7.2. Production profile of the reference model. Only the history matching period is shown.**

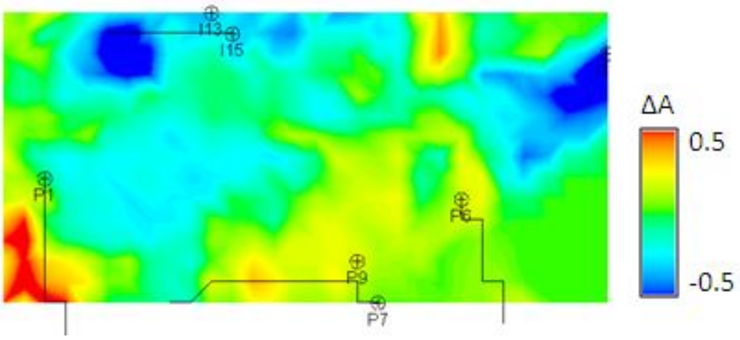

**Figure 7.3. Map of 4D seismic attribute (mean of coloured inversion, see Chapter 5, section 5.5.3) calculated for time difference Aug 2002-Aug 1998 with the reference model: 'historic' seismic data. Red indicates (acoustic) softening of rocks, and blue indicates hardening.**

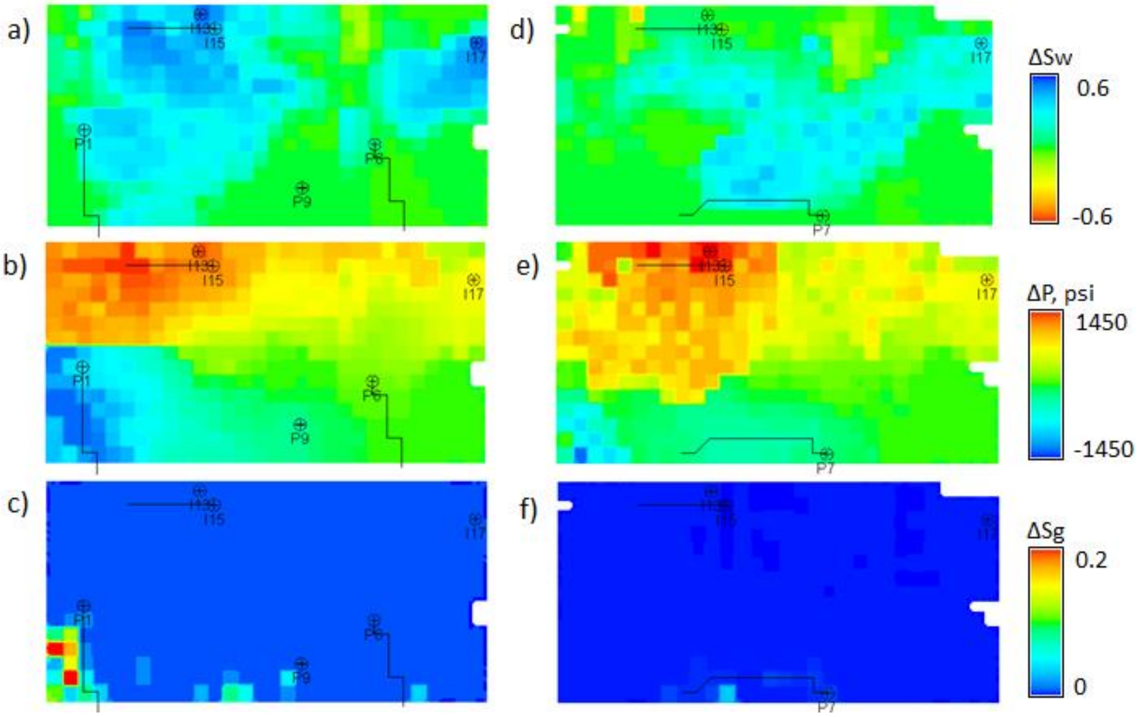

**Figure 7.4. Average maps of pressure and saturation differences between the values on 01/08/2002 and on 01/08/1998 for the reference model: a) water saturation difference in T31a, b) pressure difference in T31a, c) gas saturation difference in T31a, d-f) same as (a)-(c) but for T31b.**

In this chapter, the parameterisation of the history matching problem is based on the pilot points distributed evenly across the reservoir. The pilot points modify the permeability field. This parameterisation is chosen here because it is neutral with respect to any geological realisations of the permeability distribution unlike, for example, the parameterisation based on geobodies as shown in Chapter 6. This is important for the study of this chapter because here we are focusing on information purely from the calibration data (historic data: well rates and 4D seismic attributes) so any effect of prior information and parameterisation bias should be minimized (prior-dependent and prior-independent parameterisation methods are also discussed in Literature review chapter, section Choosing a parameterisation consistent with data resolution). However, some bias is produces by the pilot points too which is related to the sparseness of their distribution. This can be viewed as a limited resolution of the parameterisation, but are there sufficient amount of details in data to feel the resolution limit? In order to address this question, two levels of model resolution are considered here: 28-point and 77-point schemes. The layout of pilot points for these schemes is shown in Figure 7.5. The points are distributed approximately evenly across the layers T31a and T31b. The two schemes share the layout in T31b but differ in the number of points in T31a. As seen from the figure, the lower layer, T31b, is covered with fewer points as it is not the target reservoir for calculating the seismic map and also it contributes less to the oil production. Permeability values are updated at pilot point locations and then interpolated across the reservoir. Vertically, the permeability is constant within each of the layers T31a and T31b which means that the only variation of vertical heterogeneity within each of the layers is caused by varying NTG (see Figure 7.1).

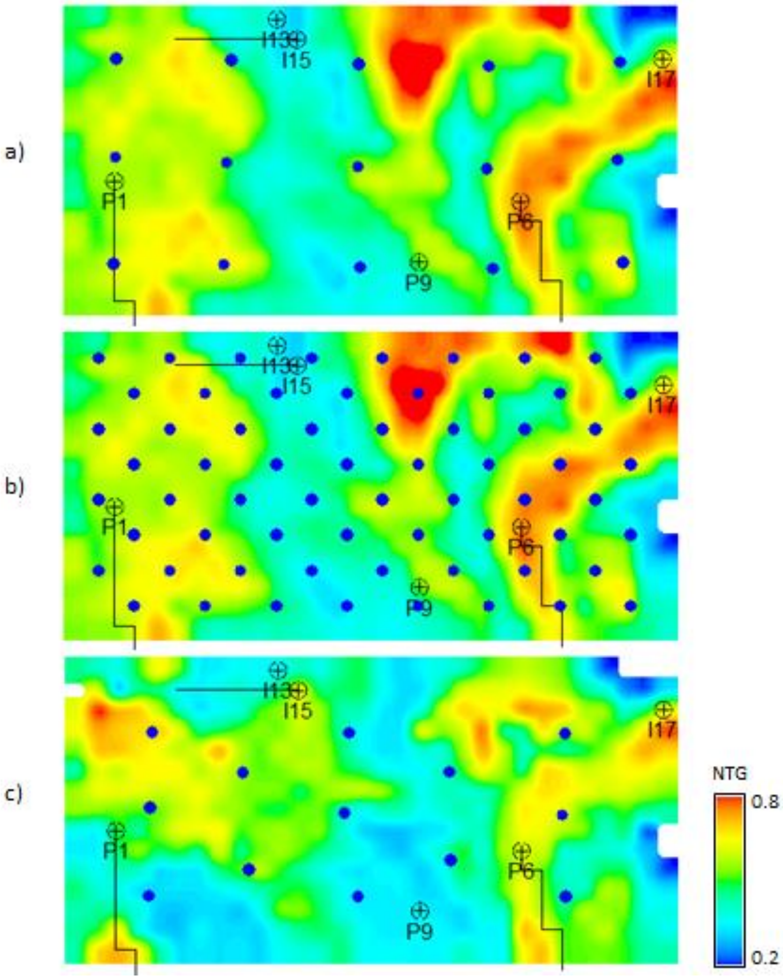

**Figure 7.5. Layout of permeability points shown on top of NTG maps of layers T31a and T31b: a) points of 28-point scheme in T31a, b) points of 77-point scheme in T31a, c) points used by both schemes in T31b.**

It is important to note that similar to the history matching setting of the previous chapter, here the reference model and the models being history matched are parameterised differently. The response of the reference model (observed data for history matching) was generated by setting the transmissibility multipliers of geobodies (on top of the constant permeability, 600 mD across the reservoir) while predictions of the history matched models are controlled by varying the permeability via pilot points as described above. This in particular means that no such values of history matching parameters exist that would cause a history matched model to generate exactly the same prediction as the reference model. History matched models will always approximate the historic data.

### *7.2.2 Feasibility of history matching with permeability points of low and high densities*

In this section, we will examine the feasibility of solving the history matching problem using the two sets of points described above as parameters. The task consists of matching well rates and seismic response of the reference model as observed data in each case. The goal in this section is to demonstrate that the algorithm is set up correctly to be able to fit the data while the solutions themselves will be discussed in the following sections. We already demonstrated that the history matching problem using the 28-point scheme can be solved for 4D seismic maps (see Chapter 6, section 6.3). For the 77-point scheme, we expect to achieve lower misfits because of the increased model resolution.

In each history matching example that will follow in this chapter, multiple history matched models are considered (that is the history matching loop is re-run several times with exactly the same input in each experiment) in order to a) study the variability of solutions where necessary and b) avoid outliers which may occur because of the stochastic nature of the optimization process (using the PSO algorithm).

In the first experiment only the production data is matched. The data consists of oil and water rates for the wells P1, P6, P7 and P9. During the history matching, models are run under the historic liquid control which is read from the output of the reference model. In the same way the historic rates are maintained in the injectors. The history matching period is 01/08/1998-01/08/2002. The objective function consists of misfits of water and oil rates which accounts for the GOR dynamic (in particular in well P1) as well. Analogous to the previous chapter, errors are assumed uncorrelated. Due to the different levels of liquid rates in the four producers (see Figure 7.2) the misfit terms for different wells receive different actual weights. One way round this issue is forcefully balancing the terms but this is not done here for sake of ensuring the total field rates are matched as a priority. PSO algorithm is used for history matching with the following parameters: 80 particles and 70 iterations in the case of 28-point scheme, and 80 particles and 85 iterations in the case of 77-point scheme. Figure 7.6 shows the misfit functions for 5 best (with lowest misfit) history matching cases for each of the two schemes. These functions are obtained by sorting the misfits from all particles in the descending order.

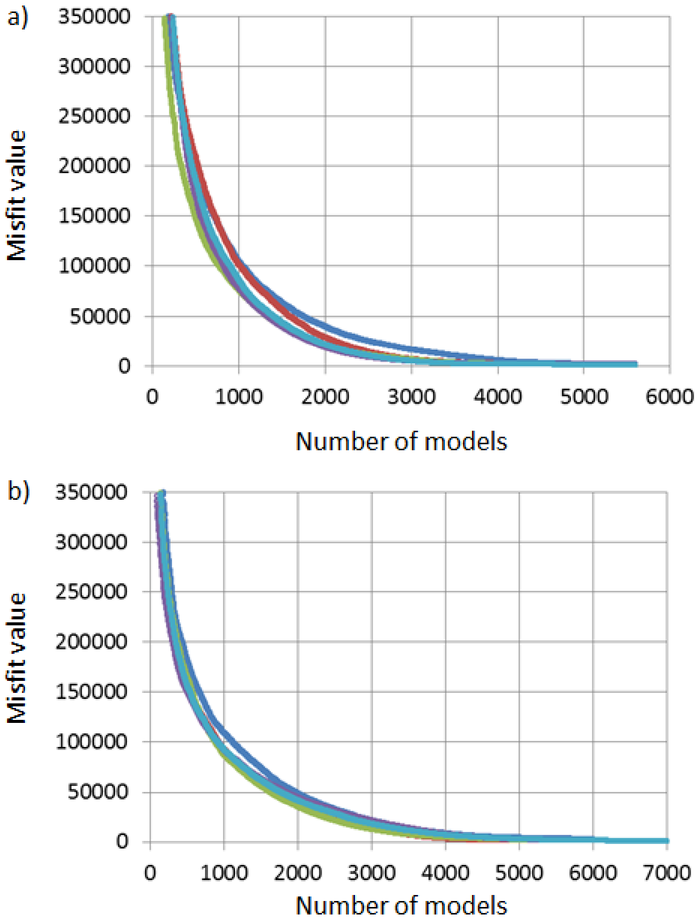

**Figure 7.6. Misfit reduction with the number of models for a) 28-point scheme, b) 77-point scheme. Each plot shows 5 misfit functions. Models history matched to production data only. Some of the initial misfits were truncated. Misfit values from all the particles were sorted in the descending order.**

Figure 7.7 shows results of history matching using the production data including the predictions of 5 history matched models using the 28-point scheme (green and blue lines), same for 77-point scheme (green and blue lines), prediction of the starting (base) model (black lines), and predictions of the reference model as observed data (red lines). The starting model here is a copy of the reference model with all information regarding the variation of permeability erased, that is it has constant permeability (600 mD) across the entire reservoir and no other modifiers of transmissibility. The results of history matching (Figure 7.7) show that the two schemes allowed us to match the rates of the reference model equally well – their predictions mostly coincide with each other and with history. Notably, the match quality is worse (although remains good) in wells P7 and P9. This is caused by the low proportion of production from these wells in the overall produced volume which stresses lesser significance of these wells and causes lower weights in the objective function.

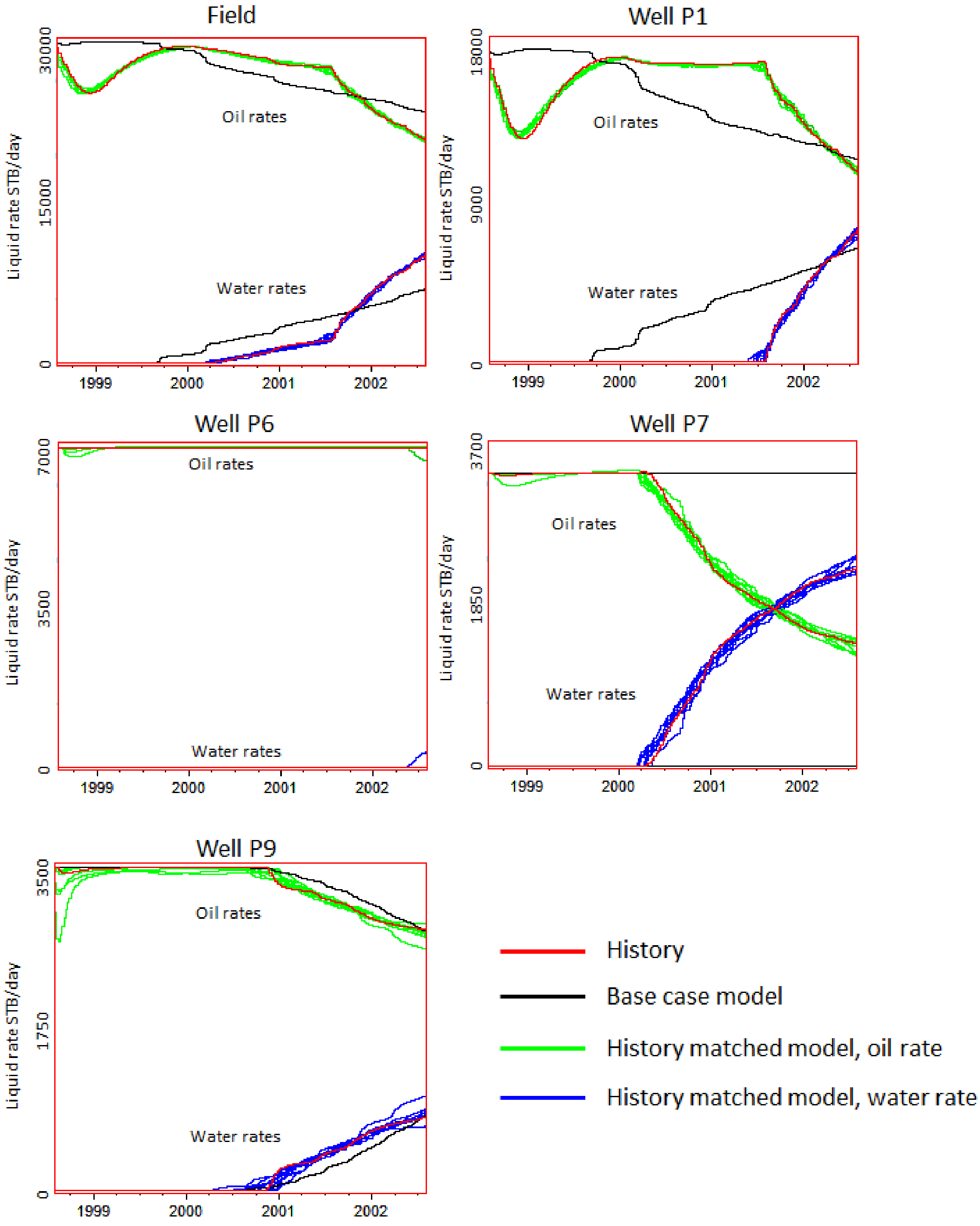

**Figure 7.7. Results of history matching to production data: oil and water rates predicted from the history matched models using 28-points and 77 points (green and blue lines for oil and water rates respectively), predictions of the starting (base) model (black lines) and predictions of the reference model ('observed' data, red lines). For each of the two schemes, predictions of 5 history matched models are shown. In this case, they mostly coincide with each other and with history.**

Another difference between the wells is the nature of produced fluids which makes a difference for the history matching process. Mainly it is the absence of water cut in well P6 which means that this wells lack any production data control. Maps of time-lapse pressure and saturation differences for one realisation of the history matched model (not called 'best' because the models within the 5 chosen are close in match quality) are shown in Figure 7.8.

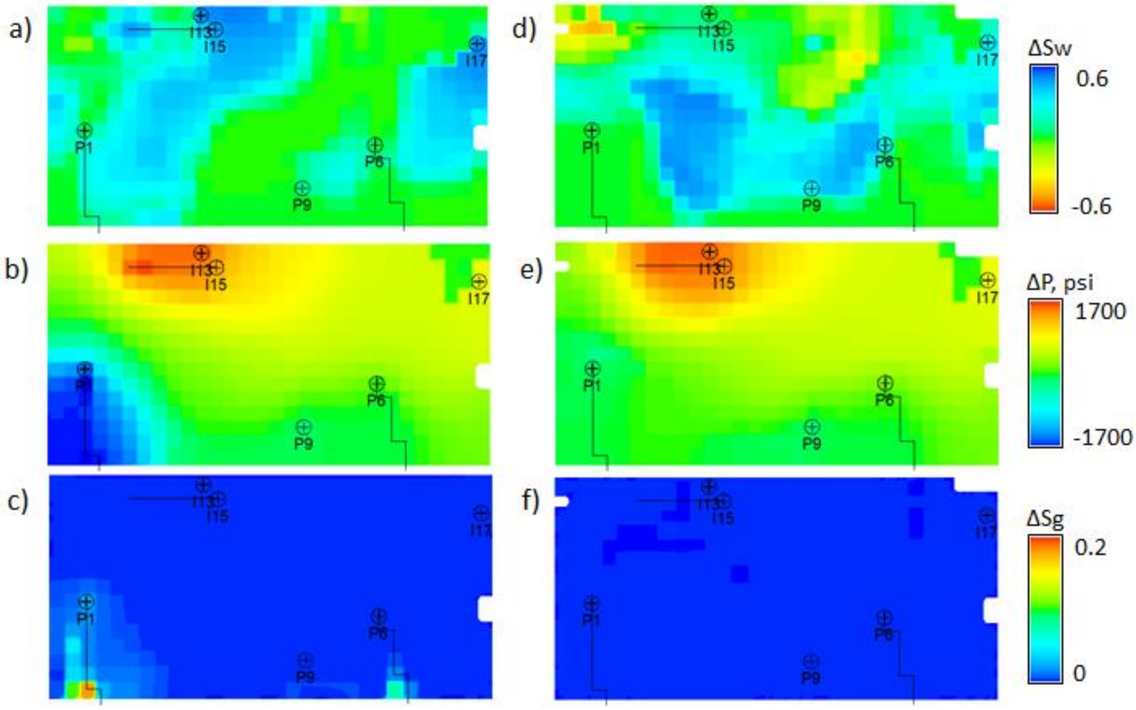

**Figure 7.8. Average maps of pressure and saturation differences between the values on 01/08/2002 and on 01/08/1998 for a model history matched to production data using 28-point scheme: a) water saturation difference in T31a, b) pressure difference in T31a, c) gas saturation difference in T31a, d-f) same as (a)-(c) but for T31b.**

In the second experiment, we will compare the ability of the models parameterised with the 28- and 77-point schemes to match the 4D seismic map. PSO algorithm is used for history matching with the following parameters: 80 particles and 75 iterations in the case of 28-point scheme, and 80 particles and 90 iterations in the case of 77-point scheme. Figure 7.9 shows the misfit functions for 5 best (with lowest misfit) history matching cases for each of the two schemes. These functions are obtained by sorting the misfits from all particles in the descending order.

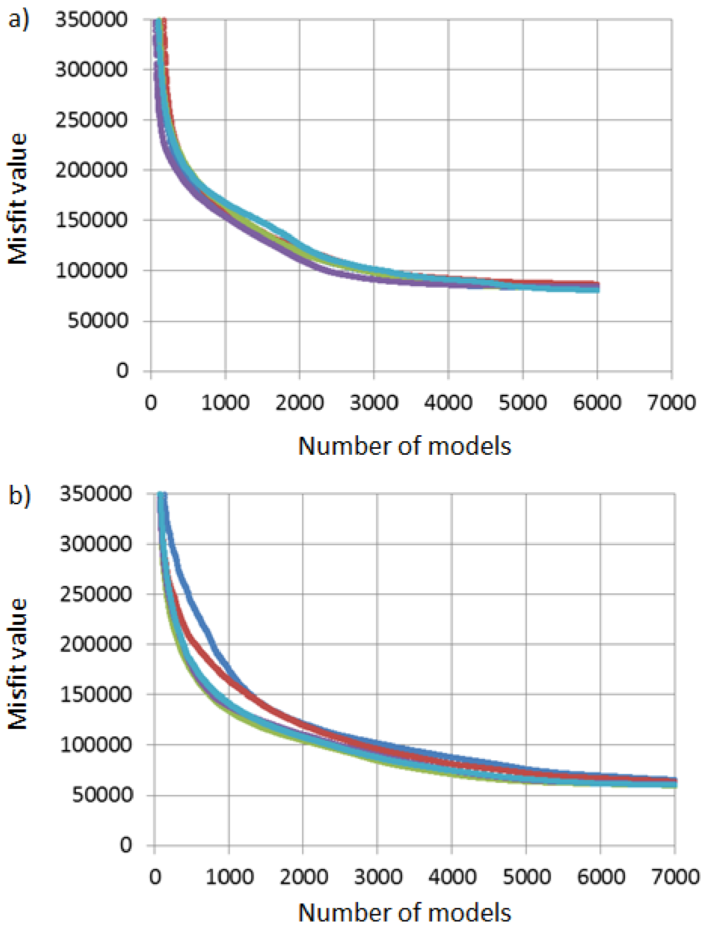

**Figure 7.9. Misfit reduction with the number of models for a) 28-point scheme, b) 77-point scheme. Each plot shows 5 misfit functions. Models history matched to seismic data only. Some of the initial misfits were truncated. Misfit values from all the particles were sorted in the descending order.**

Figure 7.10 compares 4D seismic maps of the best 2 history matched models using the 28- and 77-point schemes with the predictions of the reference and base models. The base case model is the same as the one used in the previous chapter. It has a uniform permeability across the reservoir equal to 600 mD hence its 4D seismic signal is conditioned mostly by NTG variation rather than a more complex flow pattern. Comparison of predictions of the best models with the base case and the reference predictions suggests that the history marching achieved its goals of fitting the reference seismic response with all its major features as well as the signal discontinuities replicated by model predictions. Higher resolution of the 77-point scheme allowed incorporating smaller details of the data and resulted in the lower misfit values as expected. Pressure and saturation time-lapse difference maps are shown in Figure 7.11. These indicate different state of pressure and saturation from the one in the production matched model. The different solutions by matching seismic and production data are discussed in the following sections.

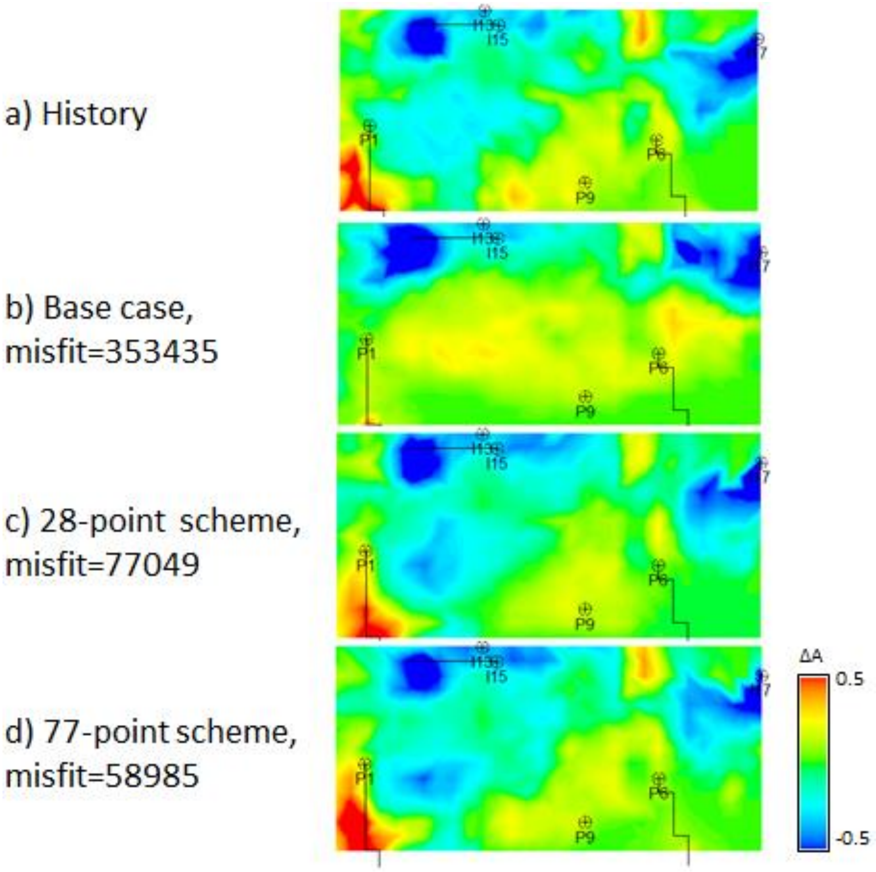

**Figure 7.10. Results of history matching to seismic data. Seismic predictions of two history matched models and the starting model are compared with 'observed' seismic map. 28- and 77-point schemes are used for history matching.**

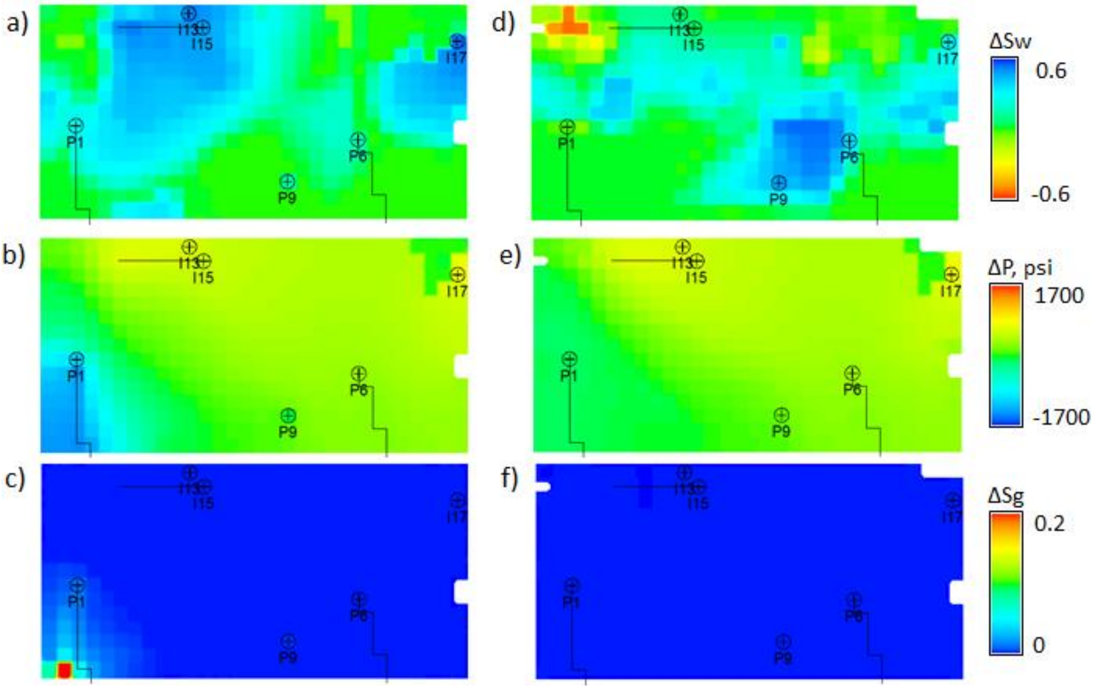

**Figure 7.11. Average maps of pressure and saturation differences between the values on 01/08/2002 and on 01/08/1998 for a model history matched to seismic data (seismic map) using 28-point scheme: a) water saturation difference in T31a, b) pressure difference in T31a, c) gas saturation difference in T31a, d-f) same as (a)-(c) but for T31b.**

Finally, Figure 7.12 compares permeability fields obtained as a result of history matching to production and seismic data using the two parameterisation schemes. The figure shows a model per parameterisation scheme (28- and 77- point) and per data type (the variety of solutions will be shown and discussed in the following sections). It is in the domain of permeabilities (input to simulation) where the different scales of the 28- and 77-point schemes can be directly observed, while in the domain of predicted data these are blended with the resolution of the rest of the model and simply result in different realisations rather than scales (for example, compare Figure 7.10c and Figure 7.10d). Another difference is in solutions for matching different data types (production and seismic): pairs (a)-(c) and (b)-(d) of Figure 7.12. This difference is caused by the different nature of constraint by production and seismic data which is discussed in more details in the following section.

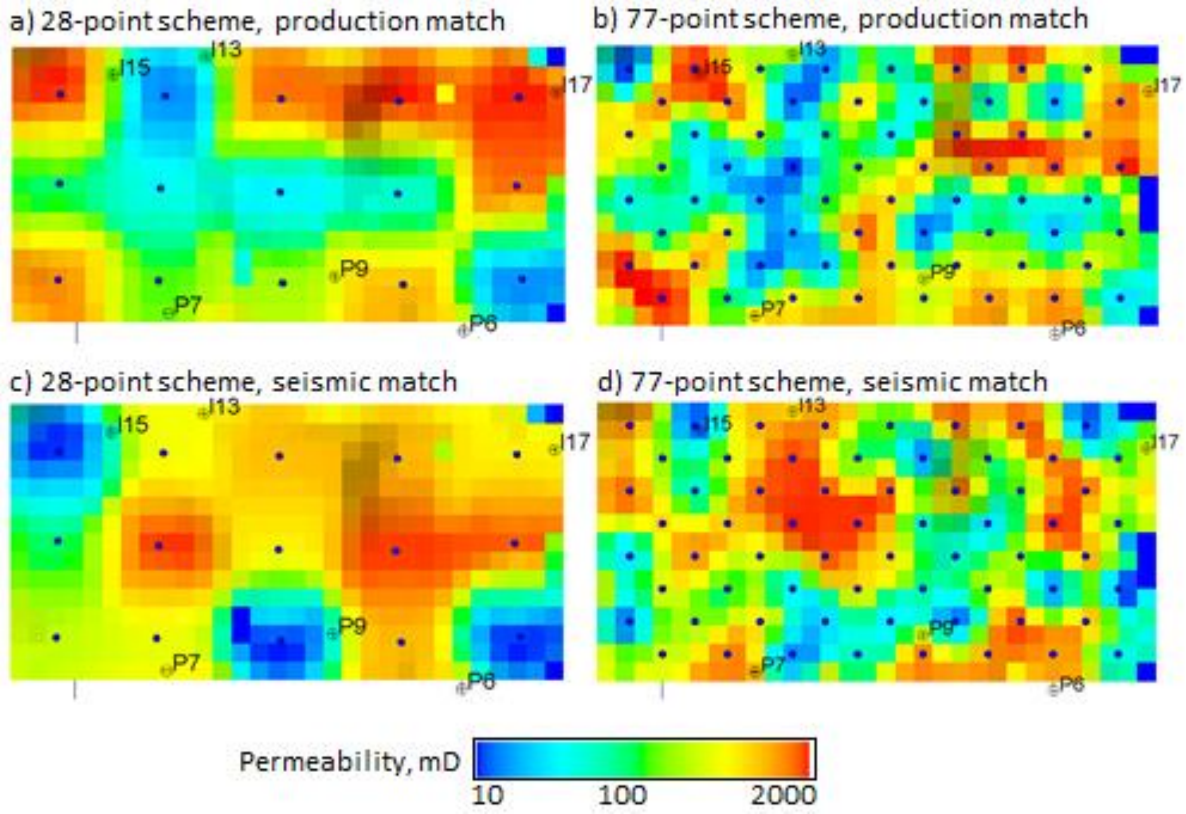

**Figure 7.12. Permeability distributions in layer T31a resulting from matching production and seismic data using 28- and 77-point parameterisation schemes.**

## 7.3 Different nature of constraint by production and seismic data

In this section, models history matched to production and seismic data will be compared in order to illustrate the difference of the constraint by these data types. In general, simulation models can be compared by their properties, such as permeability, and also by simulation results such as pressure and saturation distributions or specific predictions such as well rates and seismic responses. Comparison of models in these three domains provides different information about the simulation model. For example, the permeabilities are estimated in history matching in our case and therefore represent solutions for the history matching problem. For an ensemble of such solutions, we can study their variability by examining the permeability fields. The variability of solutions will indicate the strength of data constraint. The variability will also be different depending on how detailed the permeability solution itself is which is a function of the resolution of parameterisation. However, the goodness (goodness in terms of observed data match and predictive capability) of models cannot be assessed by examining the permeabilities only. The reason for it is that the permeabilities themselves are only (arbitrarily chosen) means for approximating a given model response. There are no ‘reference’ or ‘true’ values for permeabilities, we only have a reference model response. Moreover, there is no direct equivalent to the estimated (via pilot points) permeabilities in the reference model which was intentionally parameterised with transmissibility regions (this point was also discussed in Chapter 6, end of section 6.2.2). In a real history matching case, solutions can be examined for compliance to some prior information (although it is generally more difficult to construct a prior for permeability than, for example, NTG because the connectivity in reservoir is always an uncertainty, see for example *Govan et al, 2006*). In our case however, no prior assumptions about the permeability are made in order to concentrate on the data constraint alone.

In the first part of this section, we will study the variability of realisations of models history matched to seismic and production data and their predictions, and in the second part we will compare the models in terms of their pressure and saturation states.

### *7.3.1 Variety of solutions for the problem of history matching production and seismic data*

In the previous section devoted to feasibility of history matching experiments two scenarios were created matching production and seismic data. Here we will discuss the realisations of history matched models in those two scenarios in more details. The first scenario is matching production data only. 10 history matched models were considered in the previous section: 5 using the 28-point scheme, and 5 using the 77-point scheme. The misfit functions are shown in Figure 7.6, comparison of well rates of all 10 history matched models with the observed data and the base case are shown in Figure 7.7 (all 10 predictions look indistinguishable here because they were all able to match the observed data), pressure and saturation maps of a single model realisation are shown in Figure 7.8. The solutions themselves – permeability distributions constrained by the well rates are shown in Figure 7.13. Figure 7.14 shows seismic maps predicted from these 10 (constrained by well rates) models. These seismic maps are given here in order to analyse the resulting models and were not used in any way during the history matching. The second scenario considered in the previous chapter was matching seismic maps. 10 history matched models are considered in this scenario too. The misfit functions are shown in Figure 7.9, and the pressure and saturation maps for a single model realisation are shown in Figure 7.11. Figure 7.15 shows seismic predictions of the 10 history matched models. In this case, these are the primary predictions used in history matching, hence they show good agreement with the observed map (see also Figure 7.3 for comparison). Figure 7.16 shows the range of solutions obtained in this scenario (matching seismic maps), corresponding to the predictions in the previous figure. Finally, Figure 7.17 shows predictions of well rates for best models matched to seismic maps using 28- and 77- point schemes (again, these predictions were not used in history matching as it is a seismic-only match in this scenario).

Analysis of permeability solutions in Figure 7.13 suggests lack of spatial constraint by the production data. Specifically, one can note that the pattern of the permeability distribution (vividly presented in the 28-points case) changes significantly across the solutions. This is not the case for the models constrained by the seismic data (Figure 7.16) where a stable pattern can be traced across the solutions. This suggests that the solutions constrained to production data rather have a common integral characteristic which defines mostly the time of water arrival and phase flows but does not make any distinction between the flow paths themselves. Consequently, we may expect to get a match of production data with a wider range of spatial distributions of properties than a seismic map would allow. Being able to match data and at the same time freedom in choosing the internal structure of the model is a reminder of the ‘black box’ notion in connection with simulation models. This stresses the importance of adequate appreciation of what we can deduce based solely on data fit so that it does not trigger overly confidence in particular interpretations.

Another observation is that we are finding 2 essentially different sets of solutions by matching production and seismic data: seismic maps from the first set of models (matched to production data, Figure 7.14) show similar with each other but different from the ones of the second set (matched to seismic data, Figure 7.15) predictions which is attributed to essentially different state of pressure and saturation distribution. For this reason, matching to seismic maps in the second experiment did not lead to any good (unconstrained) prediction of well rates (Figure 7.17). Permeability distributions are also different between the two sets of solutions as seen from Figure 7.13 and Figure 7.16. These results illustrate the difference in constraints by seismic and production data as they essentially control different sides of model dynamics as mentioned in the beginning of this chapter. These differences, together with the approximate nature of models are prerequisites for difficulties in matching both data types at the same time. Experiments with combined datasets will be considered in the following sections. In our case what makes the model approximate is its parameterisation with which we can not reproduce what the reference model could predict despite the fact that the data are noise-free and the models are using exactly the same physics and assumptions. By changing the parameterisation methods, we effectively replaced the predictor itself – without needing to model any noise in data or even changing the model properties/realisations, the sets of possible realisations of pressure and saturation calculated by the reference and the variable models are different for any values of parameters.

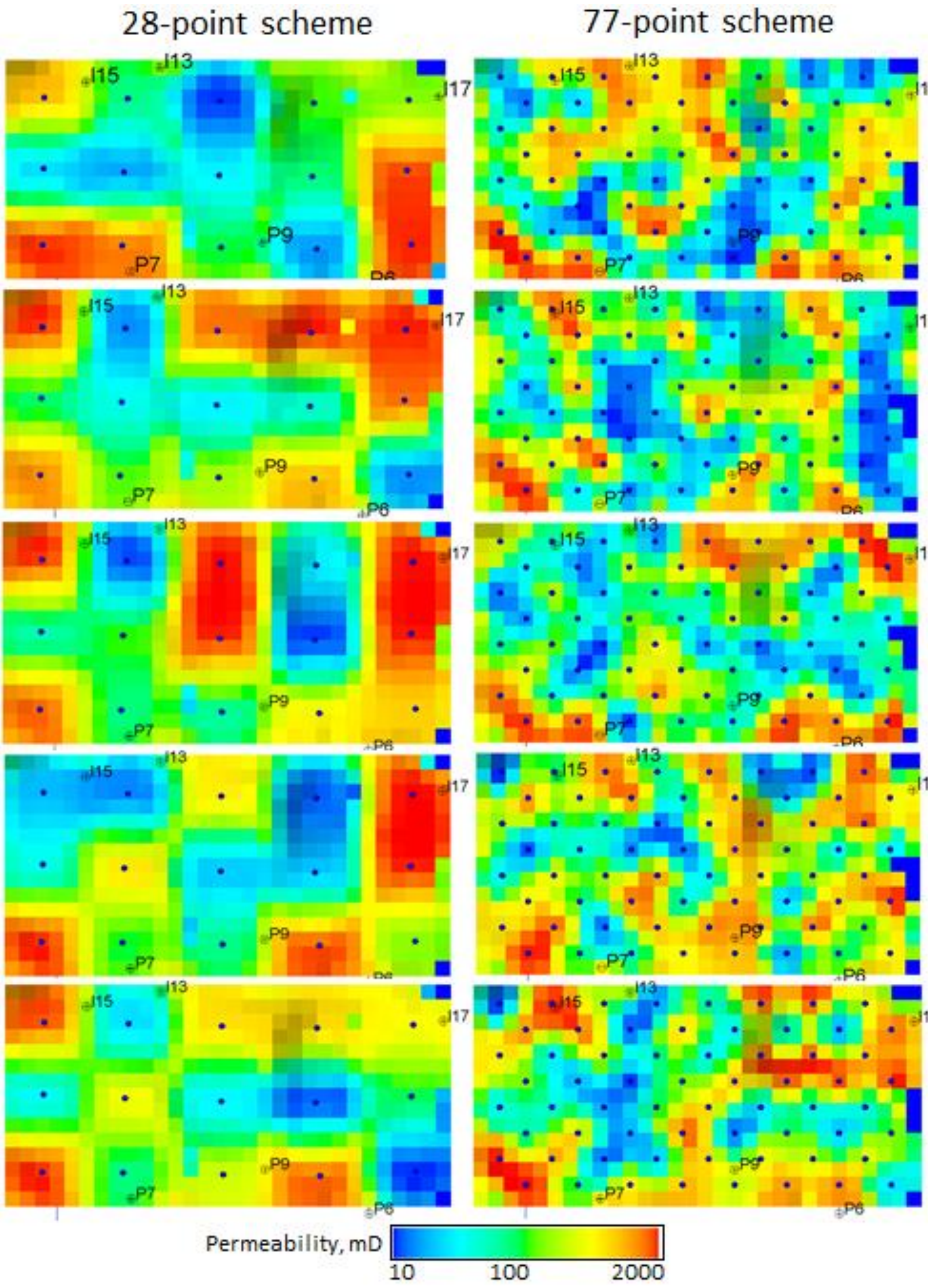

**Figure 7.13. Permeability distributions in layer T31a resulting from history matching production data using 28- and 77-point schemes.**

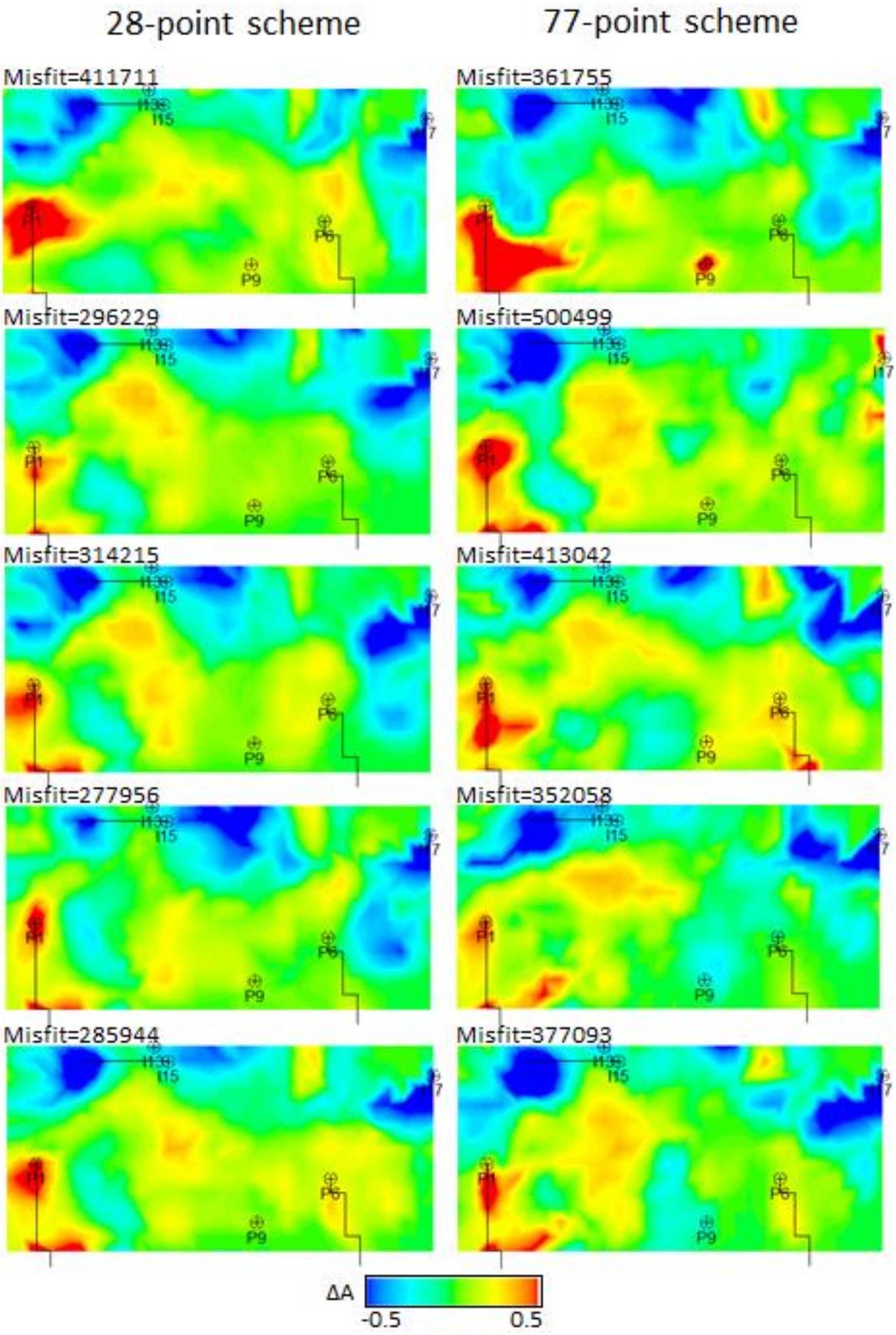

**Figure 7.14. 4D seismic attribute maps predicted by models corresponding to solutions in Figure 7.13. Misfit figures shown on top the maps indicate their deviation from the reference seismic map. These are for monitoring purposes only and were not used in history matching in any way.**

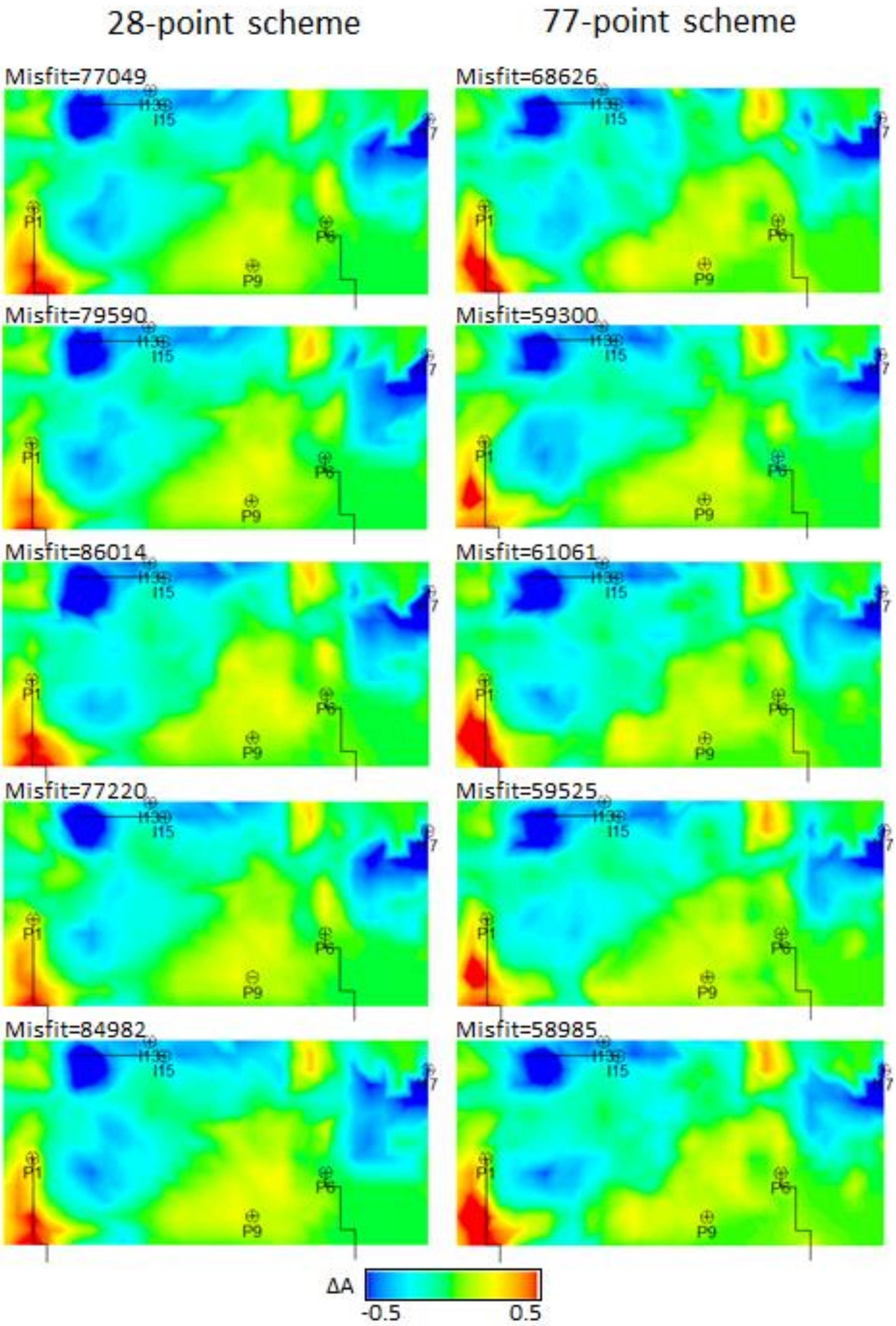

**Figure 7.15. 4D seismic attribute maps predicted by models which were history matched to seismic data using 28- and 77-point schemes.**

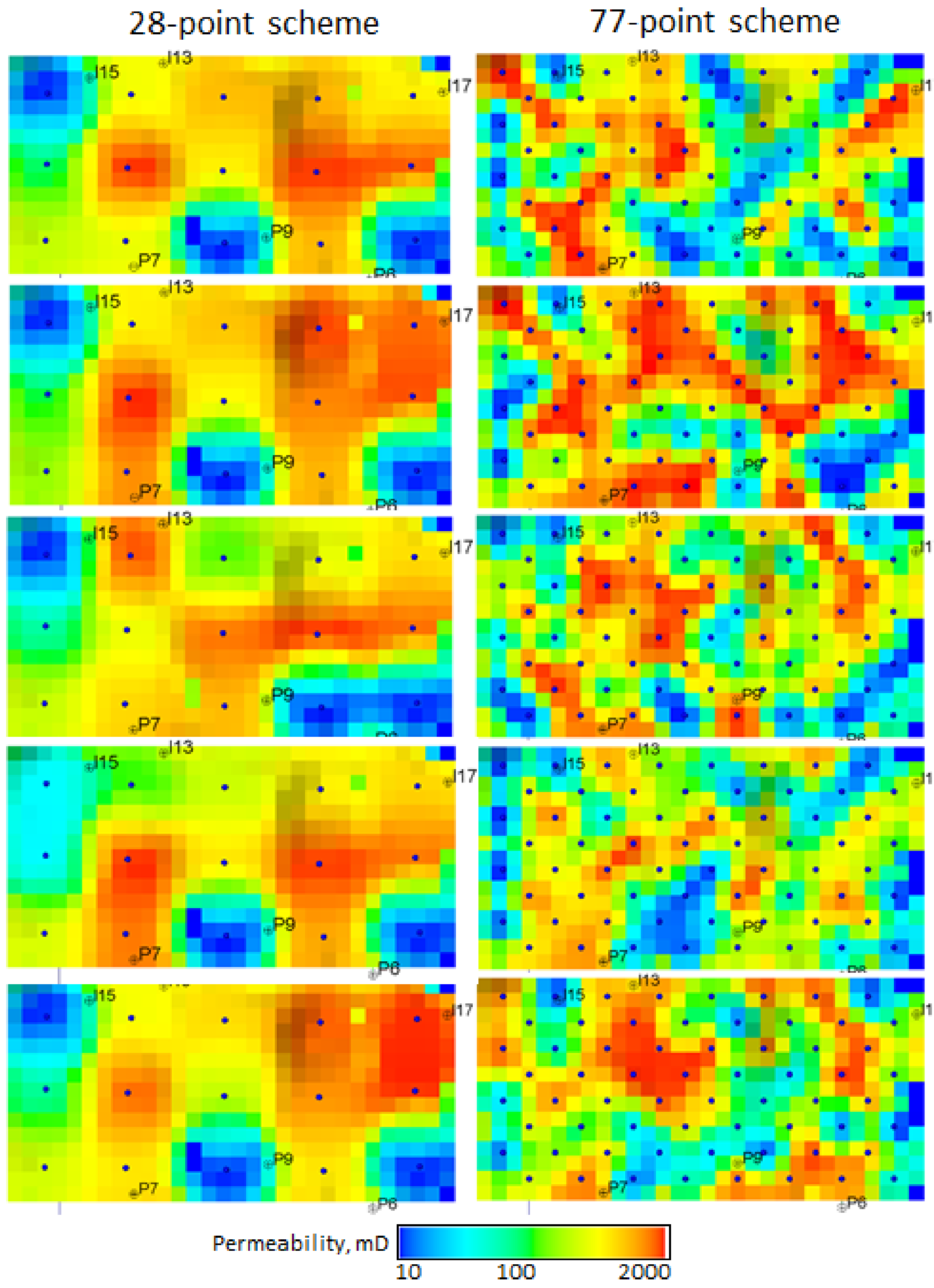

**Figure 7.16. Permeability distributions in layer T31a resulting from history matching seismic data using 28- and 77-point schemes.**

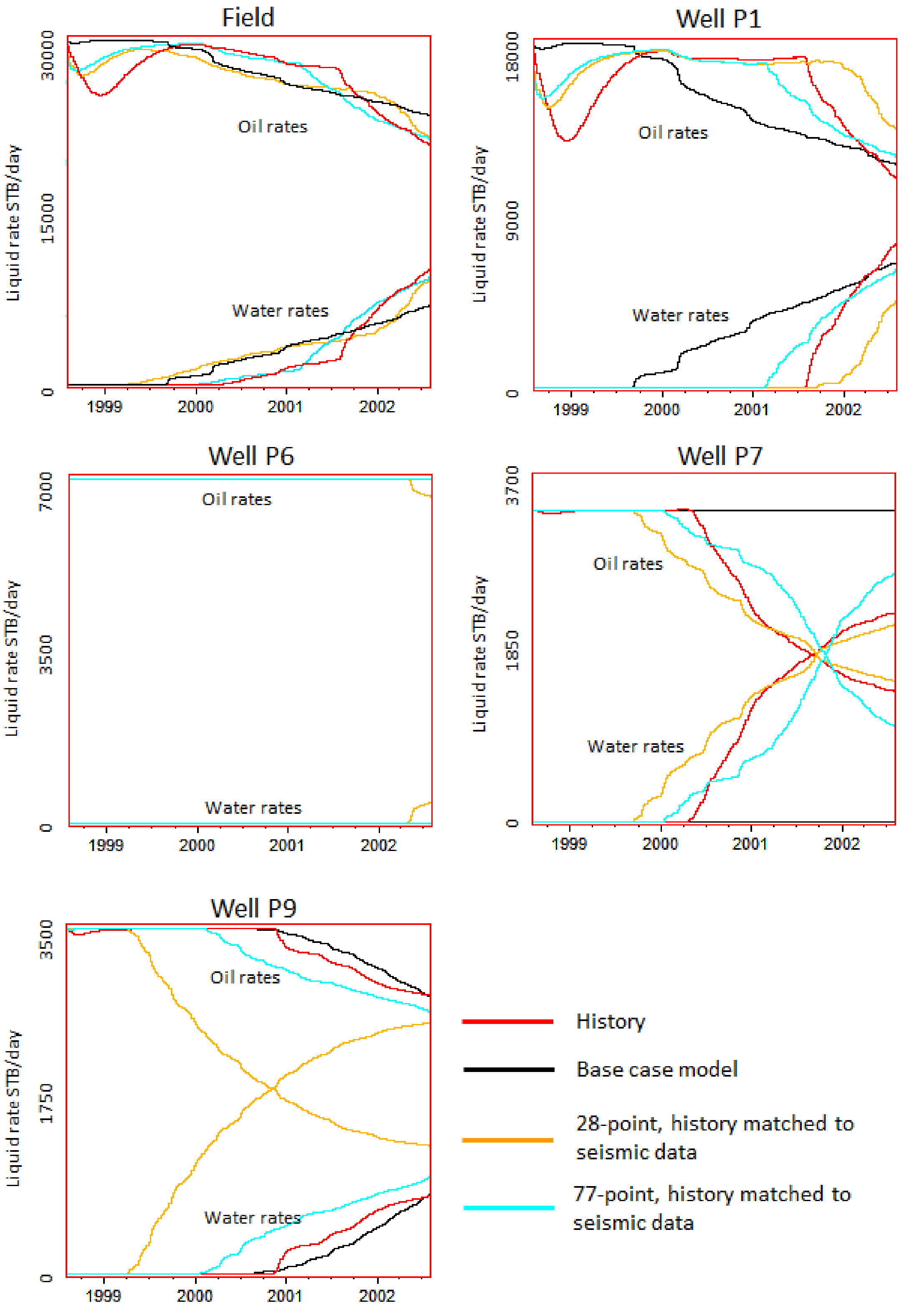

**Figure 7.17. Comparison of well rates of base case model, reference model and best models history matched to seismic maps using 28- and 77-point schemes.**

### *7.3.2 Constraints of data of different types*

The results of the two history matching scenarios above suggest that by matching to seismic and production data we had arrived at different states of pressure and saturation distribution because of different constraints by these data types. Let us now examine how these final states compare with the one of the reference model, that is how close we are getting to the reference solution by matching different data types. In this analysis, it is important to distinguish between the limitations of data (limited information content) and limitations of the history matching itself (the parameterisation makes the state of reference model unreachable). We will therefore consider an extra history matching scenarios where data have much greater information content. Such data is volumetric attributes. The remainder of this section is divided into two subsections. In the first subsection, several auxiliary history matching scenarios will be described using volumetric seismic attributes. In the second subsection, the resulting history matched models will be compared in terms of their pressure-saturation states.

#### *History matching scenarios with different data types*

In order to compare the constraints of different data types we will consider the following history matching scenarios: 1) matching production data, 2) matching seismic maps, 3) matching seismic traces, 4) matching predicted 4D impedance to the inverted one, and 5) matching predicted 4D impedance to the reference 4D impedance. Scenarios 1 and 2 have already described so far, so here we will just use the best history matched models from the previous section. Matching the seismic traces in scenario 3 is a situation where the seismic data are compared in the domain of seismic traces (different domains for seismic data comparison are discussed in Literature review chapter, section 3.4.3). This scenario provides more information for constraining the simulation model because the seismic traces cover the entire reservoir volume and therefore have greater resolution than the map-based attribute. The history matching with the seismic traces was carried out using the following PSO parameters: 80 particles and 75 iterations in the case of 28-point scheme, and 80 particles and 110 iterations in the case of 77-point scheme. Figure 7.18 shows the misfit functions for 5 best (with lowest misfit) history matching cases for each of the two schemes. These functions are obtained by sorting the misfits from all particles in the descending order. The values of misfit in scenario 3 were scaled so that the minimum misfit is at the same level as the minimum misfit in scenario 2 where the seismic maps are matched.

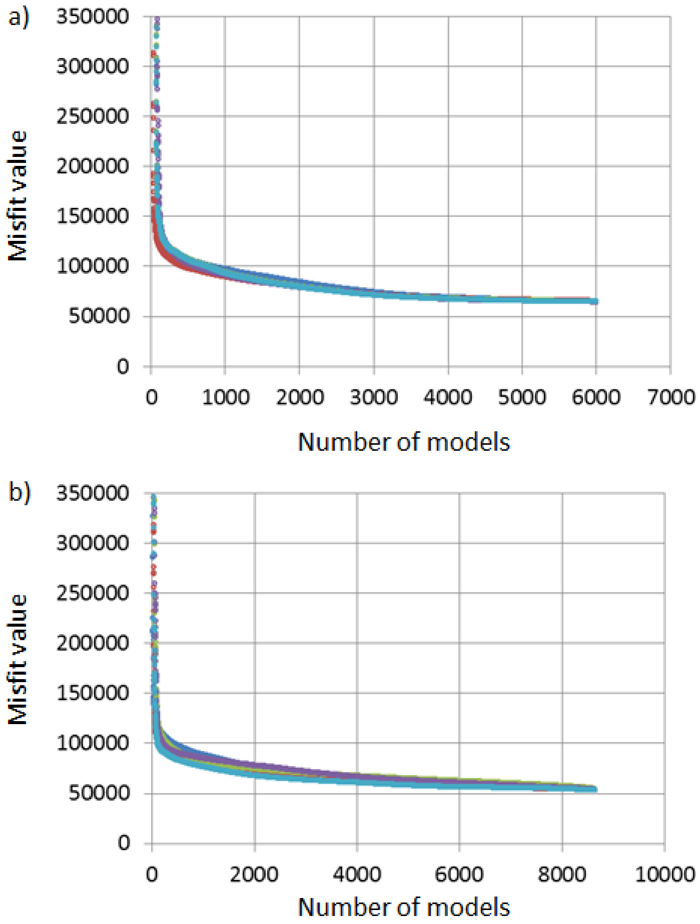

**Figure 7.18. Misfit reduction with the number of models for a) 28-point scheme, b) 77-point scheme. Each plot shows 5 misfit functions. Models history matched to seismic traces. Some of the initial misfits were truncated. Misfit values from all the particles were sorted in the descending order.**

History matching in scenario 4 uses 4D impedances as data. This is an example of situations where the seismic data are compared in the domain of petro-elastic properties, using a volumetric attribute. In this case, the observed data such as (4D) seismic traces are inverted for the (4D) impedance property which is then used as observed data in history matching. On the other hand, the predicted data in history matching are (4D) impedance properties predicted by each of the history matched models.

In such a problem setting, the first step is obtaining the observed data which is the inversion process. The inversion is carried out following the same procedure as in the case of NTG inversion described in the section 6.3.2.2 of the previous chapter but using the 4D impedance as parameters (see also Methodology chapter, section 4.7.2) which were distributed in the model according to the index property shown in Figure 7.19.

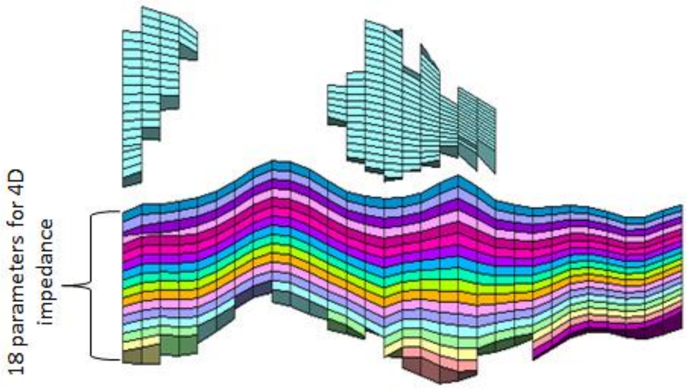

Figure 7.19. Parameter index property. Different colours indicate parameter indices.

The result of the inversion is an estimate of 4D impedance property which will be hereafter called the inverted 4D impedance. Figure 7.20 compares the inverted 4D impedance with the 4D impedance of the reference model. The two are compared here because it is the goal of an inversion to obtain an estimate of the ‘true’ impedance (in our case, the ‘true’ impedance is the one of the reference model). The comparison shows that the inverted impedance estimate is noisy and differs from the reference one in smaller details, but at the same time, the ‘events’ are repeated globally which means that they agree well on a level of lower frequency information. This is a result of narrow frequency band of the observed seismic data which does not bear information about those finer scale details, so they are left unconstrained. However, we will see further that the fine scale noise in the inverted impedance does not interfere with solutions of history matching.

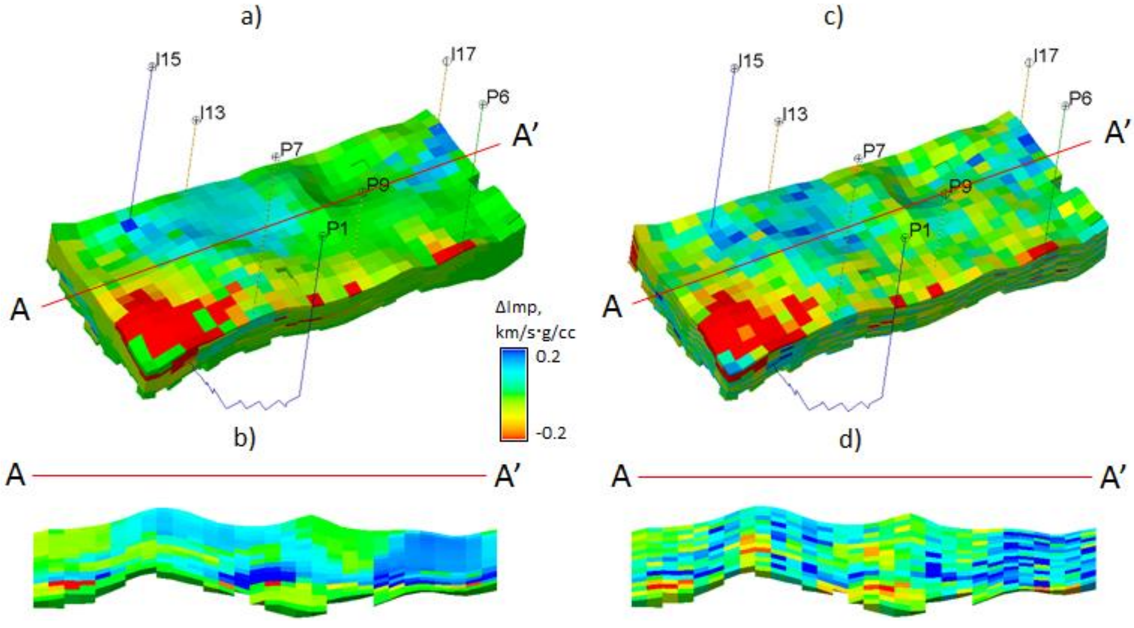

Figure 7.20. 4D impedance property: a) reference model, 3D view, b) cross-section along AA’ in (a), c) inverted from seismic response of the reference model, d) ross-section along AA’ in (c).

Finally, the scenario 5 is analogous to the scenario 4 in that the data are compared in the impedance domain. However, the scenario 5 is impossible in real history matching – it uses the reference ('true') impedance as observed data. The scenario is included here as a reference case of history matching using ideal data, that is the data of maximum resolution because it is a volumetric, and also not smoothed as the seismic traces and not distorted by the inversion noise as the inverted impedance.

History matching in scenarios 4 and 5 was carried out using the same PSO settings as in scenario 3. The best models for these scenarios history matched using the 28- and 77-point schemes are shown in Figure 7.21 and Figure 7.22. Visual inspection reveals minor differences between the predicted impedances and the reference one in Figure 7.20a, especially for the case of 28-point scheme. The analysis in the following section will show that the differences are small and that they are due to the parameterisation itself rather than due to any data errors.

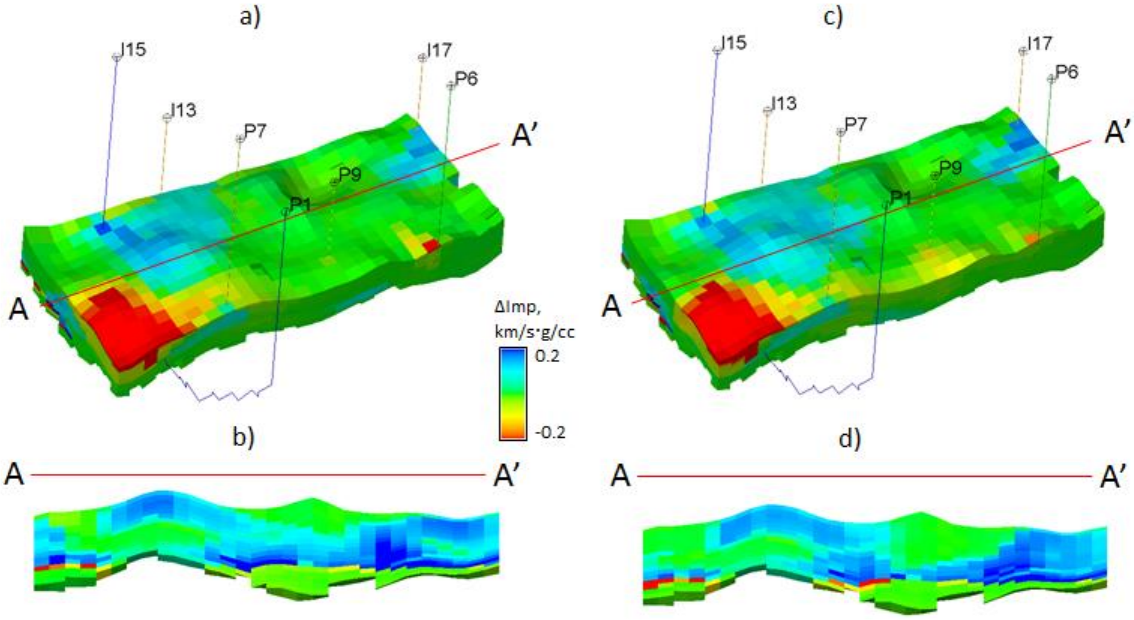

**Figure 7.21. 4D impedance property predicted by the history matched model: a) using 28-point scheme, 3D view, b) cross-section along AA' in (a), c) using 77-point scheme, d) ross-section along AA' in (c). History matching uses inverted impedance as observed data.**

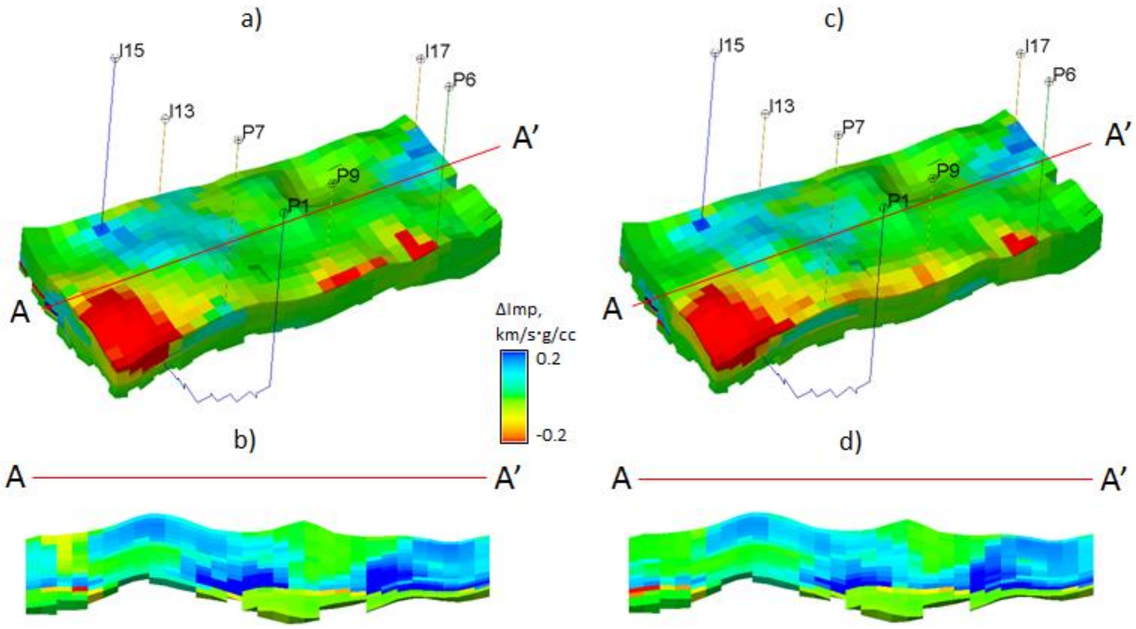

**Figure 7.22. 4D impedance property predicted by the history matched model: a) using 28-point scheme, 3D view, b) cross-section along AA' in (a), c) using 77-point scheme, d) ross-section along AA' in (c). History matching uses reference impedance as observed data.**

*Pressure-saturation states of models constrained by different data types*

In order to compare the pressure-saturation states of models (the pressure-saturation state here means the time-lapse (4D) change of pressure and saturation), one can consider calculating a misfit between pressures and saturations of the models. This leads to 3 misfits: water saturation, gas saturation and pressure misfits. In order to make the analysis more convenient, the three properties can be combined into a single property which would effectively characterise the pressure-saturation state. Given the specialisation of this work, the most relevant candidate is the 4D impedance which is controlled by changes in pressure and saturation. In general, combining three properties into a single property leads to loss of information, but in our case, this effect is negligible because realisations of simulated pressure and saturation changes are distinguished by spatial distributions of the changes rather than by magnitudes (in other words, it is highly unlikely that two simulation results would produce exactly the same distribution of impedance in the entire reservoir volume, but will be different in the underlying pressure and saturation values).

The best models from the five history matching scenarios described above will be compared here with the reference model in terms of their pressure-saturation states as described above. In particular, the pressure-saturation states of the models will be represented by the 4D impedance property. The difference between the states of history matched models and the state of the reference model is called here a misfit of state and is calculated as:

$$Misfit\ of\ state = \sum_{i=1}^{N} (\Delta I_i^m - \Delta I_i^r)^2 \qquad (7.1)$$

where $N$ is the number of cells in 3D grid of the simulation model, $\Delta I^m$ is the 4D impedance of the history matched model, $\Delta I^r$ is the 4D impedance of the reference model, symbol $\Delta$ in the last two quantities signifies that 4D impedance itself is calculated as a difference between pre-production (August 1998) and post-production (August 2002) impedances.

As a reminder, the five history matching scenarios we are considering are: 1) matching production data, 2) matching seismic maps, 3) matching seismic traces, 4) matching inverted impedance, and 5) matching reference impedance. We could just consider the misfits of states for only the final models from these scenarios which would tell us which model comes closer to the reference one. It will be more informative though to calculate the misfits of states not only for the final history matched models but also for the entire ensemble of models that were generated by the PSO algorithm in the course of history matching in each scenario. This will give us 5 ensembles of misfits of states as shown in Figure 7.23 (only 77-point cases are shown).

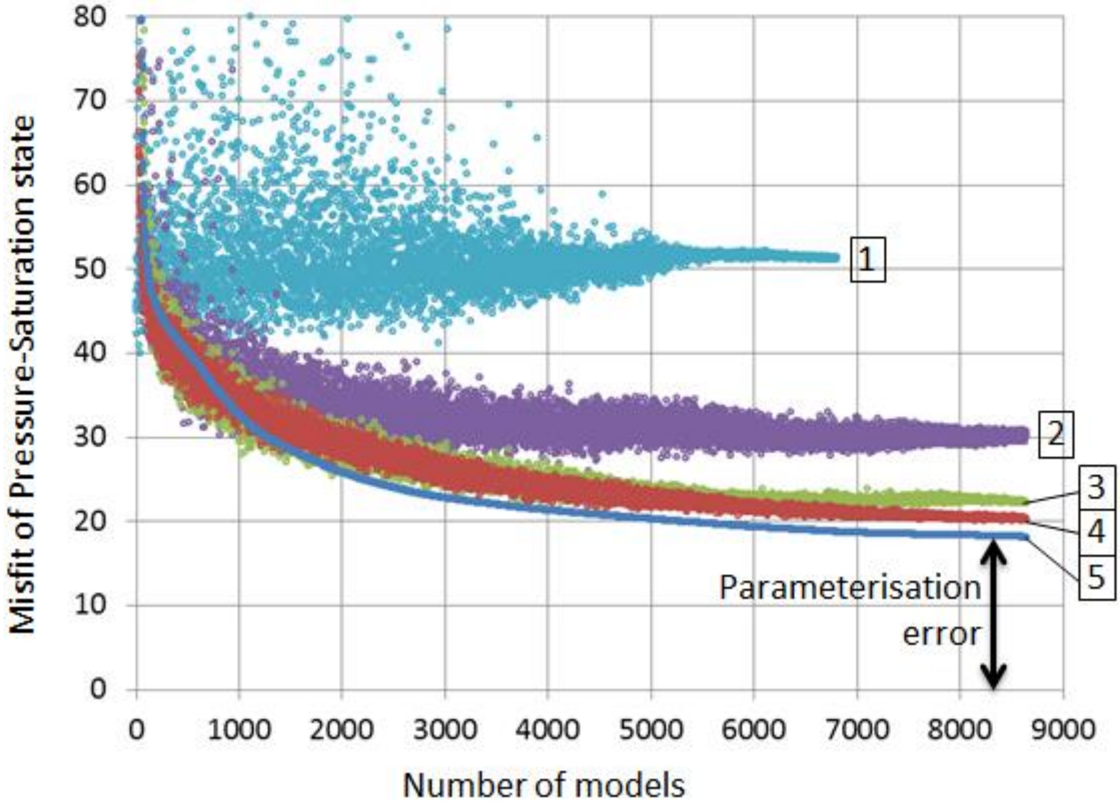

**Figure 7.23. Misfits of states of pressure and saturation represented by the states of 4D impedance for the ensembles of models generated during the history matching in 5 scenarios (indicated by numbers in boxes): 1) production match, 2) seismic map match, 3) seismic traces match, 4) inverted impedance match and 5) reference impedance match. The order of points corresponds to the descending order of the objective function values. Less points in the scenario 1 is caused by less runs required to match the production data in that scenario.**

The order of points in Figure 7.23 is determined by the order of models in the 5 ensembles (for 5 scenarios) after ranking (sorting by data misfits, that is by the misfits used in history matching such as production data misfit, seismic map misfit and so on depending on scenario). As a result, the scatter plots in the figure illustrate how much closer the pressure-saturation state of the model gets to the state of the reference model as a model’s data misfit reduces. Another way of studying the correlation between the data misfits and the state misfits would be to cross-plot the two quantities for different scenarios. However, the plot in Figure 7.23 is a better solution because there are no data-specific misfits with all associated subjectivity in choosing the weights in it whatsoever. That is in all the scenarios we are dealing with the same quantity, misfit of state, so different scenarios are perfectly comparable.

We can see in Figure 7.23 that the reduction of data misfit (that is going right along the x-axis) when matching production data in scenario 1 does not necessarily lead to the reduction of the state misfit. As discussed before, the match of production data is possible at a wider range of spatial distributions of pressure and saturation because the production data does not place a significant spatial constraint (this also explains bad seismic predictions by the models matched to production data only, see Figure 7.14). As a result, the plot in the case 1 is scattered (production misfit and state misfits are less correlated) and converges to the highest value of the state misfit among all the scenarios. Next follows the plot for the case 2 where the models are matched to the seismic maps. We can see a significant difference with the case 1 in terms of the reduced scatter and lower final state misfit value. This is in line with the stronger spatial tie of the seismic constraint as discussed before (section 7.3.1). We can say that matching the seismic map does actually bring the pressure-saturation state of the model closer to the one of the reference model.

However, the best convergence to the pressure-saturation state of the reference model is observed in scenarios 3-5 where the volumetric attributes are matched. This is explained by the fact that the volumetric attributes are the data effectively representing the pressure-saturation state itself. In scenario 5 they are even equal – the history matching is performed matching 4D impedance of the reference model which represents the state at the same time (in scenario 5, the state misfit equals the data misfit and the latter is sorted, therefore there is no scatter in the plot). In other words, in cases 3-5, we are matching ‘almost’ the pressure-saturation state itself, therefore the data misfits and the state misfits are correlated so well (low scatter, low final level). So if the data is perfect in the case 5, why do we not get a zero state misfit? The reason for this in our case is parameterisation. As discussed before, sparse pilot points cannot possibly reproduce the transmissibility field created in the reference model using the regions, therefore the pressure-saturation state of the reference model is unreachable (however, the pilot points did a good job in approximating it which makes our problem set up practical). In Figure 7.23, the level of the state misfit in the case 5 is called the parameterisation error. However, the same error causes the differences between the states in all the cases. Indeed, in an error-free model (synthetic situation), matching these data individually would lead to much more similar models as shown in Chapter 6 (section 6.3.2.1) where a close match of production data was achieved by matching the seismic maps given the parameters were the same as in the reference model. Therefore the spread of levels of the state misfits is a function of the parameterisation error.

One of the consequences of the difference between the state misfits in cases 2 and 3-5 is that matching the seismic map as close as possible leads to a pressure-saturation state different from the reference state. As long as the differences in the states are caused by the parameterisation as discussed above, we can say that the pressure-saturation state at which the model arrives when matched to the seismic map is optimal for minimizing the seismic map misfit rather than the state misfit. Let us now look at this point from the opposite side. What would the seismic maps look like for a pressure-saturation state that is actually close to the reference one, such as the state in the case 3? To answer this question, 4D seismic maps were generated for the best models history matched to seismic traces. These are shown in Figure 7.24 (all 10 history matched models (for both 28- and 77-point schemes) are shown in this figure to stress the consistency in the seismic maps errors). The misfit figures shown on top of the maps are much higher than those for the case of matching the seismic map itself (see Figure 7.15).

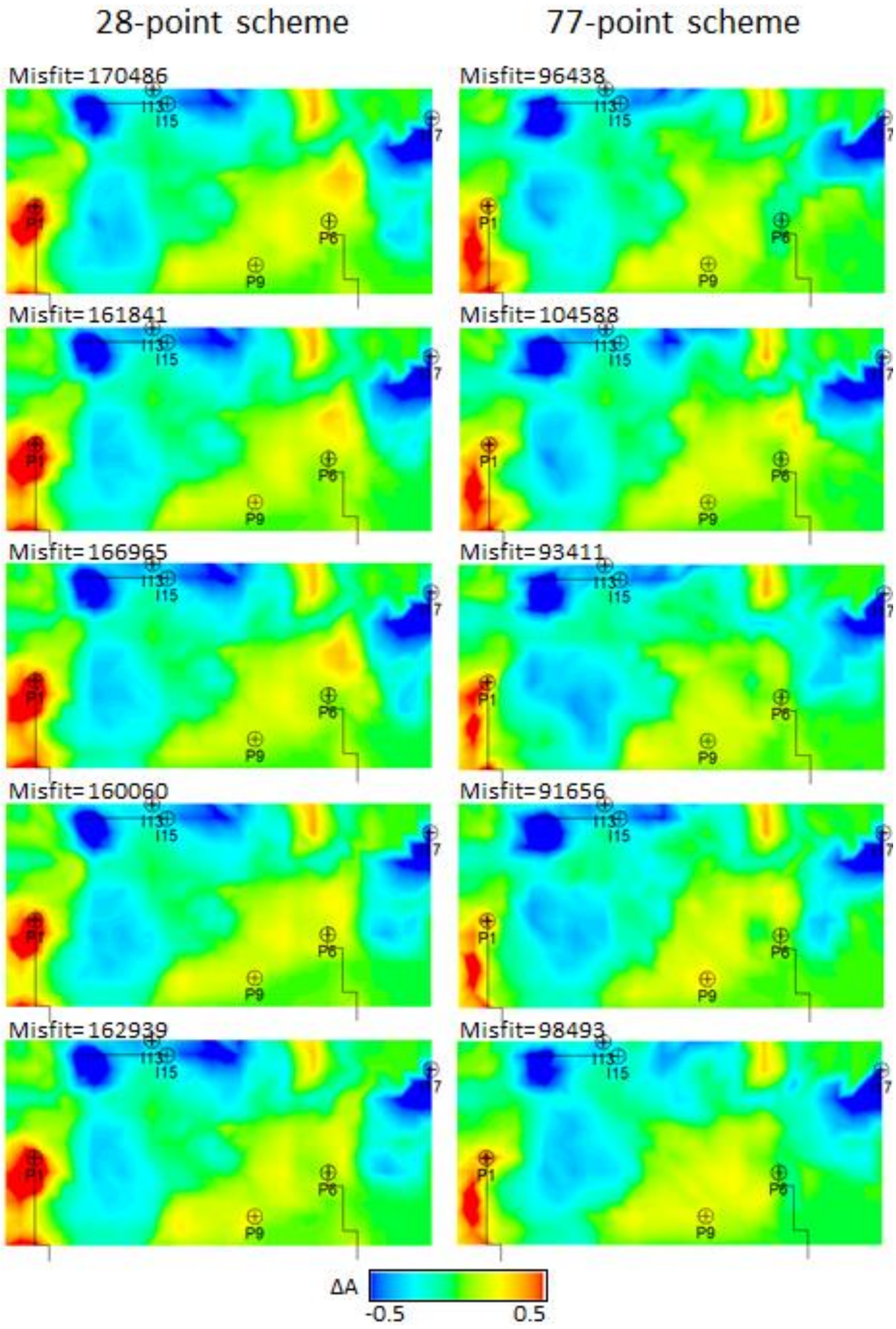

**Figure 7.24. 4D seismic attribute maps predicted by models which were history matched to seismic traces using 28- and 77-point schemes.**

Another conclusion can be drawn from the analysis of misfits of states in Figure 7.24 in the context of the question of the domain of seismic data comparison (see section 3.4.3 in Literature review chapter). By comparing the misfits of states for the scenarios 3-5, we can say that these are very close which suggests that similar models are obtained by matching the seismic traces, the inverted impedance, and the reference impedance. This means that neither the scattered noise in the inverted impedance (see Figure 7.20, b) nor the band-limited nature (smoothing effect) of the seismic traces prevented the history matching from finding the right realisation of the pressure and saturation distribution – almost the same realisation that is found by matching the error-free 4D impedance property (proxy for pressure-saturation state) itself. This suggests that in our case the controlling factor for finding the right pressure-saturation state in history matching has been the spatial distribution of 4D changes in the entire reservoir volume rather than local variation of 4D seismic signal. This in particular means that the history matching easily withstands scattered noise in the data as long as the low frequency component of the signal is right. On the other hand, the differences of states are significant in cases 1 and 2. We attributed these to the parameterisation error which means that it is a stronger factor affecting the results of history matching than for example the scattered data error in the inverted impedance although the latter appears significant visually (see Figure 7.20, b). This observation is in line with findings of *Moore and Doherty, 2006* and *Hunt et al, 2007* about the role of so called structural noise occurring due to the simplifications made to the model via its parameterisation (see Literature review chapter, section Choosing a parameterisation consistent with data resolution).

Although the volumetric attributes were shown to constrain the simulation model efficiently, these will not be considered in the future sections in combination with the production data. The reason is that there are limitations of the volumetric attributes that have not been studies here. In particular, these can be sensitive to the spatial alignment of the predicted and observed data as discussed in Literature review (section 3.4.4). Studying these uncertainties is out of scope of this work.

To sum up, in this section we demonstrated that well rates and seismic maps condition the simulation models at different levels. Production data is demanding for accurate phase rates but allows for different ways of achieving them in terms of spatial distribution of properties. As a result we may end up with distributions far from those found in the reference model. For the seismic map, it was shown that the close match of this attribute does not bring us closer to the reference pressure and saturation state. This is a prerequisite for potential overfitting effects when matching the details of the seismic map too closely.

## 7.4 Integrating production and seismic data in history matching

Combining seismic and production data into a single dataset for history matching aims to improve the predictive capability and hence utility and reliability of the resulting models compared to the case with only the production data. With this goal in mind we are investigating better ways of incorporating seismic data into the models. Appropriately weighting the seismic term in the objective function is one of the most important considerations on this route, and this to date has not been systematically studied in publications in the context of seismic history matching, in particular there is no universal answer on how to balance the seismic and production terms in the objective function (as discussed in Literature review chapter, section 3.4.1). In general, error estimates serve as measures of importance of data but it is difficult to describe the errors accurately enough to assure the right balance between the production and seismic terms. For this reason, the seismic and production terms usually are balanced empirically by combining the two terms with certain weights which leads to a compromise in match quality of these two terms (match quality of both terms usually worsens when combined compared to matching them separately as discussed in the following sections). The relative weight figures can be varied to shift the accent to either seismic or production term. If for example, bigger weight is given to the production data then some of the details of the seismic map will not be matched. The weighting effect which leads to different quality of match of either seismic or production data as described above will be the basis for the analysis in the following chapters. Different weight values will allow us to match different levels of details in the seismic map. This variation is needed to understand at which level the details of the seismic data are important for constraining the flow characteristics of the simulation model. The resulting history matched models will be assessed in terms of the production forecasts. This analysis will also be related to the findings of the previous section where a limited efficiency of the constraint by the seismic maps was demonstrated.

**Important note regarding the misfits reported in the rest of the chapter.** In the rest of this chapter, we will consider cases where seismic and production misfit terms are combined in the objective function. These are combined with certain weights so that the history matching results in a better match of either of the terms. However, absolutely every misfit value that will appear in the following text (including those appearing in figures, captions and everywhere else and no matter in what context) is calculated separately, without those extra balancing weights. That is it uses the same error-based weights as in the cases of matching production or seismic data separately discussed in the previous sections. For this reason, all the misfit values reported in this chapter (and also in Chapter 6 since section 6.3) are comparable.

### *7.4.1 Results of history matching with combined production and seismic data*

In this section, we will consider cases of (relatively) weaker and stronger seismic match in a combined dataset of well rates and seismic maps. The seismic and production terms are combined as follows. In the scenarios of matching the production data and seismic maps separately (section 7.3.1) we obtained models which characterise the best possible fits to these data types given our problem set up (algorithm and parameterisation). Based on the error figures of 100 bbl/day for the well rates and 40% of maximum amplitude of the seismic attribute, the misfits for production and seismic data were obtained at the following levels: around 1000 for the production data and around 60000 (for 77-point scheme) for the seismic data. If the two terms are combined, then these levels cannot be achieved at the same time because generally different parameter values minimize the production and seismic misfits as discussed in the previous section. If the two terms are combined, then we have to choose which term should be matched better. It was observed that if the production misfit is increased to a value not exceeding 3000, then there is no visible distortion to the production match. On the other hand, if the seismic match is a priority, then weighting the terms such that the production match is at a level around 20000 allows achieving the level of seismic match similar to one in scenario 2 of the previous section (matching seismic maps only). At this level of seismic match, production match worsens (especially GOR), but remains reasonable in terms the water-cuts. As a result, we have two cases where match of either production or seismic data is prioritised. The first will be called a weak seismic match. In this case, the production data is matched stronger and the production misfit does not exceed the value of 3000 while the seismic match is unbounded. The second case is called a strong seismic match. In this case the level of seismic match is the same as in the case of matching seismic data only (misfit value around 60000 for 77-point scheme) while the production misfit is at a level of around 20000 (misfit in the final model, not affected by extra weighting). One extra case will be considered which is combining the seismic traces and the production data. In this case, the weights are adjusted as follows. The two terms, seismic traces misfit and production misfit are combined with such weights that the production misfit is at the same level as in the strong seismic match case described above, that is at the level of around 3000.

Figure 7.25 illustrates the relationship between the production and seismic misfits in the final models resulting from the two scenarios of matching production data and seismic maps described above (as in all previous cases, multiple runs were made, and 5 best models were selected for 28- and 77- point schemes, PSO parameters are following: 80 particles and 90 iterations). Notably higher seismic misfits in the strong seismic case with 28-point scheme compared to those with 77-point scheme are explained by the lower flexibility of the 28-point scheme which prevents it from matching the seismic map better. This is in line with the results presented in Figure 7.15 where only seismic maps were matched: 28-point scheme resulted in higher misfits there.

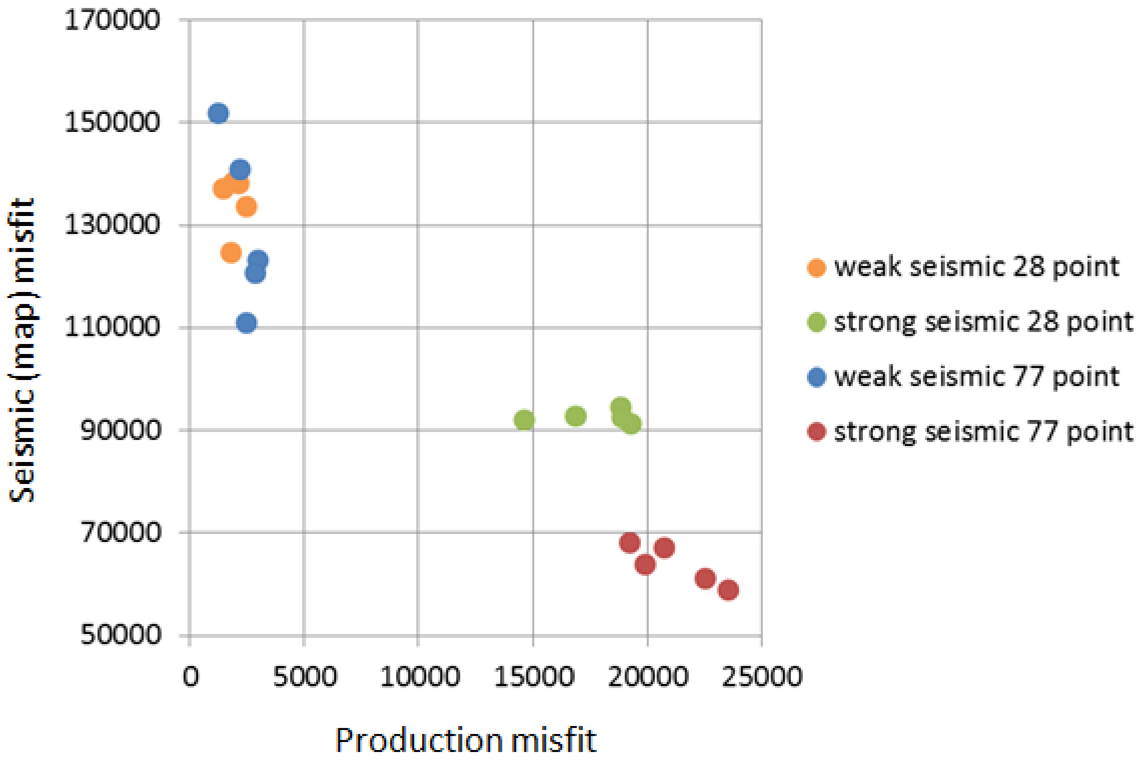

**Figure 7.25. Production and seismic misfits for ‘weak seismic’ and ‘strong seismic’ history matching scenarios (see text for details) using 28- and 77-point schemes. Misfit figures are unaffected by any weighting.**

Figure 7.25 is a Pareto-type plot showing models that match production and seismic data at the same time to the maximum extent for any given balance between the terms. Based on the data fit only, we could say that all these models are equally good. However, we have seen in the previous section that matching different data types leads to different pressure-saturation states. This allows us to assume that the models will perform differently in the forecasting period. In the following sections, these models will be compared in terms of their forecasts.

### *Well rates + seismic maps: weak seismic match*

In this case the seismic and production terms are combined in such a way that the production misfit is at the level around 3000 while the seismic misfit is unbounded. The results of history matching to a combined dataset are shown in Figure 7.26 and Figure 7.27. The black vertical line in the plots of Figure 7.26 indicates the end of the history matching period (August 2002). Figure 7.26 shows predictions of water and oil rates for wells P1 and P6. These two wells were chosen for the analysis due to their importance in terms of the volume of liquid they produce. Well P6 does not have useful information for constraining phase flows (water specifically) so its forecast relies on the seismic constraint only. This in fact can be seen in the results in Figure 7.26 and suggests that the seismic data cannot condition the rates to the same accuracy as the actual historic rates. Also, we can see that the forecasts of P6 are different between the two parameterisation schemes. In the 28-point case, the deviations of water rates in terms of the values and the shape of the curve are stronger than in 77-point case. This is in line with the argument made before about the roughness of the parameterisation function with fewer parameters, while 77-point point function is more responsive to shaping by the data control.

Figure 7.27 shows the seismic maps predicted from the history matched models in this case. It is notable that these maps fail to match the reference map compared to the ones obtained by matching seismic data only (see Figure 7.15). The misfit figures shown on top of the maps are all higher (above 100k) than those in Figure 7.15 (60-80k depending on the scheme). The observed mismatch is due to the elements of seismic signal mostly of smaller scale. However, the high level 4D pattern is captured because the maps represent a significant improvement compared to the ones from the production-only case (see Figure 7.14).

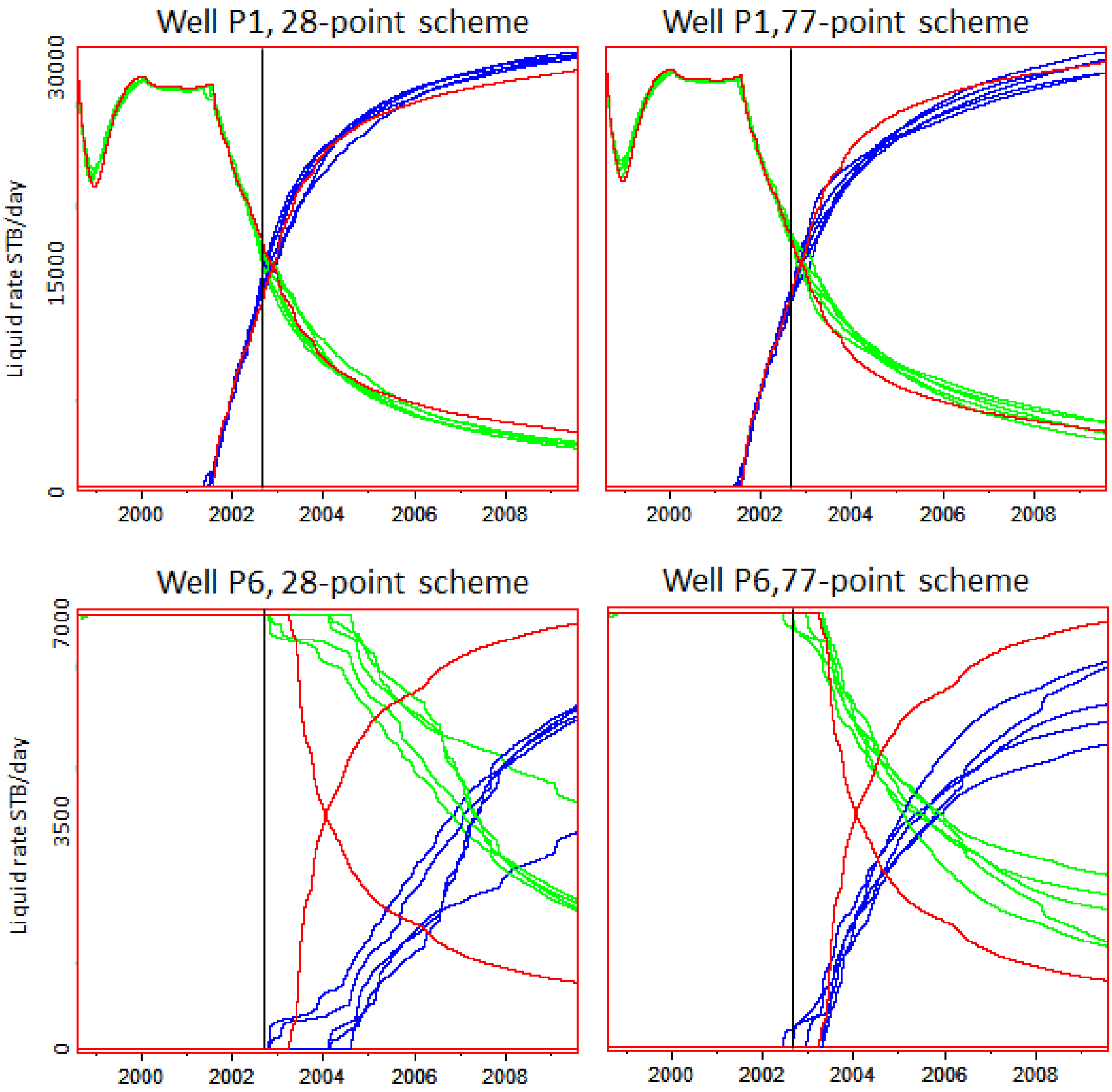

**Figure 7.26. Results of history matching using a combined dataset of well rates and seismic map with low weight of the seismic term. Shown are oil and water rates predicted from the history matched models (green and blue) and from the reference model (red). Vertical black line indicates the end of history matching period (01/08/2002). Wells P1 and P6 and 28- and 77-point schemes are shown.**

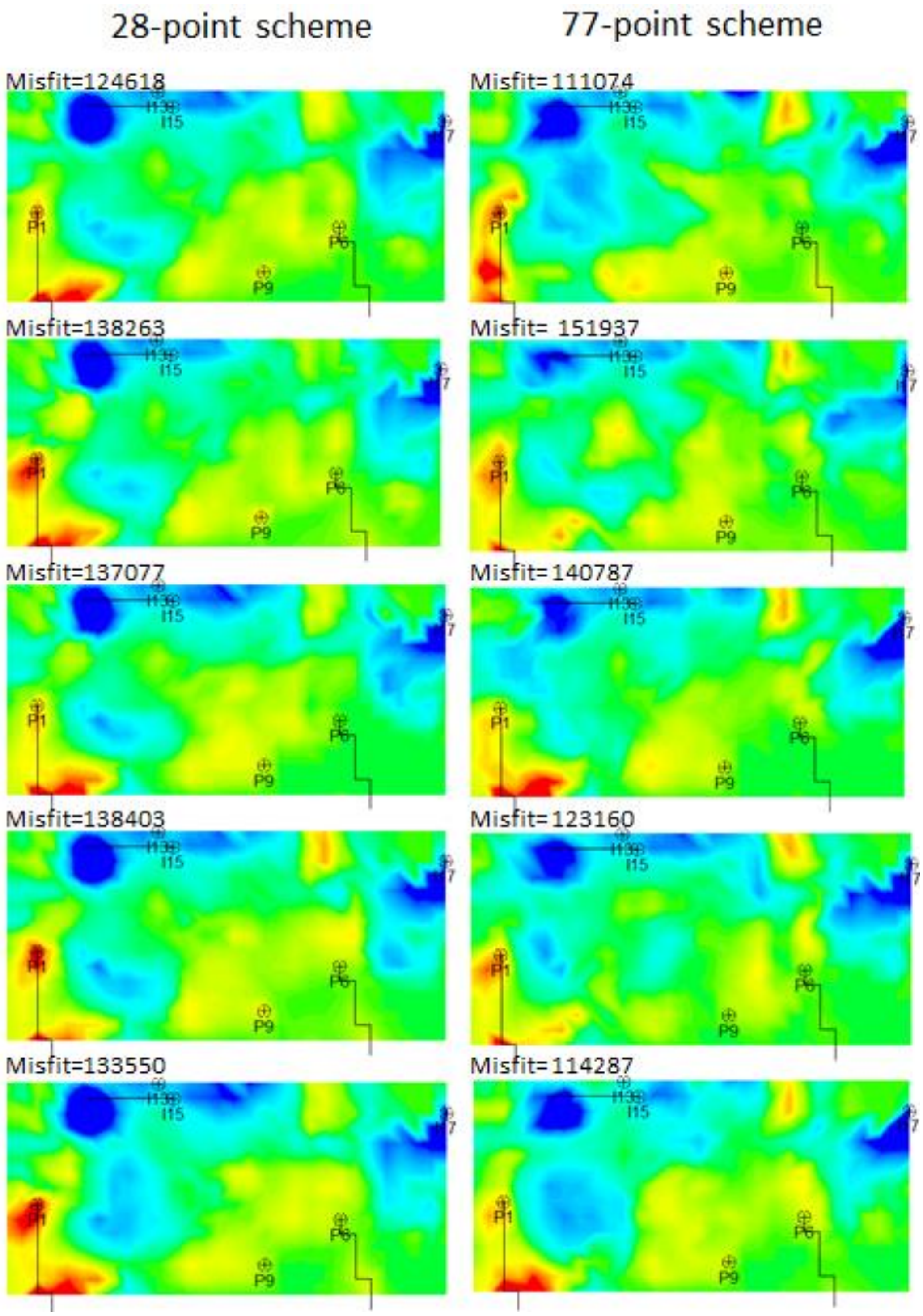

**Figure 7.27. 4D seismic attribute maps predicted from the same history matched models as in Figure 7.26. Misfit figures shown on top of each map represent deviations of those maps from the observed map – these are not the misfits driving the history matching.**

*Well rates + seismic maps: strong seismic match*

In this case the seismic map is matched as a priority in a combined dataset. The results of history matching are shown in Figure 7.28 and Figure 7.29. The black vertical line in plots of Figure 7.28 indicates the end of the history matching period (August 2002). The results show that the quality of seismic match is close to that achieved by matching seismic maps only (see Figure 7.15). The match of production data was maintained so that the water rate is matched while the match of GOR is somewhat relaxed which can be noted on the oil rate of P1 at the early stage of production (Figure 7.28). As discussed before, in this case the production misfit is around 20000. Recalling the analysis of different constraints by seismic and production data, we can conclude that this relatively uncompromised match of production data together with the maximum match of seismic maps (as good as when matching seismic only) has been possible because well rates can be matched with many possible spatial distributions of permeability, including those matching seismic maps (although they may be not optimal for the production-only match). Another observation is that at this level of seismic match we are able to see the difference between the 28- and 77-point schemes: 77-point final seismic maps have consistently lower misfit than the 28-point ones as 77-point function is easier to adjust to the data control. The difference did not show in the previous case (Figure 7.27) because the algorithm was not pursuing the level of details resolvable by the 77-point scheme. On the forecasts side, we can see that they became worse in the well P1 (Figure 7.28). The plots show that the water rate started to reflect the small, hard to reproduce details of the seismic map while following closely the observed data in the history period.

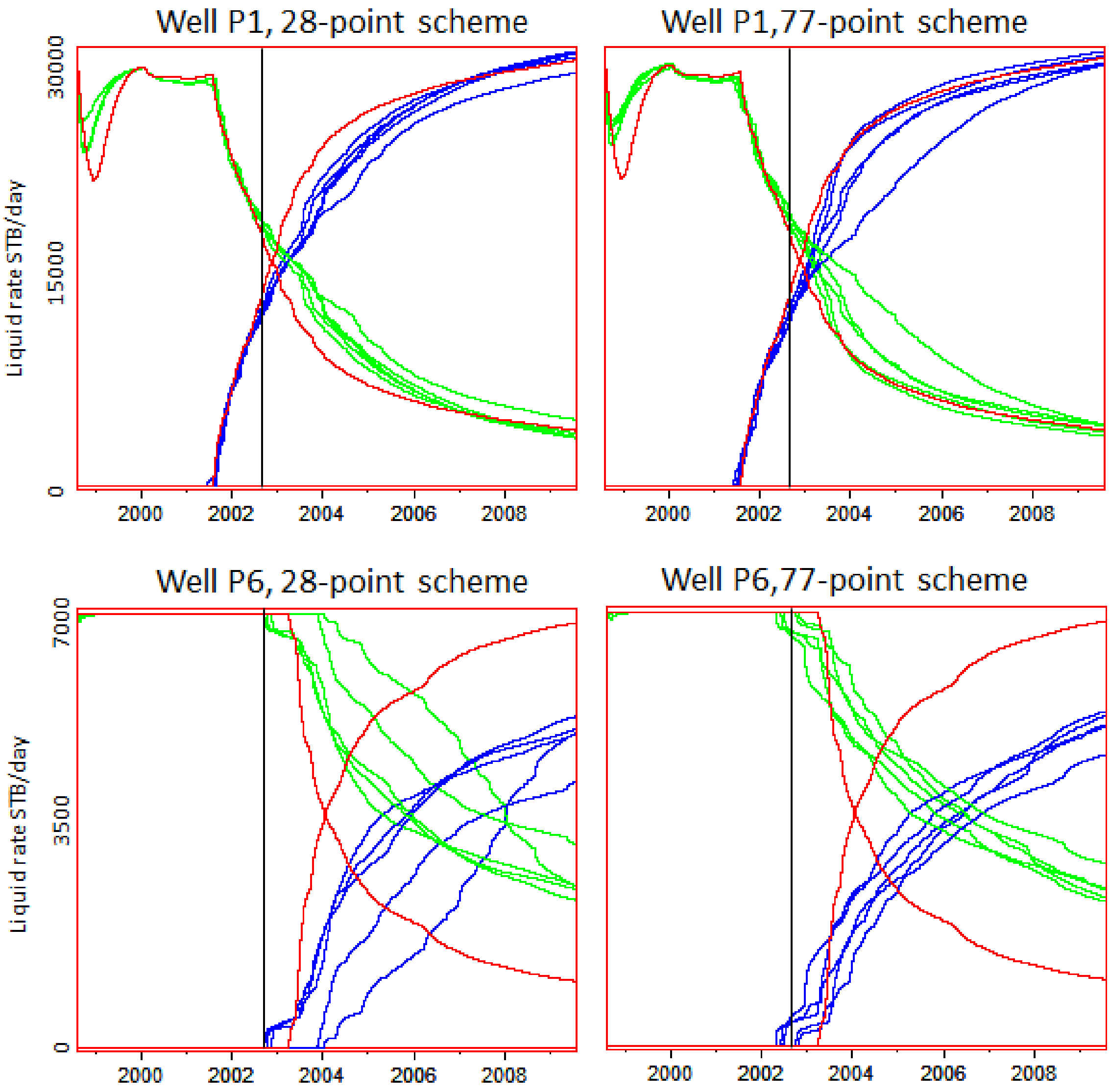

**Figure 7.28. Same as Figure 7.26, but for matching a combined dataset of well rates and seismic map with high weight of the seismic term.**

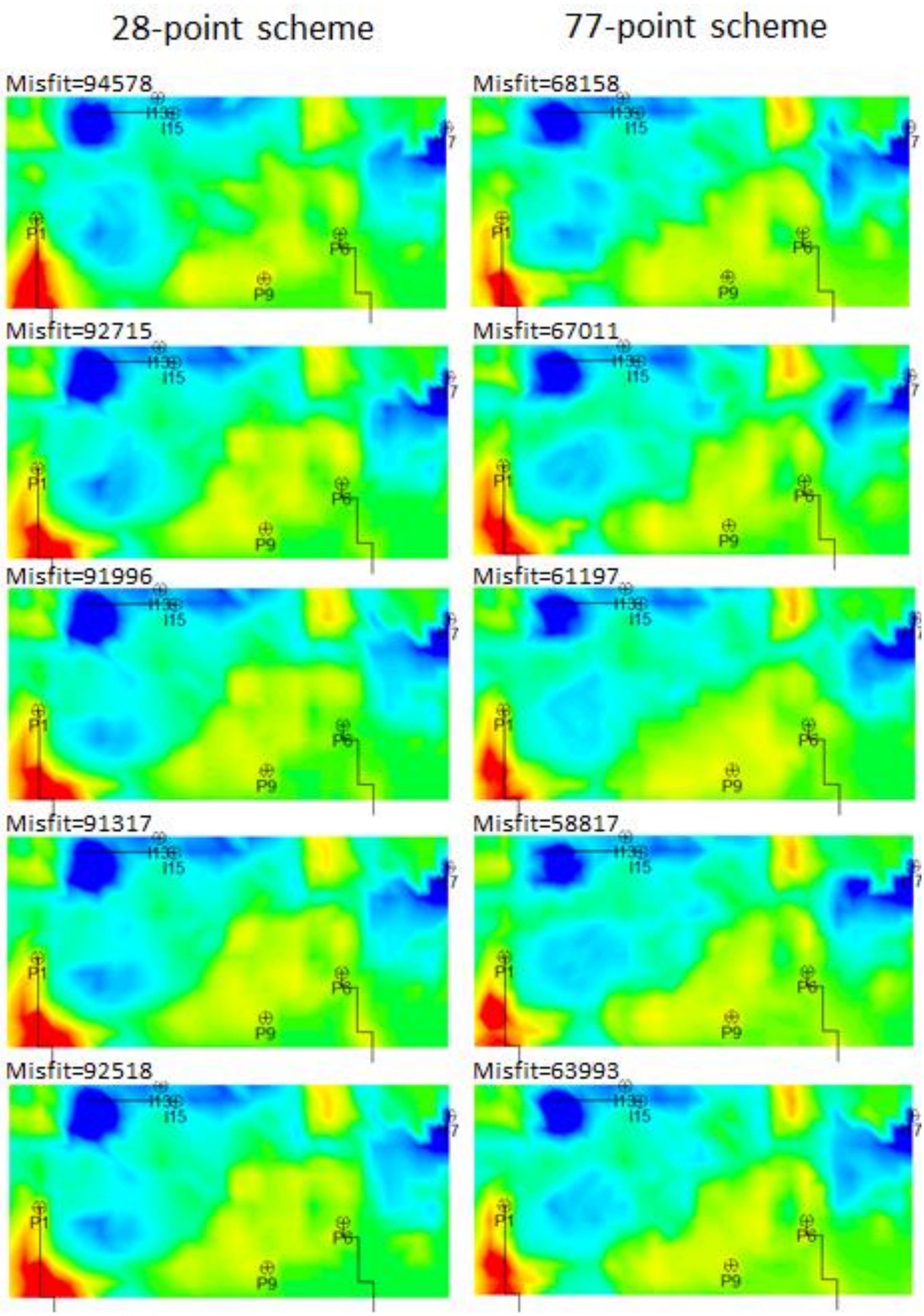

**Figure 7.29. Same as Figure 7.27 but with high weight of the seismic term.**

### *Well rates + seismic traces*

The seismic data in this case consists of cubes of seismic traces rather than seismic maps. The seismic cube actually is a cube of differenced traces because it is calculated by differencing the base- (August 1998) and monitor-survey (August 2002) seismic cubes. Because it is a volumetric attribute, we expect greater information content in the data and more effective constraint for simulation models. Moreover, as discussed before (section 7.3.2), this volumetric attribute effectively represents the pressure-saturation state of the model for which reason matching this attribute improves the similarity of model with the reference one.

Figure 7.30 shows results of history matching using a combined dataset of well rates and seismic traces. The black vertical line in the figure indicates the end of the history matching period (August 2002). The well rates demonstrate good agreement with the reference model in the forecasting period for well P1. Also, the agreement is good for well P6 – a result we could not achieve by matching seismic maps (together with well rates) so far. These circumstances indicate an effective constraint by a combination of seismic data and well rates which resulted in good forecasts. However, the results will not be used to make conclusions about the volumetric attributes in the context of our study of useful scale of seismic signal, but will be applied differently. Specifically, since the resulting history matched models represent such good solutions (to the history matching problem) with that particular parameterisation, it is interesting to see what seismic response (in terms of seismic maps) is of a ‘good’ solution. Figure 7.31 shows seismic maps predicted by models which were history matched to a combined dataset of well rates and seismic traces. One can note that these match observed data only to a degree where it slightly matches the pattern of the observed map. From that we can conclude that the details in which these maps are different from the observed map measure the effect of our parameterisation error.

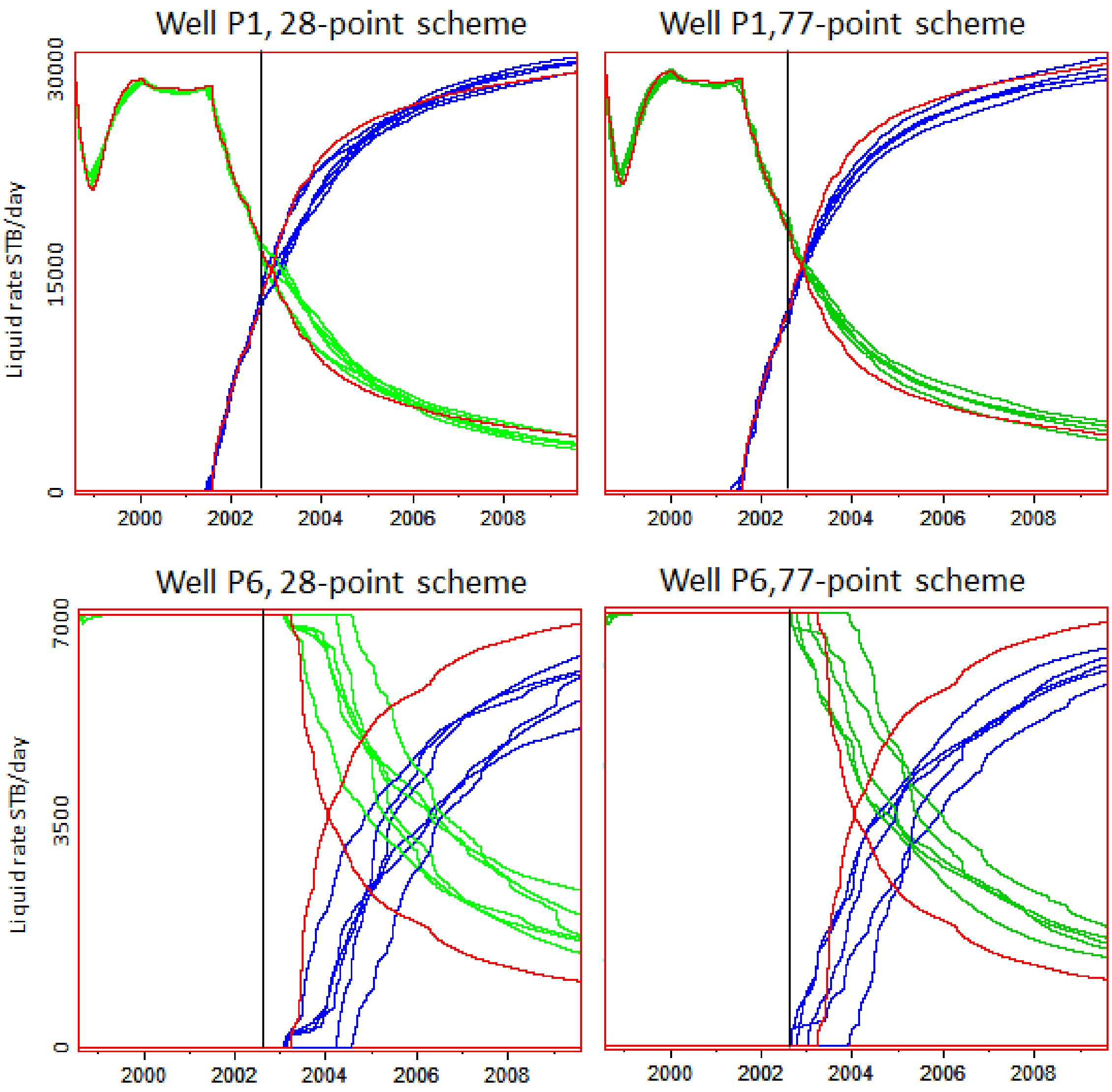

Figure 7.30. Same as Figure 7.26, but for matching a combined dataset of well rates and seismic traces.

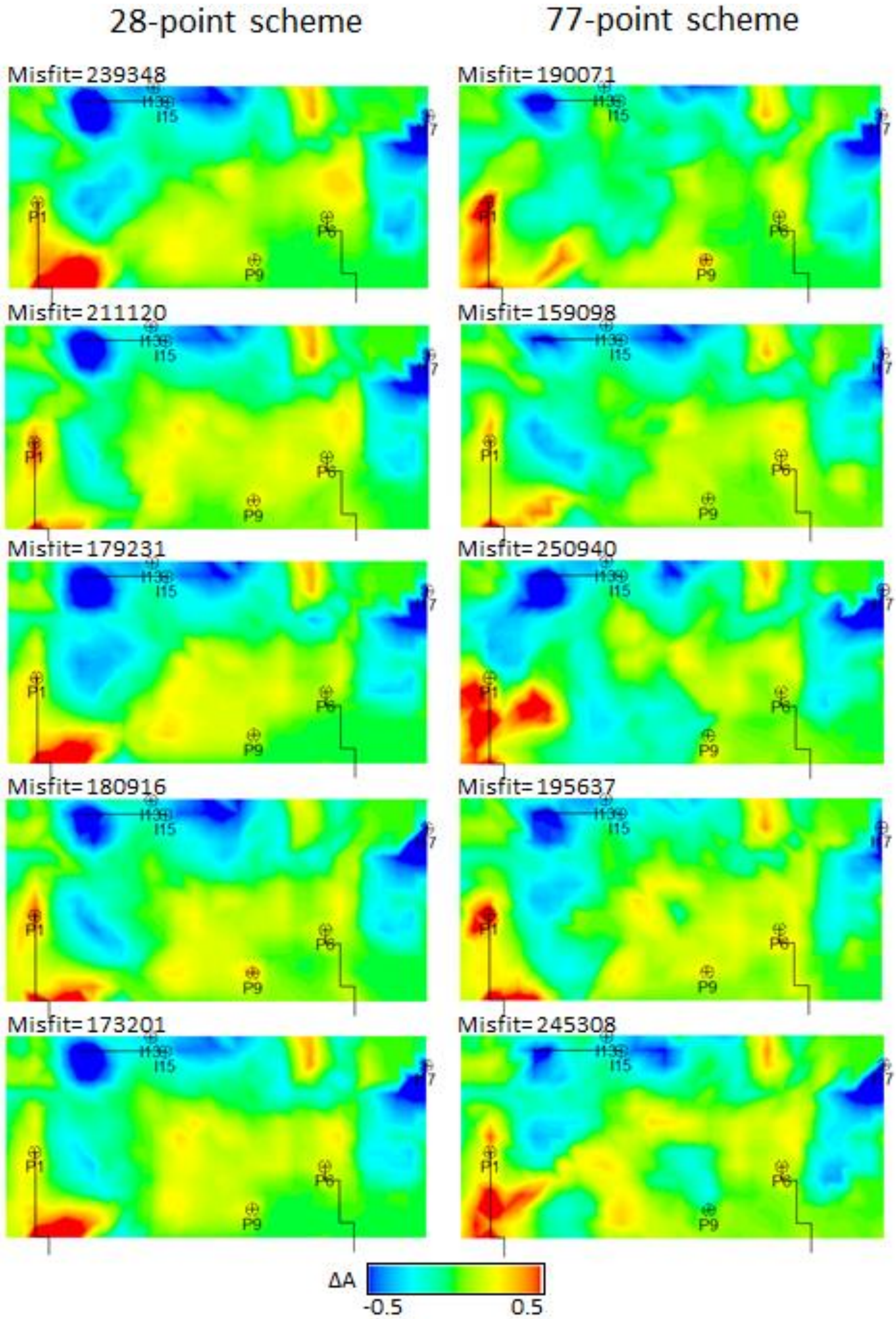

**Figure 7.31. Same as Figure 7.27, but for matching a combined dataset of well rates and seismic traces.**

### *7.4.2 Honouring seismic data: what scale?*

In the previous section it was shown that matching both seismic and production data is limited by the approximate character of the simulation model, and in particular, its parameterisation. Theoretically, we can keep increasing the complexity of the model (resolution of the parameterisation in this case) to try to improve the match. Experiments so far have shown that it will be a more challenging task to improve the match of the seismic map out of the two data types. For example the results in Figure 7.15 where the seismic map alone was matched show that we were able to match the major features and discontinuities, but there is a certain and quite prominent level of detail that is left unmatched. That is for that particular model with its parameters, we reached the limit in matching the seismic maps. Whereas the results of matching production data alone (Figure 7.7) does not seem to require any improvement. As it has been shown, this is because the constraint of the seismic map is much more spatial in nature than that of production data, so the mismatch is difficult to address with the pilot points at fixed locations. We may ask whether the better match of the seismic map needed at all, however? The key to answering this question is understanding the effective scale of the seismic signal carrying useful information for simulation model, with all the smaller details being specific to the source of that data (history matched model on one hand and the reference model or the real Earth on the other hand). If due to the incompatibility of such sources of data a special effort is required to fit the seismic map better, then we have a reason to assume that this special effort may even harm the predictive capability of the estimated model due to overfitting.

Figure 7.32 and Figure 7.33 use the results of previous sections to illustrate the point. The black vertical lines in these figures indicate the end of the history matching period (August 2002). Starting with models matched to production data only in sections (a) of both figures, we are increasing the amount of seismic information being incorporated into the simulation model as we go down to (b) and (c). Sections (a) and (c) show (relative) extremes in matching individual data types. Looking at the forecasts of water rates by well P1 we can conclude that too much of either data type reduces their quality because when data are overfitted the resulting parameter estimates become too specific to the calibration dataset (that is the model estimates loose generality). Case (b) on the other hand demonstrates the best forecasts as it is constrained by well rates and only the high level seismic signal. The role of seismic data at the scale utilised in case (b) clearly rules out realisations of the permeability field that are too data-specific, mainly those obtained by matching production data only (see Figure 7.13).

Our priority was to match production and seismic data in order to obtain plausible forecasts. In particular, case (b) can be viewed as matched to production data, with only a ‘touch’ of seismic information expressed in a high level match of the seismic map pattern. The result gives an answer to the question about the role of seismic details in describing fluid flow in reservoir. The seismic map contributes constructively by compensating for too liberal spatial constraint of well rates (well rates in fact do not care much about spatial distributions), but no more. Specifically, we should not attempt to reproduce the seismic map as it looks by means of redirecting flows in the model because both the model and the seismic map are imperfect. Imperfection of the model in our case is caused by the chosen parameterisation which makes the model predictions generally not compatible with those of the reference model as discussed before. The imperfection of the 4D seismic map is caused by the complex relationship between the values of this seismic attribute and the underlying changes in reservoir impedance as discussed in Chapter 5. As a result, 4D seismic map attribute has limited ability to track the pressure and saturation state of the reservoir as shown in the previous section (7.3.2). And vice versa, whenever the pressure-saturation state was constrained by the volumetric attributes, the corresponding predictions of the 4D seismic map attribute did not match the reference map (see Figure 7.24 and Figure 7.31) which suggests that the ‘best by seismic map’ model and the ‘best constrained by the pressure-saturation state’ model in general are different.

Regarding the resolution of parameterisation, we can say that with 28- and 77-point schemes, the production data were matched equally well. As long as the seismic data is more demanding for the spatial resolution of the model, 77-point scheme demonstrated a clear advantage in matching the seismic maps with lower misfits (see Figure 7.15). At the same time, in the scenarios where the seismic data are matched together with production data (‘weak seismic’ and seismic traces+production – good forecast scenarios), the resulting seismic maps show similar level of match for both schemes (see Figure 7.27 and Figure 7.31). This suggests that the extra resolution of the 77-point scheme is not utilised in those cases where the pressure-saturation states satisfy the common constraint of the production data and the high level pattern of the seismic data.

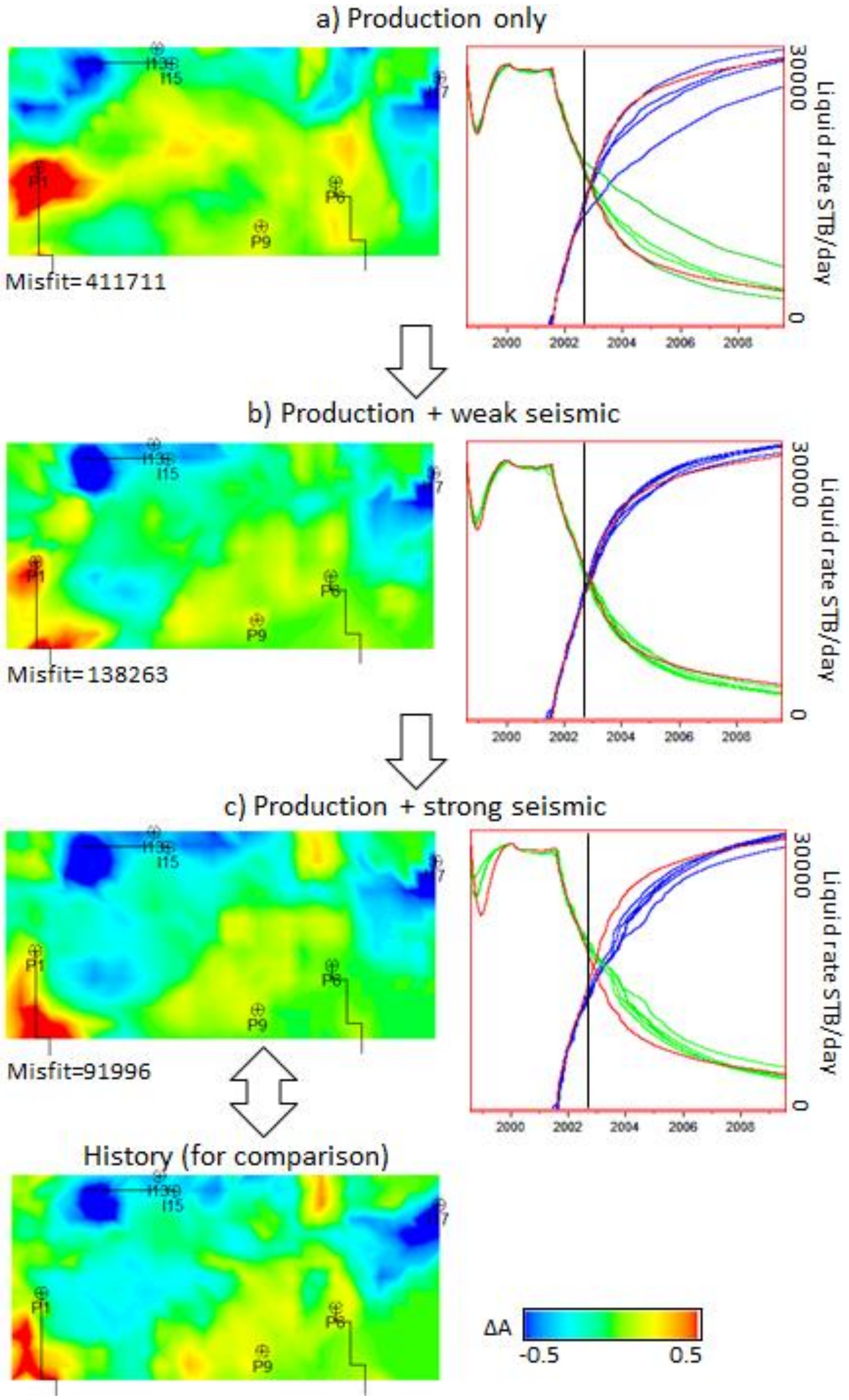

**Figure 7.32. Predicted and observed seismic maps and well rates for the following history matching scenarios: a) matching production data only, b) matching combined dataset of well rates and seismic map with low weight of seismic data, c) as (b) but with high weight of seismic data. Liquid rate plots show predictions of oil and water rates of well P1 for a series of history matched models in each scenario, annotations are the same as in Figure 7.26. History matching uses 28-point scheme.**

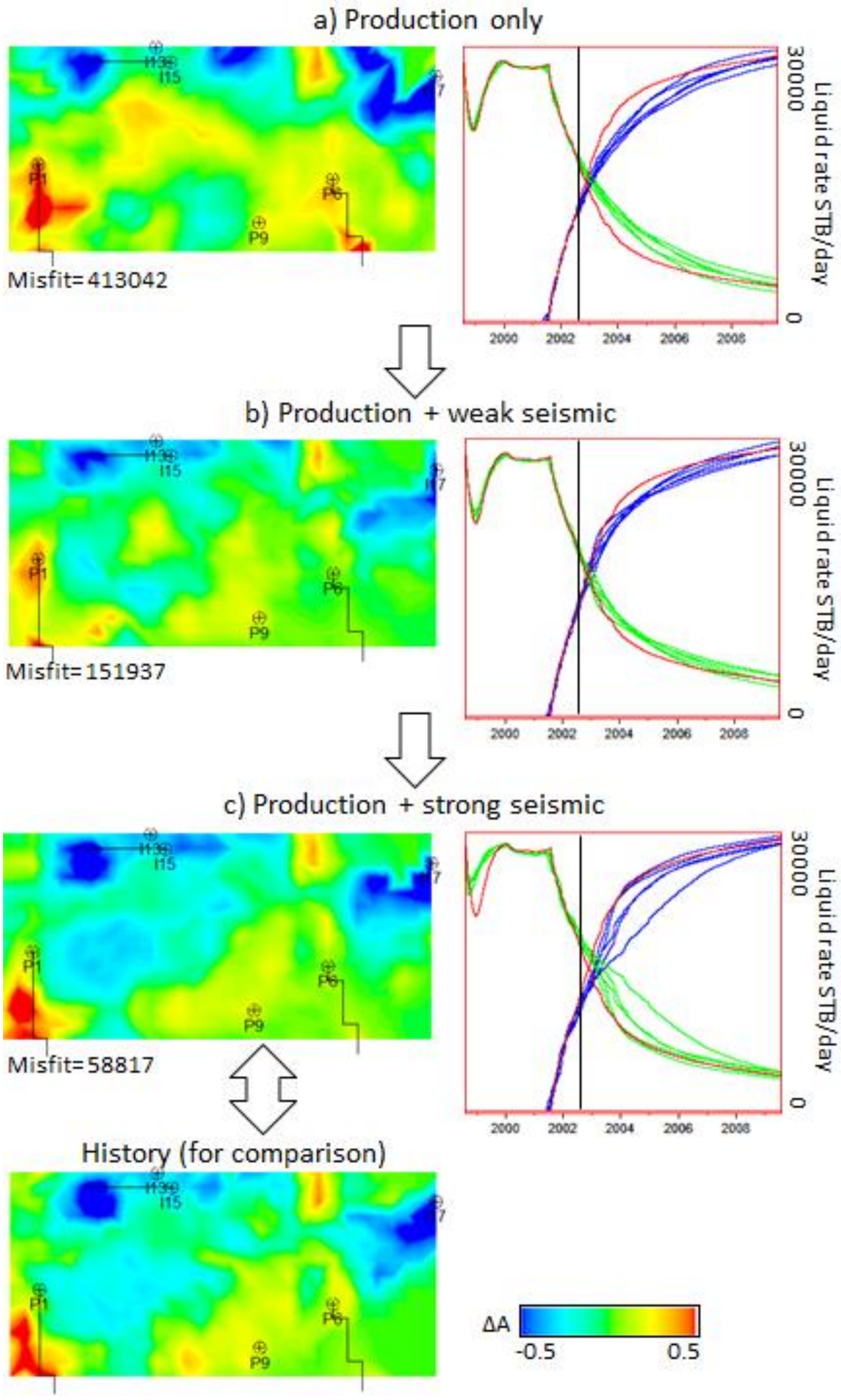

**Figure 7.33. Same as Figure 7.32 but using 77-point scheme.**

## 7.5 Conclusions

The focus of this chapter is integration of 4D seismic data into the history matching process so that it improves the forecasts of the simulation model. The integration of 4D seismic is complicated by difficulties in matching seismic and production data at the same time: we have to compromise the overall quality of match in order to honour both pieces of data. This is related to the limitations of the model itself, as well as the noise in data. In the example considered in this work, the major limiting factor was caused by the parameterisation which was specifically chosen to prevent the history matched models to match the response of the reference model precisely. In these conditions, we were able to reveal the limited ability of the 4D seismic map attribute to track the pressure-saturation state of the reservoir in the context of history matching. The smaller details in the seismic maps were found to be too specific to the process that generated that map. As a result, fitting the seismic map in details does not provide a constructive constraint for the simulation model.

These results have important implications both for the process of history matching and for sourcing 4D seismic data intended solely for seismic history matching. An engineer needs to be aware that the amount of details in the seismic data is dictated by the limiting factor of the models themselves. The characteristic scale of seismic anomalies matched in the experiment of this work suggests that the controlling effect of the seismic data was achieved rather at the field-level pattern. This raises questions about usefulness of models wholly conditioned by a single smaller anomaly of 4D seismic data: no matter how good the match is, it can well fall within a definition of modelling artefacts. On the other hand, a close replica of observed seismic map presented as a result of history matching may indicate excessive match and higher chance of overfitted models.

It was shown that the resolution of the 77-point scheme is not utilised fully when the model is matched to seismic and production data simultaneously because a common solution for these two constraints does not include the smaller details of the seismic map.

It was also shown that uncorrelated noise present in the inverted impedance does not affect the history matching because the realisations of the pressure and saturation state produced by the simulation model are constrained by low frequency 4D signal, that is by high level (larger scale) pattern, rather than by local variations of the signal. Similar history matching results were achieved by matching the seismic traces and also by matching the precise impedance. This suggests that the characteristic scale of the seismic signal that constrains the simulation realisations was larger than the resolution of the seismic traces in our case.

# Chapter 8. Conclusions and recommendations

This work is devoted to the integration of 4D seismic data within the history matching studies. In particular, the focus is on the relationship between the scale of seismic details, model resolution and complexity and flexibility of model parameterisation.

The next section summarizes the main conclusions of this work. These are based on the following studies as described in this thesis. The seismic response study of Chapter 5 is carried out on a number of models with varying geometry and distributions of properties, static and dynamic. Also, scenarios of hydrocarbon displacement were considered using the template models of the Schiehallion reservoir. The study resulted in the conclusions about the relationship between the seismic attributes and the underlying changes in the reservoir which ultimately define the detectability of the production-related effects in 4D seismic data. Chapter 6 is devoted to the parameterisation of the history matched models. The study is based on history matching experiments with the template models parameterised using the geobodies and the pilot points. By testing the schemes with different types and numbers of parameters, the conclusions about the effect of the parameterisation bias were made. The study of Chapter 7 utilises history matching experiments where the production and seismic data are combined. The central idea pursued in this study is understanding the balance between the production and seismic terms. The models obtained by varying this balance were compared by their predicting capability. The study also allowed making conclusions about the scale of the seismic details informative of the flow regime based on the results of history matching using different seismic attributes. Comparing the results in the domains of solutions (permeability), pressure-saturation states and the predictions resulted in the conclusions about the relative importance of the parameterisation bias and the noise in data.

## 8.1 Main conclusions and recommendations

1. The relationship between the values of the map-based 4D seismic attributes and the underlying changes in impedance is complex. It is affected by the interference between the signals from different reflectors within the target reservoir interval as well as outside of it. Constructive and destructive

interference effects distort the signal and reduce the detectability of pressure and saturation changes. The first order average of seismic amplitude (after coloured inversion) correlates best with impedance for the cases studied in this work.

2. Estimates of the relative impedance which result from the coloured inversion process agree very well with the band-limited version of the true impedance which makes them a useful measure of the relative impedance. On the other hand, the inverted impedance obtained using the model-based inversion is not constrained in frequencies outside of the seismic frequency band (10-80 Hz). In the absence of any informative prior, the information in this part of the spectrum (especially the high frequency component) is noisy. Despite this fact, it was found that high frequency variations of the impedance (when used as history data) do not affect the results of history matching which in turn are constrained by the larger scale signal. This explains another finding that the model estimates obtained by matching the inverted impedance are similar to those obtained by another volumetric attribute, seismic traces. This also indicates that only the information common for the data in these two domains (seismic domain and impedance domain) is important for history matching. In other words, localized data errors (resulting from the inversion) do not affect the results of history matching when the data is matched on a larger scale spatial pattern. Similar history matching results obtained by matching the precise 4D impedance (proxy for pressure and saturation state) finally suggest that the information actually constraining the simulation models (within the scope of the studied examples) has a scale equal to or larger than the seismic resolution. Importance of smaller details in seismic data is also reduced when solutions to history matching are found by fitting both seismic and production data at the same time which is further explained in the following clauses. The practical implication is that we should aim to constrain larger scale patterns such as water floods with 4D signal rather than individual smaller anomalies which may well be artefacts of data. Also, any special processing aimed at restoring smaller details in the seismic data such as the inversion may not provide a benefit for the history matching as explained above.
3. In the solution domain (that is in the domain of permeabilities), the permeability fields estimated by matching production data demonstrate high spatial variability whereas the permeability fields constrained by the seismic data are more spatially correlated with each other. Stronger spatial tie of the seismic data is

explained by the fact that the seismic response is controlled by the spatial distribution of pressure and saturation rather than by their evolution directly. The production data on the other hand is controlled by an integral characteristic of the reservoir which ensures correct phase flows but does not make any preference in terms of which path the flow will take. This difference in constraints in particular means that the production match (of phase flow rates) is possible with a wider range of spatial permeability distributions than the seismic match. The implication of this conclusion is that models estimated purely on production data constraint should be treated as realisations of well predictors rather than estimates of spatial distribution of permeability (production data do not constrain the latter).

4. In the domain of pressure-saturation states, matching to production data, seismic maps and volumetric attributes result in different states (different models) (see Figure 7.23 in Chapter 7). In particular, matching volumetric attributes leads to the states closest to the reference ones (parameterisation did not allow for a closer match as explained in the following clauses). On the other hand, matching to production data does not bring the state of the model close to the reference one which suggests that the production data is the poorest (among the studied data types) indicator of the pressure-saturation state. Although matching to seismic maps does bring the state of the model closer to the reference state, the result is worse than when matching the volumetric types. This is an important observation which has implications on joint history matching to production and seismic map as explained below.
5. It was found that combining the seismic map and production data in a way where only the high level details of the seismic map are matched provides the best constraint for the simulation model in terms of its future forecasts. In contrast, matching smaller details of the seismic map harms the predictive capability of the simulation model because in that case the solution becomes too specific to those details. This finding questions the notion of the good match of 4D seismic data in seismic history matching studies often equated to the best match possible. Optimal combinations of production and seismic match were found with a significant level of details unmatched which would seem unacceptable if judged only visually.
6. 77-point parameterisation demonstrates (within the scope of the studied examples) clearly higher flexibility in matching the seismic data (production

data do not require high flexibility) which is expressed by lower misfits. However, the extra resolution of the 77-point scheme (compared to the 28-point scheme) is not utilised when matching seismic (only high level pattern, without details) and production data simultaneously. This is explained by the fact that the pressure-saturation state that is common for production and seismic constraints is characterised by larger scale (lower frequency) signal which does not require too much of model flexibility. This finding suggests that the choice of parameterisation should not be made with the aim of matching smaller details of the seismic data but only the larger scale pattern.

7. Although the previous clause suggested that too high resolution of the parameterisation can be superfluous, using too few parameters is also a bad option as it may lead to a significant bias in parameter estimates. It was shown that too few parameters lead to over-determined models where the uniqueness is not supported by data constraint but rather is a result of imposing some prior information. This prior information in general is not compatible with the calibration data but is fixed in history matching for which reason it produces bias. The bias is a function of not only the number of parameters but also of the parameterisation itself. For example, two parameterisations, pilot points and geobodies, both with 28 parameters (as it was shown) result in different amount of bias. In particular, the bias from the pilot points is weaker because the parameterisation itself is more neutral in terms of the prior information, whereas the geobodies-based parameterisation creates structural noise due to the information (prior structure) about the geometry of the geobodies. It is therefore recommended to use generally more parameters to minimize the bias from the fixed prior information.
8. Closeness of the history matching results for the data types different only in local variation (noise in data, see clause 2) and non-achievable state of the reference model due to the parameterisation suggest that the structural noise (that is our choices in parameterisation) affect the results of history matching stronger than noise in data.
9. The PSO algorithm is easy to implement and control. However, the convergence is found to be very sensitive to the values of its two parameters ($c_1$ and $c_2$) so testing of the algorithm with a problem specific objective function is recommended prior to the actual history matching. Best results in terms of the final misfit value were achieved with the ‘circle’ topology of PSO. In the case of

> matching production data, the objective function is of simpler shape and the convergence is faster. When matching the seismic maps, convergence is slower as the case is more difficult. The most difficult case is matching production and seismic data simultaneously where the convergence is slowest.

In the introduction to this thesis, a scheme of history matching was presented (see Figure 1.1) which illustrates the standard approach to history matching (in an automatic stochastic implementation), and the areas of interest for this research were defined. Figure 8.1 below shows an updated version of the scheme where answers are given within the limited scope of this work to the questions of parameterisation and balancing the production and seismic terms when integrating 4D seismic data within the reservoir models. In the part of parameterisation, the correct balance between the prior structure (part of the model defined deterministically based on knowledge from sources other than the calibration data, for example, the geobodies) and the flexibility of the model (number and scale of parameters) which defines the effective parameterisation resolution was found to be the key to the optimal assimilation of the information from the calibration data. In the context of matching 4D seismic data, the requirement for the spatial resolution of the parameterisation is stricter due to the spatial nature of the seismic constraint. In particular, the prior structure imposed by any deterministic inclusions (implementing geological concepts), although dense in valuable information, requires thorough compensation in the part of parameterisation resolution. In what concerns the comparison of predicted and observed data and balancing the production and seismic terms, the seismic constraint was found to be effective on the large scale pattern level. This in particular accounts for seismic modelling errors and those of the entire model (prior structure!) which have strong effect on local signal variation, but as mentioned, taking the signal globally allows extracting the common part which effectively constrains the flow.

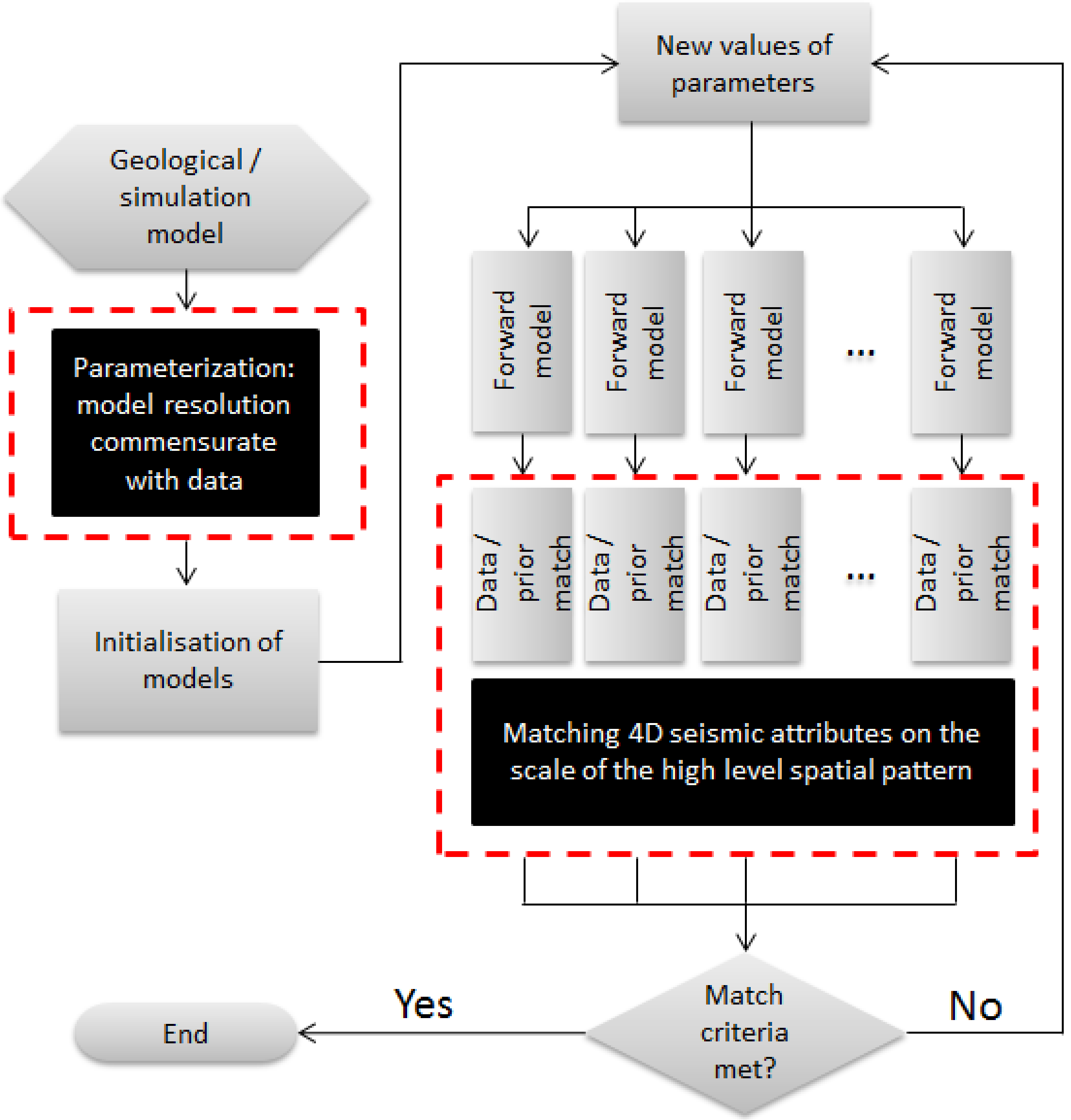

**Figure 8.1. Scheme of history matching for an iterative parameter estimation formulation using multiple-model approach such as a stochastic automatic history matching. Dashed red rectangles indicate the parts of the workflow on which the present work focusses, contributions of this work are placed in the black blocks.**

The analysis leads to many new questions which require both studying the subject of the seismic history matching further and testing the conclusions of this work on a wider range of scenarios. If the seismic signal is found to constrain the flow on a certain scale, then to what situations in terms of the reservoir size, data noise level is it applicable? In which cases do pressure-saturation distributions actually define economically significant forecasts, or when does the pressure-saturation state have control on model prediction? Is there anomaly dominance in the constraining ability of the seismic attributes (that is when a certain anomaly defines much of the reservoir simulation outcome – unfavourable situation because the anomaly-scale seismic signal was shown to be more susceptible to noise than the larger pattern scale signal)? What is the constraining ability of volumetric seismic attributes in a real situation with noisy data?

## 8.2 Limitations and future work recommendations

1. History data used in this work were generated from the synthetic reference models. As discussed before this provided a controllable environment for the experiments but at the same time it is a limitation for the scope of this study. In order to demonstrate the repeatability of the results, similar studies need to be conducted with a wider range of models including the input parameters such as the petro-elastic properties. Also, the results need to be tested in the context of real data uncertainties using the models constrained by the real observed data.
2. Mostly the particular case of the previous clause, but an important consideration about the rock physics properties assumed in the study. In this case them template was the Schiehallion field where the bubble point was high which gave plenty of gas effects in the 4D signature. Also, the water in oil was highly detectable which allowed us constraining the future model forecasts based on water flood monitoring. However, the conclusions about the constraining ability of the 4D seismic attributes may change when different petro-physical input is used.
3. Seismic modelling is based on 1D convolutional model which is known to be an approximate method. This did not cause any problems in this study because the observed data were generated with exactly the same methods. However, the modelling error due to the seismic modelling method needs to be tested with real data.
4. Flexibility of parameterisations was tested using only two parameterisations, 28 and 77 pilot points. Other parameterisation options need to be tested in order to understand how prior-dependent and prior-independent parameterisations affect the predictive capability of the history matched models.

# References

1. Aanonsen, S., Aavatsmark, I., Barkve, T., Cominelli, A., Gonard, R., Gosselin, O., Kolasinski, M., Reme, H., Effect of scale dependent data correlations in an integrated history matching loop combining production data and 4D seismic data, presented at SPE Reservoir Simulation Symposium, 3-5 February 2003, Houston, Texas
2. Aanonsen, S., Eydinov, D., A multiscale method for distributed parameter estimation with application to reservoir history matching. Comput. Geosci. 10(1), 2006, p. 97-117
3. Aanonsen, S., Nævdal, G., Oliver, D., Reynolds, A., Vallès, B., Ensemble Kalman filter in reservoir engineering – a review. SPE J. 14(3), 2009, p. 393-412
4. Abu-Mostafa, Y., Magdon-Ismail, M., Lin, H-T., Learning From Data, AMLbook.com, March 2012
5. Aggarwal, A., Du, S., King, M., Strategies in history matching: a deepwater turbiditie field example, presented at SPE Annual Technical Conference and Exhibition, 8-10 October 2012, San Antonio, Texas, USA
6. Aki, K. Richards, P., Quantitative Seismology, Theory and Methods, San Francisco: Freeman, 1980
7. Andersen, T., Zachariassen, E., Meisingset, H., Otterlei, C., Hatland, K., Hoye, T., Mangeroy, G., Liestol, F., Method for conditioning the reservoir model on 3D and 4D elastic inversion data applied to a fluvial reservoir in the North Sea, presented at SPE Europec/EAGE Annual Conference and Exhibition, 12-15 June 2006, Vienna, Austria
8. Andorsen, K., Tjetland, G., Barkved, O., Kristiansen, T., Idsoe, C., Wrobel, L., Seismic full waveform inversion improves Valhall reservoir management, presented at SPE Offshore Europe Oil and Gas Conference and Exhibition, 3-6 September, 2013, Aberdeen, UK
9. Anterion, F., Karcher, B., Eymard, R., Use of parameter gradients for reservoir history matching, presented at SPE Symposium on Reservoir Simulation, 6-8 February 1989, Houston, Texas

10. Arts, R., Chadwick, R., Eiken, O., Trani, M., Dortland, S., Synthetic versus real time-lapse seismic data at the Sleipner $CO_2$ injection site, SEG/San Antonio 2007 Annual Meeting.
11. Atkinson, J., The use of reservoir engineering in the development of the Magnus oil reservoir, presented at Offshore Europe, 10-13 September 1985, Aberdeen, United Kingdom
12. Backus, G.E., Long-wave elastic anisotropy produced by horizontal layering. J. Geophys. Res., 67, 1962, p. 4427-4440
13. Batzle, M., Wang, Z., Seismic properties of pore fluids, Geophysics, vol. 57, no. 11, 1992, p. 1396-1408.
14. Beaudoin, G., Ross, A., Field design and operation of a novel deepwater, wide-azimuth node seismic survey, The Leading Edge, April 2007
15. Bhark, E., Rey, A., Datta-Gupta, A., Jafarpour, B., A multiscale workflow for history matching in structured and unstructured grid geometries, SPE Journal, volume 17, issue 03, 2012, p. 828-848
16. Biondi, B., 3D seismic imaging, Investigations in Geophysics Series No. 14, 2006
17. Biot, M., Theory of propagation of elastic waves in a fluid saturated porous solid: I. Low frequency range, II. Higher-frequency range, J. Acoust. Soc. Am., 28, 168–191, 1956
18. Bissell, R., Calculating optimal parameters for history matching, 4th European Conference on the Mathematics of Oil Recovery, 1994
19. Bissell, R., Dubrule, O., Lamy, P., Swaby, P., Lepine, O., Combining goestatistical modelling with gradient information for history matching: the pilot point method, SPE-38730, Proc. of the SPE Annual Technical Conference and Exhibition, San Antonio, Texas, 5-8 October 1997, p. 139-154
20. Bissell, R., Sharma, Y., Killough, J., History Matching Using the Method of Gradients: Two Case Studies, SPE-28590, presented at the SPE 69fh Annual Technical Conference and Exhibition held in New Orleans, LA, USA, 25-28 September, 1994.
21. Brito, D., Moraes, R., Emerick, A., The Marlim field: incorporating time-lapse seismic in the assisted history matching, presented at SPE Latin American and Caribbean Petroleum Engineering Conference, 1-3 December 2010, Lima, Peru
22. Buckley, S., Leverett, M., Mechanism of fluid displacements in sands, Transactions of the AIME (146), 1942, p. 107-116

23. Caers, J., Hoffman, T., The probability perturbation method: a new look at Bayesian inverse modelling. Math. Geol. 38(1), 2006, p. 81-100

24. Carcione, J., Hermanz, G., Kroode, A., Seismic modelling, Geophysics, vol. 67, No. 4, July-August 2002, p. 1304–1325.

25. Castro, S., Caers, J., Otterlei, C., Andersen, T., Hoye, T., Gomel, P., A probabilistic integration of well log, geological information, 3D/4D seismic, and production data: application to the Oseberg field, presented at SPE Annual Technical Conference and Exhibition, 24-27 September 2006, San Antonio, Texas, USA

26. Chapin, M., Terwogt, D., Ketting, J., From seismic to simulation using new voxel body and geologic modelling techniques, Schiehallion Field, West of Shetlands. The Leading Edge, April 2000 19(4) p. 408-412

27. Chavent, G., Dupuy, M., Lemonnier, P., History matching by use of optimal control theory, SPE Journal, 15(1), 1975, p. 74-86

28. Chen, W., Gavalas, G., Seinfeld, J., Wasserman, M., A new algorithm for automatic history matching. SPE Journal, 14(6), 1974, p. 593-608

29. Chen, Y., Oliver, D., Ensemble-based closed-loop optimization applied to Brugge Field, Society of Petroleum Engineers Journal, 13(1), 2010, p. 56-71

30. Ching-Lai, H., Md Masud Abu, S., Multiple objective decision making, methods and applications : a state-of-the-art survey, Lecture note in economics and mathematical systems, Berlin, Springer-Verlag, 1979

31. Christie, M., Eydinov, D., Demyanov, V., Talbot, J., Arnold, D., Shelkov, V., Use of multi-objective algorithms in history matching of a real field, presented at SPE Reservoir Simulation Symposium, 18-20 February 2013, The Woodlands, Texas, USA

32. Clerc, M., Kennedy, J., The particle swarm – explosion, stability, and convergence in a multidimensional complex space, IEEE Transactions On Evolutionary Computation, vol. 6, no. 1, February 2002

33. Cole, S., Lumley, D., Meadows, M., Tura, A., Pressure and saturation inversion of 4D seismic data by rock physics forward modelling, 72nd Annual International Meeting, SEG, Expanded Abstracts, 2002, p. 2475-2478

34. Cooke, D., Cant, J., Model-based seismic inversion: comparing deterministic and probabilistic approaches, CSEG Recorder, April, 2010

35. Cooke, D., Schneider, W., Generalized linear inversion of reflection seismic data, Geophysics, vol. 48, No. 6, June 1983, p. 665-676

36. Cooley, R., A theory for modelling ground-water flow in heterogeneous media, Professional Paper 1679, Reston, Virginia, USGS, 2004

37. Cooley, R., Christensen, S., Bias and uncertainty in regression-calibrated models of groundwater flow in heterogeneous media, Advances in Water Resources, vol. 29, no. 5, 2006, p. 639-656

38. Curia, D., Seismic inversion methods, http://davidcuria.blogspot.co.uk /2009/07/seismic-inversion-methods.html

39. Dadashpour, M., Landro, M., Kleppe, J., Porosity and permeability estimation by gradient-based history matching using time-lapse seismic data, presented at SPE Middle East Oil and Gas Show and Conference, 11-14 March 2007, Kingdom of Bahrain

40. Datta-Gupta, A., King, M., Streamline simulation: theory and practice, SPE Textbook Series vol. 11, 2007

41. Davolio, A., Maschio, C., Schiozer, D., Incorporating 4D seismic attributes into history matching process through an inversion scheme, presented at SPE EUROPEC/EAGE Annual Conference and Exhibition, 23-26 May 2011, Vienna, Austria

42. de Marsily, G., Lavedan, G., Boucher, M., Fasanino, G., Interpretation of interference tests in a well field using geostatistical techniques to fit the permeability distribution in a reservoir model. In: Geostatistics for Natural Resources Characterization, Part 2, D. Reidel, 1984, p. 831-849

43. Dickstein, F., Goldfeld, P., Pfeiffer, G., Amorim, E., Santos, R., Gomez, S., A Study of the Impact of 4D-Seismic Data on TSVD-Based Schemes for History Matching, presented at the SPE Latin American and Caribbean Petroleum Engineering Conference held in Lima, Peru, 1-3 December, 2010

44. Dijksman, N., Evans, A., McCormick, D., Stammeijer, J., 4D key to Schiehallion reservoir management, Offshore digital magazine, 09 January 2007.

45. Ding, Y., Roggero, F., Local Parameterization of Geostatistical Realizations for History Matching, presented at the SPE Reservoir Simulation Symposium, 2-4 February 2009, The Woodlands, Texas

46. Dong, Y., Oliver, D., Quantitative use of 4D seismic data for reservoir description, SPE Journal, vol. 10(1), 2005, p. 91-99

47. Dong, Y., Oliver, D., Reservoir simulation model updates via automatic history matching with integration of seismic impedance change and production data,

presented at International Petroleum Technology Conference, 3-5 December 2008, Kuala Lumpur, Malaysia

48. Donnez, P., Essentials of reservoir engineering, TECHNIP, 2007

49. Dorigo, M., Optimization, Learning and Natural Algorithms, PhD thesis, Politecnico di Milano, Italy, 1992.

50. Dubrule, O., Haas, A., Geostatistical inversion – a sequential method of stochastic reservoir modelling constrained by seismic data, First Break, vol. 12, No. 11, November 1994.

51. Dubrule, O., Thibaut, M., Lamy, P., Haas, A., Geostatistical reservoir characterization constrained by 3D seismic data, Petroleum Geoscience 1998, v.4, p121-128

52. Durlofsky, L., Advanced reservoir engineering, PE222, Stanford University, California, USA, 2002

53. Eaton, D., Milkereit, B., Adam, E., 3-D seismic exploration, in “Proceedings of Exploration 97: Fourth Decennial International Conference on Mineral Exploration” edited by A.G. Gubins, 1997, p. 65-78

54. Edris, N., Stephen, K., Shams, A., MacBeth, C., Updating Barrier transmissibilies in Simulations by Successively Adding Data to an Automated Seismic History Matching Processes: A Case Study, SPE113557, Presented at the SPE Europec/EAGE Annual Conference and Exhibition held in Rome, Italy, 9-12, June 2008

55. El Ouair, Y., Lygren, M., Osdal, B., Husby, O., Springer, M., Integrated reservoir management approach: from time-lapse acquisition to reservoir model update at the Norne field, presented at International Petroleum Technology Conference, 21-23 November 2005, Doha, Qatar

56. Enchery, G., Le Ravalec-Dupin, M., Roggero, F., An Improved Pressure and Saturation Downscaling Process for a Better Integration of 4D Seismic Data together with Production History, presented at the EUROPEC/EAGE Conference and Exhibition, 11-14 June, 2007, London, UK

57. Erbas, D., Dunning, M., Nash, T., Cox, D., Stripe, J., Duncan, E., Magnus WAG pattern optimization through data integration, presented at SPE Improved Oil Recovery Symposium, 12-16 April 2014, Tulsa, Oklahoma, USA

58. Eydinov, D., Aanonsen, S., Haukas, J., Aavatsmark, I., A method for automatic history matching of a compositional reservoir simulator with multipoint flux approximation, Computational Geoscience, 12(2), 2008, p. 209-225

59. Fienen, M., Muffels, C., Hunt, R., On constraining pilot point calibration with regularization in PEST. Ground Water 47(6), 2009, p. 835-844

60. Floricich, M., MacBeth, C., Staples, R., An engineering-driven approach for separating pressure and saturation using 4D seismic: Application to a Jurassic reservoir in the UK North Sea, proceedings of the 2005 SEG Annual Meeting, 6-11 November, Houston, Texas, p. 2464-2467

61. Gardner, G., Gardner, L., Gregory, A., Formation velocity and density – the diagnostic basics for stratigraphic traps: Geophysics, 39, 1974, p. 770-780.

62. Gassmann, F., Über die elastizität poröser medien (On elasticity of porous media), Viertel. Naturforsch. Ges. Zürich, 96, 1-23, 1951

63. Gavalas, G., Shah, P., Seinfeld, J., Reservoir history matching by Bayesian estimation. SPE J. 16(6), 1976, p. 337-350

64. Gjøystdal, H., Iversen, E., Laurain, R., Lecomte, I., Vinje, V., Åstebøl, K., Review of ray theory applications in modelling and imaging of seismic data, Studia Geophysica et Geodaetica, April 2002, Volume 46, Issue 2, pp 113-164

65. Gosselin, O., Aanonsen, S., Aavatsmark, I., Cominelli, A., Gonard, R., Kolasinski, M., Ferdinandi, F., Kovacic, L., Neylon, K., History matching using time-lapse seismic, Paper presented at the SPE annual technical conference and exhibition held in Denver, Colorado, USA, 5-8 October 2003

66. Gouveia, W., Scales, J., Bayesian seismic waveform inversion: parameter estimation and uncertainty analysis, Journal of Geophysical Research: Solid Earth, vol. 103(B2), February, 1998, p. 2759-2779

67. Gouveia, W., Scales, J., Resolution of seismic waveform inversion: Bayes versus Occam, Inverse Problems 13, 1997, p. 323–349

68. Govan, A., Primmer, T., Douglas, C., Moodie, N., Davies, M., Nieuwland, F., Reservoir management in a deepwater subsea field – the Schiehallion experience, SPE Reservoir Evaluation & Engineering, Volume 9, Number 4, August 2006, pp. 382-390

69. Greaves R., Fulp, T., Three dimensional seismic monitoring of an enhanced oil recovery process, Geophysics, 52, 1987, p. 1175-1187

70. Grimstad, A., Mannseth, T., Aanonsen, S., Aavatsmark, I., Cominelli, A., Mantica, S., Identification of unknown permeability trends from history matching of production data, SPE Journal, vol. 9(04), 2004, p. 419-428

71. Grimstad, A., Mannseth, T., Nævdal, G., Urkedal, H., Adaptive multiscale permeability estimation. Comput. Geosci. 7(1), 2003, p. 1-25

72. Hajizadeh, Y., Christie, M., Demyanov, V., Comparative study of novel population-based optimization algorithms for history matching and uncertainty quantification: PUNQ-S3 revisited, presented at Abu Dhabi International Petroleum Exhibition and Conference, 1-4 November 2010, Abu Dhabi, UAE

73. Han, D.-H., Batzle, M., Velocity, Density and Modulus of Hydrocarbon Fluids - Data Measurement, SEG expanded abstracts, 2000

74. Han, D.-H., Liu, J., Batzle, M., Seismic properties of heavy oils – measured data, The Leading Edge, 27, no. 9, 2008, p. 1108-1115

75. Helgerud, M., Miller, A., Johnston, D., Udoh, M., Jardine, B., Harris, C., Aubuchon, N., 4D in the deepwater Gulf of Mexico: Hoover, Madison, and Marshall fields, The Leading Edge, September 2011, p. 1008-1018.

76. Hokstad, K., Lecomte, I., Maaø, F., Tuseth, M., Mjelva, A.E., Gjøystdal, H., Sollie, R., Hybrid modelling of elastic wavefield propagation, Extended Abstracts, 60th EAGE Annual Meeting, 1998, p. 5-56.

77. Hoos, H., Stützle, T., Stochastic Local Search: Foundations and Applications, Morgan Kaufmann, Elsevier, 2004.

78. Hu, L.Y., Ravalec, M.L., Blanc, G.: Gradual deformation and iterative calibration of truncated Gaussian simulations. Pet. Geosci. 7, 2001, p. 25-30

79. Hunt, R., Doherty, J., Tonkin, M., Are models too simple? Arguments for increased parameterization. Ground Water 45(3), 2007, p. 254-262

80. Ifeachor, E., Jervis, B., Digital signal processing: a practical approach, second edition, Pearson education limited, 2002

81. Jack, I., Time-lapse seismic in reservoir management, SEG Distinguished Instructor Series, no. 1, 1997

82. Jacquard, P., Jain, C., Permeability distribution from field pressure data, SPE Journal, 5(4), 1965, p. 281-294

83. Jafarpour, B., McLaughlin, D., Reservoir Characterization With the Discrete Cosine Transform, SPE Journal, 14(01), 2009, p. 182-201

84. Jin, L., Alpak, F., van den Hoek, P., Pirmez, C., Fehintola, T., Tendo, F., Olaniyan, E., A comparison of stochastic data-integration algorithms for the joint history matching of production and time-lapse seismic data, SPE Annual Technical Conference and Exhibition, 30 October-2 November 2011, Denver, Colorado, USA

85. Jin, L., Sen, M., Stoffa, P., Seif, R., Optimal Model Parameterization in Stochastic Inversion for Reservoir Properties Using Timelapse Seismic and

Production Data, proceedings of SEG Annual Meeting, 23-28 September 2007, San Antonio, Texas, p. 1805-1809

86. Johnston, D., Practical applications of time-lapse seismic data, 2013 DISC, distinguished instructor series, No. 16

87. Jourdan, C., Ekern, T., Integrating 3D seismic in multidisciplinary reservoir modelling projects, Offshore Technology Conference, 6-9 May 1996, Houston, Texas

88. Kaiser, J., Digital Filters, In Kuo, F. F. and Kaiser, J. F. (Eds.), System analysis by digital computer, chap. 7. New York, Wiley, 1966

89. Kazemi, A., Stephen, K., Optimal parameter updating in assisted history matching of the Nelson field using streamlines as a guide, SPE-131540, presented at the SPE EUROPEC/EAGE Annual Conference and Exhibition held in Barcelona, Spain, 14–17 June 2010.

90. Kazemi, A., Stephen, K., Shams, A., Seismic history matching of Nelson using time-lapse seismic data: an investigation of 4D signature normalization, SPE 131538, presented at the SPE EUROPEC/EAGE Annual Conference and Exhibition held in Barcelona, Spain, 14–17 June 2010.

91. Kennedy, J., Eberhart, R., Particle Swarm Optimization, proceedings of IEEE International Conference on Neural Networks IV, 1995, pp. 1942–1948. doi:10.1109/ICNN.1995.488968.

92. Kennedy, J., Eberhart, R., Shi, Y., Swarm intelligence, Morgan Kaufmann Publishers, Inc., San Francisco, CA, 2001.

93. Khaninezhad, M.,R, Jafarpour, B., Hybrid parameterization for robust history matching, SPE-146934-PA, SPE Journal, 19(3), 2014, p. 487-499

94. King, M., MacDonald, D., Todd, S., Leung, H., Application of novel upscaling approaches to the Magnus and Andrew reservoirs, European Petroleum Conference, 20-22 October 1998, The Hague, Netherlands

95. Kjelstadli, R.M., Lane, H.S., Johnson, D.T., Barkved, O.I., Buer, K., Kristiansen, T.G., Quantitative history match of 4D seismic response and production data in the Valhall Field, Presented at the Offshore Europe 2005 held in Aberdeen, Scotland, 6-9 September 2005

96. Kolstoe, E., Husby, O., Roste, T., Tyssekvam, J., Moen, A., Endresen, T., Dawodu, N., Using 4D seismic for understanding drainage pattern and optimizing infill wells placement in a heterogeneous and compartmentalised reservoir - cases from the Heidrun field

97. Koster, K., Gabriels, P., Hartung, M., Verbeek, J., Deinum, G., and Staples, R., Time-lapse seismic surveys in the North Sea and their business impact, The Leading Edge, pp286-293, 2000.

98. Kragh, E., Christie, P., Seismic repeatability. Normalized RMS, and predictability, The Leading Edge, v. 21 no. 7 p. 640-647.

99. Kravaris, C., Seinfeld, J., Identification of parameters in distributed parameter-systems by regularization. SIAM Journal, Control Optimization, 23(2), 1985, p. 217-241

100. Krebes, E., Seismic forward modelling, CSEG recorder, April 2004

101. Kumar, D., A tutorial on Gassmann fluid substitution: formulation, algorithm and Matlab code, Geohorizons, January 2006

102. Lancaster, S., Whitcombe, D., Fast-track 'coloured' inversion, SEG Expanded abstracts, 70th SEG Annual meeting, Calgary, 2000, p. 1572-1575

103. Landa, J., Horne, R., A procedure to integrate well test data, reservoir performance history and 4D seismic information into a reservoir description, The paper was presented at the SPE Annual Technical Conference and Exhibition held in San Antonio, Texas, 5-8 October 1997.

104. Landa, J., Kumar, D., Joint Inversion of 4D Seismic and Production Data, SPE-146771-MS, presented at the SPE Annual Technical Conference and Exhibition, 30 October-2 November, 2011, Denver, Colorado, USA

105. Landro, M., Discrimination between pressure and fluid saturation, changes from time-lapse seismic data, Geophysics, vol. 66, no. 3, May-June 2001, p. 836-844

106. Le Ravalec-Dupin, M., Hu, L., Combining the pilot point and gradual deformation methods for calibrating permeability models to dynamic data, Oil and Gas Science and Technology – Rev. IFP, vol. 62, no. 2, 2007, p. 169-180

107. Leach, H., Herbert, N., Los, A., Smith, R., The Schiehallion development, In: Fleet, A., Boldy, S., (eds), Petroleum Geology of Northwest Europe: Proceedings of the 5th Conference, Geological Society, London, 1999, p. 683-692.

108. Lecomte, I., Hybrid modelling with ray tracing and finite difference. Expanded Abstracts, 66th SEG Annual Meeting, 1996, p. 699-702

109. Lee, T.-Y., Kravaris, C., Seinfeld, J., History matching by spline approximation and regularization in singlephase areal reservoirs, SPE Reservoir Engineering Journal, vol. 1(5), 1986, p. 521-534

110. Lerat, O., Adjemian, F., Baroni, A., Etienne, G., Renard, G., Bathellier, E., Forgues, E., Aubin, F., Euzen, T., Modelling of 4D Seismic Data for the Monitoring of Steam Chamber Growth During the SAGD Process, Journal of Canadian Petroleum Technology, June 2010, Volume 49, No. 6

111. Li, J., Liner, C., Geng, P., Zeng, J., Convolutional time-lapse seismic modelling for $CO_2$ sequestration at the Dickman oilfield, Ness County, Kansas, Geophysics, vol. 78, no. 3, May-June 2013, p. B147–B158

112. Liberti, L., Kucherenko, S., Comparison of deterministic and stochastic approaches to global optimization. International Transactions in Operational Research, 12, 2005, p. 263–285.

113. Lindseth, R., Synthetic sonic logs – a process for stratigraphic interpretation, Geophysics, vol. 44, No. 1, January 1979, p. 3-26.

114. Liu, J., A multiresolution method for distributed parameter estimation, SIAM J. Sci. Comput. 14(2), 1993, p. 389-405

115. Lorentzen, R.J., Fjelde, K.K., Frøyen, J., Lage, A.C.V.M., Nævdal, G., Vefring, E.H., Underbalanced and low-head drilling operations: real time interpretation of measured data and operational support, presented at the SPE annual technical conference and exhibition, New Orleans, 30 September-3 October, 2001, SPE 71384

116. Lumley, D., Nur, A., Strandenes, S., Dvorkin, J., Packwood, J., Seismic monitoring of oil production: a feasibility study, presented at the 1994 SEG conference, Los Angeles

117. Lumley, D.E. Behrens, R.A., Practical Issues of 4D Seismic Reservoir Monitoring: What an Engineer Needs to Know, SPE Reservoir Evaluation & Engineering, December 1998

118. Lyons, R., Understanding digital signal processing, Prentice hall PTR, 2001

119. MacBeth, C., A classification for the pressure sensitivity properties of a sandstone rockframe, Geophysics, 69, 2004, p. 497-510

120. MacBeth, C., Stephen, K., Seismic scale saturation relations in turbidite reservoirs undergoing waterflood. Geophysical Prospecting. 56(5), 2008, p. 693-714

121. MacGregor, A., Trussell, P., Lauver, S., Bedrock, M., Bryce, J., Moulds, T., The Magnus field: extending field life through good reservoir management and enhanced oil recovery, Petroleum Geology Conference series 2005, v.6, p. 469-475

122. Makhlouf, E., Chen, W., Wasserman, M., Seinfeld, J., A general history matching algorithm for three-phase, three-dimensional petroleum reservoirs. SPE Adv. Technol. Ser. 1(2), 1993, p.83–91

123. Margrave, G., Manning, P., Seismic Modelling: An Essential Interpreter's Tool, CSEG National convention, 2004.

124. Martin, K., Macdonald, C., The Schiehallion field: applying a geobody modelling approach to piece together a complex turbidite field, presented at the DEVEX conference held in Aberdeen, Scotland, 12-13 May, 2010.

125. Marvillet, C., Hubans, C., Thore, P., Desegaulx, P., Al-Mehairi, Y., Shuaib, M., Al Shaikh, A., Seismic monitoring feasibility on Bu-Hasa field, IPTC 11640, Paper presented at the International petroleum technology conference held in Dubai, 4-7 December, 2007

126. Maucec, M., Cullick, S., Shi, G., Geology-guided quantification of production-forecast uncertainty in dynamic model inversion, presented at SPE Annual Technical Conference and Exhibition, 30 October-2 November 2011, Denver, Colorado, USA

127. Mavko, G., Mukerji, T., Dvorkin, J., The Rock Physics Handbook, First Edition, Cambridge university press, 1998

128. Mavko, G., Mukerji, T., Dvorkin, J., The Rock Physics Handbook, Second Edition, Cambridge university press, 2009

129. Meadows, M., Adams, D., Wright, R., Tura, A., Cole, S., Lumley, D., Rock physics analysis for time-lapse seismic at Schiehallion field, North Sea, Geophysical prospecting, 2005, 53, p. 205-213

130. Mezghani, M., Fornel, A., Langlais, V., Lucet, N., History matching and quantitative use of 4D seismic data for an improved reservoir characterization, Presented at the SPE Annual Technical Conference and Exhibition held in Houston, Texas, USA, 26-29 September 2004

131. Mikkelsen, P., Guderian, K., du Plessis, G., Improved reservoir management through integration of 4D-seismic interpretation, Draugen field, Norway, SPE Journal Reservoir Evaluation & Engineering, 11(01), 2008, p. 9-17

132. Miranda, D., Fault-induced bends on Schiehallion's North Channel, presented at 4th European production and development conference on subsurface techniques for maximising recovery, DEVEX 2007 held in Aberdeen, Scotland, 15-16 May, 2007.

133. Moore, C., Doherty, J., The cost of uniqueness in groundwater model calibration, Advances in Water Resources, vol. 29(4), 2006, p. 605-623

134. Moulds, T., Trussell, P., Haseldonckx, S., Carruthers, A., Magnus field: reservoir management in a mature field combining waterflood, EOR and new area developments, presented at Offshore Europe conference, 6-9 September 2005, Aberdeen, United Kingdom

135. Nocedal J., Wright, S., Numerical optimization, Second edition, Springer, 2006.

136. Nur, A., Seismic imaging in enhanced recovery, The paper was presented at the 1982 SPE/DOE Third Joint Symposium on Enhanced Oil Recovery of the Society of Petroleum Engineers held in Tulsa, OK, April 4-7, 1982

137. Ødegaard, E., Avseth, P., Well log and seismic data analysis using rock physics templates, First Break, v. 22, no. 10, 2004, p. 37-43.

138. Oldenburg, D., Scheuer, T., Levy, S., Recovery of the acoustic impedance from the reflection seismograms, Geophysics, vol. 48, No. 10, October 1983, p. 1318-1337

139. Oliveira, R., The Marlim field: incorporating 4D seismic in reservoir-management decisions, Journal of Petroleum Technology, 60(04), 2008, p. 52-110

140. Oliver, D., Chen, Y., Recent progress on reservoir history matching: a review, Computational Geosciences, vol. 15, no. 1, 2011, p. 185-221

141. Oliver, D., Reynolds, A., Liu, N., Inverse Theory for Petroleum Reservoir Characterization and History Matching, 1st edition, Cambridge University Press, Cambridge, 2008

142. Oliver, D., Reynolds, A., Liu, N., Petroleum reservoir characterisation and history matching, Cambridge university press, 2008.

143. Park, H-Y., Datta-Gupta, A., King, M., Handling conflicting multiple objectives using pareto-based evolutionary algorithm for history matching of reservoir performance, presented at SPE Reservoir Simulation Symposium, 18-20 February, 2013, The Woodlands, Texas, USA

144. Parker, R., Understanding inverse theory, Ann. Rev. Earth Planet. Sci. 5, 1977, p. 35-64

145. Parks, T., Burrus, C., Digital filter design, A Wiley-Interscience publication, John Wiley and sons, 1987

146. Pendrel, J., Seismic inversion – still the best tool for reservoir characterization, CSEG Recorder, January, 2006.

147. Pendrel, J., Seismic inversion – the best tool for reservoir characterization, CSEG Recorder, 2001.

148. Pullin, N., Matthews, L., Hirsche, K., Techniques applied to obtain very high resolution 3-D seismic imaging at an Athabasca tar sands thermal pilot, The Leading Edge, vol. 6, no. 12, 1987, p. 10-15

149. Queißer, M., and Singh, S., Time lapse seismic monitoring of CO2 sequestration at Sleipner using time domain 2D full waveform inversion, SEG expanded abstracts, presented at SEG Denver 2010 Annual Meeting

150. Reeves, C. (ed.), Modern Heuristic Techniques for Combinatorial, McGraw-Hill, 1995, ISBN 0-07-709239-2.

151. Rey, A., Bhark, E., Gao, K., Datta-Gupta, A., Gibson, R., Streamline-based integration of time-lapse seismic and production data into petroleum reservoir models, Geophysics, Vol. 77, No. 6, November-December 2012, p. M73–M87

152. Richardson S., Herbert, N., Leach, H., How well connected is the Schiehallion reservoir? SPE-38560, Presented at the Offshore Europe Conference in Aberdeen, Scotland, 9-12 September 1997.

153. Robertson, J., Reservoir management using 3D seismic data, Journal of Petroleum Technology, vol. 41(07), 1989, p. 663-667

154. Rodrigues, J., Calculating derivatives for automatic history matching, Computational Geoscience, 10(1), 2006, p. 119-136

155. Roggero, F., Ding, D., Berthet, P., Lerat, O., Cap, J., Schreiber, P., Matching of production history and 4D seismic data – application to the Girassol field, offshore Angola, Paper presented at the SPE annual technical conference and exhibition held in Anaheim, California, USA, 11-14 November 2007

156. Romero, C., Carter, J., Using genetic algorithms for reservoir characterisation. Journal Pet. Sci. Eng. 31(2-4), 2001, p. 113–123

157. Russel, B., Hampson, D., Comparison of poststack seismic inversion methods, 1991 SEG Annual Meeting, November 10-14, 1991, Houston, Texas

158. Russel, B., Hampson, D., The old and the new in seismic inversion, CSEG Recorder, December 2006.

159. Sambridge, M., Geophysical inversion with a neighbourhood algorithm-I, Searching a parameter space. Geophys. J. Int. 138, 1999, p. 479-494

160. Sarkar, S., Gouveia, W., Johnston, D., On the inversion of time-lapse seismic data, SEG Annual International Meeting, Expanded Abstract, 2003, p. 1489-1492

161. Sarma, P., Durlofsky, L., Aziz, Kh., Chen, W., A New Approach to Automatic History Matching Using Kernel PCA, Presented at the SPE Reservoir Simulation Symposium, 26-28 February 2007, Houston, Texas, USA

162. Sarma, P., Durlofsky, L., Aziz, Kh., Chen, W., Efficient real-time reservoir management using adjoint-based optimal control and model updating, Computational Geosciences 10 (1), 2006, p. 3-36

163. Schulze-Riegert, R., Axmann, J., Haase, O., Rian, D., You, Y., Evolutionary algorithms applied to history matching of complex reservoirs. SPE Reserv. Evalu. Eng. 5(2), 2002, p. 163–173

164. Seldal, M., Reime, A., Arnesen, D., Improving reservoir simulation models using 4D data at the Snorre field, presented at EUROPEC/EAGE Conference and Exhibition, 8-11 June 2009, Amsterdam, The Netherlands

165. Sengupta, M., Mavko, G., Mukerji, T., Quantifying subresolution saturation scales from time-lapse seismic data: A reservoir monitoring case study, Geophysics, vol. 68, no. 3, May-June 2003, p. 803-814

166. Shahin, A., Stoffa, P., Tatham, R., Seif, R., Accuracy required in seismic modelling to detect production-induced time-lapse signatures, SEG San Antonio 2011 Annual Meeting

167. Shi, Y., Eberhart, R., A modified particle swarm optimizer, proceedings of IEEE International Conference on Evolutionary Computation, 1998, pp. 69–73.

168. Skjervheim, J.-A., Evensen, G., Aanonsen, S., Ruud, B., Johansen, T., Incorporating 4D seismic data in reservoir simulation models using ensemble Kalman filter. SPE J. 12(3), 2007, p. 282–292

169. Spall, J., Multivariate stochastic approximation using a simultaneous perturbation gradient approximation. IEEE Trans. Automat. Contr. 37(3), 1992, p. 332-341

170. Staples, R., Stammeijer, J., Jones, S., Brain J., Smit, F., Hatchell, P., Time-lapse (4d) seismic monitoring - expanding applications, CSPG-CSEG-CWLS Convention, 2006

171. Stephen, K., Scale and process dependent model errors in seismic history matching, Oil & Gas Science And Technology, 2007

172. Stephen, K., Shams, A., MacBeth, C., Faster Seismic History Matching In A UKCS Reservoir, Paper presented at the SPE Europec/EAGE annual conference and exhibition held in London, UK, USA, 11-14 June 2007

173. Stephen, K., Soldo, J., MacBeth, C., Christie, M., Multiple-model seismic and production history matching: a case study, SPE Journal, December 2006, p. 418-430

174. Stewart, G., Well test design & analysis, PennWell Corporation, 2011, ISBN 1593702310, 9781593702311, p. 41

175. Storn, R., Price, K., Differential evolution – a simple and efficient heuristic for global optimization over continuous spaces, Journal of Global Optimization 11, 1997, p. 341–359.

176. Tarantola, A., A strategy for nonlinear elastic inversion of seismic reflection data, Geophysics, v. 51, no. 10, October 1986, p. 1893-1903

177. Tarantola, A., Inverse problem theory: methods for data fitting and model parameter estimation. Elsevier, Amsterdam, Netherlands, 1987

178. Tavassoli, Z., Carter, C., King, P., Errors in history matching. SPE Journal, v. 9, 2004, p. 352–361

179. Thedy, E.A., Salomão, M.C., Corá, C.A.G., Santos, M.S., Pumputis, A. Gomes, R.M., Caletti, L. Understanding Flow Paths – New Opportunities From Time-Lapse Seismic Data, The paper was presented at the SPE Europec/EAGE Annual Conference and Exhibition held in London, United Kingdom, 11–14 June 2007.

180. Tikhonov, A., Arsenin V., Solution of Ill-posed Problems, Washington: Winston & Sons, 1977

181. Tillier, E., Le Ravalec, M., Roggero, F., Using time domain seismic data for history matching processes, First Break, 29, March 2011

182. Vasco, D.W., Datta-Gupta, A., He, Z., Behrens, R., Rickett, J., Condon, P., Reconciling Time-Lapse Seismic and Production Data Using Streamline Models: The Bay Marchand Field, Gulf of Mexico, Presented at the SPE Annual Technical Conference and Exhibition, 5-8 October 2003, Denver, Colorado.

183. Waggoner, J.R., Cominelli, A., Seymour, R.H., Improved reservoir modelling with time-lapse seismic in a Gulf of Mexico Gas Condensate reservoir, Presented at the SPE Asia Pacific Oil and Gas Conference and Exhibition held in Melbourne, Australia, 8-10 October 2002.

184. Walden, A., Hosken, J., An investigation of the spectral properties of primary reflection coefficients. Geophysical Prospecting, 33, 1985, p. 400-435

185. Walker, G., Allan, P., Trythall, R., Parr, R., Marsh, M., Kjelstadli, R., Barkved, O., Johnson D., Lane, S., Three case studies of progress in quantitative seismic-engineering integration, The Leading Edge, September 2006

186. Watanabe, S., Han, J., Datta-Gupta, A., King, M., Streamline-based time lapse seismic data integration incorporating pressure and saturation effects, presented at the SPE Annual Technical Conference and Exhibition held in New Orleans, Louisiana, USA, 30 September-2 October 2013

187. Watts, G., Permanent reservoir monitoring still facing challenges in bod for industry acceptance, First Break, 29, no. 5, 2011, p. 13-15

188. Wen, X.-H., Lee, S., Yu, T., Simultaneous integration of pressure, water cut, 1 and 4-D seismic data in geostatistical reservoir modelling. Math Geol. 38(3), 2006, p. 301-325

189. Wetter, M., Wright, J., A comparison of deterministic and probabilistic optimization algorithms for nonsmooth simulation-based optimization, Building and Environment, Volume 39, Issue 8, August 2004, p. 989-999

190. Widess, M., How thin is a thin bed? Geophysics, 38, 1973, p. 1176-1180

191. Williams, M., Keating, J., Barghouty, M., The stratigraphic method: a structured approach to history-matching complex simulation models, SPE Reservoir Evaluation & Engineering Journal, vol. 1(2), 1998, p. 169-176

192. Winter, G., Periaux, J., Galan, M., Genetic Algorithms in Engineering and Computer Science, John Wiley & Son Ltd., 1995.

193. Wood, A.W., A Textbook of Sound, New York: McMillan Co., 1955

194. Wu, Z., Reynolds, A., Oliver, D., Conditioning geostatistical models to two-phase production data. SPE Journal, 4(2), 1999, p. 142–155

195. Yang, D., Fehler, M., Malcolm, A., Liu, F., Morton, S., Double-difference waveform inversion of 4D ocean bottom cable data: application to Valhall, North Sea, SEG expanded abstracts, presented at SEG Houston 2013 Annual Meeting

196. Yang, Y., Thompson, C., McCarthy, J., The generation of grid block permeabilities from core data, presented at SPE Asia Pacific Oil and Gas Conference, 7-10 November 1994, Melbourne, Australia

197. Yilmaz, O., Seismic data analysis, Second edition, Society of exploration geophysicists, 2001.

198. Yoon, S., Malallah, A., Datta-Gupta, A., Vasco, D., Behrens, R., A multiscale approach to production data integration using streamline models, SPE Journal, 6(2), 2001, p. 182-192

199. Zhang, F., Reynolds, A., Optimization algorithms for automatic history matching of production data, Proceedings of 8th European Conference on the Mathematics of Oil Recovery, 2002

200. Zhang, F., Reynolds, A.C., Oliver, D.S., The impact of upscaling errors on conditioning a stochastic channel to pressure data. SPE Journal, 8(1), 2003, p. 13-21

201. Zhang, R., Sen, M., Phan, S., Srinivasan, S., Stochastic and deterministic seismic inversion methods for thin-bed resolution, Journal of geophysics and engineering, 9, 2012, p. 611–618

202. Zhang, Y., Oliver, D., History Matching Using the Ensemble Kalman Filter With Multiscale Parameterization: A Field Case Study, SPE-118879-PA, SPE Journal, 16 (02), 2011, p. 307-317